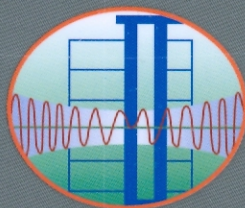


2008
NCREE Research Programs and Accomplishments



National Center for Research on Earthquake Engineering



NCREE



2008 NCREE Research Programs and
Accomplishments

Keyword

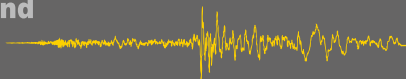
This 2008 Report on Research Progress and Accomplishments is the ninth issue of its kind. It highlights some important ongoing research projects conducted in NCREE. The 32 articles contained in this report are divided into seven categories. It covers a broad spectrum of research efforts made in 2008. A brief description of the seven categories and some specific research topics are listed as follows :

- Research on performance-based seismic design methods: “The microzonation of Seismic design earthquake for Taipei Basin” , “Preliminary Improvement for Performance-Based Seismic Design for Buildings in Taiwan (II)” .
- Research on seismic performance assessment and retrofit techniques for building structures: “Verification of Pushover Analysis on In-Situ Test of School Buildings” , “Progressive Collapse of Reinforced Concrete Buildings during Earthquakes” , “Seismic Performance Assessment of Low-rise RC Buildings: Part II” .
- Enhancement on Taiwan Earthquake Loss Estimation System: “A Preliminary Study on the Performance Assessment of Water Network Systems Following Earthquakes” .
- Research on innovative seismic-resisting technologies: “Bayesian Damage Classification using AR-ARX Array Expression Data” , “Mechanical behavior of stainless steel rebars for earthquake engineering applications” , “Applications of Viscous Dampers to Vertically Irregular Building Structures” .
- Development of advanced numerical simulation and experimental technologies: “Image-based Surface Strain Field Measurement in an RC-Wall Cyclic Test” , “A Preliminary Study on Online Updating Hybrid Simulation” .
- Integrating seismology and earthquake engineering: “Development of A Prototype of Strong Ground Motion Estimation System” .
- Research on geotechnical engineering: “Earthquake Source Parameters and Micro-tremor Site Characteristics Study - Geochemical Monitoring (IV)” , “A Study of Soil-structure Interaction Using In-situ Tests of School Buildings” .

It is our sincere hope that with the publication of the annual reports, the research endeavors of all NCREE researchers can be evaluated and recognized by the global earthquake engineering community. This report should provide opportunities to exchange the research findings with others. Hopefully, this could make contributions to enhance the national coordinations and international collaborations on earthquake engineering research.

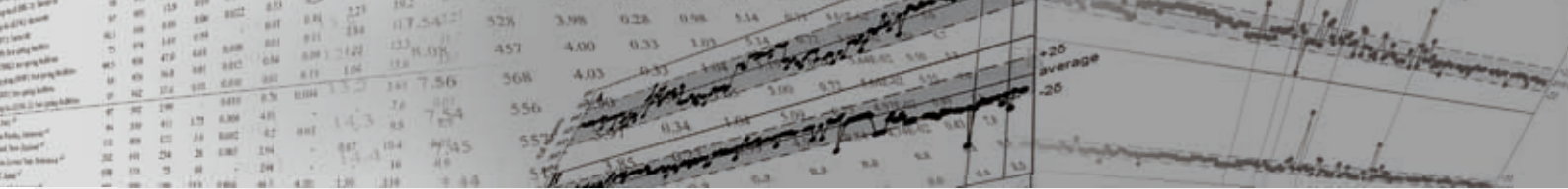
This report is a collection of some of the research efforts made in NCREE in 2008. The full research paper or report of each of the topics listed in this report can be requested from the corresponding authors. The electronic version of this report, in PDF format, can also be downloaded from the official NCREE web site (<http://www.ncree.org>).

Keh-Chyuan Tsai, Director



Contents

- 1 Preliminary Improvement for Performance-Based Seismic Design for Buildings in Taiwan (II)**
Tsung-Jen Teng, Juin-Fu Chai, Wen-I Liao, Wen-Yu Jean, Yuan-Tao Weng, Shyh-Bin Chiou, Fan-Ru Lin and Te-Kuang Chow
- 5 The Microzonation of Seismic Design Earthquake for Taipei Basin**
Yu-Wen Chang, Shyh-Bin Chiou, Wen-Yu Jean and Juin-Fu Chai
- 9 Case Studies of the Confidence-based Seismic Performance Evaluation Procedure**
Yuan-Tao Weng and Tsung-Jen Teng
- 13 Seismic Performance Assessment of Low-rise RC Buildings: Part II**
Yuan-Tao Weng and Shyh-Jiann Hwang
- 17 Experiment of RC Building Frame Subjected to Bi-directional Cyclic Loading**
Chien-Chuang Tseng, Shyh-Jiann Hwang, Yeong-Kae Yeh and Yi-Tsung Lee
- 21 Verification of Pushover Analysis on In-Situ Test of School Buildings**
Yeong-Kae Yeh, Wen-Cheng Shen, Fu-Pei Hsiao and Te-Kuang Chow
- 25 Damage Record and Material Test of Taitung Fire Bureau Building in the 0401 Earthquake**
Yeong-Kae Yeh, Wen-Cheng Shen, Wen-Ching Jaung, Wen-Ching Wang and Lap-Loi Chung
- 29 Progressive Collapse of Reinforced Concrete Buildings during Earthquakes**
S. Yavari, S.H. Lin, K.J. Elwood, C.L. Wu, P.W. Weng and S.J. Hwang
- 33 Study on Seismic Performance Curves of Reinforced Concrete Columns Failed in Shear**
Yi-Ton Hwang and Shyh-Jiann Hwang
- 37 Assessment of Current Pushover Analysis for Irregular Continuous Bridges**
Hsiao-Hui Hung and Kuo-Chun Chang
- 41 Cable Dynamic Stability Experiment of the “Ji-Lu” Cable-stayed Bridge on Taiwan Provincial Highway 139**
Zheng-Kuan Lee and Kuo-Chun Chang
- 45 Mechanical Behavior of Stainless Steel Rebars for Earthquake Engineering Applications**
Yu-Chen Ou, K.C. Chang, Mu-Sen Tsai, Yihui Zhou and George C. Lee
- 49 Seismic Performance of Skew Bridge with Sliding/Friction Rubber Bearings**
Kuang-Yen Liu, Kuo-Chuan Chang, Wei-Jin Cheng and Chi-Hung Lu
- 53 Bayesian Damage Classification using AR-ARX Array Expression Data**
Wei-Sung Lin, Tzu-Kang Lin and Kuo-Chun Chang



- 57 **Seismic Analysis of Asymmetric-Plan Buildings with Supplemental Damping**
Jui-Liang Lin and Keh-Chyuan Tsai
- 61 **Preliminary Study on the Seismic Design of Nonstructural Components in A Hospital**
Juin-Fu Chai, George C. Yao and Fan-Ru Lin
- 65 **Applications of Viscous Dampers to Vertically Irregular Building Structures**
Jenn-Shin Hwang, Wang-Chuen Lin and Shiang-Jung Wang
- 69 **A Study of Three Full-Scale 2-Story Steel Concentrically Braced Frames**
Keh-Chyuan Tsai, Ker-Chun Lin, Chih-Yu Wei, Chih-Han Lin, Ching-Yi Tsai, Jacob Powell, Kelly Clark and Charles Roeder
- 73 **Turning the Building into A Smart Structure: Integrating Health Monitoring**
Kung-Chun Lu, Jian-Huang Weng and Chin-Hsiung Loh
- 77 **Numerical Simulation and Experimental Verification of Semi-active Control of Cable Vibration Using MR Damper**
Pei-Yang Lin, Shieh-Kung Huang, Kweu-Shi Cheng and Chin-Hsiung Loh
- 81 **A Study of Soil-structure Interaction Using In-situ Tests of School Buildings**
Yung-Yen Ko
- 85 **Seismic Retrofit of Rectangular RC Columns Using CFRP Wrapping and CFRP Anchors**
Min-Lang Lin, Pei-Ching Chen, Ying-Han Wu, Keh-Chyuan Tsai and Chih-Tsung Lin
- 89 **Shaking Table Tests on Model Piles in Liquefiable Sand**
Tzou-Shin Ueng, Chia-Han Chen and Yong-Cheng Tseng
- 93 **Parametric Study on Ductility Capacity of Fixed-Head Piles**
Juinn-Shyang Chiou
- 97 **An Investigation on the Effective Damping Ratio Considering Soil-Structure Interaction (I)**
Shang-Yi Hsu, Cheng-Hsing Chen and Juinn-Shyang Chiou
- 101 **Preliminary Study of Seismic Response and Disaster Prevention Information System**
Hui-Ping Wang, Wei-Jen Chen, Wei-Chang Chen and Chin-Hsun Yeh
- 105 **A Preliminary Study on the Performance Assessment of Water Network Systems Following Earthquakes**
Gee-Yu Liu and Hsiang-Yuan Hung
- 109 **Development of A Prototype of Strong Ground Motion Estimation System**
Tao-Ming Chang



- 113 **The Engineering Geological Database for Strong Motion Stations in Taiwan**
Kuo-Liang Wen and Hung-Hao Hsieh
- 117 **Preliminary Study on Online Updating Hybrid Simulation**
Yuan-Sen Yang, Keh-Chyuan Tsai, Amr S. Elnashai, Oh-Sung Kwon and Sheng-Lin Lin
- 121 **Image-based Surface Strain Field Measurement in an RC-Wall Cyclic Test**
Yuan-Sen Yang, Chang-Wei Huang, Bei-Ting Chen and Chiun-lin Wu
- 125 **Construction and Application of NCREE Information and Knowledge Services**
Kuang-Wu Chou, Wen-Hsiang Tu, Chun-Yi Lin, Shang-Hsien Hsieh and Hsien-Tang Lin
- 129 **Earthquake Source Parameters and Micro-tremor Site Characteristics Study-Geochemical Monitoring (IV)**
Vivek Walia, S. J. Lin, T. F. Yang and K. L. Wen
- 133 **Development of an Object-Oriented Program for Structural Collapse Analysis of Framed Structures**
Ren-Zuo Wang, Keh-Chyuan Tsai and Ming-Chieh Chuang

Preliminary Improvement for Performance-Based Seismic Design for Buildings in Taiwan (II)

Tsung-Jen Teng¹, Juin-Fu Chai², Wen-I Liao³, Wen-Yu Jean⁴,
Yuan-Tao Weng⁵, Shyh-Bin Chiou⁶, Fan-Ru Lin⁷, and Te-Kuang Chow⁸

鄧崇任¹、柴駿甫²、廖文義³、簡文郁⁴、翁元滔⁵、邱世彬⁶、林凡茹⁷、周德光⁸

Abstract

The objective of this study is to link up efficiently the current classical force-based design code to the future version of performance-based design guideline. For the purpose, a transition design framework has been proposed in this report to combine the concepts of seismic use group and seismic design category, which are both recommended by FEMA450 and IBC2006. Therefore, the seismic design code developed in the next stage can be expected to serve as an intermediate version. In addition, this report would like to address and discuss key issues in the proposed design framework transition.

Keywords: intermediate version of performance-based design, seismic use group, seismic design category, performance evaluation, acceptance criteria, design framework

Introduction

In general, the seismic performance of a building includes both strength and deformation capacity. The main objective of the traditional seismic design code is to achieve the strength requirement based on a predefined deformation capacity. The global ductility of each specific building system is assumed first, and then the associated seismic design force can be determined. In addition, based on the LRFD method, the earthquake effect can be considered using the specified loading combination rule to design the building, such that the strength performance of the designed building satisfies the strength demand. However, there is no procedure specified to validate the predefined global ductility and the deformation capacity of the main lateral resistance components for the multi degrees of freedom system (e.g. story drift).

In the early stage of developing the performance-based design guideline, the direct displacement-based design that considers the reliability in the preliminary design phase was adopted as the preliminary design method. Besides, combined with the performance objectives, analysis procedures, and the acceptance criteria recommended by FEMA 356, the first version (draft) of performance-based design guideline for new buildings has been completed in 2006. However, there exist some difficulties indeed in the engineering design practice regarding the draft of performance-based design guideline. The first difficult is that although we have adopted the direct displacement-based design method and considered the reliability in the preliminary design phase, the direct displacement-based design is still in its development and further, not so familiar to most of the structural engineers. The

¹ Research Fellow, National Center for Research on Earthquake Engineering, tjteng@ncree.org.tw.

² Research Fellow, National Center for Research on Earthquake Engineering, chai@ncree.org.tw.

³ Associated Professor, Department of Civil Engineering, National Taipei University of Technology, wiliao@ntut.edu.tw.

⁴ Research Fellow, National Center for Research on Earthquake Engineering, wychien@ncree.org.tw.

⁵ Associated Research Fellow, National Center for Research on Earthquake Engineering, ytweng@ncree.org.tw.

⁶ Assistant Research Fellow, National Center for Research on Earthquake Engineering, sbchiou@ncree.org.tw.

⁷ Assistant Research Fellow, National Center for Research on Earthquake Engineering, frlin@ncree.org.tw.

⁸ Assistant Technology Fellow, National Center for Research on Earthquake Engineering, tkchow@ncree.org.tw.

second one is that the acceptance criteria adopted in the proposed draft is merely in a sense of performance evaluation of local members therefore only the median values are needed in the approach. Nevertheless, the check approach for local members is more suitable for the retrofit of existing buildings rather than the design of new buildings. Thus, it is more difficult to present or evaluate the performance capability of a building in the global sense, i.e. in the IM (intensity measure) versus DM (damage measure) format.

In order to avoid the aforementioned difficulties, a design framework to link up to the newly proposed performance-based design guideline is proposed as an intermediate version for the next stage of development, and Figure 1 illustrates the outline for the undertaking. The aim is to link the current classical force-based design code to a future version of the performance-based design guidelines smoothly. In order to develop this intermediate version, the direct displacement-based design method must be set aside and instead, the current sophisticated force-based design methodology incorporated with the concepts of seismic use group and seismic design category which are recommended by FEMA450 and IBC2006 must be retained as shown in Fig. 2.

The objective of this study was to propose a design framework that can serve as an intermediate version. In the following, the key issues in the proposed design framework transition will be addressed and discussed briefly.

Performance Matrix

It is known that, for the traditional force-based design, the engineering parameters (e.g. PGA, spectral acceleration parameters at short periods and at one second) corresponding to strong ground motions can be determined and illustrated by the seismic hazard curve. As a result, the target seismic demand for the specified return period can be determined to design the building. On the other hand, if the deformation performance is taken as the design goal instead of the strength requirement, the seismic hazard curves of the index for the deformation demand (e.g. maximum story drift) should be determined. Figure 3 is the proposed performance matrix, which indicates the discrete hazard curves of the deformation demand (e.g. maximum story drift) for different seismic use groups.

In reality, both FEMA 450 and IBC 2006 do not contain direct methods to evaluate and verify the actual performance capability of structures, nor do they provide a direct means to design for performance characteristics other than those implied in Fig. 3. Therefore, for buildings in which it is desired to attain other performance rather than what is implied by the current code, or for where which it is desired to have greater confidence that the building will actually be capable of attaining the desired performance, both the design procedures and the detailed procedures for

performance evaluation as illustrated in Fig. 1 will be applied.

Implement Strategy

In order to implement the performance matrix while considering the continuity of the current seismic design code, the key practice strategies are proposed as follows:

- (1) The deformation demand at the specified hazard levels can be determined by the indirect method. It means that the spectral acceleration parameters corresponding to strong ground motions at the specified hazard levels should be determined first, and then the associated deformation demand (e.g. maximum story drift) can be evaluated using the specified analysis procedures. Furthermore, the acceptance criteria for the deformation capacity is defined at the design level (10%/50 yrs) only, and can be ignored at the other two hazard levels (i.e. 50%/50 yrs and 2%/50 yrs).
- (2) Each building or structure should be assigned to one of three Seismic Use Groups on the basis of their intended occupancy and use. Buildings in each of Seismic Use Groups II and III are intended to provide a better performance than buildings in Seismic Use Group I. In addition, each structure may be assigned a Seismic Design Category in accordance with the provisions as depicted in Table 1. The Seismic Design Category is used in the provisions to define the permissible structural system, the limitation on height and irregularity, the structural components that must be designed for seismic resistance, and the types of lateral force analysis that must be performed. Buildings designed in accordance with the provisions for each specified Seismic Use Group are intended, as a minimum, to be able to provide the default seismic performance as indicated in Fig. 3.

Table1. Seismic Design Category based on S_{DS}

S_{DS}	Seismic Use Group		
	I	II	III
$0.5 \leq S_{DS} < 0.6$	C	C	D
$0.6 \leq S_{DS}$	D	D	D

- (3) The analysis procedures for evaluating the deformation demand (e.g. maximum story drift) should be specified in the provisions of the seismic design code. As specified by the proposed version of the seismic design code, the maximum story drift can be evaluated by either equivalent lateral force analysis, spectrum analysis, linear and nonlinear time history analysis, or pushover analysis (nonlinear static analysis) according to the Seismic Design Category of the building.

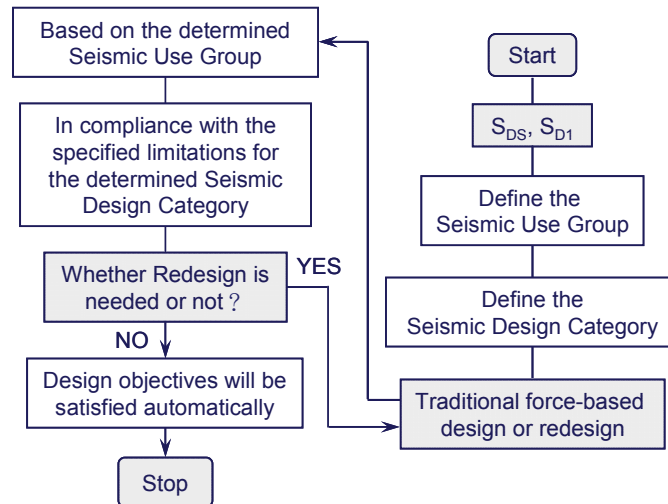


Fig. 2 Design flow chart proposed for the modification of current seismic design code (with the concept as depicted by FEMA 450 or IBC 2006)

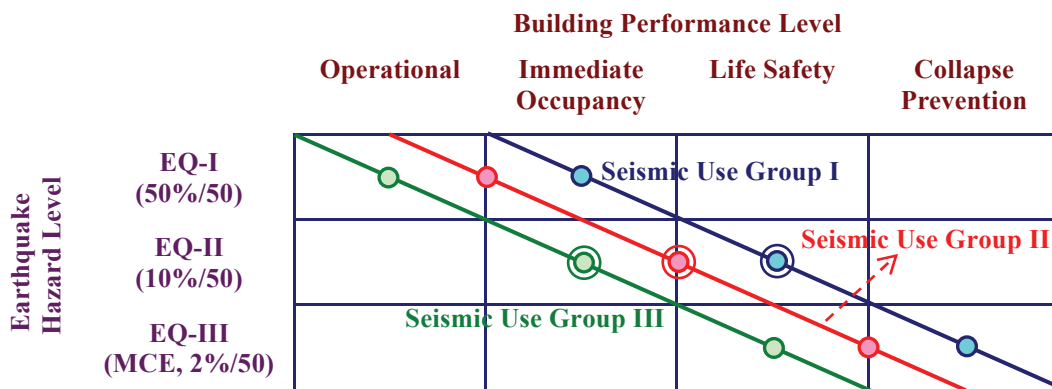


Fig. 3 Proposed performance matrix corresponding to the Seismic Use Group (The symbol ◎ indicates the deformation capacity should be checked during the performance-based design)

The Microzonation of Seismic Design Earthquake for Taipei Basin

Yu-Wen Chang ¹, Shyh-Bin Chiou ², Wen-Yu Jean ³, Juin-Fu Chai ⁴

張毓文 ¹、邱世彬 ²、簡文郁 ³、柴駿甫 ⁴

Abstract

Taipei City is the capital of Taiwan and is geographically located on a sediment-filled basin. The city has experienced several damaging earthquakes in which the most recent event occurred on March 31, 2002. Obviously, the earthquake located more than 80-100 km away, it still caused severe damages in the Taipei Basin due to the site or basin effect. The essential way to mitigate the earthquake hazard is to refine the current seismic design code by a more a proper definition of seismic demands for different site conditions so that the undesired damage of structures due to earthquake excitations can be efficiently prevented. The Central Weather Bureau has installed a very dense ground-motion array in the Taipei Basin. The earthquake data collected in the last decades was used to investigate the local site effects on the ground shaking in the Taipei Basin. Finally, performing the probabilistic seismic hazard analyses with the proposed site amplification factors, the more proper microzonation of the Taipei basin is proposed for the current seismic design code.

Keywords: microzonation, seismic design code, basin, amplification factor, site effect

Introduction

Taiwan is located at the convergent plate boundary where the Eurasian plate has been eastward underthrusting and colliding with the Philippine Sea plate. This tectonic environment results in high seismicity in and around the Taiwan Island. Undoubtedly, earthquake hazard mitigation is an important issue in Taiwan. It is worthy of noting that Taipei City, the capital of Taiwan and located on a sediment-filled basin, has experienced several damaging earthquakes in which the most recent has occurred on March 31, 2002. Eventhough the earthquake epicenter located more than 80-100 km away, it still caused the severe damages in the Taipei Basin due to the site or basin effect. The essential way to mitigate the earthquake hazard is to refine the current seismic design code through a more proper definition of seismic demands for different site conditions so that the undesired damage of structures due to earthquake excitations can be prevented efficiently. This paper aims at modifying the current

seismic microzonation using more intact earthquake records that includes sufficient damaging earthquakes.

The procedure in determining the controlling earthquakes and developing a seismic hazard information base is based on a de-aggregation of the probabilistic seismic hazard in terms of earthquake magnitudes and distances. It has been found that the basin effect is significant especially when the controlling earthquake is a major, shallow and far-field earthquake such as the 1999 Chi-Chi earthquake ($M_L7.3$) and the 2002 Hualien earthquake ($M_L6.8$).

Due to the fact that the seismic microzonation within the Taipei Basin in the current seismic design code was determined based on the earthquake data recorded by the limited stations from 1993 to 1999, i.e., the 1999 Chi-Chi earthquake record has been excluded, thus, this study proposed to modify the current seismic microzonation using the more intact earthquake records including recent and sufficient damaging earthquakes. The local site effect (basin

¹ Assistant Researcher, National Center for Research on Earthquake Engineering, ywchang@ncree.org.tw

² Assistant Researcher, National Center for Research on Earthquake Engineering, sbchiou@ncree.org.tw

³ Research Fellow, National Center for Research on Earthquake Engineering, wychien@ncree.org.tw

⁴ Research Fellow, National Center for Research on Earthquake Engineering, chai@ncree.org.tw

effect) on the Taipei Basin can be discussed as follows:

1. The parameter C_v , the spectral acceleration at 1 second spectral period, for defining the site-dependent normalized design response spectrum can be determined based on the average response spectrum of the observed strong ground motions at each observation station within the Taipei Basin and the surrounding areas. Among the earthquake events occurred from 1991 to 2007, ninety-three earthquake events with the magnitude greater than $M_L 5.0$ were selected. Using an extensive database analysis, the more adequate distribution of parameter C_v for the Taipei Basin can be determined. Therefore, the current seismic microzonation is necessary to be modified based on the more intact earthquake records, i.e., plenty of damaging earthquake records.
2. Based on the recorded data corresponding to the controlling earthquakes such as the 1999 Chi-Chi earthquake and the 2002 Hualien earthquake, the associated acceleration response spectra were determined for each observation station in Taipei Basin. Having had calculated the normalized response spectra for each station, all the response spectra of each event were compared with current seismic code to facilitate examination of the corner period of response spectrum for that seismic zone.

By performing the probabilistic seismic hazard analysis with either of the aforementioned information, a modified seismic microzonation within the Taipei Basin can be established. The proposed seismic microzonation considering the more intact earthquake records within the Taipei Basin is more applicable compared with the existing one discussed in the seismic design code.

Geologic Background of Taipei Basin

The Taipei Basin is triangular in shape with an area of about $20\text{km} \times 20\text{km}$. Four young formations are found sitting flat above the basement which is at most 700m deep. This one-sided subsidence made the basin's Tertiary basement in a half-graben shape. Four newly deposited unconsolidated strata were overlying the basement. The top near-surface layer, called the Sungshan Formation, is thought to carry the burden of the site-effects because of its loose sand and silt content (Wang et al., 2004).

Due to the aforementioned geologic conditions, the basin effects of the Taipei Basin are more complicated than those of the other sites with the soft soil condition. A theoretical 3D model may be developed to study the amplifications of ground motions due to the basin effects. Alternatively, an empirical procedure must be developed based on the recorded earthquake data to estimate the basin effects.

Current Seismic Design Code for Taipei Basin

For the current seismic design code for buildings in Taiwan, the elastic seismic demand is represented by the design spectral response acceleration S_{D1} corresponding to a uniform seismic hazard level of 10% probability of exceedance within 50 years. Due to the basin effects, the corner periods noted in the response spectra associated with the earthquake data observed in the Taipei Basin are generally larger than 1.0 second (Yeh et al., 2001). It implies that the parameters S_{DS} and S_{D1} prescribed in the design response spectrum for general sites can not be applied directly for sites in the Taipei Basin. Alternatively, it is based on the parameters of $C=2.5$ and $C=C_v/T$ for the normalized design response spectrum within the short and moderate period ranges, respectively. The parameter C_v and the associated corner period ($T_0 = C_v / 2.5$) can be determined from the observed strong ground motions for each observation station within the Taipei Basin. Then, based on the contours of parameter C_v and the boundaries of the municipal units, four seismic micro-zones are defined in the Taipei Basin. The representative values of corner period T_0 between short and moderate period ranges of the design response spectrum are prescribed in Table 1.

Table 1 Representative values of corner period for each micro-zone in Taipei Basin

Micro-zone	Taipei Zone 1	Taipei Zone 2	Taipei Zone 3	Taipei Zone 4
Range of C_v	3.6 – 4.6	2.8 – 3.6	2.2 – 2.8	1.5 – 2.2
T_0 (sec.)	1.60	1.30	1.05	0.85

The distribution of the four micro-zones and the shapes of their corresponding design response spectrum in Taipei Basin are shown in Fig. 1. It has been found that the microzonation map of the corner period is in accordance to the basin shape and reflects the thickness of the sedimentary soil layers in the Taipei Basin.

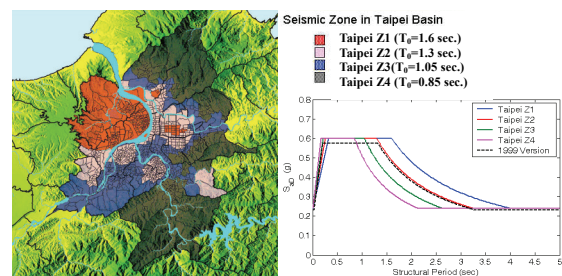


Fig.1 Distribution and the design response spectrum for each microzonation in the Taipei Basin

Earthquake Database

Criteria for Database

Among the earthquake events that occurred from 1991 to 2007, ninety-three earthquake events with the

magnitude greater than $M_L 5.0$ were selected. From these ninety-three selected earthquake events, more than 1900 earthquake histories with PGA of greater than 10gal recorded by 120 stations of the TSMIP network within and around the Taipei Basin were adopted in the desired analysis database. Fig.2 shows the locations of the 120 stations and the seismicity within and around the Taipei Basin. Besides, the locations of the epicenters of the 93 selected earthquake events are depicted in Fig.2, from which the main shock and five large aftershocks of the 1999 Chi-Chi earthquake are observed. Obviously, using the extensive analysis database instead of the existing one, the more adequate distribution of parameter C_v for the Taipei Basin can be determined.

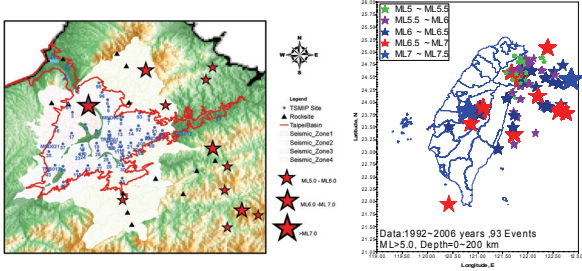


Fig.2 Distribution of the strong motion array in the Taipei Basin and the locations of epicenter of the 93 selected earthquakes

Controlling Earthquakes

Seismic demands specified in the design code were determined based on the seismic hazard analysis, which is usually to develop rock outcrop or hard site ground motion for seismic design and earthquake loss estimation. This procedure, to determine the controlling earthquakes and developing a seismic hazard information base, is based on a de-aggregation of the probabilistic seismic hazard in terms of earthquake magnitudes and distances. The seismic hazard information base summarizes the contribution of individual magnitude and distance ranges to the seismic hazard and the magnitude and distance values of the controlling earthquakes at the 10% probability of exceedance within 50 years level of the Taipei Basin. The hazard contributions corresponding to the various magnitudes and distances (or each sub-source) in the Taipei Basin are shown in Fig. 3. Comparing to the seismicity and zoning scheme, it has been concluded that these controlling earthquakes are located in the subduction zone of NE part of Taiwan. The distances and magnitudes of these controlling earthquakes are greater than 70km and $M_L 6.8$, respectively (Chang et al, 2007). Also, it has been found that the basin effect is significant especially when the controlling earthquake is a major, shallow and far-field earthquake such as the 1999 Chi-Chi earthquake ($M_L 7.3$) and the 2002 Hualien earthquake ($M_L 6.8$).

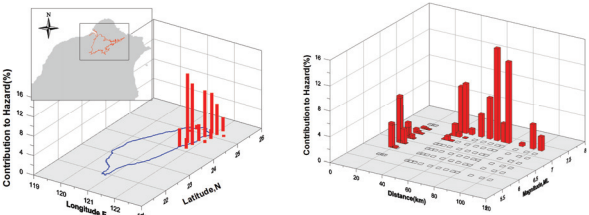


Fig.3 Distribution of hazard contribution in the Taipei Basin

Microzonation Map of Taipei Basin

The site-dependent normalized design response spectrum, C_v

The parameter C_v , the spectral acceleration at 1 second spectral period in defining the site-dependent normalized design response spectrum, can be determined based on the average response spectrum of the observed strong ground motions at each observation station within the Taipei Basin and the surrounding areas. The selected earthquake data which utilized the McGuire relationship (McGuire, 1975) was adopted to determine the seismic microzonation within the Taipei Basin being used in the existing seismic design code, and can be described briefly in the following. Once the magnitude and distance are obtained, V/A and AD/V^2 values for any earthquake history recorded by each station can be estimated approximately using the McGuire relationship. In which A , V and D represent the recorded maximum ground acceleration, velocity and displacement responses, respectively. Accordingly, the earthquake records with a larger V/A value in each station are selected for the calculation of the parameter C_v .

It is still believed that the distribution of the parameter C_v obtained from the earthquake records selected based on the McGuire relationship is not capable of revealing the realistic characteristics of the basin effect due to the consideration that there are insufficient damaging earthquake records such as the 1999 Chi-Chi earthquake. Therefore, the current seismic microzonation is necessary to be modified based on the more intact earthquake records, i.e., involving damaging earthquake records. In addition, ten observed strong ground motions with a larger V/A value in each station are selected to re-calculate the average normalized response spectrum and the corresponding parameter C_v .

In Fig.4, the modified distribution of the parameter C_v proposed in this study (denoted by a line contour) and the seismic microzonation specified in the current seismic design code (denoted by a fill contour) are illustrated for easier comparison in the Taipei Basin. It has been found that the modified distribution is in accordance to the basin shape and reflects the thickness of the sedimentary soil layers much better compared with the current seismic microzonation.

The Source Effect on the Seismic Response Spectrum

Based on the recorded data corresponding to the controlling earthquakes such as the 1999 Chi-Chi earthquake and the 2002 Hualien earthquake, the associated acceleration response spectra were determined for each observation station in Taipei Basin. Having had calculated the normalized response spectra for each station, all the response spectra of each event were compared with the existing seismic code to facilitate examination of the corner period of response spectrum for that seismic zone.

In general, the recorded earthquake data with larger PGA were selected to develop the design response spectrum. However, as shown in the present study, focusing only on seismic intensity while ignoring the earthquake source effect and including the data of controlling earthquakes, the adoption of this approach would result in significantly underestimating the seismic demand. A comparison of the design response spectrum and the average response spectrum is shown in Fig.5. The design response spectra specified by the seismic design code are more or less in conformity with the average response spectra from actual earthquake records. The design spectrum, including the corner period and the spectral acceleration at long periods, as specified by the current seismic design code for all micro-zones in Taipei Basin can thus be considered to be acceptable. However, for individual observation station, some adjustments still need to be done. In total, 30 sites within the Taipei Basin require adjustment (Chiou et al, 2007). The distribution of these sites and the corresponding needed adjustments are shown in Fig. 6.

Conclusions

The basin effect is not negligible in particular when the controlling earthquake is a major, shallow and far-field earthquake such as the 1999 Chi-Chi earthquake or the 2002 Hualien earthquake. In addition, since the seismic microzonation within the Taipei Basin in the current seismic design code was determined using the earthquake data recorded by the limited stations before 1999, the current seismic microzonation is needed to be modified using the more intact earthquake records including the sufficient data of damaging earthquakes. The analytical results show that the modified seismic microzonation is in accordance with the basin shape and the thickness of the sedimentary soil layers much better compared with the current seismic microzonation. It is also evident that the basin effect can be well depicted by using a modified distribution of parameter C_v incorporating data of recent damaging earthquakes.

References

Chang Y.W., Jean, W.Y., Chai J.F. Loh C.H. and Wen K.L.(2007). *The Microzonation of*

Seismic Design Earthquake for Taipei Basin, 14th World Conference on Earthquake Engineering, **07-145**.

Chiou,S.B., Jean, W.Y. and Chai J.F. (2007). *Study on Spectrum Shape for Performance Based Design in Taipei Basin*, 14th World Conference on Earthquake Engineering, **07-146**.

Wang, C.Y., Lee Y.H., Ger M.L. and Chen Y.L. (2004). *Investigating subsurface structure and P- and S-wave velocities in the Taipei basin*, TAO 15:4, 609-627.

Yeh C.S., Teng T.J., Chai J.F. and Liao W.I. (2001). *Seismic Microzonation and Design Response Spectrum in Taipei Basin*. Research Report, Architecture and Building Research Institute Ministry of the Interior Taiwan. (Chinese Version)

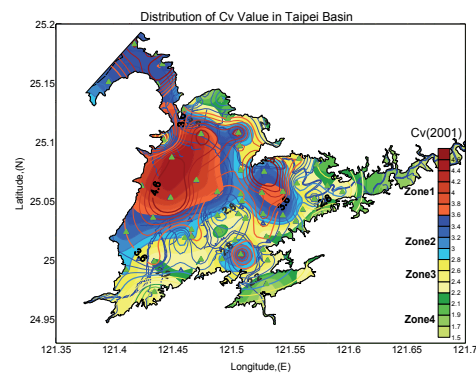


Fig.4 Distribution of the parameter C_v in the Taipei Basin

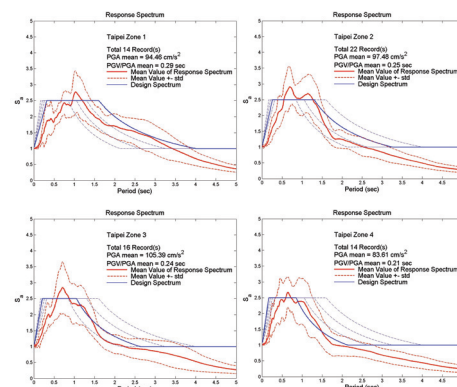


Fig.5 Averaged response spectra for 921 and 331 earthquakes

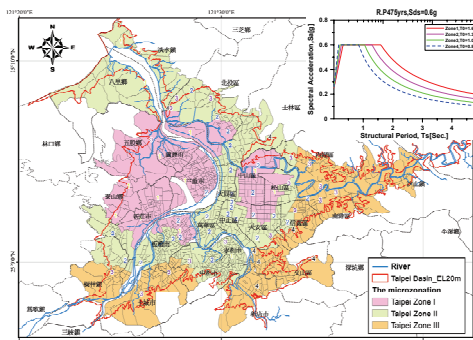


Fig.6 Microzonation map of Taipei Basin

Case Studies of the Confidence-based Seismic Performance Evaluation Procedure

Yuan-Tao Weng¹ and Tsung-Jen Teng²

翁元滔¹、鄧崇任²

Abstract

Following the Northridge earthquake, the FEMA/SAC Steel Project extended the application of reliability methods to assess the seismic performance of steel moment-resisting frame buildings. In this case, the deformation demands on a system were compared to estimates of the capacity of the system against seismically-induced displacements, globally and locally, in order to estimate the ability of the structure to prevent collapse (or achieve other performance goals, such as continued occupancy) for a stipulated seismic hazard level (FEMA, 2000). In this research, the reliability framework as used to assess Special Moment Resisting Frame (SMRF) structures during the FEMA/SAC Steel Project was employed to assess the confidence criteria used with different ground motion scaling methods.

Keywords: confidence, hazard analysis, seismic evaluation, reliability,

Confidence-based Seismic Performance Evaluation

Quantification of the confidence level that a performance goal can be achieved for a particular structure and seismic hazard level includes several inter-related steps: site-specific hazard assessment, structural demand estimation, and structural capacity evaluation. In the procedure implemented herein, median peak inter-story drift demands were computed for an ensemble of earthquake records representative of the seismic hazard level of interest, dynamic interstory drift capacities were estimated, and various types of aleatoric and epistemic uncertainties were characterized. Nonlinear dynamic analyses were used in this study to estimate seismic demands and capacities. From the data obtained, a confidence parameter, λ_{con} , can be determined from equation 1:

$$\lambda_{con} = \frac{\phi C}{\gamma_a D} \quad (1)$$

This confidence parameter is associated with the probability of a specific performance being met, given a specific hazard level (Lee and Foutch, 2000). The

following sections discuss the assumptions used to calculate each of the coefficients in equation 1 for the 34-story building mentioned above. Because of the lack of supporting tests and data, several significant assumptions were made. As such, the values of confidence computed are only approximate, but the computations illustrate the process and help identify areas requiring further refinement. This study also investigates the factors influencing the confidence parameter using two ground motion scaling methods: 1) the MMS method proposed by Weng et al (2009), and 2) the Code method prescribed by Taiwan seismic provision (ABRI, 2006).

Structural Demand Assessment

Limit States

In general, inter-story drift ratios and axial load demands are the primary damage intensity parameters used in characterizing the behavior of SMRF structures. Prediction of inter-story drifts in SMRF structures is relatively insensitive to modeling assumptions and analytical procedures, and computed drifts can be readily related to expected damage in and around connection regions. Inter-story drift has also been adopted in this study to characterize the global

¹ Associate Research Fellow, National Center for Research on Earthquake Engineering, ytweng@ncree.gov.tw.

² Research Fellow, National Center for Research on Earthquake Engineering, tjteng@ncree.gov.tw

dynamic response of a frame system braced with eccentrically braces and BRB elements. However, additional studies are needed to assess the validity of this assumption (for example, it may be necessary to monitor local damage in connections, gusset plates, braces, etc.). For this study, the peak inter-story drift predicted in any story was used to characterize the damage for a specific ground motion. Computation of median values and standard deviations over a suite of ground motions was based on an assumed lognormal probability distribution (see Hamburger et al. 2003).

Modeling

The Platform of Inelastic Structural Analysis for 3D Systems (PISA3D), developed in NTU and NCREC (Lin and Tsai, 2006), is an object-oriented general-purpose computational platform for nonlinear structural analysis. It provides more than 35 different characteristics of structural elements for simulation of structural responses. In particular, its beam-column element can conveniently simulate the shear yielding or flexural yielding responses of steel wide flange sections. Thus, PISA3D has been applied to carefully model the welded moment connections, BRBs and EBFs in order to investigate the seismic performance of the 34-story steel structure under severe earthquakes.

All BRB members were modeled using plastic hardening truss elements. The vibration periods of the 1st to 6th mode of the original and the redesigned structures computed by PISA3D are listed in Table 1, respectively.

Table 1. 1st to 6th modal periods of the example structure.

	Redesigned (unit: second)
1 st Mode	3.75
2 nd Mode	3.59
3 rd Mode	3.21
4 th Mode	1.21
5 th Mode	1.18
6 th Mode	1.08

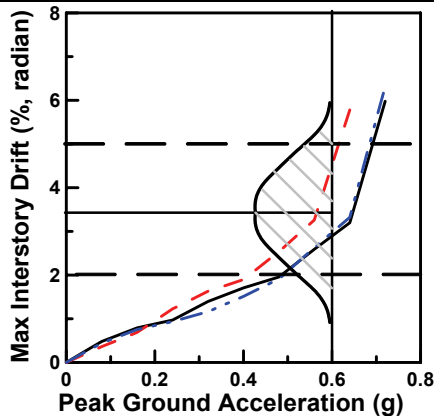


Fig. 1 The relationship between the seismic drift demand and earthquake strength

Demands and Demand Uncertainties

Seismic demands were characterized by extracting the maximum inter-story drift from the analysis output for the seven 2% in 50 year events (Weng et al, 2009). The variability (uncertainty) of response for this hazard level was represented by the standard deviation of the natural logarithms of the drift demands (β_{DR}). β_{DR} was used in conjunction with parameters characterizing the variability of ground motion intensity at the site for the stipulated seismic hazard to compute a demand variability factor, γ . Figure 1 illustrates the relationship between the seismic drift demand and earthquake strength. Table 2 shows the results of the factored demand of the example building in the two ground motion scaling methods.

Table 2. Demand and Capacity Results and Randomness Parameters

	MMS	Code
k	2.40	2.40
b	1.00	1.00
β_{DR}	0.14	0.26
β_{DU}	0.25	0.25
β_{CR}	0.02	0.02
β_{CU}	0.25	0.25
γ	1.02	1.08
γ_a	1.08	1.08
ϕ_R	1.00	1.00
ϕ_U	0.93	0.93
$\gamma_a D$	1.14	2.27
ϕ_C	3.02	3.02

Capacity assessment

To estimate the seismic capacity of an SMRF, the FEMA/SAC guidelines suggest Incremental Dynamic Analysis (IDA) procedure. Default values are provided based on application of this method to various model structures. These default values are not appropriate for braced frame structures, so direct computation is necessary. The IDA method involves carrying out several nonlinear dynamic analyses, in which the intensity of the ground motion accelerograms considered are increased incrementally until a limit state “failure” is observed (Lee and Foutch, 2000). In the FEMA/SAC methodology, failure is defined when the rate of increase of peak inter-story drift with increasing ground motion intensity exceeds five times that associated with an elastic system (or at a prescribed maximum inter-story drift ratio beyond which the reliability of the analysis

is considered doubtful (e.g., 10%). Other criteria have been suggested by other investigators (Vamvatsikos and Cornell, 2002). To be consistent with procedures used for assessing SMRF, the criteria suggested in FEMA 351 (FEMA, 2000) were used herein.

For this study, a total of 77 nonlinear incremental dynamic analyses were computed, requiring approximately 3 hours to complete and plot the results. In these plots, the peak inter-story drift obtained at any level from an inelastic analysis was plotted for a specific ground motion as a function of the intensity of the ground motion. Here, the measure used to quantify the ground motion intensity is the pseudo-spectral acceleration of the scaled ground motion at the first mode period of the structure. Each of the curves on these plots corresponds to one of the twenty FEMA/SAC ground motions from the 2% probability of exceedance in 50-year database. The circled points on the curves correspond to the ground motion intensity (and inter-story drift) where the rate of increase in drift exceeds the criteria stated in the FEMA/SAC guidelines. Because a nonlinear dynamic analysis of the system was carried out in performing these analyses, and member yielding and failure were accounted for, these capacities are not based on the initial yielding or even failure of a single element, but rather on the situation where the rate of increase of lateral displacement of the overall system becomes excessive. This high rate is taken to be an indication of the onset of failure. As can be seen, the seismic capacity predicted in this way is different for each ground motion.

The dispersion of the results obtained for different ground motions can be seen clearly in Figure 2, and the median capacities of the seismic capacities are listed. It is clear that the example building has a relatively large seismic “capacity” based on this method. This does not necessarily signify that collapse or failure always occurs, due to the probabilistic scatter of demands and capacities. Consequently, a statistical interpretation of the demands and capacities is needed to assess the likelihood that the collapse prevention performance goal is violated.

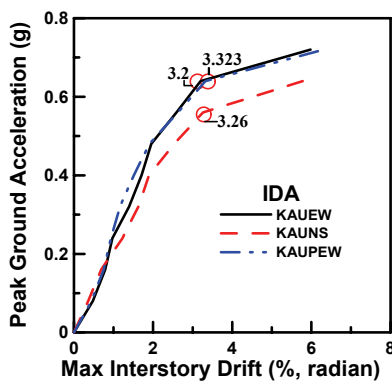


Fig. 2 The relationship between the seismic drift demand and earthquake strength

Moreover, it is noted that the IDA analyses can identify situations where the rate of increase inter-story drifts with increasing ground motion intensity becomes quite large, but then decreases drastically before suddenly increasing again. This is an artifact of the methodology, as previously noted by Vamvatsikos and Cornell (2002) and others for single-degree-of-freedom structures. In these cases, a pulse in a waveform may cause the structure to yield substantially in one direction. When a larger intensity is imposed, an earlier pulse in the record may cause the structure to yield in the opposite direction. This yielding may shield the structure from the effect of the later pulse that was critical for a lower intensity record.

Similarly, using different interpretations of the slope of the IDA curves to define failure may lead to substantially different estimates of capacity. Thus, it is clear that additional work is needed to fully assess methods in estimating the dynamic global capacity of braced frame systems

Table 2 also summarizes the median capacities along with the standard deviation term β_{CR} . It also includes a statistically-based capacity reduction factor ϕ_R derived which accounts for the variability in the computed capacity and statistics related to the ground motion hazard.

Several other sources of uncertainty need to be accounted for in this PBEE methodology. For example, Table includes assumed β_{CU} and ϕ_U values associated with inherent randomness in capacity estimates (taken from the FEMA/SAC guidelines). Because very few full-scale or nearly full-scale tests of modern SCBF component or sub-assemblages have been compared to analytical predictions, actual uncertainty parameters are most certainly different from those assumed.

Confidence Assessment

When all of the parameters for equation 1 are determined, the next step is to evaluate the confidence parameter, λ , for the studied structure. Once determined, the standard Gaussian variation can then be computed by using equation 2:

$$K_X = \left[\ln(\lambda_{con}) + \frac{1}{2} \cdot k \cdot \beta_{UT}^2 \right] \cdot \frac{1}{\beta_{UT}} \quad (2)$$

Conclusions

In this study, performance-based earthquake evaluation methodologies like those implemented in FEMA 351 and elsewhere provide a consistent means in assessing the potential seismic performance of various forms of construction currently in use or proposed. As shown herein, application of these methods to steel braced frame systems introduces various practical and theoretical problems that require further study. Nonetheless, the results presented suggest that low-rise SCBFs designed according to

modern code provisions may be far more vulnerable to earthquake effects than generally accepted for SMRF structures. For instance, the confidence that the 34-story example building designed according to the 1989 Taiwan seismic provision is able to achieve the collapse prevention performance goal was less than 99% for a seismic hazard corresponding to a 2% probability of exceedance in 50 years using the MMS method, which satisfy the confidence requirement 95% proposed by FEMA-350, but that of the results using the Code method is only 85%.

It is the goal of the authors to work towards a unified, performance-based evaluation approach for characterizing and improving the performance of steel braced frames incorporating conventional bracing, buckling-restrained braces, friction and hysteretic devices and viscous dampers. Clearly, achievement of this goal requires the collaborative participation of many professional engineers, researchers, fabricators, erectors, regulatory officials and other experts.

References

- ABRI. *Recommended Provisions for Building Seismic Regulations*. Taipei, 2005. (in Chinese)
- FEMA, *FEMA-351: Recommended seismic evaluation and upgrade criteria for existing welded steel moment frame buildings*, Federal Emergency Management Agency, Washington, DC, 2000.
- Hamburger, Ronald O., Foutch, Douglas A, and Cornell, Allin C., *Translating research to practice: FEMA/SAC Performance-based design procedures* Earthquake Spectra, Special issue: Welded Steel Moment-Frame Structures-Post-Northridge; Vol. 19, No 2, May 2003
- Hooper, J., *Evaluating and upgrading welded steel moment frame buildings using FEMA-351*, Earthquake Spectra, Special issue: Welded Steel Moment-Frame Structures-Post-Northridge; Vol. 19, No 2, May 2003
- Lee, K. and Foutch, D. *Performance prediction and evaluation of steel special moment frames for seismic loads*, Tech. Rep. SAC/BD-00/25, SAC Joint Venture, 2000.
- Mahin, S. A., Malley, J. O., Hamburger, R. O., and Mahoney, M., *Overview of the U.S. program for reduction of earthquake hazards in steel moment-frame structures*. Earthquake Spectra, Special issue: Welded Steel Moment-Frame Structures-Post-Northridge; Vol. 19, No 2, May 2003.
- Somerville, P., *Development of ground motion time histories for phase 2 of the FEMA/SAC Steel Project*. Background Document, SAC/BD-97/04, SAC Joint Venture, Sacramento, Calif., 1997.
- Vamvatsikos, D. and Cornell, A., *Incremental Dynamic Analysis*, Earthquake Engineering & Structural Dynamics, vol. 31, pp. 491-514, March 2002.
- Weng, Y. T., Tsai, K. C., Chen, P. C., Chou, C. C., Chan, Y. R., Jhuang, S. J. and Wang, Y. Y. (2009). "Seismic performance evaluation of a 34-story steel building retrofitted with response modification elements." *Earthquake Engineering and Structural Dynamics*. (accepted)

Seismic Performance Assessment of Low-rise RC Buildings: Part II

Yuan-Tao Weng¹ and Shyh-Jiann Hwang²

翁元滔¹、黃世建²

Abstract

Damage indices aim to provide a means of quantifying numerically the damage in concrete structures sustained under earthquake loading. The development and application of damage indices has, until now, concentrated almost exclusively on flexural modes of failure, thus there is a clear need to investigate the ability of the indices to represent shear damage. This study, first, has chosen and shifted out a lot of experimental results from five reinforced concrete columns including numerical data and images. These existing experimental results obtained by NCREE could be interpreted by specific representative damage indices followed by a discussion of the damage measures relating structural seismic responses. From the comparison between experimental images and damage states expressed by specific damage indices in all experimental process, qualitative and quantitative descriptions of seismic performance could be constructed for different seismic design hazard levels and the corresponding results could be a good reference for next generation performance-based seismic design provision.

Keywords: captive columns, existing school building, damage indices, seismic demand

Introduction

In Taiwan, many typical school buildings suffered severe damage caused by the 1999 Chi-Chi earthquake. Most school buildings were constructed and expanded in a patchy way which caused insufficient seismic resistance during the event. The structural systems of school buildings have intrinsic defects. In order to utilize the natural light and ventilation, windows and doors fully occupy both sides of the corridor. The upper portion of the columns is constrained by the window frame made of aluminum or wood. The lower portion of the column is restricted by the windowsill made of brick walls. Since the windowsill is rigid compared with the window frame, the effective length of the column is shortened. The shorter the column, the larger the shear force. Therefore, the columns tend to fail in the shear mode rather than in the flexural mode. In preventing a possible damage in the future, it is urgent to develop the seismic evaluation and retrofit technology for the existing schools. Therefore, this study focuses on understanding the seismic demands of the existing

columns and quantifying the damage status using damage indices. In this research, the failure modes of columns subjected to the horizontal and vertical loads were identified.

In addition, traditional seismic performance evaluation methods such as capacity spectrum method proposed by ATC-40 (1996) or FEMA-356 (BSSC, 2000) can only represent maximum deformational demands and cannot show local damage states, failure modes and low-cycle structural damage process. In this, the study also aimed to develop a practical seismic assessment approach based from the static pushover analysis considering damage assessment which provides a measure of the physical response characteristics of the structure and is better suited for non-linear structural analysis.

Description of Column Specimens

The experimental program consists of five tests under cyclic, lateral, and vertical load. Three parameters of the specimens such as height-to-width ratio, ductile or non-ductile detailing, and axial load

¹ Associate Research Fellow, National Center for Research on Earthquake Engineering, ytweng@ncree.org.tw.

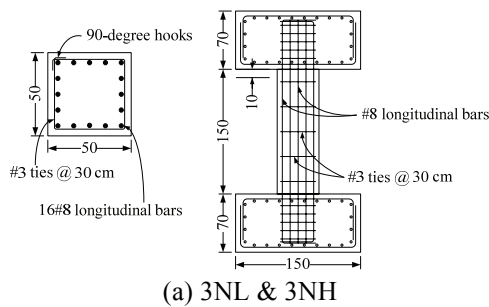
² Professor, National Taiwan University, sjhwang@ncree.org.tw

ratio were varied in the design of the five test specimens. The specimens were divided into four groups and every group has two specimens. These two specimens were subjected to low axial load ($0.1f'_cA_g$, where f'_c = designed concrete compressive strength and A_g = gross cross-sectional area) and high axial load ($0.3f'_cA_g$) separately. Table 1 shows the parameters of the specimens, 3 and 4 represent the height-to-width ratio, D and N represent ductile detailing and non-ductile detailing, and L and H represent low axial load ($0.1f'_cA_g$) and high axial load ($0.3f'_cA_g$). Figure 1 shows the reinforcement details of the specimens. The first group of specimens is the non-ductile shorter columns shown in Figure 1(a). The second group is the ductile shorter columns shown in Figure 1(b). The third and fourth group is the non-ductile longer columns shown in Figure 1 (c) and the ductile long columns shown in Figure 4 (d), respectively. The heights of the columns are 150 cm and 200 cm and the columns have a cross section of 50×50 cm.

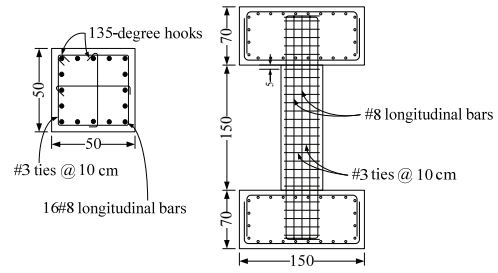
Table 1. Specimens Layout

Specimens	Parameters		
	Aspect ratio	Detailing	Axial load
4DL	4	Ductile (D)	$0.1f'_cA_g$ (L)
4DH			$0.3f'_cA_g$ (H)
4NL		Nonductile (N)	$0.1f'_cA_g$ (L)
4NH			$0.3f'_cA_g$ (H)
3DL	3	Ductile (D)	$0.1f'_cA_g$ (L)
3DH			$0.3f'_cA_g$ (H)
3NL		Nonductile (N)	$0.1f'_cA_g$ (L)
3NH			$0.3f'_cA_g$ (H)

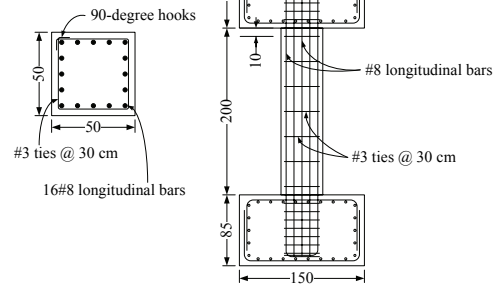
Unit : cm



Unit : cm



Unit : cm



Unit : cm

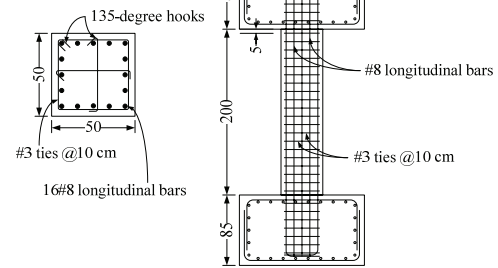


Figure 1 Specimen Details

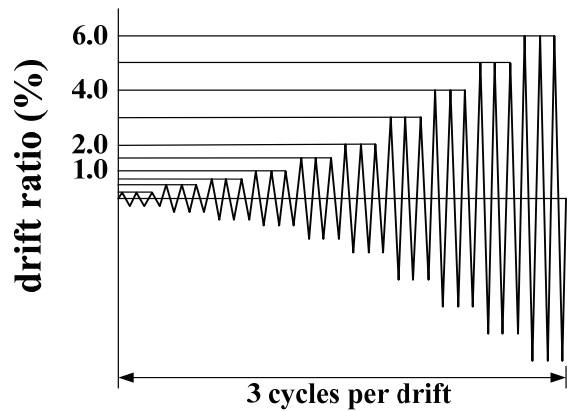


Figure 2. Loading history

Table 2. Strength parameters of specimens.

	V _{test}	V _{response2000}		V _{test}	V _{response2000}
4DL	73.11	71.6	3DL	78.13	71.6
4DH	78.38	81.3	3DH	86.12	81.3
4NL	47.62	42	3NL	48.02	42
4NH	67.4	62	3NH	71.24	62

Figure 2 shows the loading history of the following lateral drift cycles: three cycles each at 0.25%, 0.5%, 0.75%, 1%, 1.5%, 2%, 3%, 4%, 5%, 6%, 7% and 8%. The control of actuator loading system was mixed with displacement and force controls.

Comparison of Experimental and Analytical Results

The strength of all specimens evaluated from the analytical and test results are listed in Table 1. All the analytical models of the column group were constructed by PISA3D (Lin and Tsai, 2006). Figures 4 to 5 show the load-displacement hysteretic relationship of each ductile column specimen obtained from the analytical and test results, respectively. Figures 6 to 7 show the load-displacement hysteretic relationship of the non-ductile column specimens obtained from the analytical and test results. It should be noted that the maximum strength of the specimens 4NH and 4NL did not reach the flexural strength. Therefore, it is evident that all the tested non-ductile columns were failed by shear. More details of the test results can be found in the works of Weng (2007). In addition, the damage index presented in equation (1) proposed by Park and Ang (1985) was applied to quantify the damage status of all column specimens. The crack patterns and the peak values of the damage index corresponding to the specimen 4DL at each of the following lateral drift cycles: three cycles each at 2%, 4%, 6% and **finale**, are also shown in Figures 8 to 11.

$$DI = \frac{\phi_m - \phi_y}{\phi_u - \phi_y} + \beta_e \frac{\int dE}{M_y \phi_u} \quad (1)$$

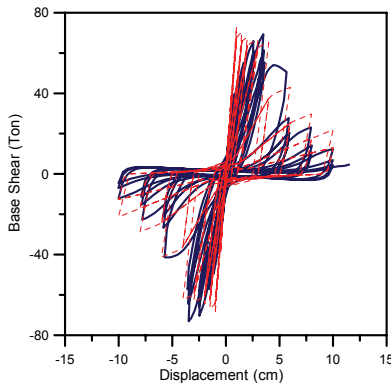


Fig. 4. Load-displacement hysteretic relationship of the specimen 4DL

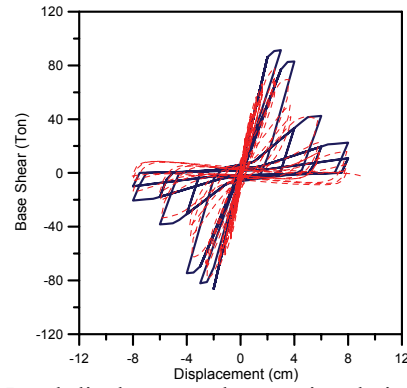


Fig. 5. Load-displacement hysteretic relationship of the specimen 4DH

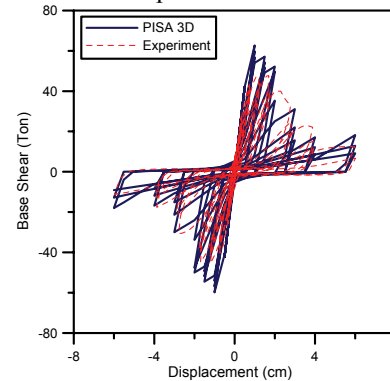


Fig. 6. Load-displacement hysteretic relationship of the specimen 4NL

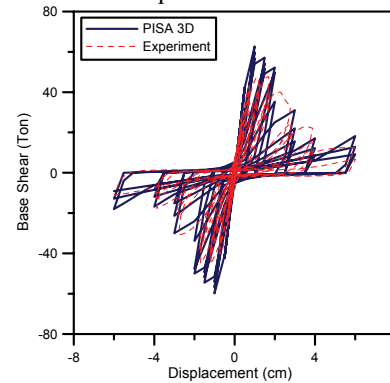


Fig. 7. Load-displacement hysteretic relationship of the specimen 4NH

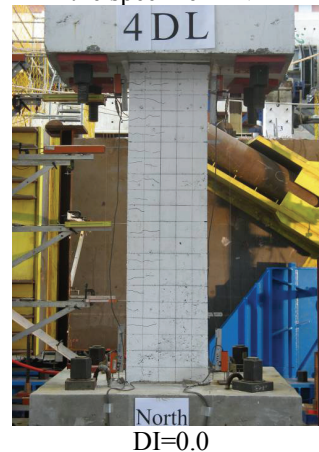


Fig. 8. Failure pattern and damage index value of the normal column C1 (column drift ratio reached 0%)

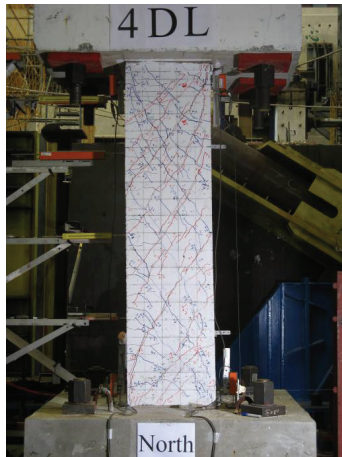


Fig. 9. Failure pattern and damage index value of the normal column C1 (column drift ratio reached 2%)



Fig. 10. Failure pattern and damage index value of the normal column C1 (column drift ratio reached 4%)



Fig. 11. Failure pattern and damage index value of the normal column C1 (column drift ratio reached 5%)

Conclusions

According to the test result, it can be observed that the failure mode of the tested short columns is of

shear failure. Besides, it has been noted that the bond splitting is another failure mechanism involved with the short columns. As the test parameters were varied, different behavior was observed. The inclined angle of the principal cracks with respect to the horizontal axis is larger when the axial load applied on the specimens is higher. The displacement of the nonductile detailing specimens at the ultimate strength is lower than that of ductile detailing; and the displacement of the specimens with high axial load is also higher than that of low axial load. This study also presents the comparison between the experimental and analytical results. Results of the tests are reported, analyzed and interpreted in this study. The damage index proposed by Park and Ang (1985) was applied to quantify the damage status of all column specimens. The crack patterns and the peak values of the damage index were correlated to estimate the seismic demands of the existing non-ductile RC columns at each different lateral drift cycles. Moreover, more research works are needed to better understand the behavior of low-rise reinforced concrete buildings.

References

- ATC, (1996) "Seismic evaluation and retrofit of concrete of concrete buildings, Vol. 1", ATC-40, Applied Technology Council, Redwood City.
- FEMA-356, (2000) "NEHRP Guidelines for the Seismic Rehabilitation of Buildings", BSSC, Federal Emergency Management Agency, Washington, D. C.
- Weng, P. W. (2007), "Study on the Seismic Performance Curves of Reinforced Concrete Short Columns Failed in Shear," Master Thesis, Department of Construction Engineering, National Taiwan University of Science and Technology, Taiwan. (in Chinese)
- Bo-Zhou Lin and Keh-Chyuan Tsai, Platform of Inelastic Structural Analysis for 3D Systems-PISA3D R2.0.2 User's Manual, National Center for Research on Earthquake Engineering, Taiwan(2006).
- Park Y. J. and Ang, H. S. (1985), "Mechanistic Seismic Damage Model for Reinforced Concrete," Journal of Structural Engineering, ASCE, Vol. 111, No. ST4, 722-739.

Experiment of RC Building Frame Subjected to Bi-directional Cyclic Loading

Chien-Chuang Tseng¹, Shyh-Jiann Hwang², Yeong-Kae Yeh³ and Yi-Tsung Lee⁴

曾建創¹、黃世建²、葉勇凱³、李逸聰⁴

Abstract

The theories of reinforced concrete (RC) structures can be divided into two distinct categories, namely “flexure governed member with axial load” and “shear or torsional member”, while the former has already had sophisticated analytical models and has been accepted by the design code, but the latter one lacks experimental support by performing a systematic study. Because of this lacking experiments, we have performed tests on a 2-story RC building subjected to bi-directional reversed cyclic loading to examine the torsional effect caused by the eccentricity at National Center for Research on Earthquake Engineering (NCREE) in Taiwan. This is an internationally-cooperated project between NCREE and the University of Houston (UH). Emphasis is placed on using simulation response histories to provide actuation forces applied to the reinforced concrete buildings subjected to reversed cyclic loading. The associated simulated response will be fed back into building characteristics for additional shake table simulations. The results will be used to correlate analytical tools and the new design methodologies.

Keywords: reinforced concrete building frame, bi-directional cyclic loading, stiffness irregularity, torsional moment, eccentricity

Introduction

The objective of this integrated experiment is proposed to address the complex behavior of reinforced concrete buildings subjected to multi-directional earthquake loading and the subsequent interactions resulting from the nonlinear response of individual components that compound further the multi-directional affect of the ground motion. The entire effort is led by a diverse team of participants from institutions around the country and the National Center for Research on Earthquake Engineering (NCREE) in Taiwan. Emphasis is placed on using simulation response histories to provide actuation forces applied to the reinforced concrete buildings subjected to reversed cyclic loading. The associated simulated response will be fed back into building characteristics for additional shake table simulations. This project is international cooperation with University of Houston (UH). The results will be used to correlate analytical tools and the new design methodologies.

Design of the RC Specimen

Fig.1 shows the specimen is two stories, the short direction is one bay, and the long direction is two bays. The net height of column on 1st floor is 2000 mm, on 2nd floor is 1500 mm. The cross section size of each column is 400 x 400 mm, and of each beam is 300 x 400 mm.

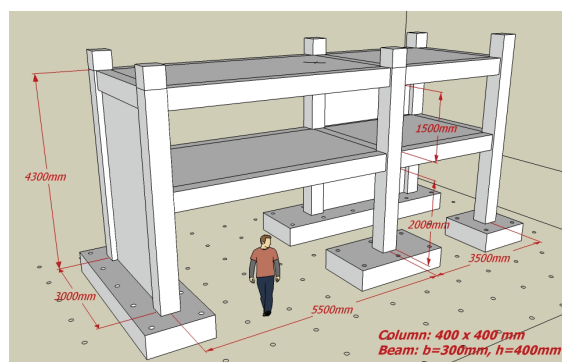


Fig.1 Drawing of RC building frame

¹ Associate Research Fellow, National Center for Research on Earthquake Engineering, cctsens@ncree.org.tw

² Professor, Department of Civil Engineering, National Taiwan University

³ Research Fellow, National Center for Research on Earthquake Engineering

⁴ Graduate Student, Department of Civil Engineering, National Taiwan University

Experiment Procedure and Allocation

In order to test torsional moment effect, we designed the walls of the specimen to be stiffness irregularity. We allocated three low-rise walls at east and north sides, as shown in Fig. 2. The short span of east side at the long direction has disposed Wall 1 (Height/Width Ratio is 0.48) and Wall 2 (Height/Width Ratio is 0.64), and the north side of specimen has disposed Wall 3 (Height/Width Ratio is 1.5) at the short direction. Walls 1 and 2 are shear critical, while Wall 3 is both shear and flexure critical. Hence, the characteristics of various types of walls can be identified. Columns A and C are short (shear critical) and normal (flexure critical), respectively, that are subjected to biaxial loading and axial compression ($0.2 f_c'$); Columns B and D are short (shear critical) and normal (flexure critical), respectively, that are subjected to biaxial loading only. The structural behavior of columns with various conditions can also be examined by this arrangement.

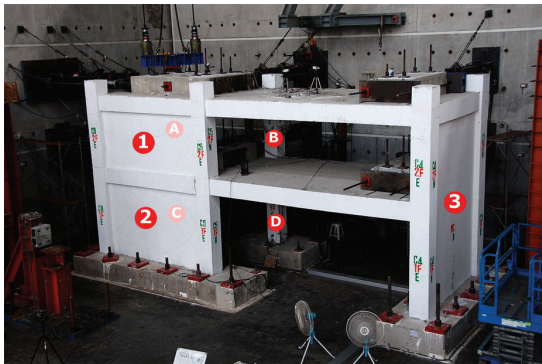


Fig.2 Global photo of the test structure (shows the allocation of beams and columns.)

The thickness of the slab depends on the strength of the specimen. During the test, the hydraulic power supply provided force to RC block, and finally the force will be transmitted to every component element. We did not want the experiment to fail due to slab damage and considering this we designed the thickness of the slab to be 200 mm.

The details of columns are shown in Fig.3. There are 12 main reinforcements and their size is no.6; the size of columns' stirrups is no.3, and the nominal strength of them is 4200 kg/cm^2 . It is worth paying attention to two columns beside Wall 3, the space between each stirrups on 1st and 2nd floor are identical to be 100 mm.

The details of beams are shown in Fig.4. There are 8 main reinforcements, the size is no.6; the size of beams' stirrups is no.3, and the nominal strength of them is 4200 kg/cm^2 .

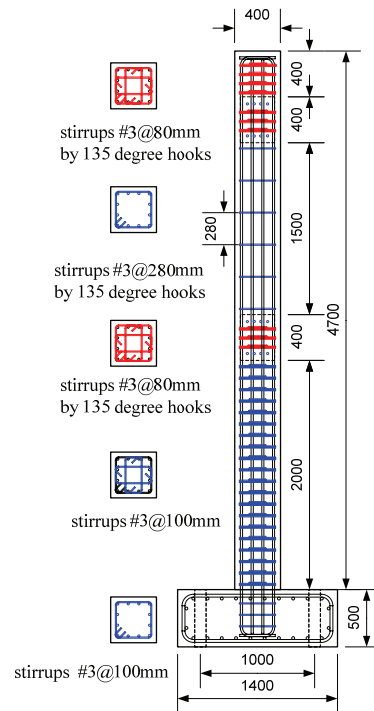
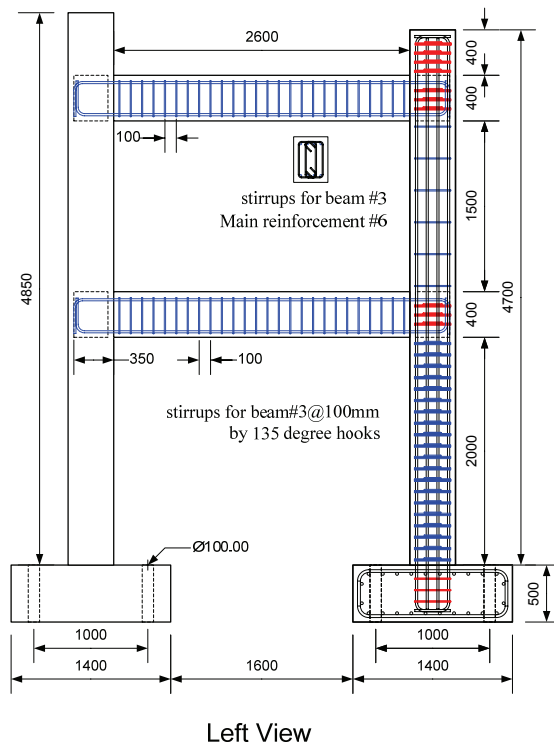


Fig.3 The details of columns



Left View

Fig.4 The details of beams

This experiment used 10 sets of static hydraulic actuators, and the capacity is 981 kN for each actuator. We allocated 5 sets of actuators at the long direction. There were 2 sets on 1st floor and 3 sets on 2nd floor. In the same way, there were 2 sets on 1st floor and 3 sets on 2nd floor at the short direction.

For the purpose of this experiment, loading history must satisfy two conditions. First, to control displacement of mass center on 2nd floor is 1:2 on NS (North-South) and EW (East-West) direction. Second, the ratio of horizontal force is 1.83 equal to the ratio of story height. Fig. 5 shows the loading history which is consisted by the following drift cycles: 0.25%, 0.375%, 0.5%, 0.75%, 1.0%, 1.5%, 2.0%, 3.0%, and each of them are three cycles.

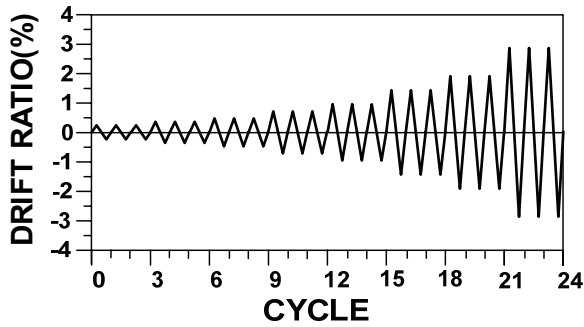


Fig.5 Loading history

Results of Experiments

Fig.6 shows the relationship between base shear and roof displacement. The red curves are base shear versus roof displacement hysteresis loops. When drift ratio is -3.0%, the specimen occur shear critical to cause base shear decay on 2nd floor. The blue curve on Fig.6 means a component of base shear and roof displacement at NS direction, and the green curve means a component of base shear and roof displacement at EW direction. When drift ratio reach 3.0 %, there are soft appearance about stiffness on 1st floor. It can shown form Fig.7 and Fig. 8: The positive displacement is large than negative displacement. It means the 1st floor occur soft appearance of stiffness. Then, the column occurred shear failure on 2nd floor to cause soft appearance. The red curve on Fig.7 shows that(this) condition. The results of this experiment will focus on developing new constitutive models for RC under combined axial/bending/shear/torsional loading in conjunction with available inelastic beam-column and shell elements.

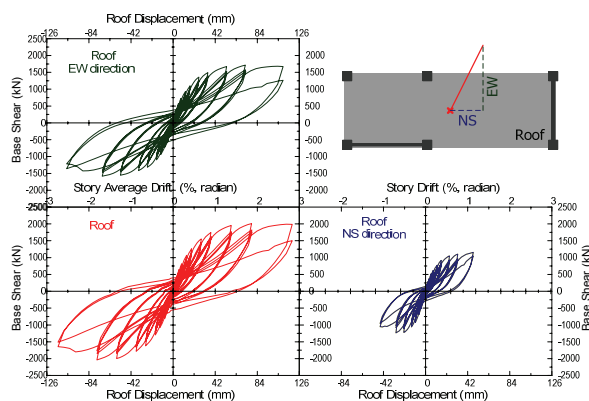


Fig.6 Base shear v.s. roof displacement hysteresis loops.

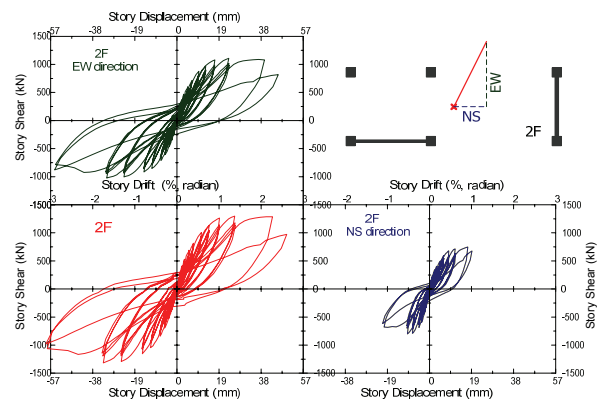


Fig.7 2nd floor story shear v.s. 2nd floor story displacement hysteresis loops.

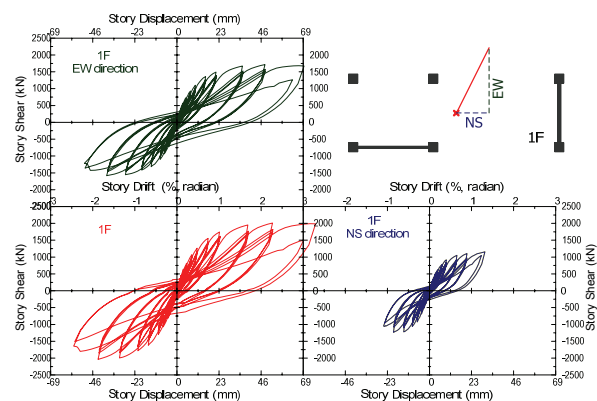


Fig.8 1st floor story shear v.s. 1st floor story displacement hysteresis loops.

Fig.9 shows 1st floor column C1 (Column C) concrete crack pictures in different phases. There are extra vertical loading (0.2 fc') at Column C1. Compared with Column C2, concrete crack on Column C1 gather on the bottom of column. Finally, the failure mode of Column C1 and C2 are flexure critical in the same result. Fig.11 shows the concrete crack of Column C2 (Column B) on 2nd floor, and the failure mode is shear critical. When drift ratio is 3.0 %, Column C2 had large concrete crack suddenly.

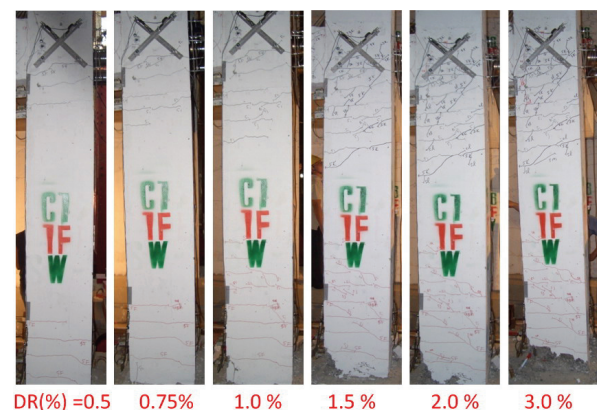


Fig.9 1st floor Column C1 (Column C) concrete crack pictures in different phases.

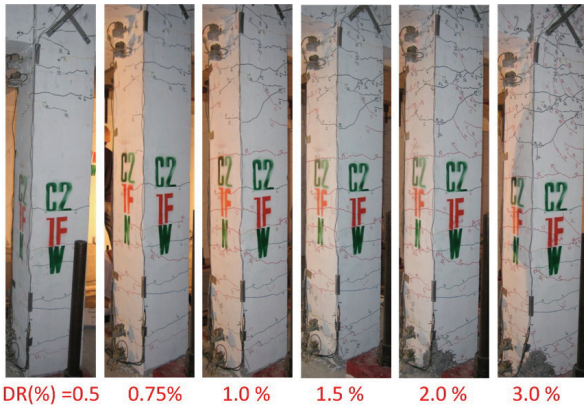


Fig.10 1st floor Column C2 (Column D) concrete crack pictures in different phases.

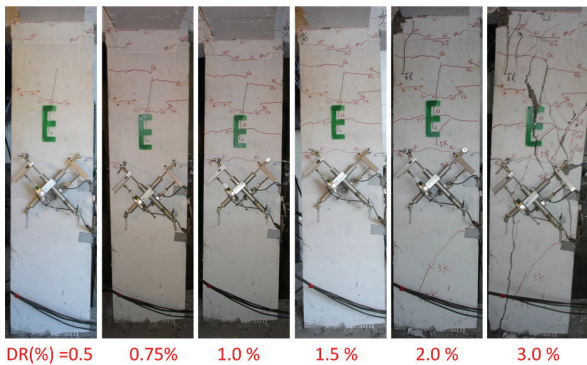


Fig.11 2nd floor Column C2 (Column B) concrete crack pictures in different phases.

Conclusions

We have tested a 2-floor RC building frame subjected to bi-directional cyclic loading experiment in NCREE. The results of this experiment will be used on some related analytical tools and new design methodologies. The brief conclusions of this paper are as follows:

1. The purpose that we control displacement of mass center on 2nd floor is 1:2 on NS (North-South) and EW (East-West) direction is to test torsional moment effect cause by stiffness irregularity.
2. During bi-directional cyclic loading experiment, the displacement of bi-direction and torsion at 1st and 2nd floor caused Column C1 and C2 compression failure on the button of columns. And, there is also concrete compression failure on Out-of-Plan walls.
3. When the center of stiffness and the center of mass do not coincide at each story, torsional moment is induced in the building and torsion vibration occurs. The torsional moment may increase the shear stress of structural components (such as: columns and walls). Hence, torsional moment needs to be considered in the interaction simulation of axial, flexural, and shear forces.

References

1. Experiments and Simulation of Reinforced Concrete Buildings Subjected to Reversed Cyclic Loading and Shake Table Excitation, 4ICEE, Taipei, Taiwan, Oct. 12-13, 2006, Paper No.175.
2. Mansour, M. and Hsu, T. T. C. (2005a). "Behavior of Reinforced Concrete Elements under Cyclic Shear: Part 1 – Experiments," Journal of Structural Engineering, ASCE, Vol. 131, No. 1, January, 2005, pp. 44-53.
3. Kunnath, S.K. and Reinhorn, A.M. (1990). "Model for inelastic biaxial bending interaction of reinforced concrete beam-columns," ACI Structural Journal, Vol.87, No.3, pp.284-291.
4. Kunnath, S.K. and Reinhorn, A.M. (1989). "Inelastic three dimensional response analysis of reinforced concrete building structures (IDARC-3D) Part –I Modeling," NCEER report no. 89-0011, State University of New York at Buffalo, New York.

Verification of Pushover Analysis on In-Situ Test of School Buildings

Yeong-Kae Yeh¹ Wen-Cheng Shen² Fu-Pei Hsiao³ Te-Kuang Chow⁴

葉勇凱¹、沈文成²、蕭輔沛³、周德光⁴

Abstract

A method of seismic evaluation for existing buildings needs to be confirmed. Based from the capacity spectrum method of ATC-40, NCREE has developed a seismic evaluation method using pushover analysis. The properties of nonlinear hinges for nonlinear pushover analysis of low-rise RC structure have been determined. However, different definitions of nonlinear hinges will cause different solutions, thus in-situ test is the best way to verify the assumptions made for pushover analysis. In the past four years, four in-situ tests of school buildings have been carried out. The experimental results are valuable to our researches. In this paper, the ETABS pushover analysis results are compared with the experimental results to verify the accuracy of the present study. Not only this discusses the mechanism of nonlinear hinges but also delivers a reference for modifying the properties of nonlinear hinges in the future. The proposed seismic evaluation method is beneficial for engineers in doing seismic evaluation of low-rise buildings.

Keywords: ETABS, In-situ test, Pushover analysis, Detail evaluation

Introduction

There are few large-scale experimental data that can be utilized to compare with the analytical results because of the huge cost and fabrication of such tests. Although the reduced-scale or single-frame models are usually adopted in the laboratory, the size effect is always a problem to be solved. In order to receive seismic test data of structures more directly, the in-situ test of school buildings which is also an important breakthrough in the field of large-scale testing was carried out in 2005 (Jaung et al., 2008). Two types of experiments were conducted: 1) lateral load tests to identify the lateral strength, stiffness and toughness of the building, and 2) vertical load tests to study the vertical load-carrying mechanism after part of members failed. The brick wing-wall along the corridor was dismantled and only the long and short columns were reserved before test. One half of this building was reinforced by steel bracings to provide reaction support, while the other half was pushed to failure. The oil jacks were aligned to push the school specimen in its weak axis along corridor direction.

During the test, the oil jacks were controlled through their pressure valve areas to keep the ratio of loads acting on 1F and 2F being 1:2, which is the proportion of lateral load distributed by the fundamental mode.

Based from the successful experience of the in situ test in Hua-Lien County, two retrofitting specimens using brick wall infill and RC wing-wall and one contrastive specimen were prepared. The effect of the above two different retrofitting methods was also investigated. Before the demolition of the old school buildings, NCREE applied for the permission to perform the said in-situ tests during the school break between school semesters. The behavior under lateral load for static pushover test, pseudo-dynamic loading test and cyclic loading test (Weng et al., 2008) was investigated. The monotonic pushover test on retrofit of school building by adding composite columns to partition brick wall was also carried out (Chung et al., 2007). In 2007 summer vacation, three specimens were utilized to prove the retrofitting methods: RC frame with steel plate jacketing, RC jacking on column, and RC frame with

¹ Research Fellow, National Center for Research on Earthquake Engineering, ykyeh@ncree.org

² Assistant Research Fellow, National Center for Research on Earthquake Engineering, wcschen@ncree.org

³ Associate Research Fellow, National Center for Research on Earthquake Engineering, fphsiao@ncree.org

⁴ Assistant Technician, National Center for Research on Earthquake Engineering, tkchow@ncree.org

post-tensioned rods. Through the comparison on the capacity curve from in-situ tests, the above retrofitting methods were found economical and justified valid for school buildings.

Detailed Seismic Evaluation Method

According to the capacity spectrum method proposed by ATC-40 (ATC-40, 1996), the pushover analysis is used to obtain the base-shear-to-roof-displacement relationship of school buildings termed as the capacity curve. The capacity curve can be transferred to capacity spectrum curve on the first mode of the structure. The seismic capacity of buildings can be specified with the performance peak ground acceleration determined from the pushover curve and the corresponding performance point. The capacity curve from nonlinear pushover analysis displays the load-deformation relationship. Moreover, not only the strength but also the toughness of building provided the seismic capacity.

Many commercial programs like ETABS and SAP2000 can process nonlinear static analyses which are also called pushover analyses. In ETABS, the elastic behavior of structural members is simulated through the elastic properties of material. The nonlinear response of a structure is restricted to nonlinear hinges which are assigned on the structural elements of that structure. The accuracy of the pushover analysis is dependent on the well-defined properties of nonlinear hinges of structure elements. These nonlinear hinges in ETABS can be divided to two types: default and user-defined hinges. The parameters of the default nonlinear hinges were constructed from FEMA-273 and ATC-40. The built-in nonlinear hinges have four types: (1)Default-P; (2)Default-PMM; (3)Default-M3 and (4)Default-V2. The user-defined nonlinear hinge properties can be modified from the built-in nonlinear hinges or can be added freely as a new one.

The conservative built-in hinge properties resulted in a disparity after comparison with the experimental data. On the other hand, no such nonlinear hinge property in ETABS software is supplied to do the nonlinear pushover analysis when the RC frames with wall. Therefore, Yeh and Hsiao (Hsiao et al., 2006 and 2007) proposed the nonlinear hinge properties for column, brick wall and RC shear wall according to the load-deformation relationship of elements. They also developed MATLAB programs (Chung et al., 2008) for engineer to calculate the parameters of nonlinear hinges.

Correction of Capacity Curve

Lateral load tests consist of monotonic static pushover test, pseudo-dynamic test and cyclic loading test were performed at Ruei-Pu Elementary School in

2006. From the comparison between results of monotonic static pushover test and cyclic loading test, all the monotonic static pushover test results can be corrected to consider the effect of cyclic loading.

The monotonic static pushover test cannot suitably describe the cyclic deformation of structure under the real earthquake. In order to simulate the real behavior under an earthquake, the cyclic loading curve from the Ruei-Pu in-situ test was employed to correct the nonlinear part of the monotonic static pushover curve in this study. Then, a pseudo-cyclic loading curve was derived. The pseudo-cyclic loading curve is much similar to the cyclic loading curve. As shown in Figure 1, the monotonic static pushover curve and the pseudo-cyclic loading curve revealed similar stiffness and strength behavior. However, the cyclic loading specimen demonstrated more pronounced degradation in the post-strength behavior. The post-strength slope of the cyclic loading specimen is as twice as steeper than that of the monotonic loading specimen. We defined the relationship for correcting the monotonic pushover curve to pseudo-cyclic loading curve as follows:

- (1) If the base shear is less than $0.97V_{monotonic,max}$, the pseudo-cyclic loading curve is defined by equation (1)

$$\delta_{pseudo} = \delta_{monotonic}, V_{pseudo} = V_{monotonic}, \quad (1)$$

In Equation (1), δ_{pseudo} indicates the roof displacement in pseudo-cyclic loading curve; $\delta_{monotonic}$ indicates the roof displacement in monotonic pushover curve; V_{pseudo} indicates the base shear in pseudo-cyclic loading curve; and $V_{monotonic}$ indicates the base shear in monotonic pushover curve.

- (2) If the roof displacement is bigger than the roof displacement corresponding with $0.97V_{monotonic,max}$ in monotonic pushover curve and also the corresponding base shear is less than $0.97V_{monotonic,max}$ in the monotonic pushover curve, the pseudo-cyclic loading curve is defined by equation (2)

$$\delta_{pseudo} = \delta_y + \frac{\delta_{monotonic} - \delta_y}{2}, V_{pseudo} = V_{monotonic}, \quad (2)$$

In Equation (2), δ_y indicates the roof displacement corresponding with $0.97V_{monotonic,max}$ in monotonic pushover curve. In order to express the post-strength behavior, equations (1) and (2) were applied to correct the monotonic pushover curves to pseudo-cyclic loading curves.

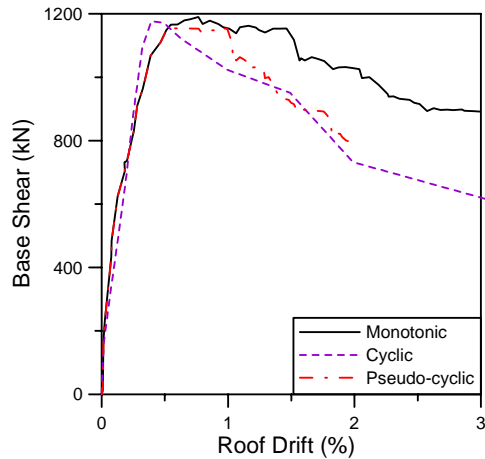


Figure 1 Cyclic loading curve and monotonic pushover curve

Verification of In-situ Test

In this brief report, we only show the test results in Hsin-Cheng Junior High School. A two-story RC school building with strengthened brick wall was dedicated by Hsin-Cheng Junior High School to the pushover test. The school building is a beam-column framed structure with 7.7 meters high, 30 meters long and 10.3 meters wide. There are three classrooms in each story and an 1B brick wall between classrooms. Most windowsills are seventy-five centimeters high along the corridor.

After assigning the nonlinear hinges on the structural members in ETABS model, the capacity curve was obtained through nonlinear pushover analysis and was plotted in Figure 2. Figure 2 shows the comparison of analytical and experimental capacity curves. The maximum strength of experimental data is obtained at 2914.7kN corresponding to the roof displacement about 149.5mm. And the maximum base shear of analytical results obtained by ETABS is at 2554.8kN. The initial stiffnesses of experimental and analytical results were very close. However, it is a disparity in the maximum lateral strength between the experimental and analytical results. Because the length of windowsill columns was much longer than usual columns, the short-column effect was not observed. The test result showed that the failure modes of columns are mostly flexure or flexure shear failure.

The behavior of nonlinear hinges near the corridor side was discussed in this paper. Figure 3 shows the illustration of nonlinear hinges under the maximum strength. Some nonlinear hinges occurred in the first floor under the maximum strength condition, but no column has cracked in the second floor. It indicates that the phenomenon of weak story exists in the bottom layer. The short columns have flexure shear failure before the long ones. These analytical results are extremely close with the experimental data. Figure 4 describes the photo of failure and the illustration of nonlinear hinges near the

corridor side.

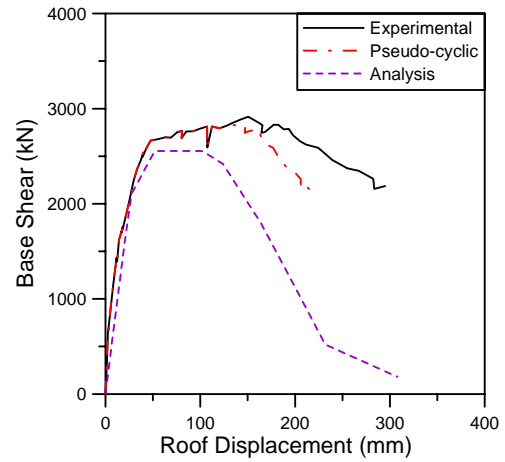


Figure 2 Capacity curve of prototype specimen

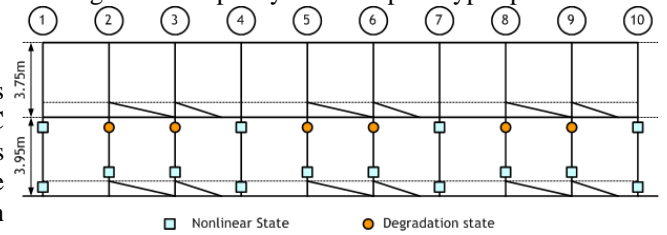


Figure 3 Illustration of nonlinear hinges near the corridor side

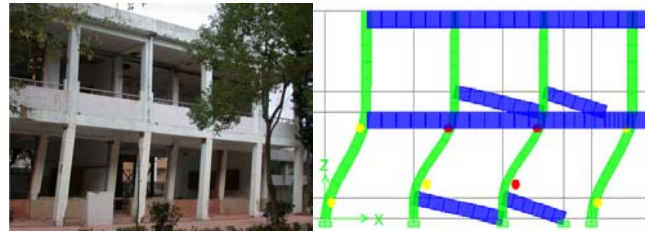


Figure 4 The failure mechanism of prototype specimen in the final step

Conclusions

Through the verification with the experiment data from in-situ tests done by NCREE in Taiwan, the pushover analytical results obtained by ETABS can provide a good approximation of the seismic behavior of RC school buildings. The failure mechanism of structure elements can be predicted well under the present method. The detailed seismic evaluation method proposed in this paper can reasonably provide a measure to determine the seismic capacity of buildings. The seismic evaluation process suggested can provide engineers a good way to precisely perform seismic evaluation of RC school buildings. The effect of hinge properties under variation of axial load will be investigated in the further work. The present method extending to the high-rise RC buildings is our goal.

References

- Jaung, W. C., Chiou, T. C., Hsiao, F. P., Tu, Y. H., Chien, W. Y., Yeh, Y. K., Chung, L. L. and

- Hwang, S. J. (2008), "In-Situ pushover test of school building structure in Sin-Chen junior high school," NCREE Report, NCREE-08-008. (In Chinese)
- Weng, Y. T., Lin, K. C., Hwang, S. J. and Chiou, T. C. (2008), "In situ pseudo-dynamic test and cyclic pushover test of existing school buildings," NCREE Report, NCREE-08-004. (In Chinese)
- Chung, L. L., Wu, L. Y., Yang, Y. S., Huang, Y. C., Lien, K. H., Chien, W. Y., Yeh, Y. K., Hwang, S. J., Hsiao, F. P. and Chiou, T. C. (2007), "In situ monotonic pushover test on retrofit of school buildings by adding composite columns to partition brick walls," NCREE Report, NCREE-07-058. (In Chinese)
- ATC-40 (1996), "Seismic evaluation and retrofit of concrete buildings. Report No. SSC 96-01," Applied Technology Council.
- Chung, L. L., Yeh Y. K., Chien W. Y., Chai J. F., Hsiao F. P., Shen W. C., Chiou T. C. Chow T. K., Chao Y. F. Yang Y. S. and Hwang S. J. (2008), "Technology handbook for seismic evaluation and retrofit of school buildings," NCREE Report, NCREE-08-023. (In Chinese)
- Hsiao F. P., Yeh Y. K. and Lin C. L. (2006), "Seismic evaluation and experimental verification of school buildings," Proceedings of the 8th National Conference on Structure Engineering, Nantou, Taiwan. (In Chinese)
- Hsiao F. P., Yeh Y. K. and Tseng C. C. (2007), "Seismic evaluation of building with pushover analysis (I)," NCREE Report, NCREE-07-049. (In Chinese)

Damage Record and Material Test of Taitung Fire Bureau Building in the 0401 Earthquake

Yeong-Kae Yeh¹, Wen-Cheng Shen², Wen-Ching Jaung³, Wen-Ching Wang⁴,

Lap-Loi Chung¹

葉勇凱¹、沈文成²、江文卿³、王文清⁴、鍾立來¹

Abstract

The building of Taitung's Fire Department shows some structural weaknesses because of its special configuration in the first storey. The 0401 earthquake caused serious damage on the said building. NCREE (National Center for Research on Earthquake Engineering) researchers visited the area to make a full exploration and sampling of concrete and steel to analyze the building's structural strength. All the gathered data can serve as a reference for further works.

Under the Taiwan Strong Motion Instrumentation Program, accelerographs had been installed in the Taitung Fire Bureau Building by the Central Weather Bureau. The strong motion records, damage records and material test data are considered as important references in the detail evaluation of the building. In this paper, the detailed damage records, concrete compression test and steel tensile strength test were carried out. Besides, the seismic motion records such as 921, 1022 and 0401 earthquakes were also introduced in the manuscript.

Keywords: 0401 earthquake, Taitung Fire Bureau Building, earthquake exploration, seismic motion record

Introduction

The 0401 earthquake measured 7.3 on Richter scale and the epicenter was located 7.2 kilometers near Taitung city occurred at 16:01 PM of April 1, 2006. NCREE researchers left for Taitung area to investigate the building's damage after the earthquake. Most of the injured people are living in Taitung city. On the other hand, some buildings have slight damages except to the Taitung Fire Bureau Building.

Under the Taiwan Strong Motion Instrumentation Program (Wen, 1998), accelerographs had been installed in strategic locations of the Taitung Fire Bureau Building by the Central Weather Bureau. The earthquake records including 921 Chi-Chi earthquake and other strong earthquakes were collected periodically. This building has been damaged severely

by the Taitung earthquake. At the same time, the time-history responses of main and after shocks were stored using the accelerographs. The obtained seismic records can be considered as an in situ test result of a real earthquake. In this paper, the detailed damage records, concrete compression test and steel tensile strength test were carried out. The strong motion records, damage records and material test data were considered as important references in the detail evaluation of the Fire Bureau Building.

Description and Damage Record of 0401 Earthquake

The 0401 earthquake measured 7.3 on Richter scale and the epicenter was located 7.2 kilometers north of the Beinan Mountain near Taitung city at

¹ Research Fellow, National Center for Research on Earthquake Engineering, ykyeh@ncree.org

² Assistant Research Fellow, National Center for Research on Earthquake Engineering, wcshen@ncree.org

³ Associate Professor, Dahan Institute of Technology, jwc@ms01.dahan.edu.tw

⁴ Associate Professor, National Taitung University, wcwang@nttu.edu.tw

around 16:01 PM, April 1, 2006. The emergency response was carried out in NCREE. During the seismic event, not only the Taitung Fire Bureau Building has been damaged but also other pertinent buildings in Kaohsiung city. From the earthquake reconnaissance, most of the losses were due to the damage of buildings. Statistics revealed that there were some casualties (NCREE and NCDR, 2006) after the event.

The damages of the Taitung Fire Bureau Building were discovered in every location inside the building such as supply room, duty room and staircase. Besides, some cracks were obvious in the partition walls. The damage states of columns in the first floor were depicted by Prof. Wang of Taitung University. A part of the crack pattern is shown in the Figure 1.

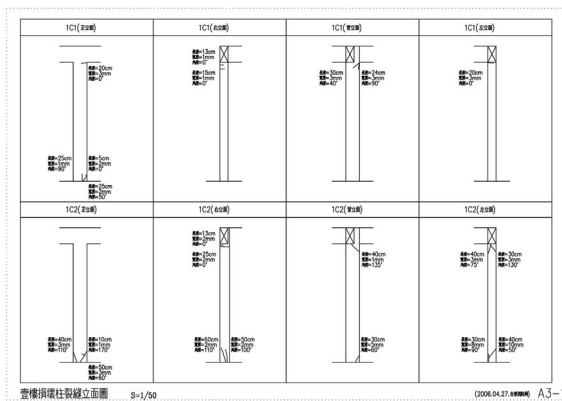


Figure 1 Sketch of crack damage columns in first storey

Sampling of Concrete and Reinforcement

In order to investigate the material parameters in the building, 50 concrete cylinders and 27 reinforcement bar samples were tested. The length of all reinforcement samples was reduced to 60 centimeters before the material test. Two indentations with a distance about 20 centimeters were struck to set up the strain gauge. The material testing machine was adopted to test the mechanical properties of the sampled reinforcements. The yield load and maximum load were recorded during the test. The concrete cylinders were extracted from columns. Before testing, the diameters of the samples were modified to two times diameter high. Gypsum was used to flat the surface of the concrete cylinders. The material test was conducted by material testing machine. The maximum load was obtained after the test.

Records of Three Earthquakes

Twenty-two strong-motion instruments were installed at each floor of the Taitung Fire Bureau Building to measure and gather seismic data. The allocation of these instruments is listed in Table 1. The measured signals shown in this paper consist of 921 Chi-Chi earthquake, 1022 Chiayi earthquake and 0401 Taitung earthquake.

Table 1 Allocation of strong-motion instruments

Item	Direction	Location
CH01	X	Free Field, near Back Door
CH02	Y	Free Field, near Back Door
CH03	Z	Free Field, near Back Door
CH04	X	Above the B1 Floor Slab near Stairway
CH05	Y	Above the B1 Floor Slab near Stairway
CH06	Z	Above the B1 Floor Slab near Stairway
CH07	X	Under the First Floor Slab
CH08	Y	Under the First Floor Slab
CH09	X	Above the First Floor Slab near Column
CH10	Y	Above the First Floor Slab near Column
CH11	Z	Above the First Floor Slab near Stairway
CH12	X	Under the Second Floor Slab near Stairway
CH13	Y	Under the Second Floor Slab near Stairway
CH14	X	Under the Second Floor Slab near Column
CH15	Y	Under the Second Floor Slab near Column
CH16	X	Under the Roof Floor Slab (at Office faced Back Door)
CH17	Y	Under the Roof Floor Slab (at Office faced Back Door)
CH18	Z	Under the Roof Floor Slab (at Office faced Back Door)
CH19	X	Under the Roof Floor Slab (at Meeting Room)
CH20	Y	Under the Roof Floor Slab (at Meeting Room)
CH21	Z	Under the Roof Floor Slab (at Meeting Room)
CH22	Z	Under the Roof Floor Slab (at Balcony)

Through the seismic response signals collected in the 921 Chi-Chi earthquake, it has been estimated that the duration of the earthquake is 103.7 seconds with an interval of 0.005. Table 2 shows the maximum acceleration measured by each instrument. The maximum peak ground acceleration in the 921 Chi-Chi earthquake is 21.51 gal measured by Channel 02. Figure 2 shows the plot of time history in the free field. The maximum sum of squares of acceleration is $1.19 \times 10^6 \text{ gal}^2$ measured by Channel 19 in the x-direction at the roof level. The plot of time history of Channel 19 is shown in Figure 3.

Table 2 Max acceleration (unit: gal)

		921	1022	0401
X-direction (B1)	CH04	18.89	4.71	165.48
Y-direction (B1)	CH05	Bad Data		
Z-direction (B1)	CH06	10.99	2.33	230.85
X-direction (1F)	CH01	18.59	4.98	211.92
	CH07	19.57	5.19	176.99
	CH09	19.39	5.04	210.22
Y-direction (1F)	CH02	21.51	4.36	382.49
	CH08	21.79	4.14	365.40
	CH10	21.90	5.08	375.78
Z-direction (1F)	CH03	10.84	2.45	126.18
	CH11	14.38	2.53	206.59
X-direction (2F)	CH12	28.10	8.87	196.13
	CH14	29.35	13.57	313.85
Y-direction (2F)	CH13	Bad Data		
	CH15	23.32	5.85	401.24
X-direction (RF)	CH16	33.73	13.13	289.09
	CH19	37.48	15.95	357.98
Y-direction (RF)	CH17	32.22	9.55	520.34
	CH20	25.91	8.22	506.69
Z-direction (RF)	CH18	11.60	2.56	151.10
	CH21	11.76	3.01	219.66
	CH22	15.55	3.50	221.18

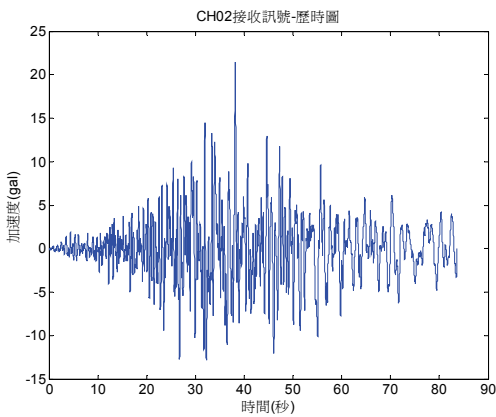


Figure 2 Plot of time-history in the free field (921 Chi-Chi earthquake)

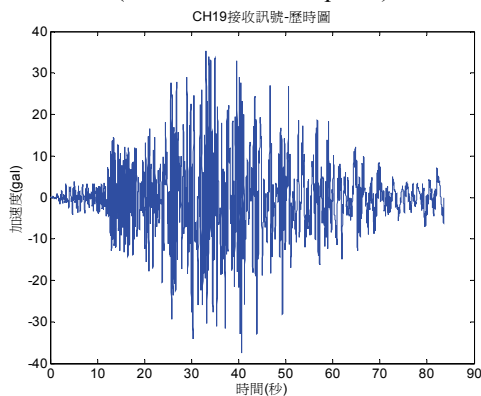


Figure 3 Plot of time-history of channel 19 (921 Chi-Chi earthquake)

Through the seismic response signals collected in 1022 Chiayi earthquake, the duration of the earthquake was found to be 62.75 seconds with an interval of 0.005. The maximum peak ground acceleration is 4.98 gal measured by Channel 01. Figure 4 shows the plot of time history in the free field. The maximum sum of squares of acceleration is $8.07 \times 10^4 \text{ gal}^2$ measured by Channel 19 in the x-direction at the roof level. The plot of time history of Channel 19 is shown in Figure 5.

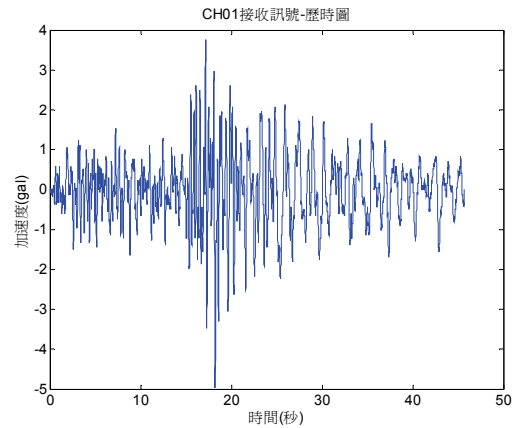


Figure 4 Plot of time-history in the free field (1022 Chiayi earthquake)

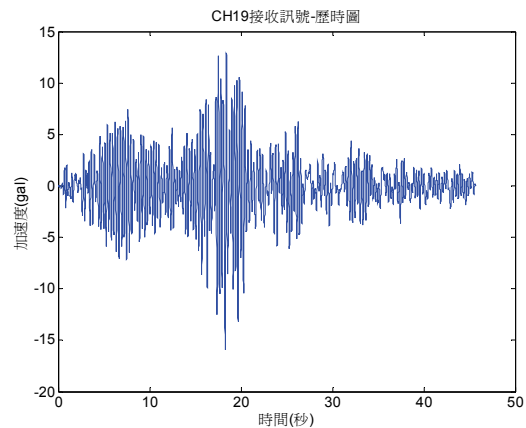


Figure 5 Plot of time-history of channel 19 (1022 Chiayi earthquake)

From the seismic response signals collected in 0401 Taitung earthquake, the duration of the earthquake was calculated at 103.7 seconds with an interval of 0.005. The maximum peak ground acceleration is 382.49 gal measured by Channel 02 in the y-direction located in the first floor. Figure 6 shows the plot of time history in the free field. The maximum sum of squares of acceleration is $2.97 \times 10^7 \text{ gal}^2$ measured by Channel 19 in the x-direction at the roof level. The plot of time history of Channel 19 is shown in Figure 7. It can be observed that the values of seismic data measured in 0401 Taitung earthquake are much bigger than the other two earthquakes.

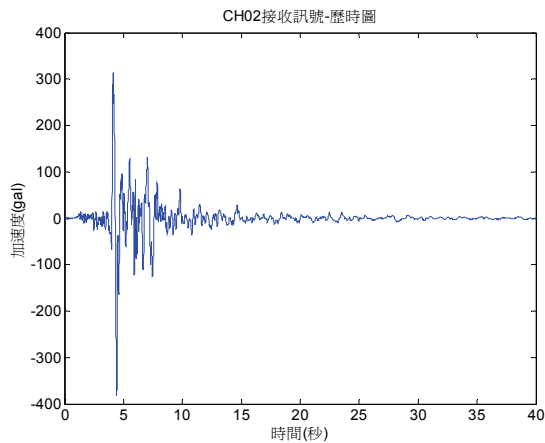


Figure 6 Plot of time-history in the free field (0401 Taitung earthquake)

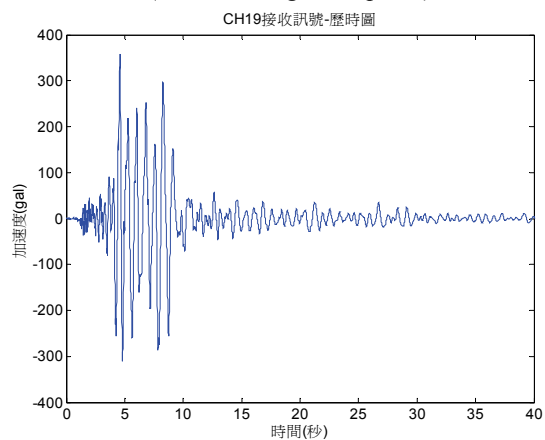


Figure 7 Plot of time-history of channel 19 (0401 Taitung earthquake)

From the recorded maximum peak ground acceleration seismic data measured in 0401 Taitung earthquake are much bigger than the other two earthquakes. The maximum peak ground accelerations in each direction are bigger than 150 gal. The 0401 Taitung earthquake, indeed, has caused significant damages of buildings and vital lines in Taitung area, including the Taitung Fire Bureau Building. This building was confronted to demolish finally.

Conclusions

The Taitung Fire Bureau Building has been seriously damaged and demolished after the 0401 Taitung earthquake. Under the Taiwan Strong Motion Instrumentation Program, the accelerographs were installed in the said building by the Central Weather Bureau. The seismic response of the 0401 Taitung earthquake was recorded completely by the installed instruments. Not only the material properties but also the damage states of structural elements (i.e. columns) were introduced in the study. Moreover the results are important for researchers to understand the response and the damage mechanism of a building during a strong earthquake.

References

- Wen, K. L., Liu, L. F., Chiu, S. J. and Chen, K. C. (1998), "Detection of free field strong motion instrumentation and structure monitoring system in Taipei and Yilan area," CWB Report, Vol. 21. (In Chinese)
- NCREE and NCDR (2006), "Reconnaissance report on earthquake in Taitung on April 1, 2006," NCREE Report, NCREE-06-006. (In Chinese)

Progressive Collapse of Reinforced Concrete Buildings during Earthquakes

S. Yavari¹, S.H. Lin², K.J. Elwood³, C.L. Wu⁴, P.W. Weng⁴, S.J. Hwang⁵

Abstract

In order to observe the interaction of structural elements at the onset of collapse, six frame specimens were planned to be tested at the National Center for Research on Earthquake Engineering (NCREE), Taiwan in 2008 and 2009. Each specimen is made of a half-scale model of a two-bay two-storey reinforced concrete frame. The specimens were tested under high and low gravity loads to investigate the influence of axial loads on the collapse vulnerability of the structures. The same tests will also be employed to study the interaction of the beams, columns and joints as collapse is initiated. After the conduct of shaking table tests, the results of analytical models were compared to the experimental data. This comparison illustrated the limitations, weaknesses, and strengths of available analytical models. Such studies will lead to a better prediction of the behavior of existing reinforced concrete structures, and consequently, more cost-effective retrofit strategies.

Keywords: collapse, shaking table tests, non-ductile concrete frames, concrete columns, concrete beam-column joints, shear and axial failure

Introduction

A recent study has concluded that in a repeat of the devastating 1906 San Francisco earthquake, the largest number of casualties will occur from concrete buildings (Kircher et al., 2006). Similar results have been observed after earthquakes in Turkey and Taiwan and can be expected for other countries facing significant seismic hazards. But not all concrete buildings pose a threat to life and safety. Typically, building owners are frustrated with the high costs of retrofitting large inventories of existing buildings, while engineers struggle to identify the vulnerable buildings that are likely to collapse in future earthquakes. Indeed, researches are needed to help engineers and building owners faced with the challenging task of reducing the seismic risks of existing structures especially in urban areas (NRC, 2004).

Based from earthquake reconnaissance worldwide, strong earthquakes can result to a wide range of damage in older concrete buildings ranging from minor cracking to collapse (Otani, 1999).

Current guidelines on the seismic assessment of existing concrete buildings are not sufficiently refined to enable engineers to distinguish between buildings which are expected to collapse and those that may only sustain minor damage. This lack of refinement, and the inherent conservatism in the guidelines, has resulted in nearly all older concrete buildings being considered collapse hazards during earthquakes. However, this result is not reasonable enough considering the extensive building infrastructure constructed prior to the introduction of seismic provisions in modern building codes in the mid-1970's and the limited funds available for seismic retrofit. A modest investment in earthquake engineering research can result to a significant improvement in the assessment of existing buildings by providing the appropriate tools to understand the complex nonlinear behavior of structural systems during seismic events. In particular, given an understanding of the mechanisms leading to the progressive collapse of older concrete buildings, appropriate public policy measures can be initiated to mitigate the risk of multiple building collapses

¹ M.Sc. Candidate, Dept. of Civil Engineering, National Taiwan University, Taipei, Taiwan

² PhD Candidate, Dept. of Civil Engineering, University of British Columbia, Vancouver, Canada

³ Associate Professor, Dept. of Civil Engineering, University of British Columbia, Vancouver, Canada

⁴ Associate Research Fellow, National Center for Research on Earthquake Engineering, Taipei, Taiwan

⁵ Professor, Dept. of Civil Engineering, National Taiwan University, Taipei, Taiwan

during a major earthquake and provide the maximum possible earthquake resilience in communities considering the limited resources available for infrastructure renewal.

The following sections describe a research project that directly addresses the significant life-safety risk facing millions of people living and working in existing concrete buildings of Taiwan and worldwide. The research will be conducted in collaboration with researchers from Canada and the United States, hence enables to leverage knowledge gained through international research programs.

Significance of the project

The current project is part of a large research project entitled, “*Seismic Upgrading of Existing Concrete Buildings*” at NCREE Taiwan. The focus of the current work is a series of a shaking table tests to investigate the complex mechanisms that lead to the collapse of concrete frame buildings during severe earthquakes. Shaking table studies provide the most accurate means of assessing the performance of structures when subjected to earthquakes.

Other participants in this NCREE project include the University of British Columbia, Canada and the Network for Earthquake Engineering Simulation (NEES) in the United States. Currently, NEES has a project which includes large-scale testing of existing concrete building components, soil-structure interaction studies, collapse modeling, and regional simulations, all geared toward identifying seismically hazardous older concrete buildings and promoting effective mitigation strategies. The NEES project, however, does not include shaking table tests, but instead relies upon international collaboration among the University of British Columbia, Canada and NCREE to provide the critical data. The overall objective of the NCREE-UBC-NEES collaboration is to provide engineers, building owners and policy makers with tools to mitigate effectively the significant life-safety risks posed by the collapse of concrete buildings during future earthquakes. This important objective can only be achieved through the close collaboration of many participants each undertaking complimentary tasks with specific expected outcomes. The expected outcome of the research proposed herein is to provide benchmark data for the development and refinement of numerical models used in the assessment of existing concrete buildings. The benchmark data from the proposed shaking table tests will be provided to all participants in the UBC-NCREE-NEES collaborative project. Refinement of the numerical models will allow for more accurate predictions of collapse potential in concrete buildings and enable engineers to identify the highly dangerous structures in need of immediate rehabilitation.

Project background and description

The collapse of a reinforced concrete frame during an earthquake can be caused by failure of beams, columns, or beam-column joints. Older gravity-based design methods resulted in a system of weak columns and strong beams, and therefore, most building frames designed using such methods are expected to experience failure of columns or joints. To date, there have been relatively few tests on lightly-confined reinforced concrete frame systems that are found in the literature and rarely been conducted dynamically to collapse. None of these tests investigated the effects of high axial load on the failure of non-ductile columns. In an attempt to provide the needed information, this study involves dynamic testing to collapse of six two-dimensional, two-bay, two-story, and half-scale reinforced concrete frames. Each frame contains non-seismically detailed columns whose proportions and reinforcement details allow them to yield in flexure prior to shear strength degradation and ultimately reach axial collapse (these columns are commonly referred to as flexure-shear-critical columns). The influence of non-confined joints on the collapse behavior of the frame was also investigated.

The NCREE shaking table tests planned for 2008-2009 will provide critical data to validate and improve numerical models on the assessment of the collapse vulnerability of concrete frame buildings, and, in turn, allow for the refinement of guidelines used for seismic assessment both in Canada and abroad. In particular, the NCREE tests will focus on two previously unexplored issues: (1) the interaction of multiple vulnerable concrete components (i.e. beams, columns and joints) within a building frame as collapse is initiated, and (2) the influence of high gravity loads on the collapse vulnerability of a structure. Past shaking table collapse tests have focused on the performance of one specific component (i.e. columns) and only considered low to moderate gravity loads, however this simplifies the building response to such an extent that the results from these tests may not be representative of the true collapse behavior of real concrete frame buildings

Figure 1 describes the types of shaking table specimens to be tested. Comparison of the results from MCFS and HCFS will reveal the influence of axial load on shear and axial behavior of flexure-shear-critical columns, while observations from MUF and MUFS will demonstrate the effects of unconfined joints on overall behavior of the frame near the point of collapse and sequence of failure in the elements. Details of the specimens are described in the following section. Two MCFS and Two HCFS specimens were tested, while one MUFS and one MUF specimens will be tested.

Specimen MCFS: <u>M</u> oderate Axial Load <u>C</u> nfinied Joints <u>F</u> lexure- <u>S</u> hear Columns	Specimen HCFS: <u>H</u> igh Axial Load <u>C</u> nfinied Joints <u>F</u> lexure- <u>S</u> hear Columns
Specimen MUFS: <u>M</u> oderate Axial Load <u>U</u> nconfined Joints <u>F</u> lexure- <u>S</u> hear Columns	Specimen MUF: <u>M</u> oderate Axial Load <u>U</u> nconfined Joints <u>F</u> lexure Columns

Fig. 1. Description of shaking table specimens

Specimens and Test Setup:

Figure 2 shows the dimensions of the two-dimensional concrete frame to be tested at NCREE. The geometries and details were selected to be representative of elements used in a seven-story frame building. Final dimensions and reinforcement details of the frames were influenced by the following considerations: laboratory and shaking table limitations, replication of column details used in existing buildings, desired failure mode, and cost. In the six specimens designed, four has been constructed in the fall season of 2008 and two will be constructed in winter of 2009. The target failure mode was intended to be damage leading to collapse that would enable examination of gravity load redistribution during the test. The column details and loadings were chosen to be typical of 1960s and 1970s hospital building construction, with widely spaced ties formed with 90° hooks. The ratio of beam stiffness to column stiffness was considered to be similar to existing buildings. Since the overall width of the frame, and consequently the beam length, were limited by the dimensions of the shaking table, the beam depth was adjusted to achieve the target beam-to-column stiffness ratio. Beam transverse reinforcement with closed stirrups and 135° hooks provide sufficient shear strength to develop full flexural strength, while longitudinal reinforcement was chosen to create a weak-column-strong-beam mechanism typical of the older concrete construction scheme. Neither beams nor columns have lap splices to eliminate the splicing effects from the scope of this study. Slabs were casted with the beams to include the effect of slabs on the beam stiffness and the joint demands.

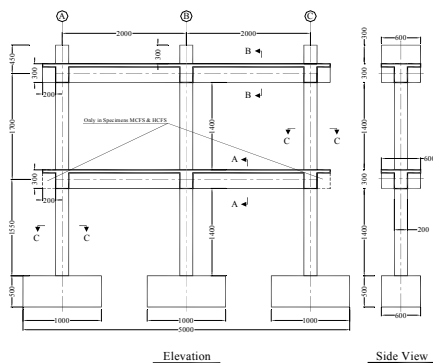


Fig. 2. Shaking table test specimen

As shown in Figure 3, to account for the seven-story building, post-tensioning will be used to achieve high axial loads on the columns marked by red rectangular. A lumped mass, marked by red circle, will be placed on the rollers of the shaking table and have those connected to the top of the specimen --- an innovative approach which will enable the demands from upper stories to be captured while ensuring the structure can be tested safely up to the collapse limit state.

A stiff steel frame bolted to the table was used to brace the specimens in the out-of-plane direction by means of frictionless rollers at each beam level which allow free in-plane motion (both horizontal and vertical) of the frame. Rigid transverse steel beams were connected to the supporting frame to catch the specimen after collapse and prevent or minimize any damage to the shaking table.

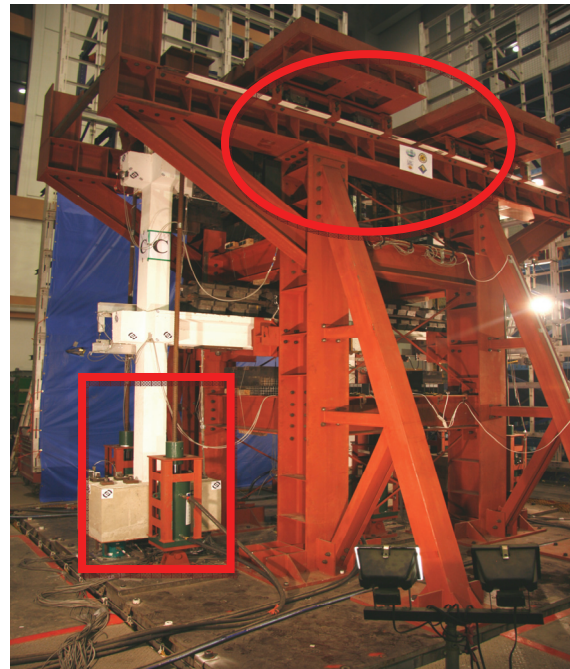


Fig. 3. Specimen, Steel Supporting Frame and Mass system

Specimen instrumentation includes: 1) force transducers (or load cells) that measured shear, axial load, and bending moments at the base of the frame footings; 2) strain gauges on longitudinal and transverse reinforcement of columns, beams and joints; 3) accelerometers for horizontal and vertical accelerations; and 4) displacement transducers to measure both local column and global frame deformations. Figure 4 shows the instrumentation used for the measurement of exterior joint deformations in the experimental test last December 2008.

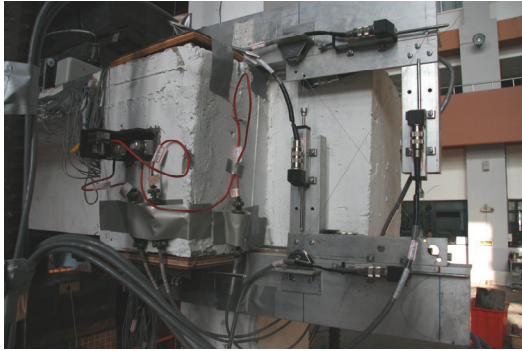


Fig. 4. Instruments for measuring the joint deformations

Experimental Test

The first experimental test in the series of planned tests described earlier was performed in December 2008. The specimen had some imperfections from the construction phase. The second story had about 1% out-of-plane drift that caused some difficulties regarding the top mass system.

The first shaking table experiment was basically a test to observe the performance of so many innovative elements employed for the series of the tests, including the hydraulic jacks for pre-stressing of axial load system, top inertia mass system, local instrumentation of the columns and joints, rotational hinges at the connecting point of inertia mass system to the specimen, etc. The specimen was first subjected to a white noise to obtain its natural period and followed by a scaled table motion selected from Chi-Chi earthquake records. Most of the above-mentioned components performed very well during the test. However, the rotational hinges could not transfer the lateral dynamic force from the top inertia mass system to the specimen because they could not be tightened up fully. Therefore, the specimen did not collapse during the predicted scale of table motion. Furthermore, a system was considered to prevent the rocking of the top inertia mass; however, some rocking of the mass was also observed. Increasing the scale of the PGA of the table motion finally caused the second story of the frame to collapse. Figure 5 shows the shear failure followed by the axial failure of column A in the second floor.

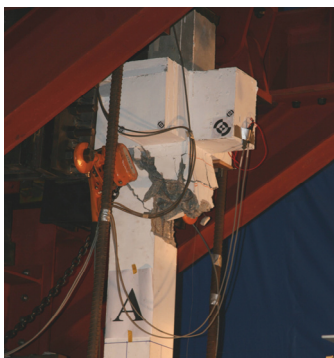


Fig. 5. Failure of column A at second floor

It was observed that although the details of columns A, B and C were identical, columns A and B were severely damaged during the test, while column C experienced flexural deformations and minor shear cracks (figure 6) only.



Fig. 6 Failure of the frame during the test

Conclusions

Six reinforced concrete frames were designed to be tested at the National Center for Research on Earthquake Engineering (NCREE) in 2008 and 2009. The results of the tests are expected to shed light on the effects of high axial load on lateral and axial behavior of flexure-shear-critical columns, the behavior of unconfined joints, and the overall behavior of non-ductile concrete frames which are tested up to the point of collapse. Details of the specimens and setup of the tests were described. Comparison of the results from the analyses with the result from the shaking table tests will reveal the accuracy of the existing analytical models leading to refinement of the models and more accurate prediction of the behavior of flexure-shear-critical frames in future earthquakes.

References

Kircher, C.A., Seligson, H.A., Bouabid, J., and Morrow, G.C. (2006) "When the Big One Hits Again - Estimated Losses due to a Repeat of the 1906 San Francisco Earthquake," *Earthquake Spectra*, Vol. 22, No. S2, pp. S297-S339.

National Research Council, (2004) "Preventing Earthquake Disasters: The Grand Challenge in Earthquake Engineering – A Research Agenda for the Network for Earthquake Engineering Simulation (NEES)," Committee to Develop a Long-Term Research Agenda for the Network of Earthquake Engineering Simulation (NEES), The National Academy of Science Press, Washington, D.C., <http://www.nap.edu/catalog/10799.html>.

Otani, S. (1999), "RC Building Damage Statistics and SDF Response with Design Seismic Forces," *Earthquake Spectra*, Earthquake Engineering Research Institute, Vol. 15, No. 3, pp. 485 - 501.

Study on Seismic Performance Curves of Reinforced Concrete Columns Failed in Shear

Yi-Ton Hwang¹ and Shyh-Jiann Hwang²

黃益堂¹、黃世建²

Abstract

During the 921 Chi-Chi Earthquake, a lot of reinforced concrete buildings failed in shear condition. Shear failure is brittle and therefore should be avoided. In order to provide ventilation, mounting of air conditioner, door frame, etc. most often extreme-short columns are encountered. These columns will be the weakest elements due to its small lateral displacement. Thus, this research is aimed to study the seismic resistant behavior of extreme-short columns under constant axial force through observation in laboratory experiments and analysis.

There are several important variables which can affect the strength and behaviour of extreme-short columns, i.e. aspect ratio, axial load magnitude, and stirrup detailing. Eight specimens were tested under double curvature and constant axial load by repeating loading test to observe their behaviour under shear and axial failure. Test results show that under different magnitude of axial load, the collapse behaviour will be different in a sense that higher axial load can accelerate the failure mechanism. Columns with transverse reinforcement using ductile detailing can resist higher lateral force and lateral displacement capability.

Keywords: extreme-short columns, brittle failure, double curvature

Introduction

During 1999 Chi-Chi Earthquake in Taiwan, column failure was found to be the major damage among reinforced concrete (RC) buildings, especially low-rise RC school buildings. In order to provide ventilation, mounting of air conditioner, door frame, etc., most often extreme-short columns are encountered, thus these columns became the weakest elements in the structure due to their small lateral displacement. However, it has been noted that the columns still possess gravity load-carrying capacity even if they have been failed by shear. Therefore, this study focuses on the understanding of the post-strength behavior of extreme-short columns after shear failure.

From the gathered data during the Chi-Chi earthquake, it has been found that low-rise RC school buildings collapsed due to the failure of the columns in the first story. The collapse of low-rise RC school buildings results from the lost of the gravity load-carrying capacity of columns. In order to

understand the seismic behavior of low-rise RC school buildings, failure modes of extreme-short columns subjected to the horizontal and vertical loads should be determined. In this research, three different parameters of extreme-short columns were varied in the tests conducted, such as height-to-width ratio, the amount of transverse steel, and axial load ratio.

Experimental Program

The experimental program consists of eight tests under cyclic lateral and vertical load. Column parameters such as height-to-width ratio, ductile or non-ductile detailing, and axial load ratio were varied. The specimens were separated into four types and every type has two specimens. These two specimens are subjected to low axial load ($0.1f'_cA_g$, where f'_c = designed concrete compressive strength and A_g = gross cross-sectional area) and high axial load ($0.3f'_cA_g$) separately. The first type is the non-ductile shorter columns shown in Fig. 1. The second is the

¹ Master, Department of Civil Engineering, National Taiwan University, coldboy1941@hotmail.com.

² Professor, Department of Civil Engineering, National Taiwan University; also serves as Division Head, National Center for Research on Earthquake Engineering, sjhwang@ncree.gov.tw

ductile shorter columns shown in Fig. 2. The third is the non-ductile longer columns shown in Fig. 3. The fourth is the ductile longer columns shown in Fig. 4. In order to show the details of the specimens, L and H represent low axial load ($0.1f'_cA_g$) and high axial load ($0.3f'_cA_g$), respectively, D and N represent ductile detailing and non-ductile detailing, respectively, and 3 and 4 represent the height-to-width ratio, and 3 and 4 represent the height-to-width ratio. The height of the columns is 50 cm and 100 cm since the columns have a cross section of 30×50 cm. The specified concrete compressive strength was 3000 psi at 28 days. Mean concrete strengths obtained from standard compression tests on 152×305 mm cylinders on the day of column testing ranged from 6228 to 6813 psi. Mean yield and ultimate strengths of the 25.4-mm diameter (No.7) deformed longitudinal bars were 63 ksi and 93 ksi, respectively. Mean yield and ultimate strengths of the 9.5 mm-diameter (No.3) deformed longitudinal bars were 66 ksi and 100 ksi, respectively. The axial load of the specimens L and H is 63.75 tf and 191.25 tf, respectively.

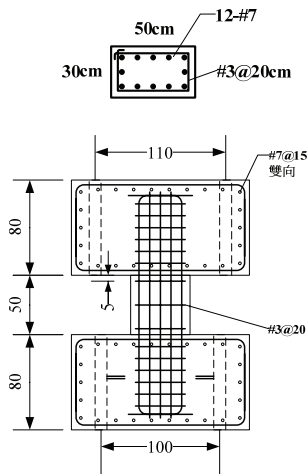


Fig. 1 The detail of nonductile short ercolumns

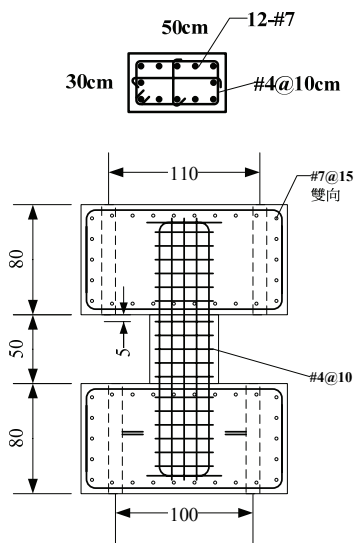


Fig. 2 The detail of ductile shorter columns

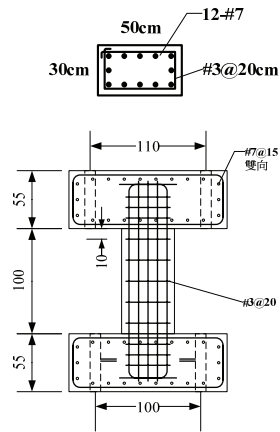


Fig. 3 The detail of nonductile longer columns

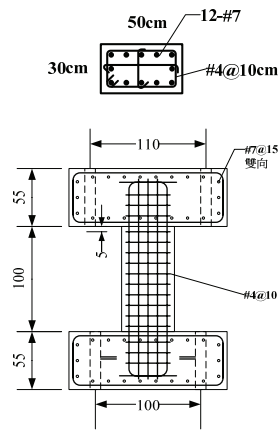


Fig. 4 The detail of ductile longer columns

The test setup was designed to restrain the test columns against lateral movement. Fig. 5 shows the test setup. Fig. 6 depicts the loading history consisted of the following lateral drift cycles: three cycles each at 0.25%, 0.5%, 0.75%, 1%, 1.5%, 2%, 3%, 4%, 5%, 6%, and until to collapse. The loading systems consist of four actuators are shown in Fig. 7. The horizontal actuator 1 is the displacement control. The horizontal actuator 2 follows the strength of the actuator 1. The displacement of the vertical actuator 3 is equal to actuator 4 ($\Delta_3 = \Delta_4$). The axial load applied on the specimen is the resultant of the vertical actuator 3 and 4 ($P_3 + P_4 = 0.1f'_cA_g$ or $0.3f'_cA_g$). This kind of loading systems has been chosen to make sure that the test column will have a double curvature deformation.



Fig. 5 Test setup

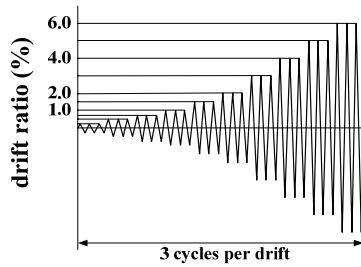


Fig. 6 Loading history

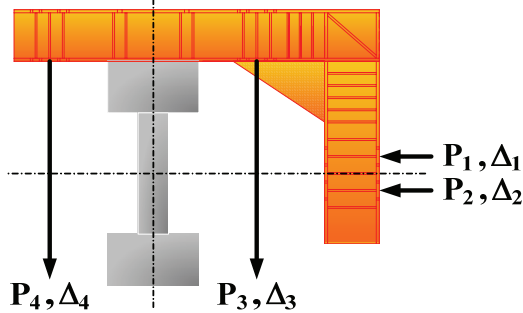


Fig. 7 Actuator control

Experimental Results

According to the crack patterns shown in Fig. 8, it has been observed that not only a lot of diagonal cracks were found after the specimens reached their maximum strength but also vertical cracks especially for ductile detailing columns. From Fig. 8, it is noted that the inclined angle of the principal cracks with respect to the horizontal axis is larger when the axial load applied on the specimens is higher. Figs. 9 to 12 show the test results containing the peak point of the test data and the observed failure modes. It can be stated that the failure mode of the extreme-short columns is the shear failure because of the diagonal crack patterns on the specimens. However, it has been noted that there is another failure mode of the short columns--- the vertical bond splitting along the column longitudinal bars.

Figures 9 to 12 depict the load-displacement hysteretic relationship of the specimens. It can be seen that the maximum strength of the specimens did not reach the flexural strength. The nominal flexural strength (M_n) of the test columns in Figs. 9 to 12 were calculated according to ACI Committee 318-05. Therefore, it can be confirmed that all the tested short columns were failed by shear. According to the hysteretic loop from tests, it can be concluded that the displacement of the non-ductile detailing specimens at the ultimate strength is lower than the ductile detailing specimens, and that the displacement of the specimens with high axial load is also higher than those of low axial load.

Some empirical equations to predict the drift ratio of the flexural shear failure (Elwood and Moehle, 2005a) and the drift ratio of the axial failure (Elwood

and Moehle, 2005b) are available. Some of these findings were incorporated into the ASCE 41 (2007). Figures 9 to 12 show the prediction of strength and displacement by the ASCE 41 (2007) and the envelope of the test results. According to the ASCE 41 (2007) the 2DL specimen has been failed by flexural-shear failure and the others are by shear failure. This observation is different from the test observation because all specimens were found to have been failed by shear failure. Also, the post-strength behavior predicted by the ASCE 41 (2007) is too conservative. The predicted displacement at the ultimate strength and at failure is much smaller than test data. Therefore, the prediction of the ASCE 41 (2007) is too stiff prior to strength and too conservative to post strength.

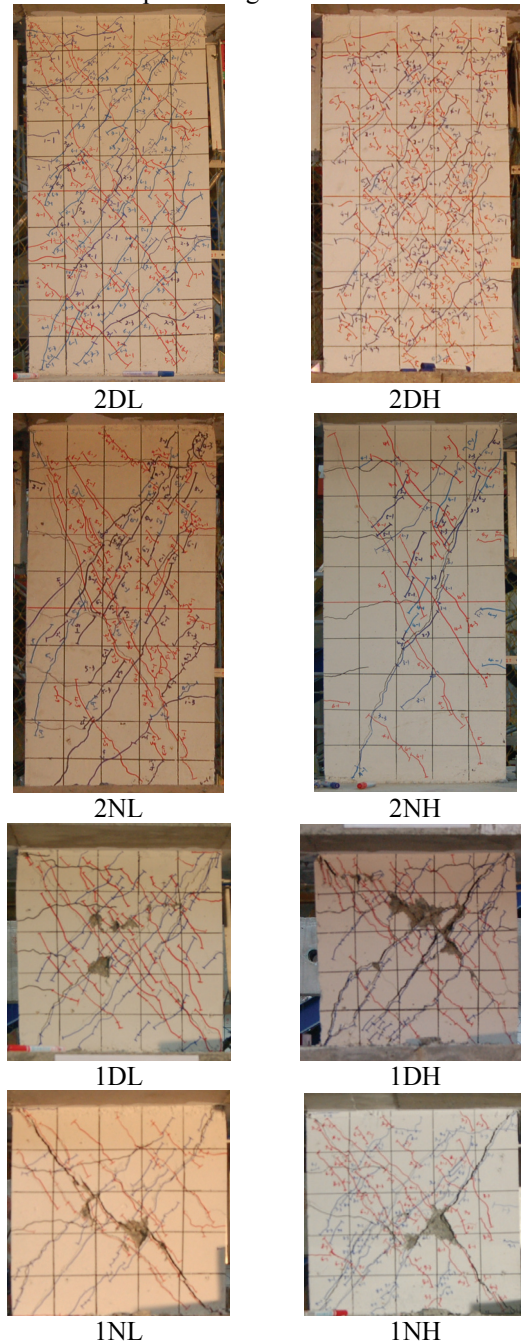


Fig. 8 crack patterns of specimens

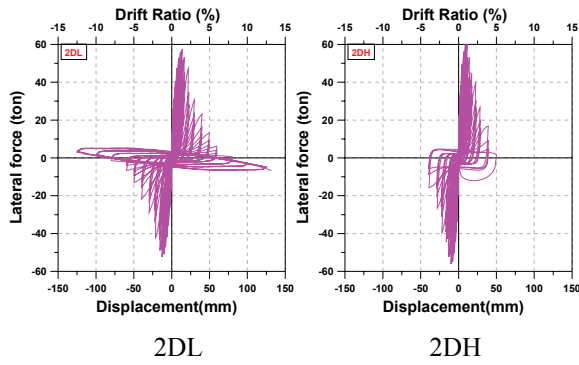


Fig. 9 Hysteretic loop of ductile longer columns

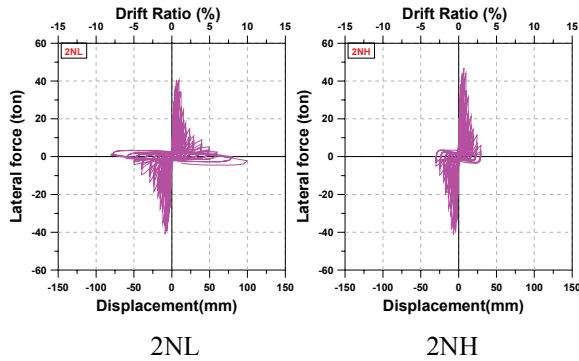


Fig. 10 Hysteretic loop of nonductile longer columns

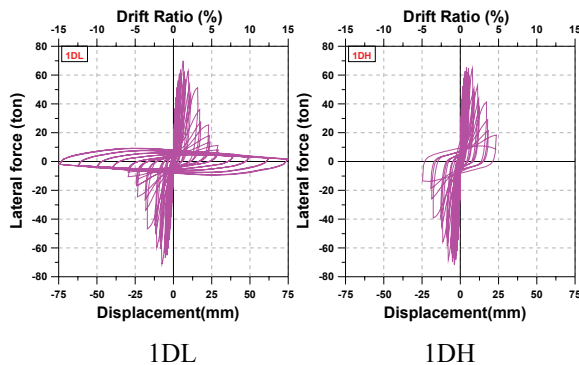


Fig. 11 Hysteretic loop of ductile shorter columns

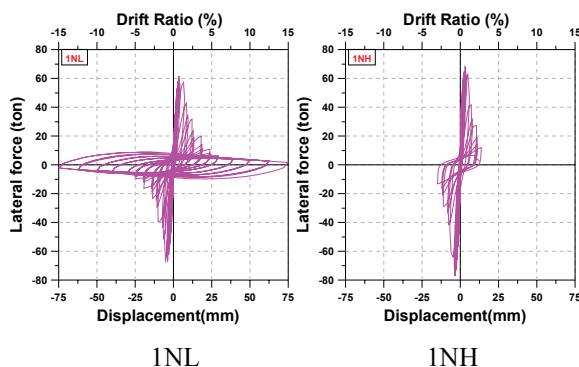


Fig. 12 Hysteretic loop of nonductile shorter columns

Conclusions

According to the test result, it can be observed that the failure mode of the tested short columns is shear failure. Besides, it has been found that the bond splitting is another failure mechanism involved with the short columns. As test parameters were varied,

different behavior was observed. The inclined angle of the principal cracks with respect to the horizontal axis is larger when the axial load applied on the specimens is higher. The displacement of the non-ductile detailing specimens at the ultimate strength is lower than that of ductile detailing; and the displacement of the specimens with high axial load is also higher than that of low axial load.

The prediction of the ASCE 41 is too stiff prior to strength and too conservative to post-strength. More research works are needed.

References

- ACI Committee 318 (2005), "Building Code Requirements for Structural Concrete (ACI 318-05) and Commentary (ACI 318R-05)," American Concrete Institute, Farmington Hills.
- Elwood, K. J., and Moehle, J. P. (2005a), "Drift Capacity of Reinforced Concrete Column with Light Transverse Reinforcement," *Earthquake Spectra*, Vol. 21, No. 1, pp. 71-89.
- Elwood, K. J., and Moehle, J. P. (2005b), "Axial Capacity Model for Shear-Damaged Columns," *ACI Structural Journal*, Vol. 102, No. 4, pp. 578-587.
- Weng, P. W. (2007), "Study on the Seismic Performance Curves of Reinforced Concrete Short Columns Failed in Shear," Master Thesis, Department of Construction Engineering, National Taiwan University of Science and Technology, Taiwan. (in Chinese)
- ASCE/SEI 41 (2007), "Seismic Rehabilitation of Existing Building," American Society of Civil Engineering, Reston, Virginia.

Assessment of Current Pushover Analysis for Irregular Continuous Bridges

Hsiao-Hui Hung¹ Kuo-Chun Chang²

洪曉慧¹ 張國鎮²

Abstract

Pushover analysis provides a simple process in studying the nonlinear behavior of structures, thus, it has rapidly become popular for the seismic evaluation of bridges in recent years. Before its comprehensive application in the earthquake engineering community, it has been an urgent issue to clarify quantitatively the limitation of this method in order that the erroneous results that might be produced by the direct application of current procedure to all types of bridges can be prevented. Pushover analysis which originally developed for building structures has two inherent drawbacks: that it is restricted with a single-mode response, and that the lateral force distribution during pushover process is invariant. As such, the procedure can be reliably applied only to regular structures and it can not account for the variation of inertial force pattern after structure yields. Several researchers in the past few years have proposed some improved methods to overcome this problem. However, again, most of these refined procedures were aimed at solving problems related to building structures. Due to the intrinsic difference of seismic responses between building structures and bridge structures, further clarification of the circumstances under which these improved methods can produce reliable estimates for bridges in the practice is needed. This research attempts to specify the scope of applicability for current pushover analysis on multi-span continuous bridge structures. Also discussed are the contributions of higher modes for bridges with different degrees of irregularities.

Keywords: pushover analysis, higher modes, continuous bridges, adaptive pushover

Introduction

Recently, due to the impact of several disastrous earthquakes on the seismic performance of bridges in several different countries, engineers and researchers started to agree that a rational seismic evaluation and design of a bridge has to be based on its inelastic deformation. With an aim to enhance seismic performance of newly-designed bridges or to predict precisely the seismic capacity of existing bridges, the nonlinear behavior of bridge has to be calculated accurately. As such, displacement-based seismic evaluation and design has increasingly become the main stream. Presently, two most widely recognized displacement design and evaluation approaches, i.e., FEMA-273 and ATC-40, both need pushover analysis to obtain the controlled displacement. In addition, two widespread-used commercial engineering software

ETABS and SAP2000 both provide pushover analysis capacity. Therefore, because of the accessibility of these softwares, the simplicity of analysis and their ability to predict failure mechanism of structures, pushover analysis has become an essential analysis tool for seismic design and evaluation of bridges. However, the conventional single-mode pushover procedure provided by SAP2000 has its limitation. Single-mode pushover is performed by applying a monotonically increasing invariant lateral forces pattern on the structure until a pre-determined target displacement is reached. Both the distribution of lateral forces and the calculation of target displacement are all based on the assumptions that structural behavior is influenced predominately by its fundamental mode and the fundamental mode of structure remains the same even as the structure yields. Obviously, these two assumptions are not accurate for

¹ Associate Research Fellow, National Center for Research on Earthquake Engineering, hhung@ncree.org.tw

² Professor and Chairman, Department of Civil Engineering, National Taiwan University, kcchang@ncree.org.tw

irregular bridges where the higher modes are relatively important. In order to overcome this problem, various improved multi-mode pushover analyses were developed during the last few years. However, most were developed for building structures, and a widely-acceptable procedure is also not yet available. Thus, further investigation on the applicability of multi-mode pushover analysis to bridge is still needed.

In practice, pushover analysis has become a typical tool for engineers to evaluate the seismic performance of structures. Albeit there are still some concerns over the reliability of pushover analysis, its practical application continues. Therefore, in order to prevent this method being used erroneously, to establish a reasonable and generally acceptable analysis procedure is urgent. In this work, adopting the results of inelastic time history analysis as the benchmark, the applicability of conventional single-mode pushover analysis and multi-mode adaptive pushover analysis (Antoniou and Pinho, 2004) on continuous bridges with unequal pier heights was evaluated and compared. Some conclusions and suggestions were also made.

Pushover Procedure

As mentioned previously, the main objective of this study is to evaluate and compare the applicability of single-mode pushover analysis and multi-mode adaptive pushover analysis on continuous bridges. Thus, both procedures are introduced briefly in the following. The first step within pushover analysis is the computation of the pushover curve. For single-mode pushover, the structure is subjected to a monotonically increasing lateral force with an invariant spatial distribution, which is generally the fundamental modal load pattern, until a pre-determined target displacement is reached, then the pushover curve that records the relation between lateral displacement and total base shear can be obtained. At this stage, the major shortcoming of the single-mode pushover is that the influence of higher modes and the change of inertial force pattern after the pier yields are not taken into account. On the other hand, the multi-mode adaptive pushover redefines the applied load pattern which is determined from the instantaneous dynamic properties of the structure at each analysis step. As such, the effect of higher mode and the inertial force redistribution following yielding are both considered.

Pushover curve represents the relation between total base shear and displacement observed at a selected reference point. In order to compare structural capacity to design earthquake demand, the pushover curve for a MDOF system has to be converted to a capacity spectrum for an equivalent SDOF system. In literature, the capacity spectrum curve that relates the spectral acceleration $S_{a,k}$ to the spectral displacement $S_{d,k}$ can be obtained from the pushover curve ($V_{b,k}$ vs

$\Delta_{r,k}$) by the following equation:

$$S_{a,k} = \frac{V_{b,k}}{M_n^* g}, \quad S_{d,k} = \frac{\Delta_{r,k}}{\Gamma_n \times \phi_{rn}} \quad (1)$$

In which, $\Delta_{r,k}$ is the lateral displacement at reference point r , $V_{b,k}$ is the total base shear, and k represents the analysis step. M_n^* is the effective modal mass of the fundamental mode n , also referred to as the mass of the equivalent SDOF system, Γ_n is the modal participation factor of the fundamental mode n , ϕ_{rn} is the value of mode shape ϕ_n at the reference point r . As can be seen, the curve obtained from Eq. (1) depends strongly on the selection of the reference point r . Different choices of reference point will lead to different capacity spectrum curves, and in turn lead to different seismic evaluation results for the same structure. In reality, a more rational way for deriving capacity spectrum curve should consider the displacement contributions from all important nodes. Accordingly, the concept of system displacement and system mass (Kowalsky, 2002) was recommended in the current study to calculate the equivalent SDOF capacity curve,

$$S_{a,k} = \frac{V_{b,k}}{M_{sys,k} g}, \quad S_{d,k} = \Delta_{sys,k} \quad (2)$$

where $M_{sys,k}$ and $\Delta_{sys,k}$ is the effective system mass and equivalent system displacement at analysis step k , respectively,

$$M_{sys,k} = \frac{\sum_i m_i \Delta_{i,k}}{\Delta_{sys,k}}, \quad \Delta_{sys,k} = \frac{\sum_i m_i \Delta_{i,k}^2}{\sum_i m_i \Delta_{i,k}} \quad (3)$$

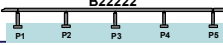
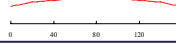
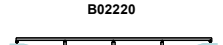
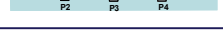
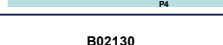
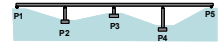
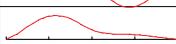
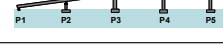
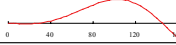
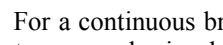
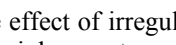
The estimation of system displacement $\Delta_{sys,k}$ is based on the assumption that work done by the original MDOF bridge and the equivalent SDOF structure is equal. The system effective mass $M_{sys,k}$ is similar to effective modal mass M_n^* , except that M_n^* only takes the fundamental mode shape in elastic state into account, whereas $M_{sys,k}$ is obtained from the instantaneous displacement profile of the structure at analysis step k . Thus, the value of $M_{sys,k}$ is not an invariant value as M_n^* does, but varies with the increase of time step. In Eq.(3), i represents every node of the structure that is regarded important, and m_i is the mass tributary to node i . For a bridge structure, the important node can be the deck nodes that are located immediately above piers.

Case Studies and Modeling

In order to identify the feasibility of the single-mode pushover analysis and the multi-mode adaptive pushover analysis for bridges, both pre-mentioned pushover procedures as well as inelastic dynamic analysis were performed on a set of continuous bridges with piers of different heights. By taking the results of inelastic dynamic analysis as reference values, the influence of higher modes on the accuracy of pushover analysis for irregular bridges can be identified. The bridge configurations

considered are listed in Table 1, which consists of five types of four-span continuous bridges with different pier heights. The length of each span is taken as 40m, the total length is 160m, and the superstructure weight is 15ton/m all throughout. The bearing systems are pinned support at the intermediate piers P2, P3 and P4, and roller supports at expansion joints P1 and P5. All piers are circular RC columns with a diameter of 2.5m and have the same design details of 74-32 ϕ longitudinal reinforcing bars, and were transversely reinforced with 19 ϕ hoop spaced at 8cm. However, the pier heights are varied to cover both regular and irregular bridges. These bridges are named as B22222, B02220, B22132, B02130 and B01234, in which each number represents the height of pier from P1 to P5. Numbers 1, 2, 3, 4 represent 5m, 10m, 15m and 20m, respectively, whereas 0 represents abutment.

Table 1 schematic representation of analysis bridges

Bridge Configurations	Modal Properties	Mode Shape for Transverse Mode
	Mode 1 T = 0.457 sec α = 89.07%	
	Mode 1 T = 0.411 sec α = 69.06%	
	Mode 1 T = 0.495 sec α = 21.61%	
	Mode 2 T = 0.167 sec α = 12.33%	
	Mode 1 T = 0.429 sec α = 53.32%	
	Mode 2 T = 0.269 sec α = 57.80%	
	Mode 1 T = 0.315 sec α = 22.25%	
	Mode 2 T = 0.925 sec α = 42.28%	
	Mode 2 T = 0.444 sec α = 19.18%	

For a continuous bridge, the effect of irregularity due to unequal pier heights mainly reacts on the transverse response. As a result, only the analysis along transverse direction is included. By a standard modal analysis, the transverse modal properties for each bridge type are also given in Table 1. In which, T is the vibration period, and α is the modal mass participation factor. As can be seen, Bridge B22222 represents a regular bridge because its modal mass participation factor of the first mode has already reached 89.07%. On the other hand, B02220, due to the constraint of the transverse movement at the abutments, only when the number of transverse modes considered is more than two, the bridge can have an accumulative modal mass participation factor over 80%. As for bridges B22132 and B02130, the first transverse modes for both are anti-symmetric modes with modal mass participation factors only around 20%, whereas the second modes with modal mass participation factors beyond 50% are the dominant ones. So, both can be classified as rather irregular bridge. The last type of bridge B01234 can also be considered irregular since its modal mass participation factor in the first mode is less than 50%.

Analyses in this current study, including nonlinear static pushover analysis and inelastic dynamic analysis, were carried out using the SeismoStruct (Seismosoft, 2007), which can be downloaded freely from the internet. Here, piers are modeled by nonlinear fiber elements, superstructures are simulated by elastic beam elements, and abutments are modeled by fixed boundary conditions. In order to obtain the plot of lateral displacements versus shear forces of bridge from elastic range into inelastic range of different levels, inelastic dynamic analysis is performed using incremental dynamic analysis (IDA), which involves a series of nonlinear time history analyses at increasing PGA. The input ground motions for the time history analyses are shown in Fig. 1, which includes two code-compatible design earthquake accelerations for Pouli in Nantou. Before the execution of IDA, each original input motion shown in Fig. 1 is multiplied by a series of intensity scaling factors S from 0.1 to 3.0 to be the actual input motion. Therefore, the earthquake intensities considered were within 0.1 to 3 times the design earthquake.

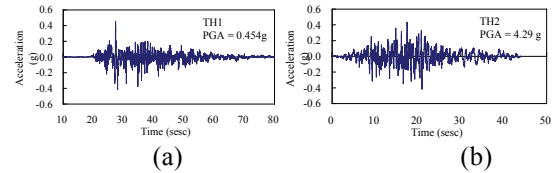


Fig. 1 input earthquake motions (a) TH1 ; (b)TH2

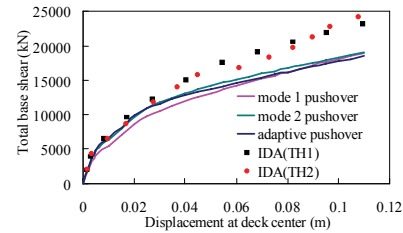


Fig. 2 Comparison of pushover curves

Analysis Results and Discussions

Two key factors in the pushover analysis procedure are the selection of lateral force pattern and of monitored points. The major influence of lateral force pattern is on the pushover curve, whereas that of monitored points is on the capacity spectrum. Accordingly, both the comparisons of pushover curves and capacity spectra calculated by different methods for different bridge types were investigated. However, due to the limit of space, only the results obtained from the most irregular one, i.e., B02130, were presented. The pushover curves obtained from various pushover procedures and IDA have been plotted in Fig. 2, where the total base shear is plotted with respect to the displacement at the mass center of the deck, i.e., the location of deck above P3. As can be seen, since the nonlinearity of the abutments at the two ends was neglected, the total base shear after the piers yield is mostly contributed by the resistant forces of the abutment.

Thus, the pushover curves obtained by adaptive pushover and single-mode pushover look similar. However, if we further observe the calculated transverse displacement profiles from different methods in Fig. 3, we can find that the adaptive pushover analysis can fully capture the development of displacement profile that is observed from IDA as the level of excitation increases. For instance, as shown in Fig. 4 for IDA curve, before pier P3 yields, the displacement at the location above central pier P3 is smaller than those above pier P2 and P3. On the other hand, after P3 yields, the deck displacement at P3 gradually becomes the largest one. This variation trend for displacement profile can be captured well by adaptive pushover, but not by single-mode pushover analyses. The displacement distributions derived by both single-mode pushover analyses almost remain the same as the excitation increases.

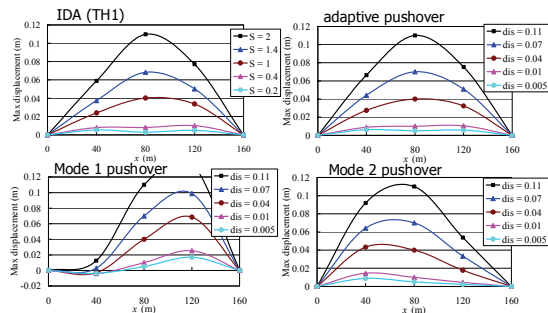


Fig. 3 Displacement pattern for B02130.

As a further comparison, the capacity spectra obtained from different approaches were also computed. By taking B02130 as an example, the results are plotted in Fig. 4. In which, the thick blue line was obtained by adaptive pushover using point 2, 3 and 4, i.e., the deck nodes above piers P2, P3 and P4, as reference points. The pink lines and green lines were obtained by 1st mode pushover and 2nd mode pushover using different reference points as specified in the legend. In addition, symbol \times and \circ respectively are denoted as the instants when two different performance limit states are reached. Symbol \times represents the crushing of core concrete as the strains of core concrete reaches -0.006, while symbol \circ represents the first yielding of steel as steel strain reach 0.0025. As can be observed, the five curves shown in Fig. 4 are totally different. This observation further reveals the problem mentioned previously for a conventional approach that different choices of reference point will most likely lead to different seismic evaluation results for a same structure. From the capacity spectrum curve, the ground acceleration corresponding to each performance limit state can also be derived based on the design spectrum value corresponding to the effective damping ratio and effective structural period at the same performance point. This is a typical seismic assessment procedure often being performed in Taiwan. Following the same procedure, the ground accelerations corresponding to steel

yielding and concrete crushing, respectively referred to as A_y and A_u were obtained and given in Table 2. In addition, according to the dynamic pushover curve obtained from IDA, the range of A_y and A_u can also be obtained: $A_y=0.21\sim 0.27g$; $A_u=0.68\sim 0.75g$. Obviously, the values predicted by 1st mode pushover with a reference point 3 overestimate the results estimated by IDA. However, if the reference points of 2 and 4 are also included, the prediction is improved. The result for 2nd mode analysis shows a similar trend. As for the results obtained by adaptive pushover with reference points 2, 3, and 4, the corresponding ground accelerations are clearly more representative of the actual behavior of the bridge.

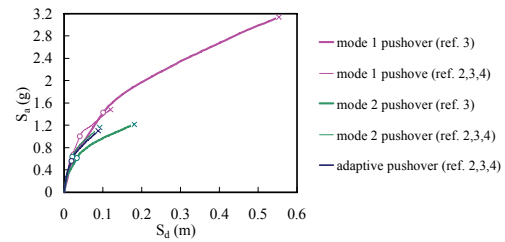


Fig. 4 Comparison on capacity curve.

Conclusions

Based on this study, two conclusions can be drawn: (1) Single-mode pushover analysis is only applicable to a regular bridge where the fundamental mode is dominant. For an irregular bridge, multi-mode adaptive pushover analysis is a better choice; and (2) the value of capacity spectrum curve as well as the ground acceleration corresponding to a performance point strongly depends on the selection of reference points. For a continuous bridge system, it is recommended to take every significant nodes of a bridge as reference points, such as the nodes above piers, in deriving the capacity spectrum.

Table 2 Ground acceleration A_y and A_u

Pushover methods	A_y (g)	A_u (g)
Mode 1 pushover(ref. 3)	0.57	2.06
Mode 1 pushover(ref. 2,3,4)	0.40	0.95
Mode 2 pushover(ref. 3)	0.25	0.78
Mode 2 pushover(ref. 2,3,4)	0.25	0.74
Adaptive pushover(ref. 2,3,4)	0.23	0.70

References

- Antoniou, S., Pinho, R., "Advantages and Limitations of Force-based Adaptive and Non-Adaptive Pushover Procedures," *Journal of Earthquake Engineering*, 8(4), pp.497-522 (2004)
- Kowalsky, M. J., "A displacement-based approach for the seismic design of continuous concrete bridges," *Earthquake Engineering and Structural Dynamics*, 31, pp. 719-747 (2002).
- SeismoSoft, "SeismoStruct- A computer program for static and dynamic nonlinear analysis of framed structures" [online]. Available from URL: <http://www.seissoft.com>. (2007)

Cable Dynamic Stability Experiment of the “Ji-Lu” Cable-stayed Bridge on Taiwan Provincial Highway 139

Zheng-Kuan Lee¹ Kuo-Chun Chang²

李政寬¹、張國鎮²

Abstract

This research project involved appraisal of the ability of the steel cable used in cable-stayed bridges to withstand rain-wind-induced vibration. Studies in other countries have shown that rain and wind can cause strong vibration in the cables of cable-stayed bridges resulting to damage of the transition pipes and speeding up the degradation of the anchor sections and corrosion protection grout, which in turn decreases the lifespan service of the steel cables. In serious cases, the impact of the cable striking the bridge can cause damage to the bridge deck. Moreover, this study used forced vibration testing and field observation techniques during typhoons to evaluate the stability of cable against rain-wind induced vibration, and thereby to design a suitable viscous vibration damper. On-site testing and recording help clarify engineering issues, thereby making it possible to determine whether restrainer cables or viscous dampers are needed.

Key Words: stability of cable to withstand rain-wind induced vibration; rain-wind effect; restrainer cables; viscous vibration damper

Introduction

The “Ji-Lu” Bridge is a cable-stayed bridge across the Jhuoshuei River that links Jiji Township and Lugu Rural Township in Nantou County, Taiwan. As shown in Fig. 1, it is a double-cell box beam bridge with a bridge deck width of 24 m (four lanes) and a single tower (58 m high), using a twin-cable fan design with 17 sets of 4 cables each, for a total of 68 cables. The span length is 120 m + 120 m. The original design incorporated restrainer cables to reduce the extent of free vibration of the steel cables, thereby minimizing rain-wind induced vibration. However, the use of restrainer cables would have severely compromised the aesthetic appeal of the bridge. It was also suggested that, given that the total span length was only 120 m + 120 m, the problem of rain-wind induced vibration would probably not be as severe as it is with long-span cable-stayed bridges. As a result, no consensus was reached regarding the need for restrainer cables.

There have been numerous reports in other countries of severe rain-wind induced vibration affecting the cables of cable-stayed bridges and such

vibration has been found to cause damage to the transition pipes (Fig. 2), speeds up the deterioration of the anchor sections and the corrosion protection grout. In the most serious case, the impact of the cable striking the bridge can cause damage to the bridge deck.

This study used forced vibration testing and field observation techniques during typhoons to evaluate the ability of steel cable against rain-wind induced vibration. In situ testing and recording help to clarify engineering issues thus making it possible to determine whether restrainer cables or viscous dampers are required.

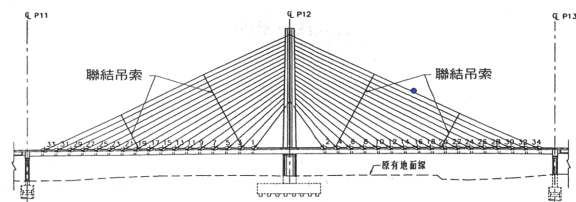


Fig. 1 Ji-Lu Cable-stayed Bridge profile with restrainer cables

¹ Associated Research Fellow, National Center for Research on Earthquake Engineering, zklee@ncree.org

² Professor of the Department of Civil Engineering, National Taiwan University, ciekuo@ntu.edu.tw



Fig. 2 Damage to the transition pipes

Forced Vibration Testing of Bridge Cables

There are two ways in implementing forced vibration testing: (1) Using a cable exciter system, and (2) Pull and quick release testing. Cable exciter systems are currently unavailable for rental in Taiwan, thus in the present study, the pull and quick release method was used to obtain the damping parameters of the bridge cable and evaluate the resistance of the cable to rain-wind induced vibration. In the available method, a cable wire was tied to a high point on the cable, and then clipped on to the bridge deck. The cable wire was pulled down, and then the clip was released quickly causing the cable to experience free vibration (Fig. 3).

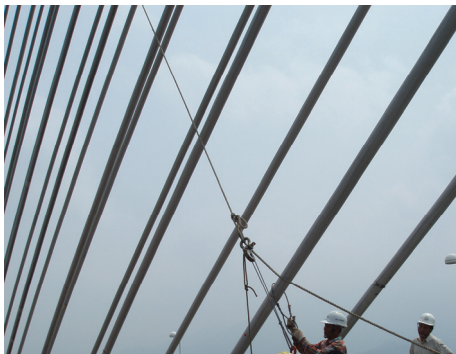


Fig. 3 Pull and quick release testing for cables

Cable Vibration Signal and Modal Damping Analysis

R33 cable pull and release testing was performed. The Fourier diagram for the vibration signal recorded in the testing is shown in Fig. 4, in which the vibration frequencies at different modes can be seen. The signal for the first mode (surrounded by a red box in Fig. 4) was selected for inverse Fourier transform analysis to obtain the time-domain signal and changes in the damping value as shown in Fig. 5.

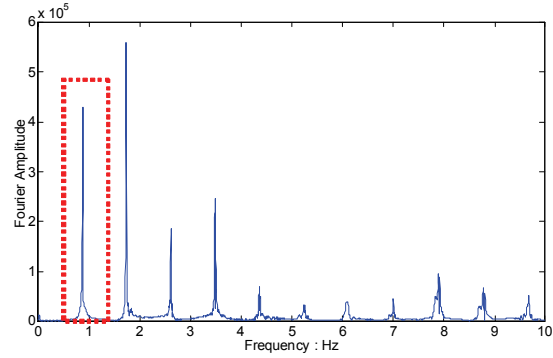


Fig. 4 Fourier diagram for the vibration signal recorded in the pull and quick release testing

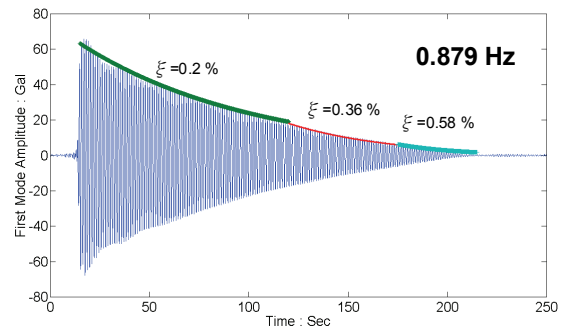


Fig. 5 The first-mode time-domain signal and the changes in the damping value

Evaluation of Resistance to Rain-Wind Induced Vibration

According to a study by the Post-Tensioning Institute (PTI), when the Scruton number (Sc) is greater than 10, the incidence of rain-wind induced vibration will be relatively low, and when the Sc value is less than 1.7, rain-wind induced vibration is sure to occur.

$$Sc = \frac{m\xi}{\rho D^2} \quad (1)$$

where m is the mass per unit length, ξ is the damping ratio, ρ is the air density, and D is the diameter of the cable. Calculations showed that, for several modals, the Scruton number of R33 cable is less than 1.7. According to the PTI report, this means that rain-wind induced vibration is inevitable; the stability of the bridge cables is inadequate.

Observation of Resistance to Rain-Wind Induced Vibration during Typhoon Conditions

On July 28, 2008, Typhoon Fung Wong struck Taiwan, following the path shown in Fig. 6. On-site observation showed that the rain and wind accompanied with the typhoon has indeed induced vibration in the R33 cable. At 3:29 p.m. on July 28, 2008, the wind was blowing from the south at a wind

speed of 11 m/sec. At this time, the R33 and R31 cables were not experiencing rain-wind induced vibration. At 6.35 p.m. on the same day, the wind had veered round to southwest (220°), and the wind speed has increased to 13 m/sec and this time, on-site observation revealed rain-wind induced vibration in the R33 cable. This in situ observation during typhoon conditions confirmed that the cables of the cable-stayed bridge have inadequate resistance to rain-wind induced vibration.

To minimize rain-wind induced vibration, either the restrainer cables provided for in the original design should be installed, or else some other measure should be adopted to improve resistance to wind and rain during typhoons, such as the installation of extra dampers.

Vibration Resistance Damping Reinforcement Design for Bridge Cables

The original design for the “Ji-Lu” Bridge included restrainer cables. However, because the bridge’s span length was relatively short, and because of concerns regarding the impact on the aesthetic appearance of the bridge, the plan including restrainer cables was abandoned, as shown in Fig. 1. In practice, cables’ resistance to wind and rain can also be strengthened by installing dampers to raise the value of the Scruton number, thereby preventing rain-wind induced vibration. The vibration reduction parameter curve shown in Fig. 7 is taken from the paper by Pacheco et al., “Estimation Curve for Modal Damping in Stay Cables with Viscous Damper.” It can be seen from Fig. 7 that: (1) the size and location of the dampers determine the increase in the damping ratio ξ_i at different modes, where i denotes the mode, (2) the greatest damping ratio ξ_i is approximately half of the length ratio X_c/L , and (3) damping design needs to be optimized to achieve the maximum increase in the damping ratio ξ_i with respect to the modes which the designers wish to control.



Fig. 6 Typhoon Fung Wong path on July 28, 2008

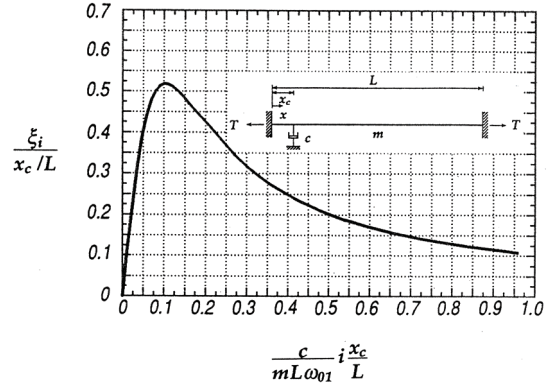


Fig. 7 Increase the damping ratio determined by the damper size and its location

The idea of implementing wind resistance reinforcement of R33 cable with respect to the first, second, and third modes (Fig. 8) was applied. The known parameters are as follows: cable length, $L = 126.4$ m, cable mass density = 48 kg/m, first fundamental wavelength $\omega_{01} = 0.879 \times 2\pi$ rad/s, $X_c/L = 3.0/126$, cable diameter, $D = 0.2$ m, air density $\rho = 1.2$ kg/m³, thus,

$$\xi_1 = 0.42 \times \left(\frac{3.0}{126}\right) = 0.010$$

$$Sc_1 = \frac{m(\xi_{1,original} + \xi_1)}{\rho D^2} = \frac{m(0.010 + 0.002)}{\rho D^2} = 11.2$$

$$\frac{c}{mL\omega_{01}} \times 1 \times \left(\frac{X_c}{L}\right) = 0.05$$

$$\therefore C = 7.0 \times 10^5 \text{ N-sec/m}$$

When the value of C has been obtained, the increase in the modal damping ratio ξ_i for damper C can be calculated for the second mode and third mode, together with the value of the Scruton number for the second mode and third mode.

$$\xi_2 = 0.52 \times \left(\frac{3.0}{126}\right) = 0.012$$

$$Sc_2 = \frac{m(\xi_{2,original} + \xi_2)}{\rho D^2} = \frac{m(0.0012 + 0.012)}{\rho D^2} = 12.3$$

$$\xi_3 = 0.47 \times \left(\frac{3.0}{126}\right) = 0.011$$

$$Sc_3 = \frac{m(\xi_{3,original} + \xi_3)}{\rho D^2} = \frac{m(0.0013 + 0.011)}{\rho D^2} = 12.3$$

The additional damping wind resistance reinforcement design outlined above can raise the Scruton number for the first, second and third mode of R33 cable to over 10. According to the PTI report,

when the Scruton number is over 10, the likelihood of rain-wind induced vibration is very low.

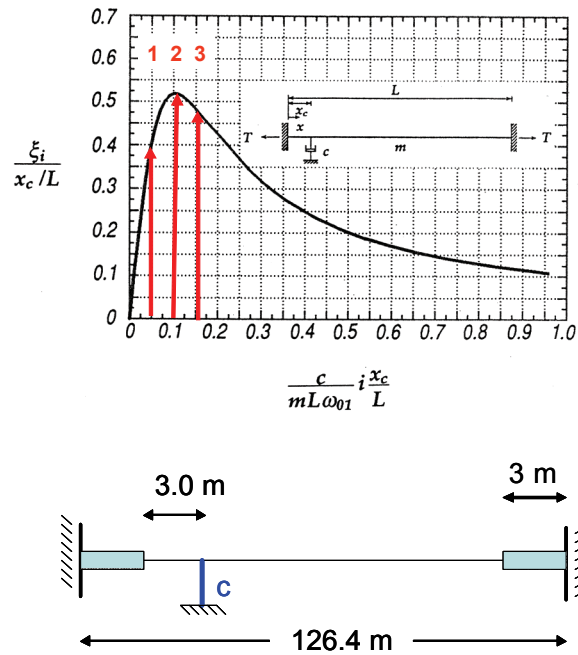


Fig. 8 Wind resistance reinforcement of R33 cable with respect to the first, second and third modes

Conclusions

This study utilized forced vibration testing and field observation technique during a typhoon to evaluate the ability of the steel cable used in the “Ji-Lu” Bridge against rain-wind induced vibration, and to clarify engineering issues, thereby to determine whether restrainer cables are required, and to recommend design of vibration reduction damping system as an alternative solution.

References

- Post-Tensioning Institute (PTI) "Recommendations for Stay Cable Design, Testing, and Installation," 1993.
- Benito M. Pacheco, Yozo Fujino, and Ajai Sulekh, "Estimation Curve for Modal Damping in Stay Cables with Viscous Damper," Journal of Structural Engineering, Vol. 119, No. 6, June 1993, pp. 1961-1979.
- Y. B. Lin, K. C. Chang, J. C. Chern, L. Wang,(2005), "Packaging Methods of Fiber Bragg Grating Sensors in Civil Structure Applications," IEEE Sensor Journal, Vol.5, pp.419-424.

Mechanical Behavior of Stainless Steel Rebars for Earthquake Engineering Applications

Yu-Chen Ou¹ K.C. Chang² Mu-Sen Tsai³ Yihui Zhou⁴ George C. Lee⁵

歐昱辰¹、張國鎮²、蔡木森³、周毅輝⁴、李兆治⁵

Abstract

Use of stainless steel in reinforced concrete structures is a promising solution to the corrosion issues. However, for stainless steel rebars to be used in seismic applications, several mechanical properties need to be investigated. These include specified and actual yield strengths, tensile strengths, elongations. Three types of stainless steel rebars including 316LN rebar, Enduramet 32 rebar, and 2205 Duplex rebar were tested and the results are reported in this paper. They were compared with the properties of A706 carbon steel rebars, which is typical for seismic applications, and MMFX II rebar, which is a high strength, corrosion resistant steel rebar. Test results show that the stainless steel rebars have lower moduli of elasticity, higher elongations at rupture than A706 rebars and MMFX II rebars. All five types of rebars tested satisfy the requirements of the ACI 318 code on the lower limit of σ_u / σ_{y2} and the upper limit on actual yield strength. Among the three types of stainless steel rebars tested, Enduramet 32 rebar possesses the highest elongation at rupture.

Keywords: Stainless steel; rebar

Introduction

Corrosion of structural steel and concrete reinforcing bars has contributed to the premature failure of highway bridge decks, columns and superstructures and thus shortened the service lives of bridges. Two important causes for corrosion of rebars are chloride attack due to deicing salts and seawater and carbonation of concrete due to carbonic acid from carbon dioxide. While chloride-induced corrosion is generally more pernicious and expensive to repair, carbonation-induced corrosion of reinforcement may

affect a far wider range of reinforced concrete structures. Solid stainless steel rebar is a promising solution for addressing these issues because of its superior corrosion resistance compared to carbon steel and surface treated steel such as epoxy coated rebar, galvanized rebar, and stainless clad rebar (Smith 2007). Despite its higher initial cost, the use of solid stainless steel rebar in bridges and highways has been growing over the past 20 years (IMO, 2008). The expected lower life cycle cost associated with a corrosion resistant structure is undoubtedly the reason (Schnell and Bergmann, 2007).

¹ Assistant Professor, Department of Construction Engineering, National Taiwan University of Science and Technology, Taipei, Taiwan.

² Professor, Department of Civil Engineering, National Taiwan University, Taipei, Taiwan.

³ Ph.D Student, Department of Construction Engineering, National Taiwan University, Taipei, Taiwan.

⁴ Ph.D Student, Department of Civil, Structural and Environmental Engineering, University at Buffalo, Buffalo, U.S.A.

⁵ Professor, Department of Civil, Structural and Environmental Engineering, University at Buffalo, Buffalo, NY.

According to current design provisions for buildings (ACI Committee 318, 2008) and bridges (AASHTO, 2007), primary rebars located at the plastic hinge regions of earthquake-resistant reinforced concrete structures are expected to undergo large inelastic strain reversals under strong ground shaking. This can lead to low-cycle fatigue failure of the rebars. Low-cycle fatigue is defined as a fatigue life of less than 10^5 cycles (Stephens et.al, 2001) and typically results from inelastic strain reversals. This paper presents results of the low-cycle fatigue tests of three types of stainless steel rebars, using A706 carbon steel rebar and MMFX II rebar for comparison. Other mechanical properties associated with seismic design are also presented including yield strengths, elongations at rupture, actual and specified yield strengths, and ratios of tensile to yield strengths.

The Experimental Program

Testing materials

Enduramet 32 rebars, 316LN rebars, and 2205 Duplex rebars, designated as S24100, S31653 and S31803 in ASTM A955 (ASTM, 2004), respectively, were the three types of stainless steel rebars investigated. A706 carbon steel rebars, typical for seismic design, and MMFX II rebars (MMFX Technologies Corp, 2008), a high strength and corrosion resistant steel rebar, recently been introduced in the market were also tested for purpose of comparison. The three types of stainless steel rebars have more than 17% chromium (Cr). The chromium combines with the oxygen in the atmosphere to form a thin, adherent chromium oxide surface layer to protect the steel from rust (Murray et.al, 2007). A set of photos of the rebars are shown in Fig. 1.

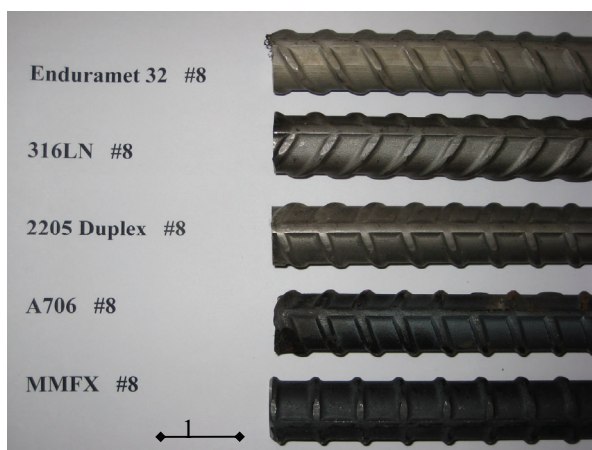


Figure 1. Rebars

Specimen design & test setup

Monotonic tension tests were carried out first to determine the basic mechanical characteristics of the rebars being investigated. These included modulus of

elasticity (E), yield strength (σ_y), tensile or ultimate strength (σ_u), and elongation at rupture. The specimen for the monotonic tests was designed and tested according to ASTM E8 (ASTM, 2004).

Fig. 2(a) shows the test setup and instrumentation, respectively. Failure of the specimen was defined as the point at which the maximum stress decreased by more than 50 % according to ASTM E606 (ASTM, 2004). Fig. 2(b) shows failure of a fatigue specimen.

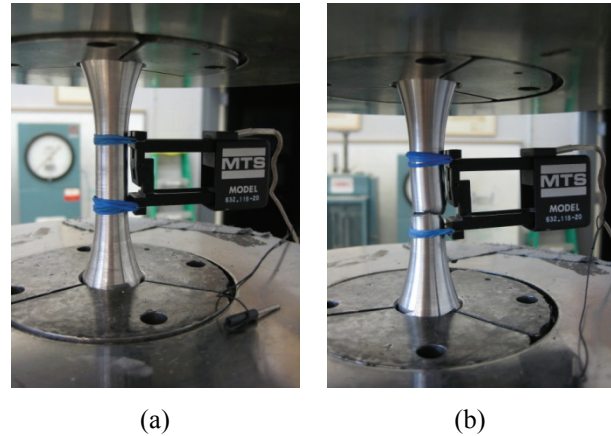


Figure 2. (a) A specimen before fatigue test; (b) A failed fatigue specimen

Results and Discussion

Fig. 3 presents stress-strain curves from the monotonic tests. The major characteristic stress-strain control parameters for each single material type are listed in Table 1. In this table, the actual yield strengths determined by the 0.2% offset method per ASTM E8 (ASTM, 2004) and the 0.35 percent strain method per ACI 318(ACI Committee 318, 2008) were denoted as σ_{y1} and σ_{y2} , respectively.

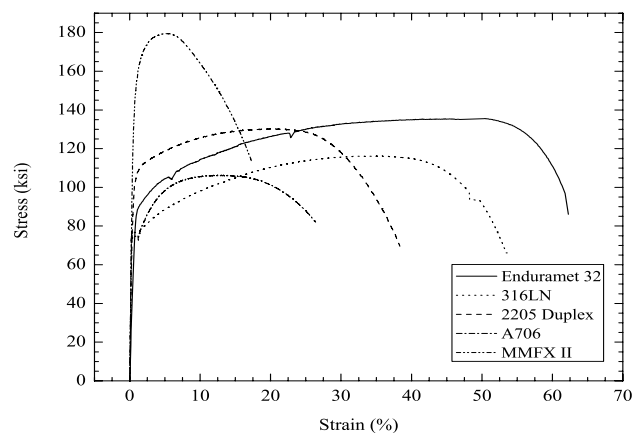


Figure 3. Stress-strain results for monotonic tension test

Steel Name	E (ksi)	Specified σ_y (ksi)	Actual σ_{y1} (ksi)	Actual σ_{y2} (ksi)
Enduramet 32	29,848	75	84.17	83.52
316LN	28,981	75	77.14	77.75
2205 Duplex	27,705	75	94.06	96.97
A706	30,244	60	73.67	72.59
MMFX II	31,533	100	137.88	100.73

Steel Name	Actual σ_u (ksi)	$\frac{\sigma_u}{\sigma_{y2}}$	Elongation (%)
Enduramet 32	136.25	1.63	58.66
316LN	116.34	1.50	52.82
2205 Duplex	130.53	1.35	38.74
A706	106.02	1.46	26.5
MMFX II	179.43	1.78	17.51

σ_{y1} is determined by 0.2% offset method according to ASTM E 8
 σ_{y2} is defined as the stress corresponding to a strain of 0.35

Table 1: Monotonic tension test results

Test results show that, compared to A706 rebar, the modulus of elasticity (E) is smaller for the three types of stainless steel rebars, and higher for MMFX II rebars. The values of E of Enduramet 32 rebars, 316 LN rebars, 2205 Duplex rebars and MMFX II rebars are respectively 98.7%, 95.8%, 91.6% and 104.3% of that of the A706 rebars. In fact, the value of E of Enduramet 32 rebar is quite similar to that of the A706 rebars.

The stress-strain curve of 316 LN rebars shows a clear yield plateau up to a strain of 1.2% similar to the A706 rebars while those for Enduramet 32 rebars, 2205 Duplex rebars and MMFX II rebars did not show a distinct yield plateau. Comparing the data of σ_{y1} and σ_{y2} in Table 1, one could conclude that the yield strengths for the stainless steel rebars and A706 rebar determined by the 0.2% offset method are similar to those defined by the stress corresponding to a strain of 0.35 percent. According to the 0.2% offset method, MMFX II rebar has very high yield strength, 138 ksi. However, the ACI 318 code (ACI Committee

318, 2008) limits the yield strength for design to 101 ksi by the 0.35% method to ensure conservative values of the member strength. Among the five types of steel rebars tested, MMFX II has the highest yielding stress, $\sigma_{y2} = 100.73 \text{ ksi}$. Rebar of such high yield strength has been accepted by the ACI 318 code (ACI Committee 318, 2008) to be used as confinement reinforcement to increase the constructability (Post, 2007). Note that the use of rebar of higher yield strength tends to result in greater crack widths and deflections of structural elements under service loads. Partly due to this reason, current building (ACI Committee 318, 2008) and bridge codes (AASHTO, 2007) generally do not allow the use of design yield strengths greater than 80 ksi and 75 ksi, respectively.

Under monotonic loading, the elongations at rupture of the three types of stainless steel rebars are substantially higher than that of the A706 rebars and MMFX II rebars. The elongation of A706 rebar (26.5%) is higher than that of MMFX II rebar (17.51%). This shows that the stainless steel rebar is much more ductile than the A706 rebar and the MMFX II rebar, and the MMFX II rebar is the least capable of elongating among the steels tested. A greater elongation means the rebar is more ductile and dissipates more energy prior to rupture, which are desirable features in seismic resistance design.

According to the ACI 318 code (ACI Committee 318, 2008), deformed reinforcement in members resisting earthquake-induced forces should have values of σ_u / σ_{y2} no less than 1.25 to ensure a sufficient length of the yield region to develop required inelastic rotation capacity. Furthermore, the actual yield strength should exceed the specified yield strength no more than 18 ksi to avoid brittle shear or bond failure modes due to unexpected higher actual yield strength. The Enduramet 32 rebars, 316LN rebars, 2205 Duplex rebars and MMFX II rebars all meet these requirements.

Conclusions

The mechanical properties of Enduramet 32, 316LN, and 2205 Duplex stainless steel rebars, A706 carbon steel rebars, and MMFX II high strength, corrosion resistant steel rebars were investigated in this paper. Important conclusions are summarized as follows.

(1) The values of the modulus of elasticity, E , for Enduramet 32, 316 LN, and 2205 Duplex stainless rebars are 1.3%, 4.2% and 8.4% lower than for A706 rebar; in contrast, it is 4.3% higher for the MMFX II rebars.

(2) All five types of rebars tested satisfy the

requirements of the ACI 318 code on the lower limit of σ_u / σ_{y2} and the upper limit on the actual yield strength.

(3) Under monotonic loading, the elongations at rupture of the three types of stainless steel rebar are substantially higher than that of the A706 rebars and the MMFX II rebars.

References

- AASHTO. (2007). AASHTO LRFD Bridge Design Specifications. American Association of State Highway and Transportation Officials (AASHTO), Washington, DC.
- ACI Committee 318. (2008). Building Code Requirements for Structural Concrete (ACI 318-08) and Commentary (ACI 318R-08), American Concrete Institute, Farmington Hills, MI.
- ASTM. (2004). ASTM Annual Book, American Society for Testing and Materials, West Conshohocken, PA.
- IMOA. 2008. "Stainless Steel Rebar." <http://www.imoa.info/_files/stainless_steel/StainlessSteelReinforcement.pdf>.
- MMFX Technologies Corp. (2008). "Revolutionary steel — Setting the standards for the future." <<http://www.mmfx.com>>.
- Murray, G., White, C.V., and Weise W. (2007). Introduction to Engineering Materials, Second Edition, CRC Press, New York.
- Post, N.M. (2007). "High-strength rebar called revolutionary." Engineering News-Record, August 27/September 3, the McGraw Hill companies.
- Schnell, R. E., and Bergmann, M. P. (2007). "Improving tomorrow's infrastructure: extending the life of concrete structures with solid stainless steel reinforcing bar," 3rd NYC Bridge Conference, New York, NY, U.S.A., Aug. 27-28.
- Smith, F. N. (2007). "The use of stainless steel reinforcement," Concrete Engineering International, Vol. 11, No. 2, pp. 25-27.
- Stephens, Ralph I., Fatemi Ali., Stephens, Robert R. and Fuchs, Henry O. 2001. Metal Fatigue in Engineering, Second Edition, John Wiley & Sons, Inc., New York.

Seismic Performance of Skew Bridge with Sliding/Friction Rubber Bearings

Kuang-Yen Liu¹, Kuo-Chuan Chang², Wei-Jin Cheng³ and Chi-Hung Lu⁴

劉光晏¹、張國鎮²、鄭維晉³、盧智宏⁴

Abstract

The seismic response of the skew bridges with rubber bearing is studied. In Taiwan, simply-supported PCI bridges are widely used with rubber bearing pads as a supporting system. It is commonly seen that, during the construction practice, the rubber bearing pads have been laid on the cement mortar-made bearing pads without any details of bolting design. This kind of arrangement potentially allows rubber bearing to slide, as the superstructure when the earthquake occurs. In addition, bridges are usually being skewed to provide transportation service, requiring a further investigation of seat width to avoid falling of the superstructure. In this study, firstly, a series of friction coefficient was conducted. Furthermore, a scale-down skew bridge model has been constructed to perform the shaking table test. According to the experimental results, the inertial forces from superstructure can be reduced because of the sliding-induced isolation effect. The analytical program, SAP2000N was used to simulate the experimental results, and it has been shown that the numerical model can well predict the displacement demand. Based on the parametric study, finally, the study will discuss the bridge behaviors with different skew angles.

Keywords: skew bridge, rubber bearing, friction coefficient, shaking table test

Introduction

A devastating earthquake with a magnitude of 7.6 struck the central region of Taiwan in the early morning of September 21, 1999. It was known as the 921 or Chi-chi earthquake. There are approximately 1,100 highway bridges spread on the provincial and county routes in the region. Major catastrophe occurred especially in Taichung and Nantou counties. About 90 percent of the bridges escaped from serious damage. The extents of bridge damages are relatively minor when compared to those observed in the 1994 Northridge earthquake and 1995 Kobe earthquake. It was observed that the friction-sliding mechanism of rubber bearings played a critical role to limit the seismic load transfer to the bridges' columns. Most of the bridge damages appeared to be caused by the movement of superstructure and separation of thermal expansion joints due to sliding or failure of the

bearings, with the exception of seven bridges collapsed due to large fault displacements which crossed indirectly to the bridges. It was also observed that the number of bridge column damage was surprisingly small. Chang in 2004 developed a bridge model to simulate slide-friction of rubber bearings, impact effect between shear key and girder, and plastic hinge at the end of the columns, providing well simulation on a bridge that was damaged in the Chi-Chi Earthquake. Since most of the bridges in the damaged area caused by Chi-Chi earthquake were designed without ductile detailing, it may be in contrast to the current seismic design concept emphasizing the design of plastic hinges. Besides, damages of skew bridges were also found in the Loma Prieta earthquake (M7.0) in 1989, Northridge earthquake (M6.7) in 1994, Kobe earthquake (M7.2) in 1995. However, studies of skew bridge with rubber bearing are seldom discussed. Besides, considering the

¹ Associate Research Fellow, National Center for Research on Earthquake Engineering, kyliu@ncree.org.tw.

² Professor, Department of Civil Engineering, National Taiwan University, ciekuo@ntu.edu.tw

³ Master, Department of Civil Engineering, National Taiwan University, r95521217@ntu.edu.tw

⁴ Ph.D student, Department of Civil Engineering, National Taiwan University, d93521020@ntu.edu.tw

route selection, engineers may face to design a skew bridge rather than a regular or straight bridge in some occasions. For example, the bridge which is across the river often has no choice but to make a column bent inclined to the axis of the superstructure. Therefore, this paper presents the experimental study on seismic performance of skew bridge with friction/sliding RB bearing (steel-reinforced elastomeric bearing) and PTFE-RB bearing (steel-reinforced elastomeric bearing coated on a thin PTFE material). The friction coefficient test was carried out first to get friction coefficient of RB bearings and PTFE-RB bearings on the surface of cement mortar, concrete, and steel plates. Two scaled bridge model was utilized in the shaking table test to understand the influence of sliding behavior of bearings on a straight and skew bridge, respectively. The force equilibrium relationship between inertial force and base shear was verified from the test results, helping to build up reasonable analytical models to perform the parametric study. The analytical program, SAP2000N, have been used to simulate the experimental results and demonstrated good accuracy in predicting the displacement demand of the skew bridge. Based on the parametric study, finally, the study will discuss the bridge behaviors with different skew angles and input directions of time histories.

Friction Coefficient Test

Figure 1 shows the test setup of the friction coefficient test. The size of bearing specimens are determined due to (1) minimal height of 15mm can only be provided by the manufactory and (2) consistent width of 150mm for same specimens to be used in the shaking table test. So, the size of the bearing specimen is 150mm×150mm×15mm. The Hardness IRHD material and shape factor of the rubber is 60 and 3.75, respectively. One SS400 shim plate is placed inside of the bearing. Based on the test requirements for rubber bearings in Chapter 18, AASHTO,2002, a total of 12 cases shown in Table 1 was performed to get friction coefficient of two types of bearing (RB and PTFE-RB) on two different surfaces (material: cement mortar, steel) with four sliding velocities (1.06, 50, 150 and 300 mm/sec). In each test, the bearing clamped by the restrain plates on the top beam was forced to slide on the prefixed blocks, either made by cement mortar or steel, within 14 cycles. The target displacement for horizontal actuator is 60 mm in both positive and negative direction, providing a sufficient friction length to develop sliding mechanism. The constant normal force around 4MPa for each bearing was applied by two vertical hydraulic actuators, while shear and friction force were measured through two load cells under a loading beam. The relative displacement was recorded by a tempersonic sensor to compare to the data from horizontal actuator.

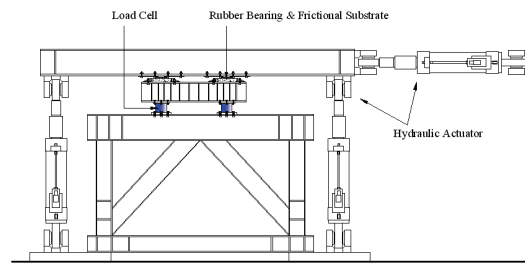


Fig. 1 Test setup of the friction coefficient test



Fig. 2 RB bearing



Fig. 3 PTFE-RB bearing

During the test, it has been found that the friction force rapidly decreases after first cycle and is getting smaller and smaller as increasing the number of cycles. There is no doubt that long accumulated sliding distance will wear bearing surface and smoothen the surface of cement mortar or steel with some residue rubber attached. The friction coefficient was determined according to ISO 15113. Since friction force is unstable in the first three cycles and affected in the last three cycles by the horizontal actuator before stopping the test, it is suggested to neglect those six cycles to obtain the coefficient with respect to cycles. Therefore, the maximum, minimum, and average friction coefficients for each case are listed in Table 1.

To reflect the construction practice of unbolted bearings, a range from 0.2 to 0.4 for the friction coefficient is more realistic than using a single value. As for the PTFE-RB, the friction coefficient from 0.1 to 0.2 can be obtained based on the test results.

Table 1 Friction coefficient test results

Group	Friction surface	Velocity (mm/sec)	Friction coefficient		
			Maximum	Minimum	Average
RB	Cement mortar	1.06	0.378	0.346	0.358
		50	0.299	0.248	0.267
		150	0.229	0.169	0.192
		300	0.231	0.168	0.193
	steel plate	1.06	0.417	0.371	0.388
		50	0.536	0.422	0.467
		150	0.477	0.359	0.409
PTFE-RB	steel plate	300	0.498	0.386	0.434
		1.06	0.130	0.101	0.112
		50	0.175	0.138	0.152
		150	0.193	0.158	0.171
		300	0.213	0.172	0.188

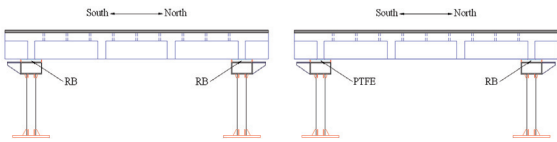
Shaking Table Test

Shaking table tests were conducted to get realistic dynamic performance from two 1/7.5 scale-down simply-supported bridge models with rubber bearings, shown in Figure 4, a straight and a skew bridge model, respectively. Based on the definition of a complex

bridge, which should be examined through dynamic analysis method, the skew angle is 20 degree. The superstructure is 10.67 tons and consists of concrete slabs, two girders and four diaphragms, supported by two rectangular hollow-section steel bents. The column bents were designed to remain elastic. The bearings used in this test are as same as in the friction coefficient test, including RB and PTFE-RB bearings. Besides, in order to compare the sliding behaviors between two different boundary conditions (B.C), as shown in Figure 5, both RB-RB cases which represent a semi-fixed B.C, and PTFE-RB cases which are like a roller-hinge B.C, were performed with peak ground acceleration (PGA) levels from 0.1g to 0.7g. The south bent may use RB or PTFE-RB bearing, depending upon the cases; while the north bent was equipped with RB bearing only. The input ground motion along the longitudinal direction of the bridge model is recorded in east-west direction of 1941 El Centro earthquake. Regarding to the instrumentation plan, acceleration on the superstructure, relative displacement of the bearing, and surface strains at the end of the columns were measured.



Fig. 4 Regular(left) and skew(right) bridge model



(a)RB-RB

(b)PTFE-RB case

Fig. 5 Boundary conditions of the bearing system

Figure 6 illustrates the test results of peak acceleration on the superstructure with respect to PGAs. The obtained acceleration is not proportional to the PGA, not only in RB-RB case or PTFE-RB case, representing the influence of sliding effect on the global performance. Especially, the trend of the line in Figure 6 is getting flat with a turning point around 0.2~0.3g. Although received same input ground motions, the accelerations in PTFE-RB case are smaller than in RB-RB case, indicating that an isolation effect is apparent when utilizing a bearing with small friction coefficient. The global structure response, particularly the force demand of the column, can be reduced due to a sliding mechanism. However, the relative displacement between superstructure and substructure is increasing.

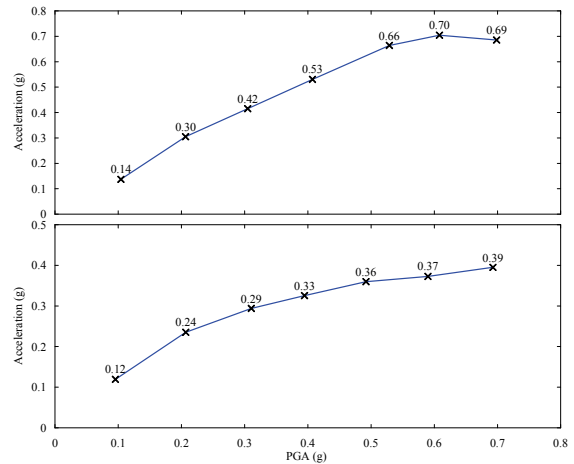


Fig. 6 Peak acceleration on the superstructure: RB-RB case (top), PTFE-RB case (bottom)

So far, friction coefficient of rubber bearing was often determined through static tests under very slow velocity. However, for bridge subjected to the earthquake excitation, the coefficient from a dynamic test, such as a shaking table test, is more realistic to describe the sliding phenomena. As shown in Figure 7, the base shear forces, which are sum of two column forces at either north or south side bent, were divided by the weight of the superstructure to determine the friction. The PGA in Figure 7 is 0.7g, and the bridge was moved according to the recorded videos. Clearly, it is due to the sliding effect that an upper and lower bound of shear forces can be identified. The friction coefficient for RB bearing and PTFE-RB bearing is around 0.4 and 0.2, respectively, close to the test results obtained in the friction coefficient test with the speed at 300mm/sec.

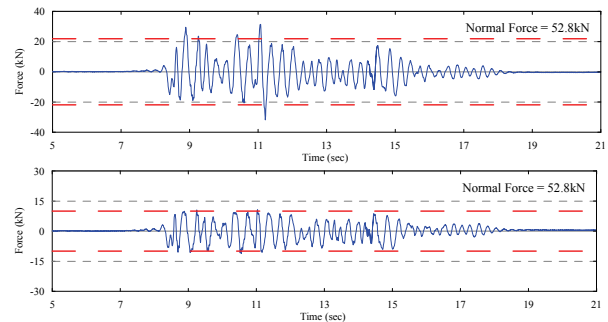
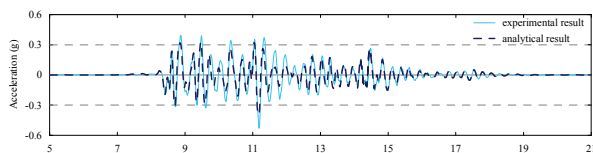


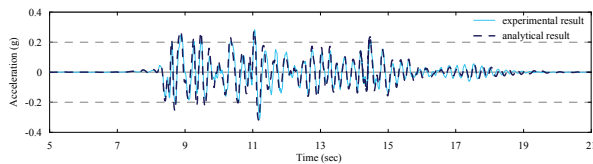
Fig. 7 Column shear forces with PGA of 0.7g: RB-RB case (top), PTFE-RB case (bottom)

Based on the structure information, both skew and straight models were established by SAP200N to compare the structure performance with experimental results. In order to simulate the sliding behavior of the rubber bearing, the friction-pendulum element [8] was utilized with proper friction coefficient given from either friction coefficient test or shaking table test. Only the bearing is considered a nonlinear element with elastic shear stiffness determined by the shear modulus, area and height of the rubber, and a constant friction coefficient of 0.4 for RB bearing, as well as 0.2 for PTFE-RB bearing. In Figure 8, the analytical

models can well predict the time history of the acceleration in the cases of 0.1g, 0.4g and 0.7g, respectively. Not only the results from straight bridge model but the skew bridge models show good accuracy.



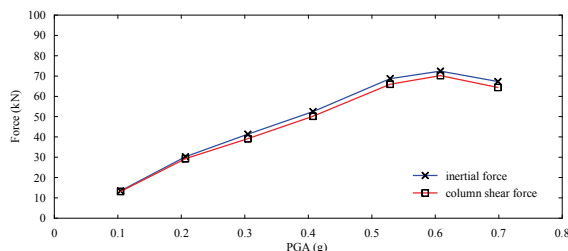
(a) RB-RB case (Skew bridge, 0.4g)



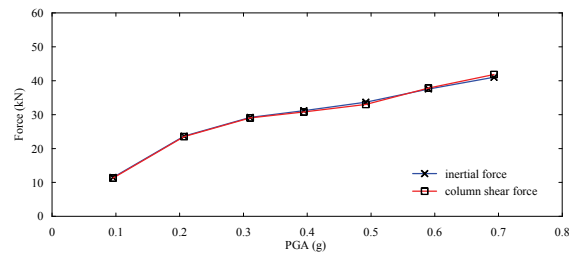
(b) PTFE-RB case (Straight bridge, 0.4g)

Fig. 8 Comparison of deck acceleration between analytical and experimental results

The shear force of the substructure is resulted from the inertial force of the superstructure, cap-beam and column bents, assumed the damping force is negligible; hence, these two loads should be identical to each other to make the loading path clearly identified through the bearing system in between. In this study, the contribution of inertial force from cap-beam and column themselves are too small to neglect because of relative small weight compared to the girder. Figure 9 represents the comparison between inertial force of the superstructure and the base shear of the substructure. The inertial force is the product of deck mass and deck acceleration at the time point corresponding to maximal acceleration of the deck; meanwhile, the base shear at the same time point was also calculated. It was found that no matter the superstructure was sliding or not, the force equilibrium relationship is satisfied in both RB-RB case and PTFE-RB case. Therefore, by taking advantage of the accuracy of the analytical model, the force demand of sliding rubber bearing and columns at different PGA levels can be quickly and precisely judged. Besides, if the skew angle is larger than 20 degree, the parametric study results in Figure 10 reveal that the structure behavior is not proportional to the skew angle. Consequently, it is suggested to use suitable bearing elements in the bridge model to get maximal response of a skew bridge.



(a) RB-RB case



(b) PTFE-RB case

Fig. 9 Comparison of inertial force and base shear force in skew bridge model

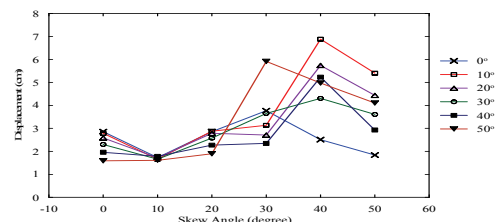


Fig. 10 Prediction of maximal displacement for RB-RB case under different skew angles (PGA = 1.0g)

Conclusions

This study aims at discussing the seismic response of the skew bridges with sliding rubber bearings. A series of friction coefficient was conducted first and followed by shaking table tests on two scale-down skew bridge models. According to the experimental results, the friction coefficient for RB and PTFE-RB bearing is 0.4 and 0.2, respectively, considering the influence of high speed may be required in a real seismic event. Besides, the force equilibrium relationship between inertial force and base shear was confirmed experimentally. The analytical models can well predict the structure performance in comparison with the test results, helping to set seat width for the skew bridge. Based on the parametric study, finally, it is suggested to use suitable bearing elements in the bridge model to get maximal response of a skew bridge under seismic excitations.

References

- National Center for Research on Earthquake Engineering. (1999) "Reconnaissance report of the 921 Chi-Chi Earthquake for bridges and transportation facilities" Report No. NCREE-99-055, Taipei, Taiwan.
- K.C Chang, K.Y Kuo, K.Y Liu, and C.H Lu. (2004) "On Seismic Retrofit Strategies of Highway Bridges - Experiences Learned from Chi-Chi Earthquake, 13th World Conference on Earthquake Engineering, Paper No. 639, Vancouver, B.C., Canada, August 1-6.
- Cheng Wei-Jin. (2008) "Shaking Table Test for Scale Down Skew Bridge Models with Rubber Bearings." National Taiwan University, Taiwan.

Bayesian Damage Classification using AR-ARX Array Expression Data

Wei-Sung Lin¹, Tzu-Kang Lin², Kuo-Chun Chang³

林偉淞¹、林子剛²、張國鎮³

Abstract

The main purpose of this research is to develop a new structural health monitoring (SHM) system which can provide on-line structural damage warning and protection. This SHM System is composed of the Naïve Bayes Classification and the array expression data, which are transplanted from bio-informatics and information technology. At the end of this report, the feasibility of the proposed SHM system with a dual-mode diagnosis algorithm is proven.

Keywords: Structural health monitoring, Naïve Bayes classification

Introduction

The purpose of this research emphasizes on the feasibility study of developing a new non-destructive structural health monitoring (SHM) system. This idea from the advanced technology of bio-informatics and information technology, where infected cancer genes can be detected by using DNA expression array. The technique of data mining and pattern recognition for data analysis and classification were also considered in the new proposed system.

As shown in Fig. 1, the developed SHM system is composed of the following components: (1) System Regression Model, which offers the feature array of the structure, (2) Pattern Sample, which comes from either finite element numerical simulation model or experimental recorded data of shaking table test, and (3) SHM diagnosis algorithm, which was chosen as the Naïve Bayes Classification in this study.

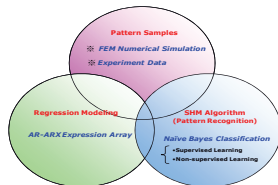


Fig. 1 Concept of the proposed SHM system

The methodology of this research is shown in Fig. 2. As illustrated, the objective of the study is to develop an on-line dual-mode SHM System which can detect both structural damage under ambient vibration or strong earthquake. In order to do this, the diagnosis core detects structural health condition by classifying the damage class of each coefficient of the training and testing arrays which are established from numerical simulation data and experimental data, respectively. Moreover, as it is not feasible to collect the damaged structural response in practice, the training database is established by using numerical finite element simulation.

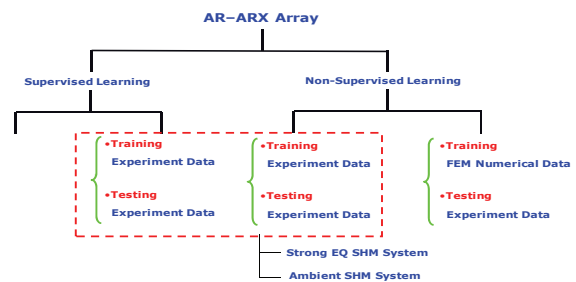


Fig. 2 the Research Methodology

The research procedure can be divided into the following steps: (1) Primary stage: structural feature comparison under supervised self-training and testing

¹ Graduate Student, National Taiwan University, Civil Engineering Department, r94521228@ntu.edu.tw.

² Associate Research Fellow, National Center for Research on Earthquake Engineering, tklin@ncree.org

³ Professor, National Taiwan University Civil Engineering Department, ciekuo@ntu.edu.tw

(SS-training and testing) condition is conducted in order to verify the classification performance of the pattern recognition algorithm --- the Naïve Bayes Classification, using experimental recorded data only. (2) Secondary stage: feasibility study of the two-mode SHM system is evaluated under non-supervised self-training and testing (NSS-Training and Testing) condition using experimental data. The optimal array structures for both ambient vibration and strong earthquake are determined in this stage. (3) Practical Application Stage: according to the suggested diagnosis array from the Secondary Stage, practical system application is conducted and the performance of the proposed structural health monitoring system is evaluated by comparing the training and testing arrays extracted from the structural response of numerical simulation and recorded experimental time history, respectively.

Databases Establishment

Three experimental databases including two shaking table experiments and one ambient vibration experiment were used for diagnosis algorithm testing. All of these experiments were conducted at the National Center for Research on Earthquake and Engineering (NCREE) with details as shown in Tables 1 and 2.

The assumed damage condition was simulated by loosening four of the sixteen connection bolts located at the beam-column joint. On the other hand, the damage level of structure was indicated by the numbers of stories. Moreover, the structural damage conditions can be categorized into four groups as listed in Tables 1 and 2, namely: (1) "Undamaged" means that all bolts are well fastened, (2) "Slight" means that the bolts are loosened in any single story of frame, (3) "Moderate" represents the condition of bolts loosened in any two stories of the frame, and (4) "Severe" shows bolts loosened in any three stories of frame.

Two shaking table experimental databases were used to verify the diagnosis performance of the proposed system under a strong earthquake. As the Bayes Classification algorithm requires large amount of samples to form the training patterns, the first strong earthquake database conducted in 2007 was only used for the feasibility study and as the benchmark of the finite element structural model in the theoretical analysis. Moreover, to verify the performance of the system in our daily life, ambient data was also collected for the feasibility study of the ambient-based SHM system.

Preliminary Study on the Proposed Algorithm

The system diagnosis algorithm is transplanted from the cutting-edge technology, which is pattern



Experiment Case Schedule, Prof. Loh et al. conducted on 2007 at NCREE

Case Number	First Stage Damage Group	Damage Floors
1	Undamaged	None
2		1F
3	Slight	4F
4		6F
5		1 & 4F
6	Moderate	4 & 6F

* Loosened Bolt (for damage simulation)

Table 1 Shaking Table Schedule in 2007



Experiment Case Schedule, T. K. Lin et al. conducted on September, 2008 at NCREE

Case	Group	Damaged Floors
1	Undamaged	None
2		1F
3		2F
4	Slight	3F
5		4F
6		5F
7		6F
8		1 & 2F
9	Moderate	3 & 4F
10		5 & 6F
11		1 & 2 & 3F
12	Severe	2 & 3 & 4F
13		4 & 5 & 6F

Loosened Bolt (for damage simulation)

Table 2 Shaking Table Schedule in 2008

recognition technique from Bio-Informatics. The feature array is first transformed from the structural response, and the SHM diagnosis algorithm, Naïve Bayes Classification, is used to detect the damage condition of the structure.

With respect to the array transformation process, the structural dynamic response data produced either from the numerical simulation program or shaking table experiment were transformed into arrays which are a series of coefficients produced by the auto-regression and auto-regression with exogenous (AR-ARX) model of system identification and modeling technique. For buildings with unknown damage condition, these arrays are always considered to represent the significant feature of structural damage situation. Furthermore, the diagnostic results were indicated by picking out the damage case of the building with the maximum value of cumulative probability. Naïve Bayes Classification, which is one of the popular data mining methods in Bioinformatics, was used for analyzing each pair of well-known or unknown training and testing array. According to the study by Keller et al., the Naïve Bayes algorithm can successfully classify and detect the infected cancer cells through the comparison process on any pairs of biological characteristic expression data, so called DNA Array.

To evaluate the performance of the proposed SHM system trained by distinct excitation databases, several

cases were combined by choosing any two of the databases among earthquake excitation, ambient vibration and white noise excitation, as shown in Figs. 3 and 5.

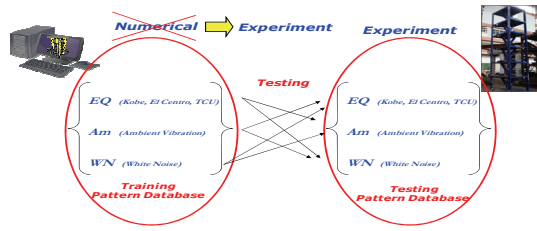


Fig. 3 SS-training and testing of different experimental database

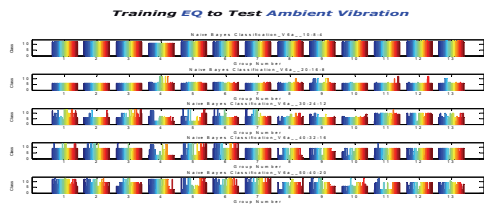


Fig. 4 Testing of cases under ambient vibration based on training database from earthquake excitation

Based from the classification performance shown in Figs. 4 and 6, several features can be concluded as follows: (1) This proposed SHM algorithm can successfully identify the current structural damage situations if the testing pattern is from the same database as the training patterns; for instance, the testing samples are chosen from the database of earthquake excitation and compared with training patterns from earthquake excitation. (2) The multi-array expression data built by one single sensor has better diagnosis accuracy than the array built by utilizing multi-channel signal or so-called multi-set expression data. (3) The array transformed from AR-ARX system model has been proven to be good in representing the structural damage characteristic from the time series data. (4) In general situation, increasing the total numbers of the array can effectively improve the classification performance on each damage situation.

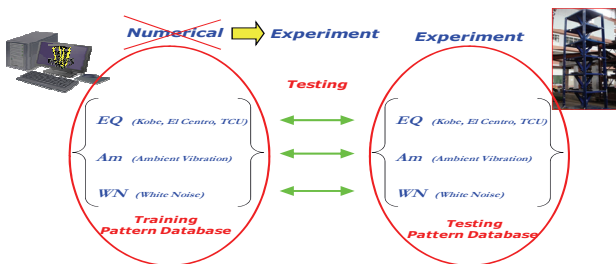


Fig. 5 SS-Training and Testing by Using Experimental Databases
According to the features mentioned above, the

preliminary study on the Naïve Bayes Classification Algorithm can provide a sound theory foundation for future SHM development and application under either ambient vibration in the daily life or during a strong earthquake.

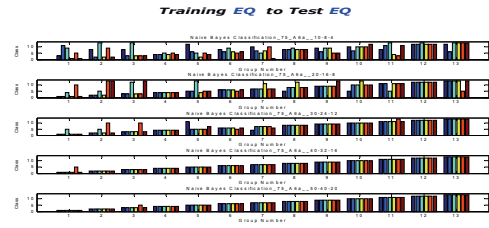


Fig. 6 Performance of self-training and testing under strong earthquakes

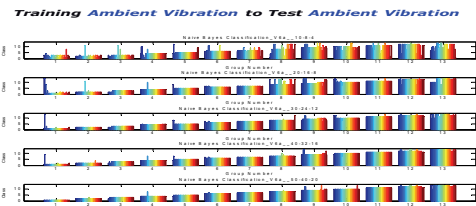


Fig. 7 Performance of self-training and testing under ambient vibration

Feasibility Verification of the SHM System

By evaluating the performance of the system with non-supervised self-training and testing with respect to both ambient vibration and earthquake experimental databases as shown in Figs. 7 and 8, the feasibility study of proposed SHM System can be confirmed.

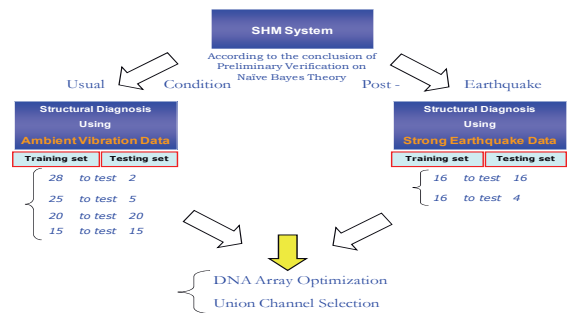


Fig. 8 Scheme of the Dual-mode SHM System

According to the initial feasibility study on the dual-mode SHM System, it shows that the ambient vibration SHM system can offer perfect classification performance for all structural damage conditions, however, the performance of the earthquake SHM system shows that the classification ability may need to be improved by properly considering the peak structural response interval of the recorded time history.

As shown in Figs. 9 and 10, the feasibility verification study on the dual-mode SHM system can be concluded as follows: the ambient vibration SHM

System can successfully identify each damage situation of structures, however, there still exists few cases of data with wrong classification result. This imperfect diagnosis result would be improved by optimizing the structural feature array.

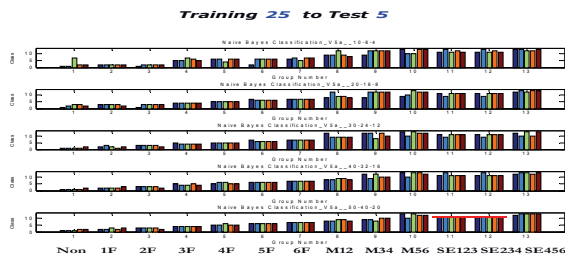


Fig. 9 Non-supervised classification of the Ambient SHM System

Training 16 to Test 4 (Short EQ Section only with Different 6 Cases)

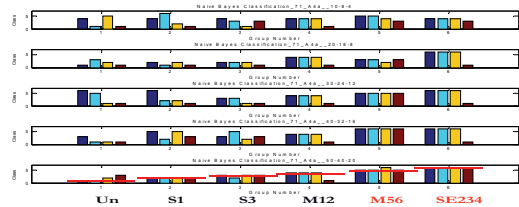


Fig. 10 Non-supervised classification of the Ambient SHM System

Meanwhile, feasibility study on the earthquake SHM system has shown that the value of the structural arrays fluctuates and highly depends on the selected structural response time history interval. By selecting the peak structural response interval of the recorded time history, the performance of the earthquake SHM system has been successfully enhanced under the test case with six different kinds of damage conditions. The research will then extend the number of the total diagnosis cases from six to thirteen damage conditions.

Practicality Study of the Earthquake SHM System

Following the success on the feasibility study of the earthquake SHM system, the Naïve Bayes Classification algorithm was applied again to distinguish the structural health conditions of a practical structure under six assumed damaged cases. The process compares each pair of training and testing array transformed from the structural response of numerical simulation program and the recorded experimental time history, respectively.

The diagnostic result, as indicated in Fig. 12, shows that the earthquake SHM system fails to identify the practical structural damage condition. However, after further analyzing the natural frequency of each structural response data, the result shows that the output data of numerical simulation model has totally different frequency distribution compared to

the frequency distribution of the experimental data.

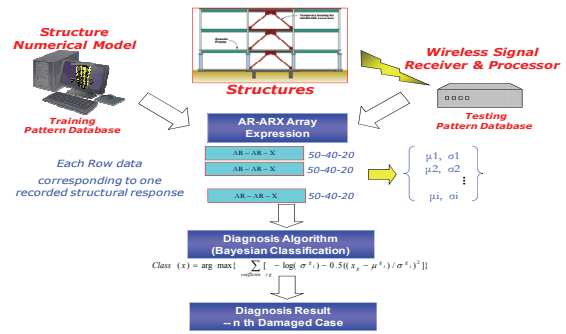


Fig. 11 Practical verification of the prospective SHM System

Training 25 to Test 5

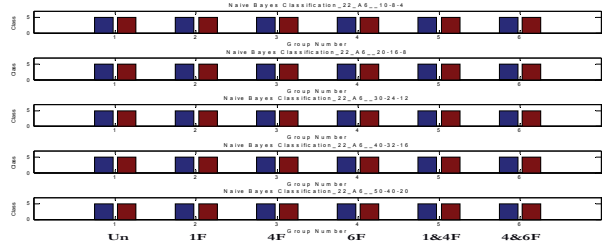


Fig. 12 Distribution of final verification for a practical structure

Conclusions

Based from the results and initial conclusions on the study, the proposed dual-mode SHM system has been proven to be feasible to identify the structural damage condition under both ambient vibration and earthquake event. For the next step, the research will try to improve the accuracy and reliability of the structural finite element model to address some key issues on applying the SHM system in practice.

References

Straser, E. and Kiremidjian, A.S., "A Modular Wireless Damage Monitoring System for Structures," The John A. Blume Earthquake Engineering Center Technical Report No. 128, Department of Civil and Environmental Engineering, Stanford University, Stanford, California, 1998.

Sohn, H., and Farrar, C. R., "Damage Diagnosis Using Time Series Analysis of Vibration Signals," Journal of Smart Materials and Structures, 10(3), pp. 446-451(2001).

Keller, A. D., Schummer, M., Hood, L., Ruzzo, W. L., "Bayesian Classification of DNA Array Expression Data," Department of Computer Science and Engineering, University of Washington, Technical Report UW-CSE-2000-08-01, Seattle (2000).

Seismic Analysis of Asymmetric-Plan Buildings with Supplemental Damping

Jui-Liang Lin¹ and Keh-Chyuan Tsai²

林瑞良¹、蔡克銓²

Abstract

This study investigates the effectiveness of the modal analysis using three-degree-of-freedom (3DOF) modal equations of motion to deal with the seismic analysis of two-way asymmetric elastic systems with supplemental damping. The 3DOF modal equations of motion possessing the non-proportional damping property enable the two modal translations and one modal rotation to be not proportional in an elastic state. The simple approximation method is to use the single degree-of-freedom (SDOF) modal equations of motion, which is obtained by neglecting the off-diagonal elements of the transformed damping matrix. One one-story and one three-story non-proportionally damped two-way asymmetric buildings under the excitation of bi-directional seismic ground motions are analyzed. The analytical results are obtained by using the proposed method, the noted simple approximation method and the direct integration of the equation of motion. It is seen that the proposed method can significantly improve the accuracy of the analytical results compared with those obtained by using the simple approximation method. Moreover, the proposed method does not substantially increase the computational efforts.

Keywords: asymmetric buildings; non-proportional damping; bi-directional ground motion; modal analysis; response history analysis

Introduction

The building with the center of stiffness (CR) not coincident with the center of mass (CM) along the two horizontal plane axes is defined as a two-way asymmetric building in this report. The noted buildings with supplemental damping, e.g. viscous dampers in the braces, usually belong to the non-proportionally or non-classically damped structures whose damping matrix can not be diagonalized by the mode shapes of the undamped systems. Although the research on the dynamic responses of non-proportionally damped symmetric structures was conducted at a much earlier time, the study of non-proportionally damped asymmetric structures was performed much later (Goel 1998). According to the literature review (Goel 2001), the analytical methods of non-proportionally damped systems were grouped into four categories and the corresponding shortcomings are briefly stated as follows: The first approach is to directly integrate the

equation of motion of the original multi-degree-of-freedom (MDOF) structure. The stated approach is numerically inefficient for structural systems with a lot of degrees of freedom. Some researchers proposed to directly integrate the truncated set of the coupled modal equations of motion, which is more efficient than dealing with the whole set of equation of motion of the original structural system. The second approach is the mode superposition method using complex mode shapes which results in doubling the size of the eigenvalue problems and difficulties associated with the use of complex numbers in the dynamic response analysis. The third approach is the hybrid time-domain procedure, which iteratively solves the coupled modal equations of motion in time domain. However, this method cannot be implemented on most commercially available structural analysis programs. The last approach, also the most common and simplest approach, is to simply neglect the off-diagonal elements of the transformed damping

¹ Associate Research Fellow, National Center for Research on Earthquake Engineering, jllin@ncree.org.tw.

² Director, National Center for Research on Earthquake Engineering, kctsai@ncree.org.tw

matrix which is appealing to the engineering practice because it enables the use of the traditional modal analysis methods.

The proposed method of this study is the modal analysis using the 3DOF modal equations of motion instead of the single-degree-of-freedom (SDOF) modal equations of motion, which are obtained by neglecting the off-diagonal terms of the transformed damping matrix. The stated 3DOF modal equations of motion, which are sets of three coupled equations, are obtained by using the partition of matrices. This paper first investigates the property of the damping matrices of the 3DOF modal equations of motion. Then the paper shows that the 3DOF modal equations of motion preserve the damping characteristics of the original multi-degree-of-freedom (MDOF) structure. The effectiveness of this proposed method is numerically verified.

3DOF modal equations of motion

The motivation of deriving the 3DOF modal equations of motion and the verification of the consistency of the stated equations with the SDOF modal equations of motion are shown in Lin and Tsai (2008a). In order to keep the completeness of this paper, the derivation of the 3DOF modal equations of motion is briefly restated in this section. The coordinate system adopted in this study is the same as that used in Lin and Tsai (2008a). Namely, the X- and Z-axis are the two horizontal axes and the Y-axis is vertically upward. When the building is under bi-directional seismic ground motions, the right-hand side of equation of motion can be written as:

$$\begin{aligned}
& -\mathbf{M}\mathbf{t}_x\ddot{u}_{gx}(t) - \mathbf{M}\mathbf{t}_z\ddot{u}_{gz}(t) \\
& = -\sum_{n=1}^{3N} \Gamma_{xn} \mathbf{M}\boldsymbol{\varphi}_n \ddot{u}_{gx}(t) - \sum_{n=1}^{3N} \Gamma_{zn} \mathbf{M}\boldsymbol{\varphi}_n \ddot{u}_{gz}(t) \\
& = -\sum_{n=1}^{3N} (\Gamma_{xn} \ddot{u}_{gx} + \Gamma_{zn} \ddot{u}_{gz}) \mathbf{M}\boldsymbol{\varphi}_n = -\sum_{n=1}^{3N} (\Gamma_{xn} \ddot{u}_{gx} + \Gamma_{zn} \ddot{u}_{gz}) \mathbf{s}_n
\end{aligned} \tag{1}$$

where \mathbf{s}_n is equal to $\mathbf{M}\boldsymbol{\varphi}_n$ and $\Gamma_{xn}\ddot{u}_{gx} + \Gamma_{zn}\ddot{u}_{gz}$ is the synthetic ground motion for the n -th mode. Γ_{xn} and Γ_{zn} are the n -th X-directional and Z-directional modal participation factors, respectively, defined as:

$$\begin{aligned}
\Gamma_{xn} &= \frac{\boldsymbol{\varphi}_n^T \mathbf{M} \mathbf{t}_x}{\boldsymbol{\varphi}_n^T \mathbf{M} \boldsymbol{\varphi}_n} & \Gamma_{zn} &= \frac{\boldsymbol{\varphi}_n^T \mathbf{M} \mathbf{t}_z}{\boldsymbol{\varphi}_n^T \mathbf{M} \boldsymbol{\varphi}_n} \\
\mathbf{t}_x &= \begin{bmatrix} 1 \\ 0 \\ 0 \end{bmatrix}_{3N \times 1} & \mathbf{t}_z &= \begin{bmatrix} 0 \\ 1 \\ 0 \end{bmatrix}_{3N \times 1}
\end{aligned} \tag{2}$$

It is assumed that only the n -th modal displacement response, \mathbf{u}_n , of the non-proportionally damped system will be excited under the excitation of

$-(\Gamma_{xn}\ddot{u}_{gx} + \Gamma_{zn}\ddot{u}_{gz})\mathbf{s}_n$, namely,

$$\mathbf{M}\ddot{\mathbf{u}}_n + \mathbf{C}\dot{\mathbf{u}}_n + \mathbf{K}\mathbf{u}_n = -(\Gamma_{xn}\ddot{u}_{gx} + \Gamma_{zn}\ddot{u}_{gz})\mathbf{s}_n \quad n=1 \sim 3N \tag{3}$$

The mass, damping and stiffness matrices shown in Eq. (3) are partitioned as:

$$\begin{aligned}
\mathbf{M} &= \begin{bmatrix} \mathbf{m}_x & \mathbf{0} & \mathbf{0} \\ \mathbf{0} & \mathbf{m}_z & \mathbf{0} \\ \mathbf{0} & \mathbf{0} & \mathbf{I}_0 \end{bmatrix}_{3N \times 3N}, & \mathbf{C} &= \begin{bmatrix} \mathbf{c}_{xx} & \mathbf{c}_{xz} & \mathbf{c}_{x\theta} \\ \mathbf{c}_{zx} & \mathbf{c}_{zz} & \mathbf{c}_{z\theta} \\ \mathbf{c}_{\theta x} & \mathbf{c}_{\theta z} & \mathbf{c}_{\theta\theta} \end{bmatrix}_{3N \times 3N} \\
\mathbf{K} &= \begin{bmatrix} \mathbf{k}_{xx} & \mathbf{k}_{xz} & \mathbf{k}_{x\theta} \\ \mathbf{k}_{zx} & \mathbf{k}_{zz} & \mathbf{k}_{z\theta} \\ \mathbf{k}_{\theta x} & \mathbf{k}_{\theta z} & \mathbf{k}_{\theta\theta} \end{bmatrix}_{3N \times 3N}
\end{aligned} \tag{4}$$

where \mathbf{m}_x , \mathbf{m}_z and \mathbf{I}_0 are the X-directional mass and the Z-directional mass and the mass moment of inertia of the building system, respectively. The subscript x , z and θ denote the sub-matrix relating to X-translational, Z-translational and Y-rotational degrees of freedom, respectively. The n -th modal displacement response is also partitioned as:

$$\mathbf{u}_n = \begin{bmatrix} \mathbf{u}_{xn} \\ \mathbf{u}_{zn} \\ \mathbf{u}_{\theta n} \end{bmatrix}_{3N \times 1} = \begin{bmatrix} \boldsymbol{\varphi}_{xn} & 0 & 0 \\ 0 & \boldsymbol{\varphi}_{zn} & 0 \\ 0 & 0 & \boldsymbol{\varphi}_{\theta n} \end{bmatrix}_{3N \times 3} \begin{bmatrix} D_{xn} \\ D_{zn} \\ D_{\theta n} \end{bmatrix}_{3 \times 1} \tag{5}$$

where $\boldsymbol{\varphi}_{xn}$, $\boldsymbol{\varphi}_{zn}$ and $\boldsymbol{\varphi}_{\theta n}$ are the components of the n -th undamped mode shape associated with X- and Z-translational and Y-rotational DOFs, respectively. D_{xn} , D_{zn} and $D_{\theta n}$ are denoted as the modal translations and the modal rotation of the n -th mode, respectively. If D_{xn} , D_{zn} and $D_{\theta n}$ are equal to each other, then they can be marked as D_n . By pre-multiplying both sides of Eq. (3)

$$\text{with } \begin{bmatrix} \boldsymbol{\varphi}_{xn} & \mathbf{0} & \mathbf{0} \\ \mathbf{0} & \boldsymbol{\varphi}_{zn} & \mathbf{0} \\ \mathbf{0} & \mathbf{0} & \boldsymbol{\varphi}_{\theta n} \end{bmatrix}_{3N \times 3}^T \text{ and substituting Eq. (5)}$$

into it, Eq. (3) becomes:

$$\mathbf{M}_n \ddot{\mathbf{D}}_n + \mathbf{C}_n \dot{\mathbf{D}}_n + \mathbf{K}_n \mathbf{D}_n = -\mathbf{M}_n \mathbf{1} (\Gamma_{xn} \ddot{u}_{gx} + \Gamma_{zn} \ddot{u}_{gz}) \tag{6}$$

where \mathbf{M}_n , \mathbf{C}_n , \mathbf{K}_n are 3×3 matrices. Eq. (6) is the so-called n -th 3DOF modal equation of motion. Each 3DOF modal equation of motion has a corresponding 3DOF modal stick (Lin and Tsai, 2008a). The modal damping matrix, \mathbf{C}_n is equal to:

$$\mathbf{C}_n = \begin{bmatrix} \boldsymbol{\varphi}_{xn} & \mathbf{0} & \mathbf{0} \\ \mathbf{0} & \boldsymbol{\varphi}_{zn} & \mathbf{0} \\ \mathbf{0} & \mathbf{0} & \boldsymbol{\varphi}_{\theta n} \end{bmatrix}_{3N \times 3}^T \mathbf{C} \begin{bmatrix} \boldsymbol{\varphi}_{xn} & \mathbf{0} & \mathbf{0} \\ \mathbf{0} & \boldsymbol{\varphi}_{zn} & \mathbf{0} \\ \mathbf{0} & \mathbf{0} & \boldsymbol{\varphi}_{\theta n} \end{bmatrix}_{3N \times 3} \tag{7}$$

If the original MDOF building is a proportionally damped system, i.e.

$$\mathbf{C} = \begin{bmatrix} \mathbf{c}_{xx} & \mathbf{c}_{xz} & \mathbf{c}_{x\theta} \\ \mathbf{c}_{zx} & \mathbf{c}_{zz} & \mathbf{c}_{z\theta} \\ \mathbf{c}_{\theta x} & \mathbf{c}_{\theta z} & \mathbf{c}_{\theta\theta} \end{bmatrix}_{3N \times 3N} = \alpha \mathbf{M} + \beta \mathbf{K} \quad (8)$$

, the modal damping matrix would be:

$$\mathbf{C}_n = \alpha \mathbf{M}_n + \beta \mathbf{K}_n \quad (9)$$

Therefore, if the original MDOF building is a non-proportionally damped system, the modal damping matrix would also be non-proportional, i.e.

$$\mathbf{C}_n \neq \alpha \mathbf{M}_n + \beta \mathbf{K}_n \quad (10)$$

It implies that a non-proportionally damped system will result in $3N$ non-proportionally damped 3DOF modal equations of motion, which are able to take the out-of-phase motions between the modal translations and the modal rotation into account. Thus, the 3DOF modal equations of motion are more appropriate to be used in the modal analysis of non-proportionally damped two-way asymmetric structures than the SDOF modal equations of motion. The n -th modal history, $\mathbf{D}_n(t)$, is obtained by direct integration of the corresponding 3DOF modal equation of motion, Eq. (6). The total displacement history of the non-proportionally damped two-way asymmetric building is calculated as:

$$\mathbf{u}(t) \approx \sum_{n=1}^p \mathbf{u}_n(t) = \sum_{n=1}^p \begin{bmatrix} \varphi_{xn} D_{xn}(t) \\ \varphi_{zn} D_{zn}(t) \\ \varphi_{\theta n} D_{\theta n}(t) \end{bmatrix}_{3N \times 1} \quad (11)$$

where p is the number of modes to be used in the modal analysis, $p \leq 3N$. The 3DOF modal equations of motion possess the non-proportionally damped property at the expense of increasing two DOFs in the modal coordinate. The proposed 3DOF modal equations of motion still can be easily computed by commercially available structural analysis programs. On the other hand, the proposed method keeps the clarity and the simplicity of the modal analysis in calculating the seismic responses of structures.

Numerical Validation

The three-story asymmetric building with viscous dampers shown in Fig. 1 is analyzed by three methods, which include the direct integration of the equation of motion, simple approximation method and the proposed method. The results obtained by using the direct integration of the equation of motion are the benchmark solutions in this study. All of the beams and columns of the noted example building are symmetric making the CR coincident with the geometric center of each floor. The CM is eccentrically located as shown in Fig. 1. The CM is eccentrically located making the values of

normalized supplemental damping eccentricities in two horizontal directions both equal to -0.75 . Choosing $\bar{e}_{sd} = -0.75$ is large enough to verify the effectiveness of the proposed method (Goel 2001). The supplemental damping ratios, ζ_{sdx} and ζ_{sdz} , used in these two prototype buildings are both equal to 30%. The properties of the example building are shown in Lin and Tsai (2008b). The floors are simulated as rigid diaphragms. Rayleigh damping is assumed as the inherent damping of this example building. The damping ratios of the first and the third mode of the example building are specified as 2%.

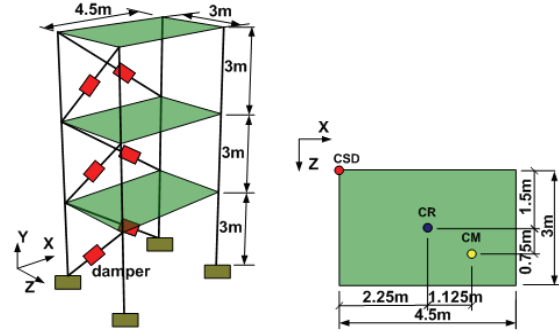


Fig. 1 The three-story example building.

The ground acceleration records used in this study are the NS and EW components of 1940 El Centro earthquake. The noted NS and EW components of ground acceleration records are scaled down and applied along the Z- and X-axis, respectively. The peak ground accelerations (PGA) of NS/EW components are equal to $0.1g/0.061g$ for the three-story building. The example building remains elastic under the excitation of the noted ground motions.

The analytical results obtained by using direct integration of the equation of motion, the simple approximation method and the proposed method are denoted as RHA, SMA and 3MA, respectively, in this paper. RHA stands for response history analysis; SMA stands for modal analysis by using SDOF modal equations of motion; 3MA stands for modal analysis by using 3DOF modal equations of motion. The 3×3 \mathbf{M}_n , \mathbf{C}_n and \mathbf{K}_n matrices of the nine modes of the three-story building are shown in Lin and Tsai (2008b). The sum of the nine elements of matrix \mathbf{M}_n is equal to one. The sum of the nine elements of matrix \mathbf{C}_n and \mathbf{K}_n are equal to the values of the n -th diagonal element of the matrix $\Phi^T \mathbf{C} \Phi$ and Λ , respectively. The first three modal responses of the three-story building obtained by using 3MA are shown in Fig. 2. The modal translations and modal rotation are not equal to each other. It reflects the non-proportional damping effect. The total responses of this non-proportionally damped three-story building obtained by using 3MA compared with those obtained by using RHA, are shown in Fig. 3. Fig. 3 shows that the analytical results obtained by 3MA are almost the same as those obtained by RHA.

However, the responses obtained by using SMA are obviously deviated from the benchmark solutions. The errors of the peak X- and Z-translational and Y-rotational responses on the roof are 0.6%, 18.2% and 28.9%, respectively. Moreover, the phases of time histories obtained by using SMA are quite different from those obtained by using RHA. The roof responses of the three-story building obtained by using 3MA and SMA considering only the first three modes are also investigated. It shows that three modes are sufficient to obtain accurate results in this example. Thus, this indicates that it is not necessary to incorporate the entire $3N$ modes (9 modes in this example) in the proposed method. It appears that the proposed method has been inherent the advantage of the modal analysis, only the first few modes are required for an earthquake response analysis.

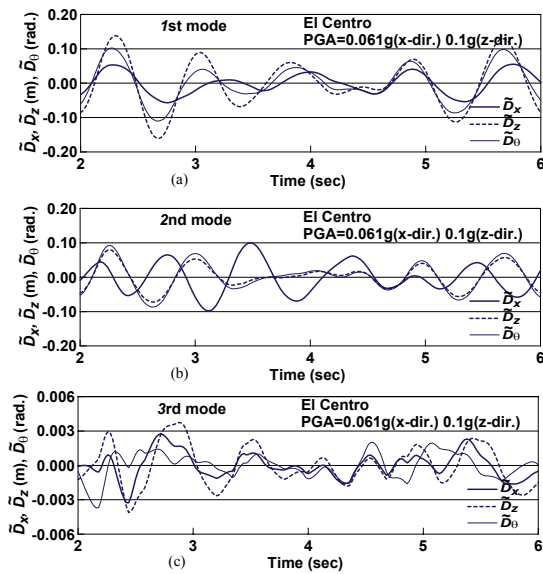


Fig. 2 The (a) 1st (b) 2nd (c) 3rd modal response of three-story building obtained by using 3MA.

Conclusions

This study develops a method to analyze the seismic responses of non-proportionally damped two-way asymmetric buildings under bi-directional seismic ground motions. The proposed method is similar to the simple approximation method except using the 3DOF modal equations of motion instead of the SDOF modal equations of motion. The proportionalities of the damping matrices in the 3DOF modal equations of motion depend on that of the damping matrix of the original MDOF building. It makes the modal translations and modal rotation to be different from each other for a non-proportionally damped structure. The 3DOF modal equations of motion are closer to the realistic structural behavior than the SDOF modal equations of motion. The accuracy of the analytical results obtained by using the proposed method is numerically verified in this study. The proposed method inherits the advantages of the simple approximation method without the complexity

of other developed methods. Hence, it is more appealing to the practical engineering.

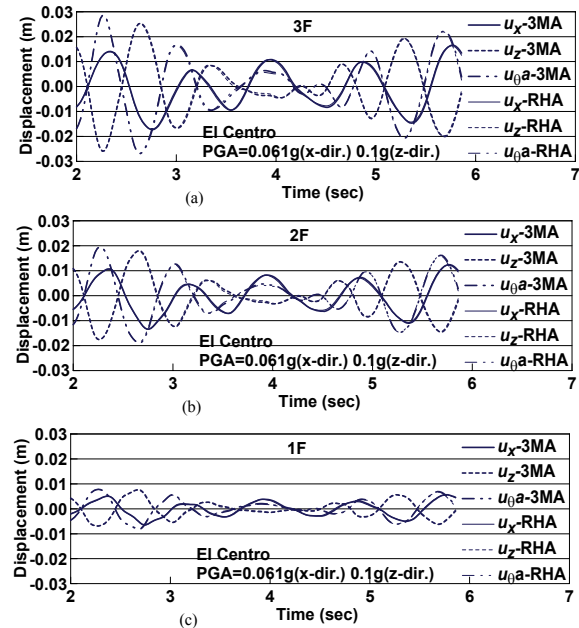


Fig. 3 The total translational and rotational responses at the (a) 3rd (b) 2nd (c) 1st floor obtained by using 3MA and RHA.

References

- Goel, R.K. (1998) "Effects of supplemental viscous damping on seismic response of asymmetric-plane systems," *Earthquake Engineering and Structural Dynamics*, 27: 125-141
- Goel, R.K. (2001) "Simplified analysis of asymmetric structures with supplemental damping," *Earthquake Engineering and Structural Dynamics*, 30: 1399-1416.
- Lin, J.L. and Tsai, K.C. (2008a) "Seismic analysis of two-way asymmetric building systems under bi-directional seismic ground motions," *Earthquake Engineering and Structural Dynamics*, 37: 305-328.
- Lin, J.L. and Tsai, K.C. (2008b) "Seismic analysis of non-proportionally damped two-way asymmetric elastic buildings under bi-directional seismic ground motions," *Journal of Earthquake Engineering*, 12: 1139-1156.

Preliminary Study on the Seismic Design of Nonstructural Components in A Hospital

Juin-Fu Chai¹, George C. Yao², and Fan-Ru Lin³

柴駿甫¹、姚昭智²、林凡茹³

Abstract

For a designated hospital, in order to preserve its capability of providing disaster rescue functions and medical treatment services after a catastrophic earthquake, the nonstructural components of the hospital should meet the “operational” requirement conforming to the seismic performance level of the performance-based design method. Due to the diversity in the categorization of nonstructural components in a hospital, before embarking on seismic design, the critical and/or vulnerable nonstructural items should be identified and prioritized. Cooperating with the National Cheng Kung University Hospital (NCKU Hospital), the criteria of screening and primary evaluation for nonstructural components are proposed in this study. In addition, appropriate seismic restraints are recommended consulting with the constructors and hospital facility manager.

Keywords: nonstructural components, seismic design, selection criteria, seismic restraint devices

Introduction

In order to promote the seismic performance of nonstructural components in the new NCKU Hospital building (phase II, under construction), the installation manual for nonstructural components in a hospital and the practical suggestions are proposed and integrated in this study, owing to the effort of hospital facility manager, designer and constructors. The first part of this study is to incorporate the design, installation, and review process for nonstructural components into the initial construction plan. Considering a great quantity and variety of hospital inventories, the second part is to identify the selection criteria and primary design methods of nonstructural components, and further, to help the designer and constructor to check the seismic performances of traditional installation devices rapidly. Finally, referred to the related studies, guidelines and constructors’ suggestions, the seismic-based drawings and specifications for installation of nonstructural components are proposed. Limited by the different schedules of this study and the construction, only the nonstructural items from ensured manufacturers with some definite types were discussed.

Current State of Design and Installation for Nonstructural Components

Nowadays, there is neither specific provision nor guideline for the seismic design and installation of nonstructural components for hospital in Taiwan. The existing installation guidelines that the contractors and constructors should comply with are according to the construction specifications established by the architect and facility manager. In the case of NCKU Hospital, the seismic restraints for nonstructural components (mainly for equipment) are regulated in Sections 15080 and 15081 of construction specifications.

Section 15080, “Vibration Isolation and Seismic Control,” regulates the equipment accompanied with operational vibration. Seismic snubbers are suggested to provide seismic restraint in all directions. At least 4 snubbers and related steel frames should be designed for chillers and pumps to resist 100 % lateral forces.

Section 15081, “Support, Anchorage and Fastener,” regulates the attachments for equipment that is attached directly to the structure. Section 15081 includes the hangers, supports and anchorage for piping systems as

¹ Research Fellow, National Center for Research on Earthquake Engineering, chai@ncree.org.tw

² Professor, Dept. of Architecture, National Cheng Kung university, gcyao@mail.ncku.edu.tw

³ Assistant Research Fellow, National Center for Research on Earthquake Engineering, frlin@ncree.org.tw

well as the bases and supports for general equipment. However, the purpose of Section 15081 is to meet the mechanical requirements without any specification for seismic protection devices. For instance, the minimum spacing of supports is specified to prevent deflection resulted from vertical load of piping, but not under the consideration of lateral force resistant.

Based on the aforementioned specification, it can be found that the seismic requirements are specified only for the vibration isolated equipment. Therefore, as shown in Fig. 1, the seismic design and installation steps as well as the associated criteria and analysis programs are proposed in this study to enhance the seismic performance of nonstructural components for hospital. Moreover, the review mechanism for seismic design and installation is suggested to be incorporated into the routine construction procedure.

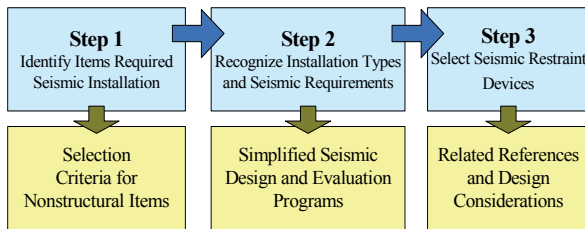


Fig. 1 Seismic design and installation steps for nonstructural components

Selection Criteria for Nonstructural Items

For the financial ability and efficiency, the first step is to identify the items, which should be designed and installed under the consideration of seismic effect, from numerous nonstructural components in a hospital. As shown in Fig. 2, the critical medical spaces and the supporting mechanical and electrical systems should be selected first. Then, the architectural components and critical medical equipment for performance levels of life safety and operational in the critical medical spaces should be identified by the hospital facility manager and architects. To decide the selected items comprehensively, the facility manager can refer to FEMA 412~414, FEMA 74, FEMA 460, IBHS, and ATC 51-2.

In addition to the nonstructural items and critical equipment listed in the aforementioned references, other nonstructural components to be evaluated under seismic consideration can be identified according to the flow chart. For the performance level of life safety, two flow charts are proposed in this study for both critical equipment and architectural component items, respectively. Figure 3 shows the flow chart for critical equipment. For architectural components, the one with height exceeding 1.5 m should be evaluated regardless of its weight.

As shown in Table 2, a simplified evaluation form was established by Excel software to determine the seismic performance of selected nonstructural items.

Users can get the evaluation results by inputting the characteristic parameters of the selected nonstructural components. However, it is noted that this evaluation form can be applied only to independent components, such as chillers, pumps, or cabinets. For systematic nonstructural items, such as suspended ceiling, access floor, or piping system, the seismic performance shall be verified by numerical analysis or shake-table tests.

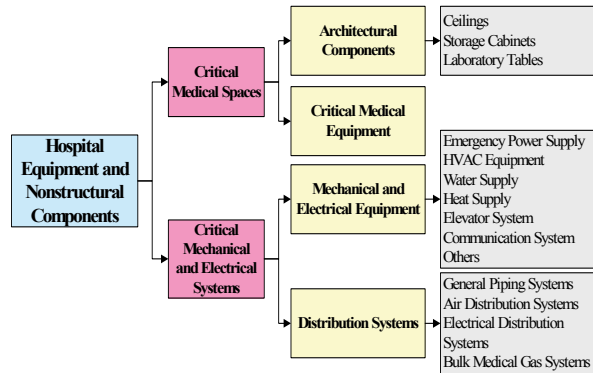


Fig. 2 Step 1 – Identify nonstructural items to be installed under seismic consideration

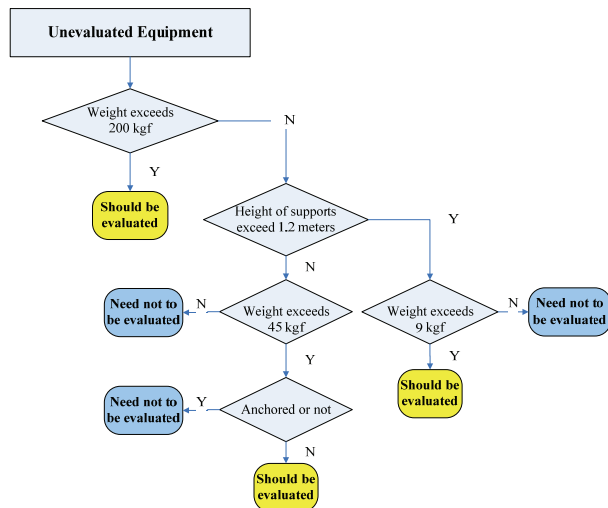


Fig. 3 Flow chart of selection criteria for equipment

Simplified Seismic Design and Evaluation Programs

After ensuring the selected nonstructural items, the second step is to recognize the installation types to meet the operational requirement. As shown in Table 1, referred to ATC 51-2, the installation types for general nonstructural components can be classified according to the installation positions and anchorage devices. For unusual nonstructural components, the types are classified for systematic, supporting, or other critical components. When the installation types of nonstructural components are determined under the functional consideration, the next work is to evaluate the seismic demand for the installation devices. Based

on the *Seismic Design Code for Buildings* in Taiwan and other references, the seismic demands on attachments of nonstructural components, including seismic forces and overturning possibility, can be determined automatically as long as the users fill out the simplified evaluation form for nonstructural components, as shown in Table 2. In view of the lack of studies for seismic performance of equipment and nonstructural components, this study is focused on the seismic design of attachments, and the capacity of the nonstructural component is assumed to be enough to resist the seismic forces.

Table 1 Category of installations for nonstructural components

General Nonstructural Components		Unusual Nonstructural Components	
Attached to Structural Components		Nonstructural System	
A	Fixed, floor-mounted components	I	Elevators
B	Vibration-isolated, floor-mounted components	J	Distribution Systems
C	Fixed, suspended or wall-hung components	K	Ceilings
D	Vibration-isolated, suspended components	Supporting Nonstructural Components	
E	Portable/mobile components	L	Raised access floors
Attached to Nonstructural Components		M	Partitions
F	Fixed components on raised access floors	N	Storage Racks
G	Fixed components on ceilings	O	Claddings
H	Desktop components	P	Critical Mechanical and Electrical Equipment

Seismic Design Requirements

When the critical nonstructural items are selected and the associated installation types are determined under the functional consideration, the next step is to improve the seismic capacity of installation devices for nonstructural components, and meanwhile, not to obstruct the functionality of nonstructural components and equipment. As shown in Fig. 4, the seismic restraint devices for general nonstructural components can be divided into four categories according to different installation types, where the component can be rigidly mounted, vibration isolated, suspended or classified as portable ones. In addition, according to the Appendix D of AC318, the size and numbers of concrete expansion anchors can be determined and displayed in the evaluation form (Table 2), if oversize or too many anchors are resulted, the designer should consider additional seismic restraint devices. Besides, referred to ATC 51-2, the design requirements and criteria for each installation type shown in Table 1 are also provided in this study.

Shop Drawings and Installation Examples

Due to the lack of seismic design requirement for nonstructural components in the Building Law, the facility manager and architect should establish the construction specifications complied with the seismic

design criteria for nonstructural components. On the other hand, before inviting the constructors to tender, hospital facility manager may request the constructors, in the tender notice, to provide seismic calculation sheet or seismic qualifications and shop drawings of critical nonstructural components before installation. However, several equipment contract awards were finished before this study, and therefore, most shop drawings of seismic restraint devices in this case were reviewed based on the seismic design experiences without any calculation sheet, numerical analysis or qualification tests.

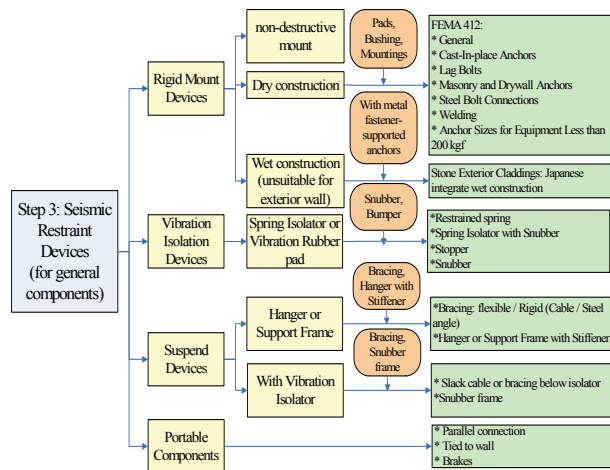


Fig. 4 Step 3—Select seismic restraint devices (for general nonstructural components)

In the following paragraphs, the fire suppression system is taken as an example to illustrate the seismic design and installation steps:

1. Identify critical items under seismic consideration

Critical equipment of the fire suppression system was identified as shown in Table 3. Facility manager should request constructors and contractors to provide the equipment catalogs, seismic calculation sheet, and shop drawings for installation.

2. Recognize the installation types and seismic requirements

Based on the catalogs or shop drawings provided by contractors, the installation types were recognized as shown in Table 3. Equipment with no seismic calculations or other seismic qualifications could be evaluated by the simplified evaluation form (Table 2). Constructors could obtain more vulnerable items and determine the associated seismic demands. Meanwhile, constructors could obtain the size and numbers of expansion anchors by simplified anchor design.

3. Select seismic restraint devices

If the expected anchors can not satisfy the seismic demand, Contractors should provide shop drawings of the additional seismic restraint devices complied with the seismic design requirement and criteria respected

to the installation types of components. As shown in Figs. 5 and 6, broadcasting cabinets were suggested to be parallel connected, and the detail drawings were provided by the contractor.

Table 2 Simplified evaluation form for nonstructural components

Structural System		Fire Suppression System					
Basic characteristics		Illustration					
No.		01	02	03	04	05	06
Equipment Name	Please fill the identifiable name	Sprink Pump	Foam Pump	Fire Suppression Pump	Water Pump	cabinet	CO2 Frame
Category	Referenced to Appendix 1	44	44	44	44	44	44
Position (Floor number)	Fill R-1 or R1F-R1F Fill R1-R2 if at R1F-R2F	-3	-3	-3	-3	-1	-1
Installation method	Referenced to Appendix 2	2	2	2	2	1	1
Position of Attachments	Referenced to Appendix 3	2	2	2	2	1	1
Number of supports	If equipment is fixed at 4 points, fill "4"	4	4	4	4	4	4
Height of the highest support (m)	floor mounted equipment needn't to be filled out						
Weight	equipment except liquid weight unit weight of piping (included contents) (kgf/m) spacing of bracing in piping system (m)	1410	660	520	1335	240	1570
Equipment Size (m)	equipment except piping						
L length		1.6	1.58	1.55	1.55	2.1	0.97
T width		1.33	1.02	1.02	1.012	0.61	0.64
3 height (included contents)		1.63	1.55	1.63	1.58	2.24	1.08
The height of the highest point of equipment (included contents)(m)		1.6	1.58	1.63	1.58	2.24	1.08
Equipment against the wall (Y or N)		Y	Y	Y	Y	Y	Y
Flexible connections with other equipment (Y or N or U)	If it's individual, please fill "U"	Y	Y	Y	Y	Y	Y
Results	"N" represents needs "I" to evaluate, "Y" represents need to evaluate "N" represents no overturning possibility, "Y" represents equipment with no anchor has overturning possibility.	Y	Y	Y	Y	Y	Y
		N	N	N	N	N	N
Horizontal seismic design force for each attachment (kgf)		814.28	381.15	300.30	770.96	95.04	621.72
Vertical seismic design force for each attachment (kgf)		407.14	190.58	150.15	385.48	47.52	310.86
Number of anchors in one attachment		4	4	4	4	4	4
Spacing of anchors in one attachment	(in) If it needs to be filled if only one anchor in a attachment.						
Anchor size	(MS M10-)	M16	M16	M16	M16	M10	M10
Anchor embedded depth	(in)	2.5	2.5	2.5	2.5	1.5	1.5
Concrete strength of structure (f _{ps})		5000	5000	5000	5000	5000	5000
	(V/FAP/SB)/NHN/C/S/Sec=1.0	0.02	0.01	0.00	0.02	0.00	0.08
Seismic capacity of attachments is enough or not		OK	OK	OK	OK	OK	OK

Table 3 Classification of installation types for fire suppression system

Fire Extinguishing System	Fire Suppression Sprinklers System	piping(J), sprinkler(J), roof tank(A), air compressor(B)
	Foam Fire Extinguishing	piping(J), sprinkler and foam head(J)
	Carbon Dioxide Fire Extinguishing	piping(J), CO2 spray head(J), CO2 Cylinder rack(A), CO2 Control Panel(C)
	Deluge Fire Suppression Sprinklers	piping(J), spray head(J), tank(A), pump(B), fire control panel(C)
Fire Alarm System	Fire Protection Alarm Equipment and Broadcasting Equipment in the Control Room	fire control panel(N), desktop equipment (H), computer(H), EPS emergency power(N), broadcasting cabinet(N)
Fire Escape Equipment		escape light(C), escape equipment(A), emergency light(C)



Fig. 5 Strengthened points for parallel connection between broadcasting cabinets

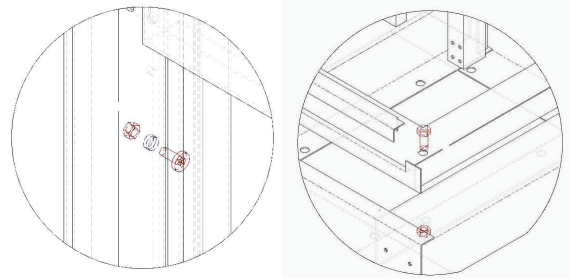


Fig. 6 Details of parallel connections and base

Conclusions

In this study, three steps and accompanied tools including the selection criteria, simplified evaluation form and seismic design requirements were proposed for the seismic design and installation of nonstructural components in a hospital. In addition, to achieve the purpose of seismic design and installation, the review mechanism for nonstructural components should be incorporated into the routine construction procedure.

References

- Vibration Isolation and Seismic Control Manufacturers Association (VISCMA), (2002). Installing Seismic Restraints for Mechanical Equipment (FEMA 412), Federal Emergency Management Agency.
- VISCMA (2004), Installing Seismic Restraints for Electrical Equipment (FEMA 413), Federal Emergency Management Agency.
- VISCMA (2004), Installing Seismic Restraints for Duct and Pipe (FEMA 414), Federal Emergency Management Agency.
- WISS, JANNEY, ELSTNER ASSOCIATES, INC (1994)., Reducing the Risks of Nonstructural Earthquake Damage (FEMA 74), Federal Emergency Management Agency.
- FEMA 460 (2005), Seismic Considerations for Steel Storage Racks Located in Areas Accessible to the Public, Building Seismic Safety Council, Federal Emergency Management Agency, Washington, D.C.
- Institute for Business & Home Safety (IBHS), (2001). A Homeowner's Guide to Earthquake Retrofit, Tampa, Florida, U.S. www.ibhs.org.
- Applied Technology Council (2003), ATC-51-2: Recommended U.S.-Italy collaborative guidelines for bracing and anchoring nonstructural components in Italian hospitals, Department of Civil Protection, Italy.
- Construction and Planning Agency (2005), Seismic Design Code for Buildings, Ministry of the Interior, Taiwan.

Applications of Viscous Dampers to Vertically Irregular Building Structures

Jenn-Shin Hwang¹ Wang-Chuen Lin² Shiang-Jung Wang³

黃震興¹、林旺春²、汪向榮³

Abstract

Since design guidelines for supplemental viscous dampers to building structures are readily available in various seismic design codes, the applications of viscous dampers to reduce the seismic damage potential to of structures and/or non-structures are extensively progressing. These design guidelines are provided often based on the added effective damping ratio contributed by added viscous dampers. However, the distribution method of damping coefficients corresponding to the desired total effective damping ratio is not specified in the current seismic design codes. Therefore, some reasonable distribution method for the damping coefficients may be needed to efficiently and economically design the viscous dampers. This is particularly needed for the vertically irregular building structures such as those with stiffness irregularity and/or mass irregularity. This study aimed at proposing and deriving the distribution methods for added linear viscous damping coefficients in different stories based on the following three concepts: (1) uniformly distributed; (2) proportional to the story shear force of each story divided by the total base shear; and (3) proportional to the elastic strain energy of each story divided by the total strain energy of the structure. For illustration, the elastic responses of three types of building structures equipped with viscous dampers designed according to the aforementioned three methods are presented. The building types include: (1) a vertically regular building; (2) a building with vertical stiffness irregularity, e.g. a building with soft stories; and (3) a building with vertical stiffness discontinuity, e.g. a setback building. The numerical study indicates that the distribution method based on the elastic strain energy, compared with the other two distribution methods, is more effective in reducing the seismic responses of the structures, particularly for the building with soft stories.

Keywords: Vertical structural irregular, viscous damper, distribution, damping coefficient

Introduction

It is not uncommon in practice to design buildings with diverse heights or plane dimensions in different stories due to architectural concerns of aesthetics and functionality. As a consequence, stiffness and/or mass irregularity may often exist in some building structures such as hospitals and fire stations. For those

structures, special care is often required in their seismic design according to the specifications by most seismic design codes [1, 2]. In order to preserve the desired functionality of the structures after an earthquake event, the implementation of viscous dampers [3] may be one of the solutions to increase the earthquake-resisting capability of said structures.

¹ Professor, Dept. of Construction Engineering, Taiwan University of Science and Technology. Also, Division Head, National Center for Research on Earthquake Engineering, jshwang@ncree.org.tw

² Ph. D. Student, Dept. of Construction Engineering, Taiwan University of Science and Technology, D9505003@mail.ntust.edu.tw

³ Assistant Research Engineering, National Center for Research on Earthquake Engineering, sjwang@ncree.org.tw

The current design guidelines for the incorporation of viscous dampers to building structures are provided based on the total effective damping ratio contributed by added viscous dampers. However, no rational distribution methods are readily available for distributing the damping coefficients along the height of the structure corresponding to the desired added effective damping ratio. The uniform distribution of damping coefficients [4] is often adopted in the current practical design. To uniformly distribute the damping coefficients along the height of the structure may be irrational and uneconomical since the seismic responses and the demands for viscous dampers are different at each story. Therefore, the objective of this research is to examine some methods other than uniform distribution for the damping coefficients such as those in which the assigned damping coefficient to each story is respectively proportional to the story shear [5, 6] and the elastic strain energy [7]. These distribution methods are numerically investigated by comparing the seismic responses of vertically regular and irregular buildings with added linear viscous dampers designed.

Distribution Formulas of Damping Coefficients

The design formula provided by FEMA 273 and FEMA 356 for calculating the supplemental damping ratio by linear viscous dampers is specified by

$$\xi_d = \frac{T \sum_j C_j f_j^2 \phi_{rj}^2}{4\pi \sum_i m_i \phi_i^2} \quad (1)$$

where ξ_d = the damping ratio contributed by linear viscous dampers; T = the fundamental natural period of the structure; C_j = the damping coefficient of the damper j ; f_j = the magnification factor of the axial deformation of the damper j to the corresponding horizontal story drift; ϕ_{rj} = the first mode relative displacement between the ends of the damper j in the horizontal direction; m_i = the mass of the i^{th} story; ϕ_i = the normalized modal displacement at the i^{th} story;

Method 1: Uniform Distribution

Assuming that the damping coefficients assigned to all stories are identical, i.e. $C_j = C_u$, the formula for determining the damping coefficient at each story is given by

$$C_u = \frac{\xi_d 4\pi \sum_i m_i \phi_i^2}{\eta_j T \sum_j (f_j \phi_{rj})^2} \quad (2)$$

where η_j = the number of dampers at the j^{th} story.

Method 2: Distribution Based on Story Shear

From structural dynamics, it is not difficult to prove that the story shear at each story is proportional to the following equation

$$\sum_j^{\text{Roof}} m_j \omega^2 \phi_j \quad (3)$$

A parameter related to the story shear is then defined as follows

$$S_j = \sum_j^{\text{Roof}} m_j \phi_j \quad (4)$$

Based on the rational assumption that the total damping coefficients in method 2 and method 1 are identical, the formula for determining the damping coefficient at each story is given by

$$(C_j)_{ss} = \frac{S_j}{\sum_j^{\text{Roof}} S_j} \sum_{j=1}^{\text{Roof}} C_u \quad (5)$$

where S_j = the story shear at the j^{th} story; ϕ_j = the first mode horizontal displacement of the damper j .

Method 3: Distribution Based on Elastic Strain Energy

Assuming that the damping coefficient is proportional to the elastic strain energy at each story, the following relationship is obvious

$$\sum_{k=1}^{\eta_j} (C_j)_{se} \propto \phi_{rj} S_j \quad (6)$$

If the total damping coefficients in method 3 and method 1 are identical, one can obtain

$$\sum_{j=1}^{\text{Roof}} \eta_j (C_j)_{se} = \sum_{j=1}^{\text{Roof}} \eta_j C_u \quad (7)$$

The formula for determining the damping coefficient at each story is given by

$$(C_j)_{se} = \frac{\sum_{j=1}^{\text{Roof}} \eta_j C_u}{\eta_j \sum_{j=1}^{\text{Roof}} \phi_{rj} S_j} \phi_{rj} S_j \quad (8)$$

Numerical Illustration

The distribution formulas corresponding to the uniform distribution (Method 1) and those proportional respectively to the story shear (Method 2) and elastic strain energy (Method 3) are shown in Equations (2), (5) and (8), respectively. In order to have a better insight on the comparison of three

distribution methods, the implementation of linear viscous dampers were added to the three types of building structures including (1) a 10-story conventional regular building given in Figure 1; (2) a 10-story building with 2 soft stories (stiffness irregularity) illustrated in Figure 2; and (3) a 12-story setback building (stiffness discontinuity) shown in Figure 3.

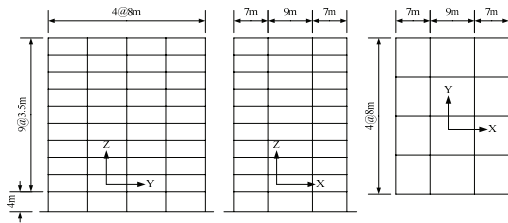


Fig. 1 Dimensions of the vertical structural regular building structure

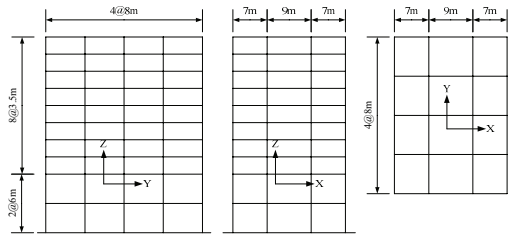


Fig. 2 Dimensions of the vertical structural irregular building structure with stiffness irregularity

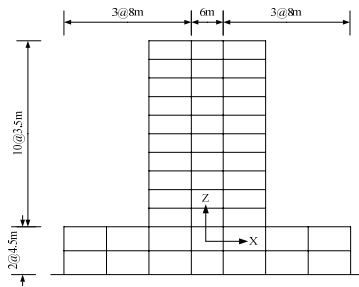


Fig. 3 Dimensions of the vertical structural irregular building structure with stiffness discontinuity

The damping coefficients corresponding to the three distribution methods for the three selected building structures are summarized in Tables 1 to 3. Assuming the buildings are to remain elastic, the dynamic response histories of the structures subjected to the 1940 El Centro Earthquake were obtained using SAP2000N. Comparisons of the seismic responses for the three building structures are summarized in Figures 4-6. It can be seen that there is no significant difference in the responses of the regular building and setback building with added dampers designed using the three different distribution methods for the viscous damping coefficients. Nevertheless, the distribution method based on the proportionality to the elastic strain energy is more effective in reducing the seismic responses of the building with soft stories as shown in Figure 5. Apparently, the distribution method based on the elastic strain

energy is beneficial to make the story drift angles become more uniformly distributed along the height of the building. In addition, significant improvement is obtained at the displacement responses of soft stories.

Table 1 Designed damping coefficients for the vertical structural regular building structure

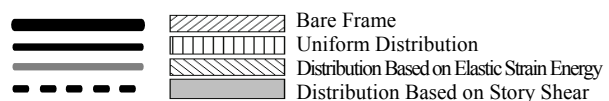
Vertical Structural Regular Building with 10 Stories ($\zeta_0 = 5\%$, $\zeta_d = 10\%$)			
Story No.	Uniform Distribution	Distribution Based on Story Shear	Distribution Based on Elastic Strain Energy
10	5979.7	1385.6	527.7
9	5979.7	2713.2	1535.8
8	5979.7	3954.6	3015.5
7	5979.7	5080.0	4704.3
6	5979.7	6064.4	6352.4
5	5979.7	7016.3	8419.9
4	5979.7	7764.1	9466.5
3	5979.7	8333.4	10124.5
2	5979.7	8675.1	9542.5
1	5979.7	8810.8	6378.3

Table 2 Designed damping coefficients for the vertical structural irregular building structure with stiffness irregularity

10-story Building with 2 soft stories ($\zeta_0 = 5\%$, $\zeta_d = 10\%$)			
Story No.	Uniform Distribution	Distribution Based on Story Shear	Distribution Based on Elastic Strain Energy
10	4931.1	1050.6	285.9
9	4931.1	2066.0	812.6
8	4931.1	3030.8	1551.3
7	4931.1	3929.6	2246.8
6	4931.1	4754.7	2881.3
5	4931.1	5616.5	3838.7
4	4931.1	6376.7	4964.1
3	4931.1	7064.1	6533.1
2	4931.1	7604.7	15739.1
1	4931.1	7817.0	10457.8

Table 3 Designed damping coefficients for the vertical structural irregular building structure with stiffness discontinuity

Setback Building with 12 Stories ($\zeta_0 = 5\%$, $\zeta_d = 10\%$)			
Story No.	Uniform Distribution	Distribution Based on Story Shear	Distribution Based on Elastic Strain Energy
10	2498.63	522.96	263.43
9	2498.63	1023.18	747.70
8	2498.63	1490.42	1385.93
7	2498.63	1915.68	2073.68
6	2498.63	2292.09	2540.57
5	2498.63	2618.47	3161.24
4	2498.63	2890.35	3632.37
3	2498.63	3138.61	3837.30
2	2498.63	3323.19	4025.06
1	2498.63	3444.70	3419.56



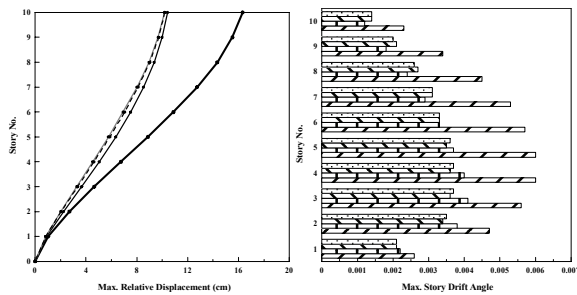


Fig. 4 Seismic responses of the vertical structural regular building structure

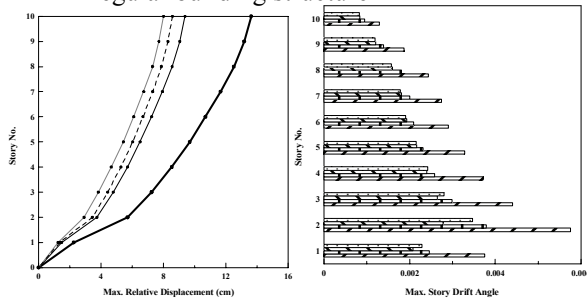


Fig. 5 Seismic responses of the vertical structural irregular building structure with stiffness irregularity

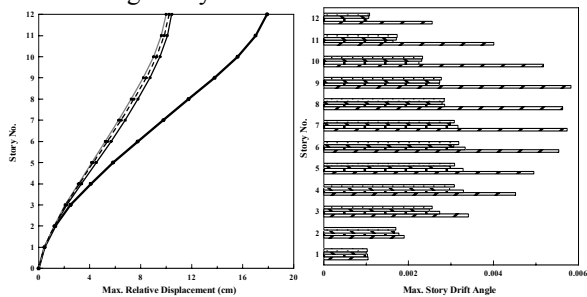


Fig. 6 Seismic responses of the vertical structural irregular building structure with stiffness discontinuity

Conclusions

The uniform distribution is a convenient and accepted method in the current design practice for adding viscous dampers to building structures. However, for the vertically irregular buildings such as the existing medical centers in Taiwan, it may not be an effective way to improve their undesired seismic responses arising from the inherent structural drawbacks such as stiffness irregularity and/or stiffness discontinuity. In this study, the analytical results disclose that the distribution method based on the proportionality to the elastic strain energy of each story is more effective in reducing the seismic responses compared with the other two distribution methods, particularly for a building with soft stories. Although the undesired behavior due to the structural drawbacks may not be perfectly improved, the method is still beneficial in making the story drift angles more uniformly distributed along the height of the structure. Significantly improvement on the displacement responses at soft stories can also be observed.

Besides, this research only concentrates on the incorporation of linear viscous dampers to the structure. In the future study, the distribution methods for nonlinear viscous dampers or the combination of linear and nonlinear viscous dampers will be further discussed.

References

- Seismic Design Code for Buildings in Taiwan (建築物耐震設計規範及解說), the Architecture and Building Research Institute, Ministry of the Interior, July, 2005. (in Chinese)
- Soong, T.T. and Dargush, G.F., "Passive Energy Dissipation Systems in Structural Engineering," John Wiley & Sons, 1997.
- Fu, Yaomin and Kasai, Kazuhiko, "Comparative Study of Frames Using Viscoelastic and Viscous Dampers," Journal of Structural Engineering, ASCE, Vol.124, No.5, pp513-522, 1998.
- Kazuhiko Kasai and Kazuyuki Oohara, "Design of Velocity-Dependent Passive Control Systems," First International Symposium on Passive Control, pp293-307, Tokyo Institute of Technology, Tokyo, 2000.
- Hwang, J. S. and Huang, Y. N., "Experimental and Analytical Study of A Structure with Supplemental Linear Viscous Dampers (使用線性黏性阻尼器建築結構之耐震試驗與分析)," National Center for Research on Earthquake Engineering, NCEE-01-022, 2001. (in Chinese)
- Hwang, J. S., Huang, Y. N. and Hong, Y. H., "Experimental and Analytical Study of A Structure with Supplemental Nonlinear Viscous Dampers (含非線性黏性阻尼器結構之減震試驗與分析)," National Center for Research on Earthquake Engineering, NCEE-02-020, 2002. (in Chinese)

Hwang, W. Y., Master thesis: "Applications of Viscous Dampers to Seismic Retrofit of Microelectronics Factories with Vertical Irregularity (黏性阻尼器於立面不規則晶圓廠之耐震補強設計)," Department of Construction Engineering, National Taiwan University of Science and Technology, 2006. (in Chinese)

A Study of Three Full-Scale 2-Story Steel Concentrically Braced Frames

Keh-Chyuan Tsai¹, Ker-Chun Lin², Chih-Yu Wei³, Chih-Han Lin⁴,

Ching-Yi Tsai⁵, Jacob Powell⁶, Kelly Clark⁷ and Charles Roeder⁸

蔡克銓¹、林克強²、魏志毓³、林志翰⁴、蔡青宜⁵

Jacob Powell⁶、Kelly Clark⁷、Charles Roeder⁸

Abstract

In this study, three full scale 2-story steel special concentrically braced frames (SCBFs) were tested. The performances of these three tests are presented in this paper, focusing on the investigations of the overall structure and local members. This paper discusses the analytical component and includes a brief description of the experimental results, which were used in the development and validation of the analytical model. The nonlinear FEM program, ABAQUS, was used to simulate the responses of the specimen. The base shear versus the story drift relationships obtained from the tests and the FEM analytical results are quite agreeable in all aspects of the responses. The analytical results confirm that the magnitude of the severe out-of-plane buckling of the braces can be accurately simulated. The test results show that ductile brace fracture occurred when the brace were subjected to a number of large out-of-plane deformation cycles and localization of the plastic hinge. This localized hinge formations can be accurately simulated in the ABAQUS model. FEM analyses also illustrate that the brace members take about 60% story shear when the inter-story drift is greater than 0.02 radians. Finally, this paper summarizes the procedures for analyzing the SCBFs.

Keywords: Concentrically braced frame, Finite element analysis, flexural buckling, local buckling.

Introduction

Special concentrically braced frame (SCBF) has been a rather common lateral force resisting system for buildings. Their high strength and stiffness properties permit to effectively achieve serviceability performance limit states during small and frequent earthquakes. In order to assure the life safety and collapse prevention during the large and infrequent seismic events, SCBFs need inelastic deformation and energy dissipation capacity. SCBFs develop cyclic inelastic deformations through axial yielding and post buckling deformations of the brace. Braces are normally connected to the beams and columns in the braced frame through gusset plate connections. The SCBF gusset plate connections must sustain large inelastic deformations and rotations when the brace buckles, and support the full tensile and compressive capacities of the brace during

significant cyclic loading. For resisting the expected yield capacity of the brace, current AISC seismic design provisions (AISC, 2005) for SCBFs require that the gusset plate be stronger than the brace. Thus, the geometric limit of “2t” requirement (illustrated in Fig. 1a) is used to assure that gusset plate will permit plastic rotations for brace out-of-plane buckling. In order to improve the behavior and performance of the gusset plate connections, the research team at the University of Washington proposed another gusset plate clearance requirement (Lehman et. al, 2008). The proposed clearance requirement uses an elliptical line to define the “8t” clearance instead of the “2t” linear clearance as shown in Fig. 1b. These two clearance requirements have been used to design the gusset plates for test specimens in this study. A full scale 2-story steel SCBF was tested three times in National Center for Research on Earthquake Engineering (NCREE) in Taiwan. This cooperative

¹ Professor, National Taiwan University and Director of NCREE, kctsai@ncree.org.tw

² Associate Research Fellow, National Center for Research on Earthquake Engineering, kclin@ncree.org.tw

³ Assistant Research Fellow, National Center for Research on Earthquake Engineering, cywei@ncree.org.tw

⁴ Assistant Research Fellow, National Center for Research on Earthquake Engineering, hank@ncree.org.tw

⁵ Former Graduate Student, National Taiwan University, r95521202@ntu.edu.tw

⁶ Graduate Student, University of Washington, jako9@u.washington.edu

⁷ Graduate Student, University of Washington, kclark4@u.washington.edu

⁸ Professor, University of Washington, croeder@u.washington.edu

project is among researchers from Taiwan and U.S. to investigate the seismic design methods for brace-to-gusset connections. Tests HSS-8t and HSS-2t were conducted using hollow structural section braces by two aforementioned brace-to-gusset details. The WF-8t test using the wide-flange section braces was conducted to compare the responses with the HSS-8t. The main purpose of this paper is to summarize the development and validation of the finite element model through comparisons of experimental and analytical responses.

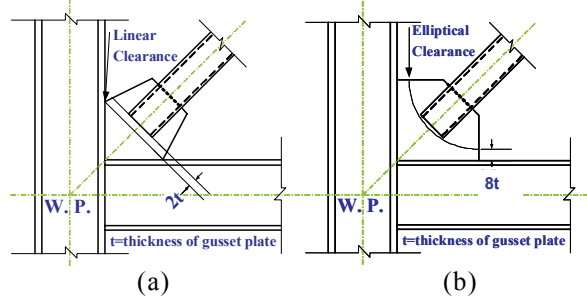
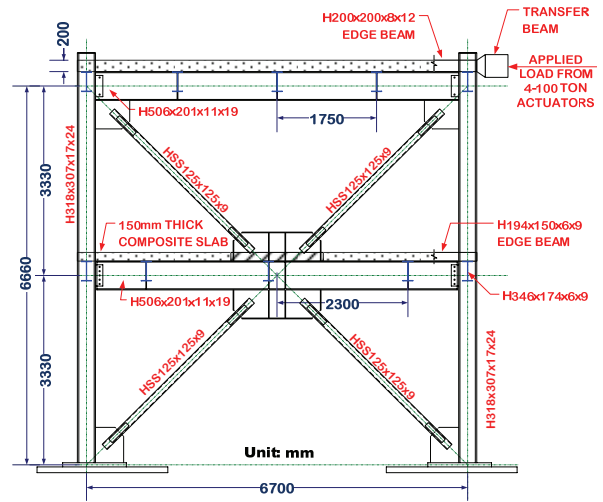


Fig. 1 Clearance requirements of gusset plates
 (a) Current AISC 2t requirements
 (b) The UW proposed 8t requirements

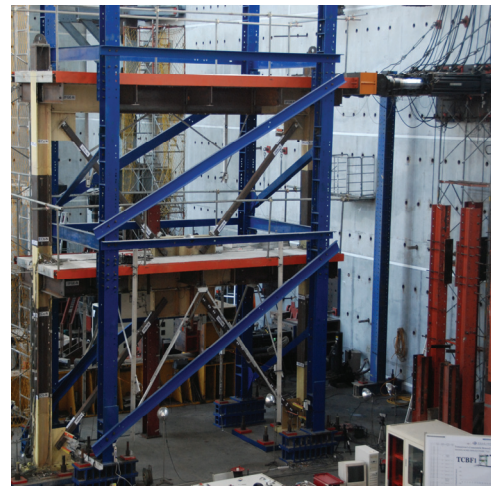
Experimental Program

The test specimen (Fig. 2) is a single bay, two-story X-bracing concentrically braced frame consisted of two beams (H506x201x19x11) and two columns (H318x307x17x24). The height of each story is 3.33 meters and the column center-to-center spacing is 6.67 meters. All beams and columns material were A572 GR50 steel. The two top beam-to-column joints were welded moment connection. Four steel braces were installed in the specimen, arranged in a multi-story cross-brace configuration and used six gusset plates to connect with the beams and columns. In the Phase I test, denoted as Test HSS-8t adopted the A500 grade steel tubes (HSS125x125x9mm) as braces, and gusset plates were designed using the 8t elliptical clearance details. In the Phase II test, wide-flange sections (H175x175x7.5x11) made of A36 steel were used. The gusset plates in the Test WF-8t were designed using the 8t elliptical clearance. In the Phase III test (Test HSS-2t), A500 steel tubes (HSS125x125x9) were used as braces and the gusset plates were designed using 2t linear clearance. The thickness of the gusset plates in 8t case is 10mm, and in 2t case it is 20mm. All gusset plates are A572 GR50 steel. The detailed dimension of specimen is shown in Fig. 2a. Additional details can be found in the references (Lin et al., 2009 and Tsai, 2008). In order to minimize the out-of-plane displacement of the two-story frame, a separate lateral supporting frame was built around the specimen. Only the in-plane displacements of the frame were imposed in the test. The experimental setup including the specimen and the lateral support is shown in Fig. 2b. The loading protocol adopted is shown in Fig. 3,

which is based on ATC-24 (ATC, 1992) and SAC recommendations. Other detailed descriptions of test specimen and test results are documented in the references (Lin et al., 2009 and Powell et al., 2008).



(a) Frame elevation



(b) Experimental setup

Fig. 2 Setup of Specimen HSS-8t

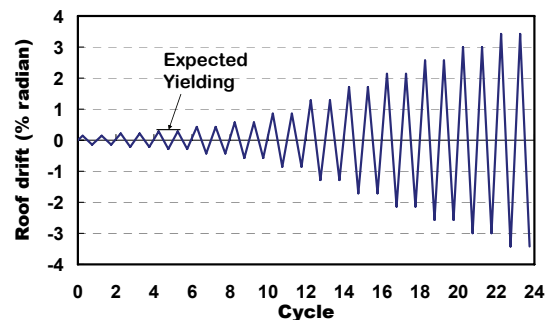


Fig. 3 Loading protocol

Comparisons of Experimental and Analytical Results

In order to access the accuracy of the analytical model and procedures, comparisons between the

FEM (ABAQUS, 2006) and experimental responses are made as following. Fig. 4 shows the base shear versus roof drift relationships of the three tests. The overall ABAQUS responses agree rather well with the test results for Specimen HSS-8t as shown in Fig. 4a. The Figs. 4b and 4c show that the ABAQUS models for Specimens WF-8t and HSS-2t can capture the elastic stiffness of the two specimens quite accurately. However, the FEM failed to predict the cyclic peak strength of the two specimens. It is important to note that the same moment resisting frame was used in all these three tests. Fig. 5 shows the detailed comparisons made between FEM and test results for Specimen HSS-8t at different test stages. It is apparent that ABAQUS model predicted the cyclic response rather satisfactorily at these different levels of frame deformations. Test results show all the braces buckled before the fracture occurred. Fig. 6 shows the analytical and experimental brace out-of-plane displacement versus roof displacement relationships. Except for Specimen HSS-8t (Fig. 6a), the other two analytical results agree with the experiment results. This is due to the fact that twisting on the lower floor slab during Test HSS-8t is much significant than other two tests. Fig. 7 shows some local analytical and experimental responses of Specimen HSS-8t. The plastic hinge location and the shape of the brace local buckling observed in ABAQUS analysis agree well with test results of Specimen HSS-8t (Fig. 7a). The severe gusset plate yielding state in the specimen and the stress distribution of the gusset plate in ABAQUS model at a roof drift of 0.026 radians are shown in Fig. 7b. Fig. 8 shows the experimental and analytical brace axial forces versus roof drift relationships for the first six cycles of loads. The experimental axial forces were computed from the averaged strains measured at the 1/4 point along the brace centerline. Fig. 8 confirms that the analytical brace forces in the elastic stage agree very well with the test results. Fig. 9 shows the positive shear forces resisted by the braces and the two columns as roof drifts increased in three ABAQUS models. The ABAQUS analytical results illustrate that the two brace members carry about 60% story shear when the inter-story drift is greater than 0.02 radians.

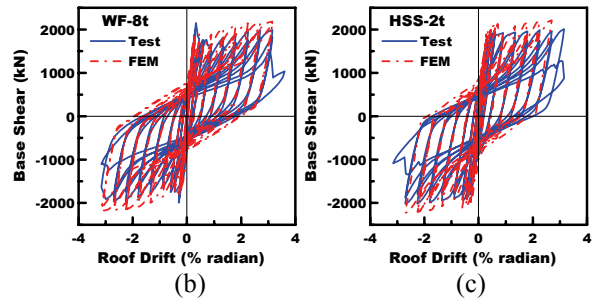
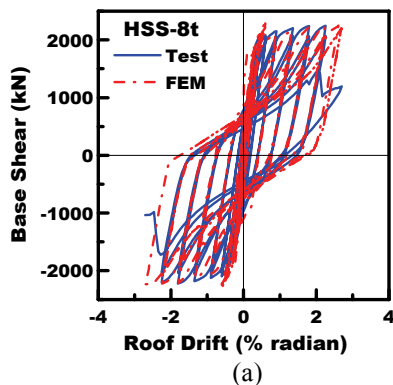


Fig. 4 Base shear versus roof drift relationships

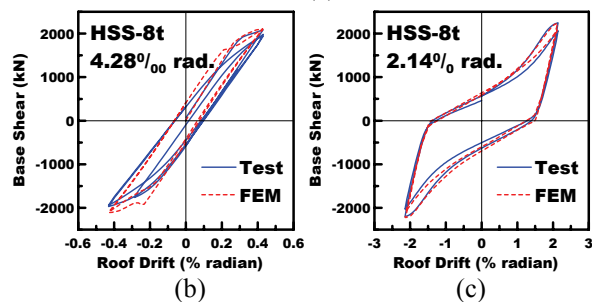
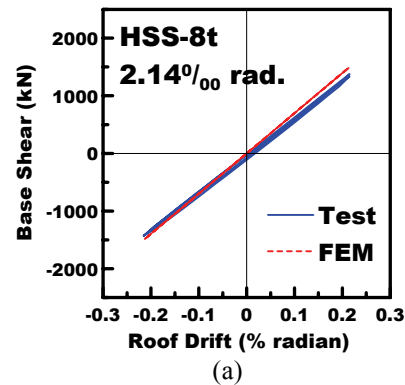


Fig. 5 Base shear versus roof drift relationships at various level of frame deformation for HSS-8t

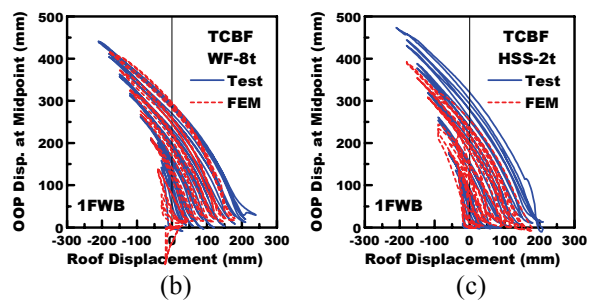
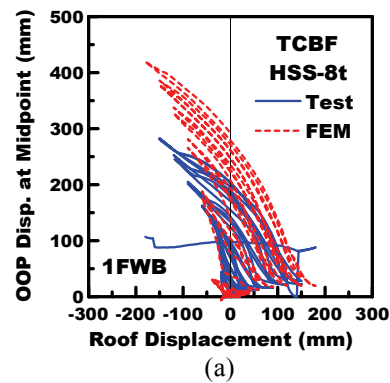


Fig. 6 Out-of-plane displacement comparisons

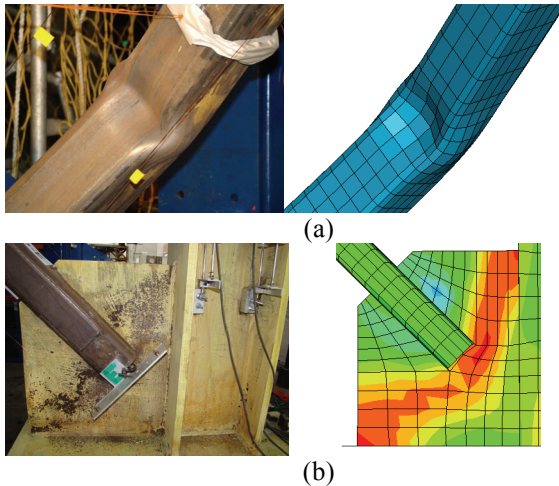


Fig. 7 Analytical and experimental buckled configurations of HSS-8t

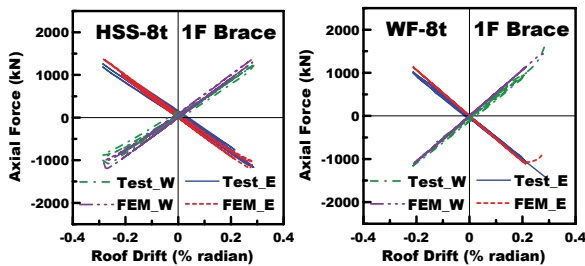


Fig. 8 Experimental and analytical brace force versus roof drift relationships

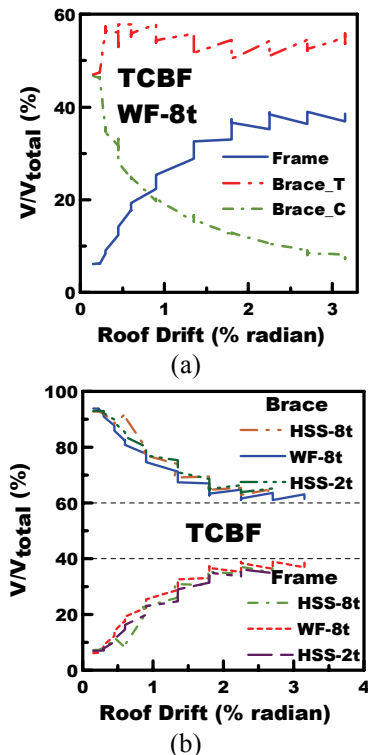


Fig. 9 Absolute shear force ratio versus roof drift relationships

Summary and Conclusions

Based on the tests and the analysis, the summary and conclusions can be drawn as follows:

- Test results show that the energy-dissipation performance of these three SCBF specimens using the X-brace configuration is quite good. No any significant strength or stiffness degradation was found before the fracture occurred in the braces during the tests.
- The total drift capacity for three tests is 4.24% (HSS-8t), 5.86% (WF-8t) and 5.44% (HSS-2t) radians, respectively. This suggests that the ductility of SCBF specimen using the wide-flange braces is better than specimen using tube braces.
- The cyclic performances of the concentrically braced frame specimens can be satisfactorily simulated by the ABAQUS models. This suggests that ABAQUS can be effectively used for research on seismic design of CBF systems.
- In the first six cycles, about 90% of the lateral forces were carried by the two braces. However, the lateral forces resisted by the braces decreased when the brace buckling occurred. The tension brace maintained to resist about 50% of the story shear as roof drift increased. The ABAQUS analytical results illustrate that the two brace members carry about 60% story shear when the inter-story drift is greater than 0.02 radians.
- The analytical assumptions in this study including initial imperfection “L/1000” and neglecting the concrete floor slab appear reasonable for the simplified models.

Reference

- ABAQUS (2006), “ABAQUS Analysis User’s Manual”, ABAQUS Inc., Version 6.6.
- AISC (2005), “Seismic Provisions for Steel Buildings”, AISC/ANSI Standard 341-05, *American Institute of Steel Construction*, Chicago, IL.
- Applied Technology Council (1992), “Guidelines for Cyclic Seismic Testing of Components of Steel Structures”, ATC-24, Redwood City, CA.
- Lehman, D. E., Roeder, C. W., Herman, D., Johnson, S. and Kotulka, B. (2008), “Improved Seismic Performance of Gusset Plate Connections”, ASCE, *Journal of Structural Engineering*, Vol.134, No. 6, Reston, VA, pp.890-901.
- Lin, C.H., Tsai, K.C., Wei, C.Y., Powell, J., Clark, K. and Roeder, C. (2009), “Cyclic Tests of A Full-Scale 2-Story Steel Concentrically Braced Frame”, Proceedings of 5th International Symposium on Steel Structures, Hotel Prima Seoul, Korea, March 12-13.
- Powell, J., Clark, K., Tsai, K.C., Roeder, C. and Lehman, D. (2008), “Test of a Full Scale Concentrically Braced Frame with Multi-story X-bracing”, *Proceedings*, ASCE SEI 2008 Structures Congress, Vancouver, Canada.
- Tsai, C.Y. (2008), “Performance and analysis of a full scale special concentrically braced frame”, National Taiwan University, Master thesis, Taipei, Taiwan. (*in Chinese*)

Turning the Building into A Smart Structure: Integrating Health Monitoring

Kung-Chun Lu¹, Jian-Huang Weng¹, Chin-Hsiung Loh¹,

盧恭君¹, 翁健煌¹, 羅俊雄¹

Abstract

The objective of this paper is to develop a novel sensing system which can conduct continuous monitoring of a building structure and generate a monitoring report. The building monitoring data will focus on the ambient vibration responses. Two servers are used in this SHM system: 1) wireless measurement server which takes care of measuring and archiving all the structural responses and environmental situation, and 2) analysis server which conducts the signal processing on the received signals. The measurement server is in charge of the collection of signals and broadcast wirelessly from all sensors to the analysis server. Dominant frequencies and mode shapes of the building will be estimated in the analysis server from the continuous monitoring of the ambient vibration data (velocity) of the building by using AR-Model, Frequency Domain Decomposition and Stochastic Subspace Identification methods. The proposed continuous monitoring system can effectively identify the building current health condition and generate a report to the owner.

Keywords: Wireless sensing system, stochastic subspace identification, frequency domain decomposition, AR-model

Introduction

Mitigation of the affects of natural hazards on civil and mechanical infrastructure requires that both sensing and control technologies be installed in structures. Specifically, sensors are responsible for recording the response of the structure to time-varying loading conditions while actuators (active and semi-active) are used to physically limit structural response so as to reduce structural damage and avoid catastrophic global collapse. More specifically, “smart” refers to the augmentation of computational intelligence with the sensor or actuator to allow each device to process its own data for determining damage and deciding optimal control actions that limit the dynamic response. Over the past decade, many innovative smart sensing and smart control devices have been explored, with test and field results showing tremendous promise for more widespread implementation in new and existing structural systems. Since the mid 1990’s, researchers have devoted in the fields of sensors, data interrogation algorithms, and smart materials as they apply to mitigation of natural hazards. The pursuit of smart structure research has

ushered in a new era of unprecedented multidisciplinary research encompassing a variety of engineering disciplines including, but not limited to, smart materials (materials science and engineering), electronics (electrical engineering), applied mechanics, structural and system dynamics (mechanical engineering), signal processing (computer science), and design and construction (civil engineering). While great advances have already been made, resulting in safer and more durable civil and mechanical infrastructure systems, catastrophes still occur.

The networks of densely deployed smart sensors have the potential to improve structural health monitoring dramatically. To effectively detect arbitrary damage in structures, a dense array of sensors distributed over the entire structure will be required. The essential difference between a standard sensor and smart sensor is the latter’s flexible communication and information processing capability. Each sensor has an on-board microprocessor that can be used for digital signal processing and self-diagnostics. Furthermore, all sensor platforms have far employed wireless communication technology. Some of the efforts in developing the

¹National Taiwan University, Department of Civil Engineering, Taipei, Taiwan

smart sensors for application to civil engineering structures were presented by [1]. Several SHM applications with smart sensors have been studied using both scale models and full-scale structure [2-7].

The objective of this paper is to develop a continuous monitoring system for building structure. Based on the wireless sensing and monitoring system the ambient vibration system was developed. The smart sensors are employed in the same manner as traditional wired sensors with all data being synchronously collected for processing at a centralized location. With the management of data processing and identification in the server, the dynamic characteristics of the building structure can be reported continuously.

Hardware Organization of Long Term Continuous Monitoring

For establishing the monitoring system the ambient vibration measurement system will be used. For this monitoring system the instrumentation system consisted of the following components:

- Transducers: Tokyo Sokushin VSE-15D velocity detectors with sensitivity factors of 0.25Volt/1 kine.
- Wireless sensing unit: each wireless sensing unit will have the voltage converters, microprocessor, AD convertor, communication module and power supply system.
- Servo Computer: one PC with wireless modem to serve as the trigger and recoding system.

The wireless sensing units used in this monitoring system replaced the traditional data acquisition system that uses cables. The wireless sensing unit includes three subsystems: the sensing interface, the computation core, and the wireless communication system. The sensing interface is responsible for converting the analog sensor signals into digital forms. The digital data is then transferred to the computational core by a serial peripheral interface (SPI) port.

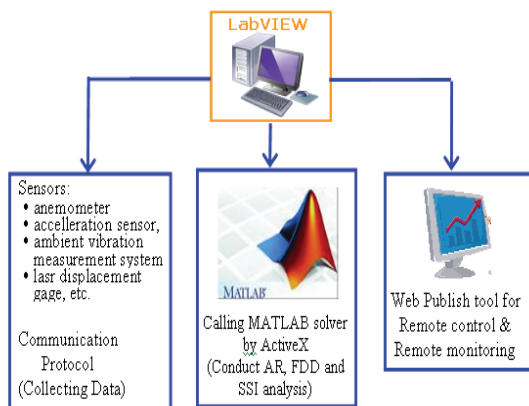


Figure 1: Hardware &Software arrangement of

structural health monitoring system.

External memory is associated with the computational core for local data storage and analysis. The Maxstream 24XStream wireless modem, operating on 2.4 GHz, is used for the wireless communication subsystem.

The hardware organization is arranged in the following steps (also shown in Figure 1):

The wireless sensing network is based on the Wireless Sensing and Monitoring Module (WiMMS sensing unit). The server program is based on LabVIEW which also supports the function of web server, remote control and monitoring.

The server is PC-based and LabVIEW can achieve MATLAB solver by ActiveX, and the engineer can easily integrate the developed structural health monitoring program into this system.

In the 2nd phase of hardware development the server will be replaced by Compaq RIO which is programmable automation controller. In this stage the embedded system will be more robust and simplified.

Depending on the objective of the structural monitoring; some computational programs will be embedded into the sensor node. The concept of distributed computation will be used and in this stage the monitoring system will be highly efficient and smart.

Software Design for Continuous Monitoring

To start the monitoring system the PC server will send a message to start the program and ask WiMMS to collect the data and send the data back to the server for analysis. Figure 2 shows the flow chart of the monitoring system. To ensure there is no mistake during the process of the monitoring, the system was design with several check points and by-pass, so as to make sure there is no error message in collecting and analyzing the data. The most important one in developing the monitoring system is the communication between the sensing unit and the receiver unit, i.e. to make sure there is no error in the communication between sensing unit and the PC server. To avoid this situation, each action in the sensing unit and in communication must be checked without any error message. First, each sensing unit is boot up to collect the vibration signal, and then check all the units are ready to broadcast the data. Second, make sure all the data was received by the server. Detail of the data communication and check pass is shown in Figure 3.

Data collected from the wireless sensing system will be processed in the server to extract the dynamic characteristics of the structure. In this report efforts will be put on the development of automatic analysis

communication and synchronized sensing. Emphasized in this paper is the procedures for error check and pass in this continuous system. The locations of smart sensors can be modified due to the irregularity of the building structure. Integration of different types of sensors can also be used, such as the laser displacement gage for measuring the deformation of isolator, Gill anemometer for measuring the wind speed, etc. Through experimental verification the proposed monitoring system demonstrate the efficacy of the monitoring system developed herein.

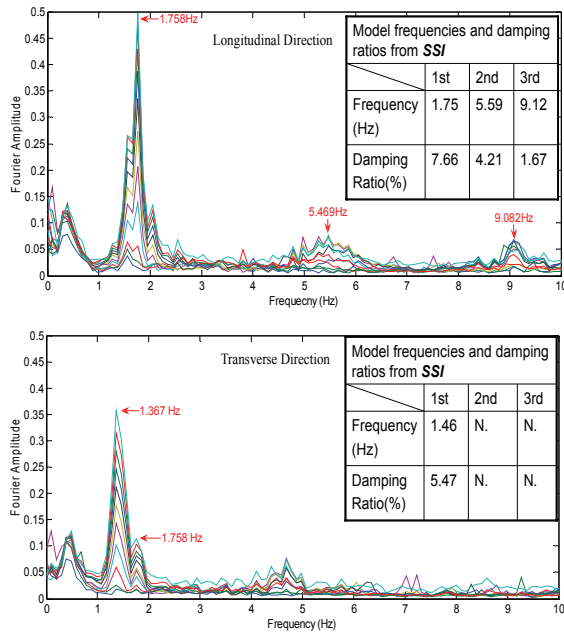


Figure 5: Fourier amplitude spectrum from the recorded ambient vibration data of CE building in both longitudinal and transverse direction. The identified natural frequencies and damping ratios from SSI method is also shown.

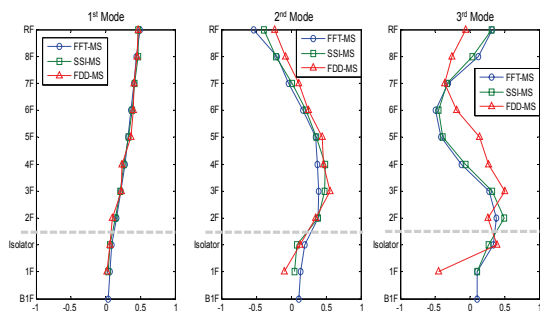


Figure 6: Identified mode shapes from three different methods: FFT, FDD and SSI (longitudinal direction).

Acknowledgements

The authors would like to thank the support from Taiwan National Science Council under contract No.

NSC 96-2221-E-002-121-MY3 and the National Taiwan University under the excellent research program of project No. 95R0066-BE03-05. Support from National Central Weather Bureau is also acknowledged.

References

- [1] Straser, E.G. and Kiremidjian, A.S. 1998. "A modular, wireless damage monitoring system for structures," The John A. Blume Earthquake Engineering Center Technical Report, 128.
- [2] Lynch, J.P., Law, K.H., Kiremidjian, A.S., Carryer, E., Kenny, T.W. et al. 2002. "Validation of a wireless modular monitoring system for structures," Proc. SPIE Smart Structures and Materials: Smart systems for Bridges, Structures, and Highways, San Diego, CA 4696(2), 17-21.
- [3] Lynch, J.P., Wang, Y., Law, K.H., Yi, J.H., Lee, C.G. and Yun, C.B. 2005. "Validation of a large-scale wireless structural monitoring system on the Geumdang bridge," Proc., the Int. Conference on Safety and Structural Reliability, Rome, Italy.
- [4] Tanner, N.A., Wait, J.R., Farrar, C.R., and Sohn, H. 2003. "Structural health monitoring using modular wireless sensors," J. of Intelligent Material Systems and Structures, 14(1), 43-56.
- [5] Nagayama, T., Ruiz-Sandoval, M., Spencer Jr., B.F., Mechitov, K.A., Agha, G. 2004. "Wireless strain sensor development for civil infrastructure," Proc., 1st Int. Workshop on Networked Sensing Systems, Tokyo, Japan, 97-100.
- [6] Nitta, Y., Nagayama, T., Spencer Jr, B.F., Nishitani, A. 2005. "Rapid damage assessment for the structure utilizing smart sensor MICA2 MOTE," Pro., 5th Int. Workshop on Structural Health Monitoring, Stanford, CA., 283-290.
- [7] Weng, J.H., Loh, C.H., Lynch, J.P., Lu, K.C., Linn, P.Y., Wang, Y., 2008. "Output-Only Modal Identification of a Cable-Stayed Bridge Using Wireless Monitoring Systems," J. of Engineering Structure, 30 (2), 1802-1830.
- [8] Rune Brincker, Lingmi Zhang and Palle Andersen, 2001. "Modal identification of output-only systems using frequency domain decomposition," Smart Materials and Structures, 10, 441-445.
- [9] P. Van Overschee and B. De Moor. 1996. Subspace identification for linear systems. *Dordrecht: Kluwer academic publishers.*
- [10] B. Peeters. 2000. System Identification and damage detection in civil engineering. *Ph.D. Thesis, Katholieke University, Leuven, Belgium.*
- [11] M. Verhaegen and P. Dewilde. 1992. Subspace model identification-Part I, *International Journal of Control*, Vol 56, 1187-1210.

Numerical Simulation and Experimental Verification of Semi-active Control of Cable Vibration Using MR Damper

Pei-Yang Lin¹ Shieh-Kung Huang² Kweu-Shi Cheng³ and Chin-Hsiung Loh⁴

林沛暘¹、黃謝恭²、鄭揆喜³、羅俊雄⁴

Abstract

This paper presents the numerical simulation and experimental verification of a semi-active cable vibration control system. The finite-element analysis “ABAQUS” was used to design and simulate the dynamic characteristics of a cable structure. The system matrixes ‘M’, ‘C’ and ‘K’ of the simplified cable model were generated from the finite element model. A 3 kN MR damper manufactured by Lord Co. was connected to the cable to reduce its vibration. Through a systematic performance test and system identification procedure, the modified Bou-Wen model was generated to represent the nonlinear behavior of the MR damper. Based from the simplified cable model and MR damper model, the LQG with continuously-optimal control was used to design the semi-active control system. The scaled-down cable structure has been designed and built according to the finite-element model of ABAQUS. Suitable mass and cable force were added to make the cable vibration more realistic. A small shaker has been designed and mounted onto the cable to generate the excitations with different amplitudes and frequencies. Both passive and semi-active control cases have been tested. Through the numerical simulation and experimental test results, the semi-active cable vibration control system with MR damper can reduce well the cable vibration under different kinds of excitations. This investigation demonstrates the feasibility and capabilities of a cable vibration control system with MR damper..

Keywords: near-fault ground motions, quasi-dynamic model, variable rupture velocities, 1992 Landers Earthquake,

Introduction

As a critical member of cable-stayed bridge, stay cables play an important role of supporting the entire structure. Besides, long stay cables are prone to vibration induced by the structure to which they are connected and by weather conditions. Inherently low damping of stay cables makes them sensitive to various vibration induced from some sources such as traffic, wind and rain-wind vibrations. To solve these hazardous vibration problems, various measures have been developed. One of the effective ways is to install mechanical dampers near the anchorages of stay

cables. A number of methods have been proposed to mitigate the cable vibration. Pacheco et al. (1993) and Krenk (2000) proposed the passive control of cables using viscous dampers attached transversely to the cables. Full-scale application of the passive viscous dampers for cable vibration control had also been applied, such as the Aratsu Bridge (Yoshimura et al. 1989) in Japan and Normandie and Tatara Bridge (Virloguex et al. 1994) in France and Japan, respectively. Besides the passive control of cables, several recent papers have also shown that semiactive dampers may provide levels of damping far superior to their passive counterparts, such as Johnson et al. (1999,

¹ Research Fellow, National Center for Research on Earthquake Engineering, pylin@ncree.gov.tw.

² Assistant Research Fellow, National Center for Research on Earthquake Engineering.

³ Master student, Department of Civil Engineering National Taiwan University.

⁴ Professor, Department of Civil Engineering, National Taiwan University.

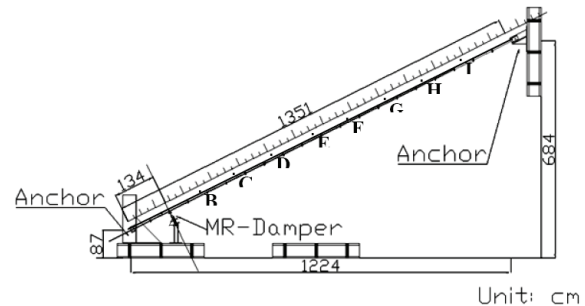
2000, 2002). It is believed that one of the effective alternatives to suppress hazardous vibration of stay cable is to use cable dampers. In order to design the cable damper (either passive or semi-active) optimally, it is necessary to exactly estimate the dynamic characteristics of existing cables. This paper concentrates on the tests of the stay cable, aimed at identifying the dynamic characteristics and comparing the damping performance of using single-damper setup in the in-plane direction. The free vibration response data of the stay cable as well as the force vibration responses were used to identify the amplitude-dependent frequency and damping of the stay cable with and without damper. From the results of these studies, more realistic model parameters of the system equation of motion can be generated for cable control research.

Experimental Setup

Fig. 1 shows the schematic diagram of vibration control testing of the cable. The suspended cable is 13.5m in length, and both ends of the cable were anchored to the reaction wall and the strong floor. The inclination angle is about 26 degrees. The cross-sectional area of the cable is 140 mm² and with a yield stress of 1670 MPa. A constant tensile force was applied to the cable. To maintain a similar dynamic characteristic to its prototype, 19 sets of mass block were hanged on the suspended cable. Each mass block weighs 16 kg, then, the total weight of the cable has risen to 320 kg. One MR damper has been connected perpendicularly to the stay cable at a distance of 10% of its total length from lower end. This MR Damper (RD-1005-3) was provided by LORD Corporation. The maximum output force of the damper is 3kN, maximum input voltage is 0.8V, maximum input current is 2.0A, and the stroke is +/-20mm. To measure the dynamic response of the cable, six accelerometers and LVDTs (Linear Variable Displacement Transformers) were mounted on points 'A' to 'E' and point 'T', as indicated in Figure 1. The implemented accelerometers are the Model 141A of SETRA, and LVDTs are the Temposonics of MTS. Moreover, two load cells were also used to measure the tensile force of the stay cable and the output force of MR damper. All those data were collected using data acquisition system (DAQ system). The DAQ system was conducted with IBM computer (ThinkPad T30) and dSPACE System (DS815), and data were recorded using ControlDesk software. For the forced vibration, a shaker working as an excitation source was placed at Node D. The shaker has a mass of 1.6kg which can rotate with a maximum of 2000rpm (corresponding to 4.44Hz). Fig. 2 shows the photo of the inclined stay cable. A photo of the shaker is also shown in the right of Fig 2.

To conduct the semi-active control of a cable, an MR damper was used. The characteristics of the MR damper must be developed. The performance test of the damper was conducted using random stroke with

constant voltage. The performance of the MR damper with a variety of currents needs to be developed. Based from the test data the Bouc-Wen model was used to simulate the hysteretic behavior of the damper. The force-displacement and force-velocity relationships of the MR damper under different applied voltage are shown in Fig 3. It must be noted that the dissipated energy increases as the supplied voltage increases (left), as well as the existing initial stiffness and Coulomb friction (right).



Yield strength (f)	233800 N
Cross section area (A)	140 mm ²
Yield force (Fy)	1670 N/mm ²
Length (L)	13.65 m
Inclined angle (θ)	26 °
Tensile force (Fc)	4.5 ton (= 44145 N)
Number of mass block	19
Mass of block (m)	16 kg

Fig. 1: A schematic diagram of vibration control testing of the cable and its related properties.



Fig. 2: Photocopy of the incline cable (left), prototype of cable exciter (right).

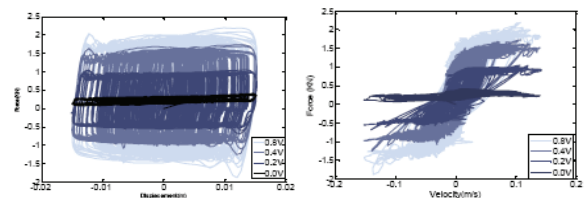


Fig. 3: the Voltage dependent force-displacement and force-velocity relationship of 3kN MR damper.

Vibration Control of Stayed Cable

To control the cable vibration using MR damper, three different control methods were used: passive

control (with constant voltage), LQR control with full-state feedback, and Sliding Mode Control using local measurement as feedback. For LQR control, the const function can be written in general discrete form

$$J_d = \sum_{k=k_0}^{k_s} \{z^T[k]Qz[k] + u^T[k]Ru[k]\} \quad (1)$$

Here, the weighting matrices, Q and R , are related to the full-state and the control forces, respectively. The goal of the objective function is to minimize the state responses from the time equal to k_0 to the time equal to k_1 . After transforming the function by the procedures of variation method, the new form of the function could imply the Ricatti equation. The solution of the Ricatti equation can be obtained by iterative calculation. The control gain, combined with the solution is given by

$$\begin{aligned} u[k] &= -(2R + B_d^T P[k+1] B_d)^{-1} B_d^T \\ &P[k+1] A_d z[k] = G[k+1] z[k] \end{aligned} \quad (2)$$

where $G[k+1]$ is the control gain, as shown

$$\begin{aligned} G[k+1] &= \\ &-(2R + B_d^T P[k+1] B_d)^{-1} B_d^T P[k+1] A_d \end{aligned} \quad (3)$$

and $P[k+1]$ can be solved from the Ricatti equation.

Due to the control gain related to the full-state as described above, an estimator to transform the measurement into the full-state is necessary for a complete control process in generating the desired force. The Kalman estimator was derived from the Kalman filter to predict the full-state vector. In this study, the cable acceleration response from node B, node E and damper force were used as feedback to calculate the commend voltage for the MR damper. As mentioned earlier, Kalman estimator was used to estimate the full-state of the system response. Four different sets of Q and R matrices were utilized in the control test. Fig. 4 shows the comparison on the displacement control performance at different node (with respect to passive-off case) among different control cases for case of excitation 780 rpm. It can be observed that most of the LQR control cases provide better displacement control performance as compare to passive-off control cases (with constant voltage). Of course, different set of Q and R values can have different control performance. It has to be pointed out that the control performance using passive MR damper with high voltage (such as 0.1 Volt, 0.2 Volt etc.) is not good at some nodes near the center portion of the cable in comparison to the passive-off case. Because the damper with high voltage will also cause the increase of the yield force of the damper, therefore, the boundary condition of the cable may be modified due to the implementation of stiffer damper and the structural model for control will be different from the original one. Similar control method was also applied to the same cable but subjected to the forced excitation

with 1400rpm.

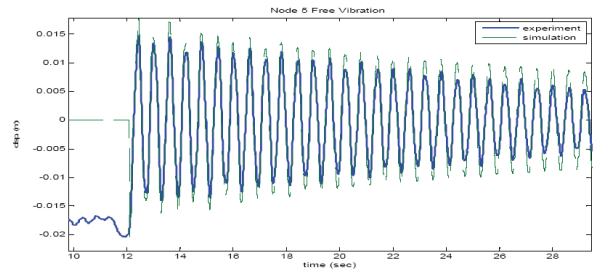


Fig. 4: Comparison on free vibration at Node 5 between simulation and experiment.

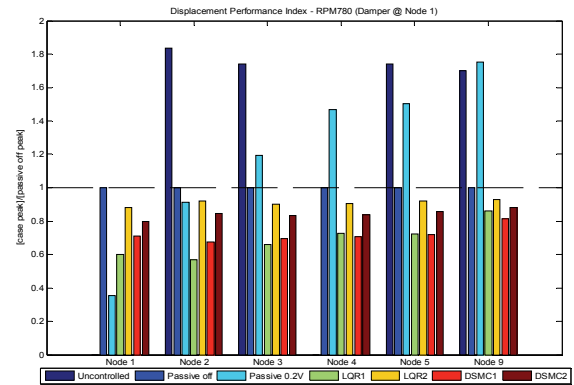


Fig. 5: Comparison on the displacement control performance among different control cases (using LQR control subject to excitation with 780rpm)

Fig. 5 shows the comparison on the displacement control performance at different node. Similar results can be observed. It can be noted that for the control of cable displacement responses the proposed LQR can provide good control performance, but on the contrary, the acceleration response can not be suppressed under the same control situation. The LQR full-state feedbacks control method is one of the centralized control algorithms which require the full-state response data to calculate the control force. In order to reduce the wiring problem as well as the accuracy in the estimation of full-state response, a decentralized sliding mode control (DSMC) algorithm was used to control the cable vibration. The theory on the sliding mode control (SMC) is to design controllers to drive the response trajectory into the sliding surface, whereas the motion on the sliding surface is stable [Lu, et al. 2008]. For linear structures, the r dimensional sliding surface $S=0$ for r controllers (dampers) can be a linear combination of the state variables, i.e.

$$S = PZ = 0 \quad (4)$$

where S is an r -vector consisting of r sliding variable, i.e.

$$S = [S_1 \ S_2 \ \dots \ S_r]^T \quad (5)$$

For the decentralized SMC, the i^{th} sliding variable S_i for the i^{th} damper is chosen as a function of x_{ki} and \dot{x}_{ki} ,

i.e.,

$$S_i = \alpha_{ki}x_{ki} + \dot{x}_{ki} \quad (6)$$

where $ki \langle$ is the pole of the sliding surface. For the motion to be stable on the sliding surface, $ki \langle$ should be positive, i.e., $\alpha_{ki} > 0$.

for $i=1, 2, \dots, r$ and the elements α_{ki} and 1 are at the locations of ki and $ki+n$, respectively. Based from the sliding mode control, the Lyapunov function is expressed as

$$V = \frac{1}{2}S^T S \quad (7)$$

Based on the model of the stay cable, G and λ can be derived. Since there is only one damper located at node A, the control force can be calculated (with $i=1$)

$$u_1 = -m_1(\alpha_1\dot{x}_1 + x_1A_{(10,1)} + \dot{x}_1A_{(10,1)}) - \delta_1(\alpha_1x_1 + \dot{x}_1)\frac{1}{m} \quad (8)$$

Where $\alpha_1 > 0$; $\delta_1 > 0$ and A is the system matrix.

Discussion on the experimental results

Two different control algorithms were applied to control the cable vibration. Comparison on the control effectiveness using these two methods (LQR and DSMC) with respect to the passive control case was made. For LQR control acceleration response from node B and node E and damper force were used as feedback signals. The achievement performance of semiactive MR damper in comparison with passive device may be seen in Fig. 5. It shows the displacement performance for different control case under the excitation of 780 rpm force excitation at node E. Four different LQR control cases were used. It is shown that under the excitation of 780 rpm at node E, the displacement control at node far away from the damper location is better than the passive control case. For displacement control of cable vibration the LQR method can provide good control effectiveness, but for acceleration control the LQR method can not provide good results.

Conclusions

Viscous dampers near the cable anchorage are a viable means to raise the model damping of long stay cables and suppress most types of vibrations, provided there is enough distance from the cable anchorage to the point of attachment of the damper. The experiments reported in this paper result in the following conclusions:

- Forced vibration tests have been conducted in a stay cable to experimentally determine the damping of the cable attached with MR damper and without the damper. The results provide information to develop theoretical model of the cable for control purpose.
- MR damper can provide considerable damping force even at passive mode. It is a good choice for adding supplementary damping to reduce the cable vibration, particularly the control of displacement response.
- Depending on the capacity of the MR damper, the control of acceleration response of cable may not be effective. With the installation of MR damper, the stiffness of the cable-MR damper system will increase (the change of boundary condition of the cable) which may cause the amplification of acceleration response.
- The proposed LQR and DSMC methods can control the displacement response of cable effectively. The DSMC can also reduce the cabling problem on the implementation of control system and, the most important one, only the local response data was used as feedback to calculate the control force.

References

- Krenk, S., "Vibrations of a taut cable with an external damper," J. of Applied Mechanics, ASME, 67, 2000, 772- 776.
- Yoshimura, T.A., Inoue, K. Kaji, and Savage, M., "A study on the aerodynamic stability of the Aratsu Bridge," Proceedings of the Canada-Japan Workshop on Bridge Aerodynamics, Ottawa, Canada, 1989
- Virloguex, M, et al., "Design of the Notmandie Bridhe," Proceedings of the International Conference on Cablestayed and Suspension Bridges, IABSE, 1994, Vol.1 605-630.
- Johnson, E.A., Spencer, B.F. Jr., Fujino, Y., "Semiactive damping of stay cable: A preliminary study," Proceedings of the 17th International Modal Analysis Conference (IMAC XVII), SEM, Bethel, Connecticut, 1999
- Johnson, E.A., Baker, G.A., Spencer, B.F. Jr., Fujino, Y., "Mitigating stay cable oscillation using semiactive damping," Smart Structures and Materials 2000: Smart Systems for Bridges, Structures, and Highways (S. C. Liu, ed.), Proceedings of SPIE, 3988, 2000, 207-216.
- Lu, K.C., Loh, C.H., Yang, J.N. and Lin P.Y., "Decentralized Sliding Mode Control of Building Using MR Dampers," Smart Material and Structures, 2008 March.

A Study of Soil-structure Interaction Using In-situ Tests of School Buildings

Yung-Yen Ko¹

柯永彥¹

Abstract

In conventional structural seismic analysis, the rigid base model is usually adopted without considering the flexibility of the ground, leading to inaccurate estimation of the vibration characteristics and the seismic response of the structure. In 2007, several in-situ tests were conducted on the school buildings at the Guanmiao Elementary School in Tainan, Taiwan. For the study of soil-structure interaction (SSI) effects, the forced vibration test was performed, and the deformation of the foundation system was measured during the pushover test. In this study, the results of these in-situ tests are presented and discussed, and the finite element (FE) models of the school buildings were generated for the simulation of the forced vibration test and for the pushover analysis in order to investigate the difference between the rigid base model and the flexible base model.

Keywords: school building; pushover test; forced vibration test; SSI effect; FE analysis.

Introduction

The ATC-40 capacity spectrum method (ATC, 1996) is often used for the seismic evaluation of RC buildings. The pushover analysis is first performed for the roof displacement versus base shear, i.e., the capacity curve. Then the design spectrum is introduced as the seismic demand. Thus, the performance point is obtained, representing the structural response under the design earthquake level. Conventionally, the rigid base model (Fig. 1(a)) is adopted in the pushover analysis without considering the soil-structure interaction (SSI) effects.

There are 3 primary categories of the SSI effects in seismic evaluation: (a) introduction of flexibility to the soil-foundation system (Fig. 1); (b) filtering of the ground motions transmitted to the structure; (c) dissipation of energy through radiation and hysteretic soil damping. (a) is partially addressed in ATC-40. The reduction of the shaking demand caused by (b) and (c) are considered in FEMA-440 (ATC, 2005). For the conservation reason, focus will be on the flexible foundation effects in this study.

For the real assessment of the seismic capacity and the verification of the benefit of retrofit measures, several field tests were executed at the Guanmiao Elementary School in Tainan, Taiwan in 2007. The

specimens included the non-retrofitted school building in its as-built form as the benchmark specimen, and the one retrofitted by post-tensioned rods which provide supplementary lateral resistance, as in Fig. 2 (Chiou *et al.*, 2008). Both were 4-bay/2-story RC frames infilled partially with brick walls.

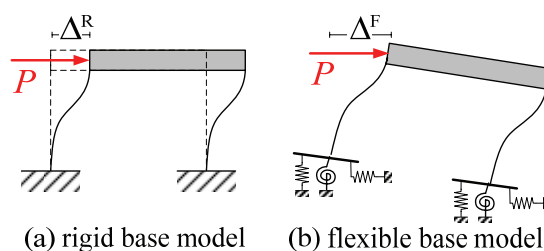


Fig. 1 Models for the pushover analysis.



Fig. 2 Post-tensioned specimen for in-situ test.

¹ Associate Research Fellow, National Center for Research on Earthquake Engineering, yyko@ncree.org.tw.

For the study of the flexible foundation effects, the forced vibration test (FVT) was conducted on the benchmark specimen. The eccentric mass vibrator system that generates harmonic force was mounted on the roof, and the loads were applied along the long and the short directions of the structure, respectively. The velocity sensors were used for vibration measurement. In addition, the deformation of the foundation system was measured during the pushover tests on both specimens, including the tilt angle, the horizontal displacement, and the settlement. The target of measurement is the intersection of the column and the foundation beam at columns C1, C3, and C5 (Fig. 2).

Test Results

Long direction Forced Vibration Test

For each test frequency, the amplitude of the harmonic velocity time history was deduced to represent the excited response. Because the forces generated in the test were frequency-dependent, the normalized response function was further calculated through dividing the response at each test frequency by the magnitude of the applied force in order to clearly characterize the vibration of the structure.

For the long direction test, the response function in the long direction at the roof is shown in Fig. 3. The response function curves of the four measured column positions are similar, the peaks all locating at 3.8 Hz. As for the response at the 1st floor, though the magnitude is much less, an obvious peak at 3.8 Hz is also observed. Therefore, the natural frequency of the entire soil-structure system for the translation mode in the long direction can be regarded as 3.8 Hz.

Short Direction Forced Vibration Test

Fig. 4 shows the roof response functions for the short direction test. The characteristics of the response functions are different between the A1-C1 and the A5-C5 sides of the structure. For columns A5 and C5, the response function curves show a local peak at 7.5 Hz, and a possible peak may be located above 8 Hz. As for columns A1 and C1, the responses are apparently smaller than those of columns A5 and C5, and the major peak locates at the frequency of 7.0 Hz.

From a further deduced response function of the roof twist angle and the modal shape of the structure, it can be seen that the response of columns A5 and C5 is dominated by the twist between the 2nd floor and the roof, which is due to the insufficient in-plane stiffness of the partition brick wall at the A5-C5 side. (Ko and Hsu, 2008). Therefore, the peak of the response functions of the A1-C1 side, 7.0 Hz, is more likely to be the natural frequency of the benchmark specimen for the translation mode in the short direction. It is believed that the configurations of typical school buildings in Taiwan make the stiffness of the structure in the short direction larger than in the long direction, which is verified by this FVT.

In general, the FVT can successfully cause the structure to vibrate, including the foundation. Besides, the larger the stiffness of the superstructure, the easier to excite the foundation. The response function of the FVT helps to characterize the soil-structure system as a whole, just as in a flexible base condition.

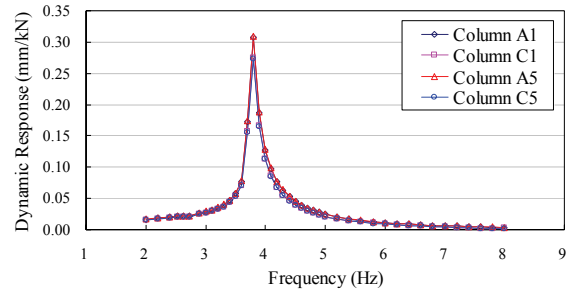


Fig. 3 Roof response functions in long direction test.

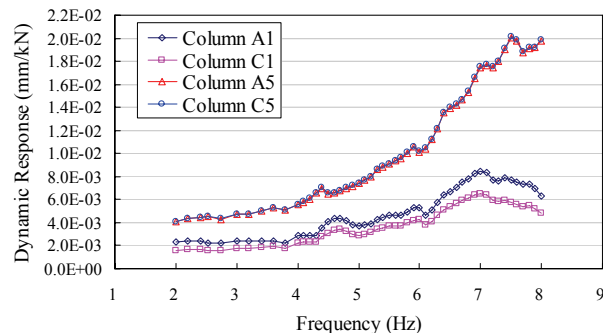


Fig. 4 Roof response function in short direction test

Foundation Deformation in Pushover Test

Since the lateral load was applied rightward in the viewpoint of Fig. 2, the clockwise tilt, the rightward displacement, and the upward displacement were taken as positive. The results of the pushover test on the post-tensioned specimen were depicted in Fig. 5. Fig. 5(a) gives the roof displacement versus the base shear. It is noted that only the foundation deformation measured before the maximum capacity reached was valid since the damage initiated with debris falling down when the strength of the structure decreased, causing great errors on the measurement.

Fig. 5(b) shows the tilt angle of the foundation at columns C1, C3, and C5 versus the base shear. At column C3 the tilt is apparently larger, yet the magnitude is only about 0.1° at the maximum capacity of the specimen. Besides, the nonlinearity is observed from the unloading and reloading curves. Fig. 5(c) shows the horizontal displacement of the foundation. Invalid leftward displacement was measured at columns C1 and C3 because of the movement of the reference frame for LVDT. At column C5, the frame was well-fixed, and the displacement is about 1.2 mm to the right at the maximum capacity. The nonlinearity is also observed. The vertical displacement of the foundation is given in Fig. 5(d). The footing rose at column C1 and settled at column C5. The structure subjected to lateral load showed an overturning tendency globally.

In the pushover test of the benchmark specimen, the trend of the foundation deformation is analogous to that of the post-tensioned specimen. The foundation deformability of these two specimens was found to be similar.

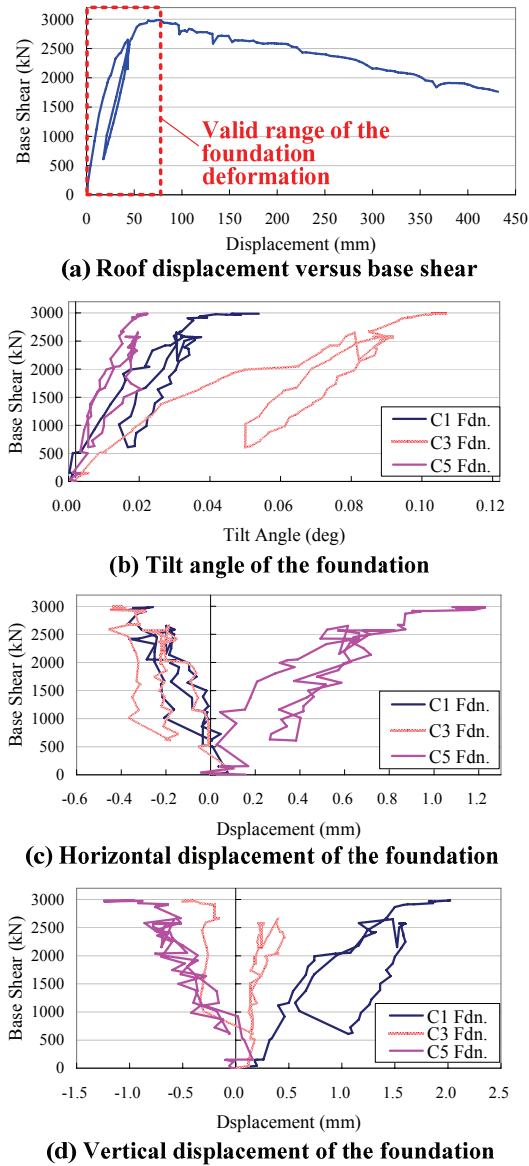


Fig. 5 Pushover test results of post-tensioned specimen

Numerical Simulation

Analysis for Forced Vibration Test

1. Analysis model

The ABAQUS code was adopted to establish the FE model of the benchmark specimen, as shown in Fig. 6. The analysis was executed in the rigid base and the flexible base conditions respectively. Only the long direction test was simulated here because of the smaller stiffness and the more regular structural behavior. Since the FVT is a small-strain test, a linearly elastic frequency domain analysis was performed for the harmonic responses of the structure.

The beam-column frame was composed of the Euler-Bernoulli beam element B33. The slab was generated by the shell element S4R. According to the suggestions proposed by Tsai *et al.* (2000), the brick wing wall was modeled as an equivalent compression-only spring, which is hinge-connected to the frame at its end and has the same stiffness as the brick wall, while the brick partition wall was modeled by the equivalent wide beam. The section and material properties of the structural components were specified according to the design and the sampling tests.

In the flexible base analysis, the soil-foundation system was modeled by the foundation beams and the spring elements placed at the intersections of the columns and the foundation beams, representing the footings. The spring stiffness was estimated based on the bearing stiffness parameters of embedded rigid plate in ATC-40 and the field soil properties.

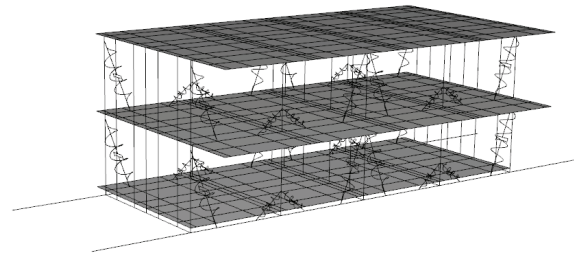


Fig. 6 FE model of the benchmark specimen.

2. Analysis results

Fig. 7 gives the response functions in the long direction at the center of the roof from the frequency domain FE analyses using the flexible base model and the rigid base model. From the comparison, it can be seen that the response function from the flexible base model is conformable to that from the field test. The peak is located at the frequency of 3.8Hz. While a smaller peak response and a higher frequency at which the peak shows (4.2Hz) is observed in the response function from the rigid base model. It can be concluded that whether the SSI effect is considered in the structural dynamic analysis brings considerable influence on the results, and the bearing stiffness parameters of shallow foundation proposed in ATC-40 are proved credible in this case.

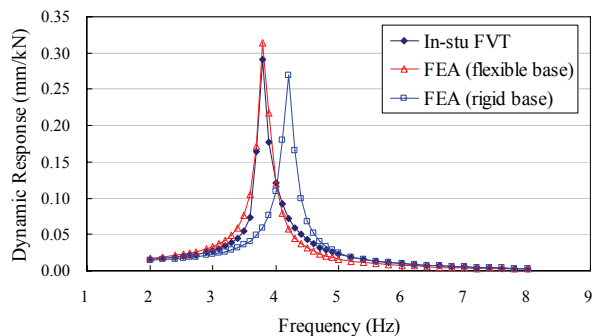


Fig. 7 Response functions from FE analysis.

Pushover Analysis for the School Building

1. Analysis model

The SAP2000 code was adopted to perform the pushover analysis for the post-tensioned specimen. Since the FE model generated for the analysis for the forced vibration test was verified to be representative of the real school building, it is introduced here with appropriate modifications for nonlinear analysis.

The tendon element of SAP2000 was used for the modeling of the post-tensioned rods. The tension limit was specified according to the yield strength of the steel rod ($F_{y,rod}$), and each tendon element was stressed to $0.5 F_{y,rod}$, as the rods were in the field test.

The nonlinearity of beams, columns, and brick partition walls was modeled by using the concentrated plastic hinge, of which the properties were specified based on Chung *et al.* (2006). The moment hinge was introduced at both ends of the beams and columns to simulate the flexural-shear failure, which usually occurred on aged school buildings in Taiwan because of insufficient stirrups in frames. The shear hinge was placed at the midpoint of the beams and columns to simulate the shear failure, which often happened to columns that are confined by half-height walls.

The nonlinearity of brick wing walls and the foundation was modeled using the multi-linear plastic link element. For the former, the load-displacement curve was referred to Tsai *et al.* (2000); for the later, the initial stiffness was specified by the ATC-40 bearing stiffness parameters, and the yielding behavior was based on the foundation deformation measurement.

2. Analysis results

Fig. 8 shows the capacity curves of the post-tensioned specimen obtained from the pushover analysis. Both the flexible base and the rigid base pushover analyses give a reasonable evaluation on the maximum lateral resistance of the school building in terms of base shear since it is controlled by the structural parts rather than the soil components of the foundation in this case. However, the pushover curve from rigid base analysis has a higher initial slope than the flexible base pushover curve and the in-situ pushover curve, possibly leading to a less conservative roof displacement when using the capacity spectrum method to evaluate the performance point.

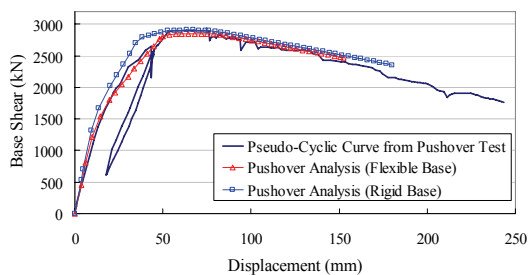


Fig. 8 Capacity curves from pushover analysis.



Fig. 9 Damage state of pushover test and analysis.

The damage state in field test and the development of the plastic hinges in the flexible base pushover analysis is shown in Fig. 9. The damages occurred mainly on the 1st floor columns in the form of flexural-shear failure. The short column behavior influenced greatly the failure mode of the school building as well.

References

- Applied Technology Council (ATC) (1996). "Seismic Evaluation and Retrofit of Concrete Buildings," *Report ATC-40*, Applied Technology Council, Redwood City.
- Applied Technology Council (ATC) (2005). "Improvement of Nonlinear Static Seismic Analysis Procedures," *Report FEMA-440*. Federal Emergency Management Agency, Washington, D.C.
- Chiou T-C, Chen S-L, Liu T-W, Hsiao F-P, Hwang S-J, and Chiou Y-J (2008). "Field Test of RC School Building Retrofitted by Post-Tensioned Rods," *The 9th National Conference on Structure Engineering*, Kaohsiung (in Chinese).
- Ko Y-Y and Hsu S-Y. (2008). "A Study of Soil-Structure Interaction by Using In-situ Tests of School Buildings," *Report NCREE-08-016*, National Center for Research on Earthquake Engineering, Taipei (in Chinese).
- Tsai, I.-C., Huang, C.-S., Tseng, Y.-P., and Chen, W.-C., (2000). "Detailed Evaluation of the Seismic Capacity of a School Building with Considering Strengthening," *Report NCREE-00-036*, National Center for Research on Earthquake Engineering, Taipei (in Chinese).
- Chung L-L, Wu L-Y, Lien K-H, Tseng C-C, Yang C-Y, and Huang Y-C. (2006). "Pushover Analysis and Experimental Verification on Retrofit of School Buildings by Adding Composite Column to Partition Brick Walls," *Report NCREE-06-010*. National Center for Research on Earthquake Engineering, Taipei (in Chinese).

Seismic Retrofit of Rectangular RC Columns Using CFRP Wrapping and CFRP Anchors

Min-Lang Lin¹ Pei-Ching Chen² Ying-Han Wu³ Keh-Chyuan Tsai⁴ Chih-Tsung Lin⁵

林敏郎¹、陳沛清²、吳穎涵³、蔡克銓⁴、林至聰⁵

Abstract

In recent years, CFRP wrapping retrofit method has been studied and became one of the most common schemes used in the retrofit industry. Research results showed that rectangular columns retrofitted by CFRP wrapping were ineffective because of concrete crushing due to the bulging of column sides. The “CFRP wrapping coupled with CFRP anchors” retrofit method was proposed in 2006 at NCREE. Preliminary research on the application of CFRP anchors showed that these anchors enabled the concentrated stress at the corners of the column spread evenly. The objectives of this study include: (1) to develop the design criteria of CFRP anchors, and (2) to evaluate the efficiency of the rectangular columns retrofitted by CFRP wrapping with CFRP anchors. A total of five full-scale specimens were constructed and tested of which one served as the as-built benchmark specimen. The other four specimens using CFRP wrapping and CFRP anchors could be divided into two major research groups: two specimens with focus on their shear capacity and the other two specimens with focus on their flexural ductility. Using a well-designed test frame, five specimens of RC columns were subjected to constant axial force and reverse-curvature moment during the cyclic loading tests. Experimental results demonstrated that the specimens retrofitted by CFRP wrapping conjugated with CFRP anchors showed improved hysteresis behavior compared with the specimen retrofitted with CFRP wrapping only. The moment capacity and ductility were enhanced as well.

Keywords: Seismic retrofit, CFRP, CFRP anchor

Introduction

A large number of reinforced concrete structures constructed following the old building codes were found to have inadequately confined transverse ties. Retrofit schemes have been suggested and since then have become an important research issue strengthening various existing building elements. Several tests on different retrofit methods have been carried out in the past to realize the performance and behavior of the building elements after being retrofitted. It has been found that the external confinement provided by CFRP wrapping is still ineffective because of the concrete crushing caused by the bulging of column sides. In the preliminary study,

test results demonstrated that the seismic performance of the rectangular RC columns can be enhanced significantly by CFRP wrapping with CFRP anchors. In this study, the design concept of the “CFRP wrapping combined with CFRP anchors” retrofit method was developed and proposed. It is hoped to decrease the concentrated stress at the column corners and to enhance its ductility. Moreover, the bulging effect of the column side is reduced as well.

A CFRP anchor is made of an anchor bolt rolled by CFRP sheet bonded with epoxy. The end of the CFRP anchor is cut to spread the fiber sheet evenly. Figure 1 shows a CFRP anchor. The general retrofitting procedures of CFRP wrapping conjugate

¹ Associate Research Fellow, National Center for Research on Earthquake Engineering, mllin@ncree.org

² Assistant Research Fellow, National Center for Research on Earthquake Engineering, pchen@ncree.org

³ Graduate Student, Department of Civil Engineering, National Taipei University of Science and Technology

⁴ Director, National Center for Research on Earthquake Engineering, kctsai@ncree.org

⁵ Associate Professor, Department of Civil Engineering, National Taipei University of Science and Technology

with CFRP anchors are: 1) Wrap the first layer of CFRP, 2) Plug the CFRP anchors into the column with the cut tail glued on the wrapped CFRP face with epoxy, and 3) Wrap the remaining CFRP. In order to keep the surface of the retrofitted columns as flat as possible, the specimens were chamfered before the application of the described procedures. Figure 2 shows a surface of CFRP wrapping with CFRP anchors after the retrofit was completed.



Fig. 1 CFRP anchor



Fig.2 The completion of retrofit using CFRP wrapping and CFRP anchors

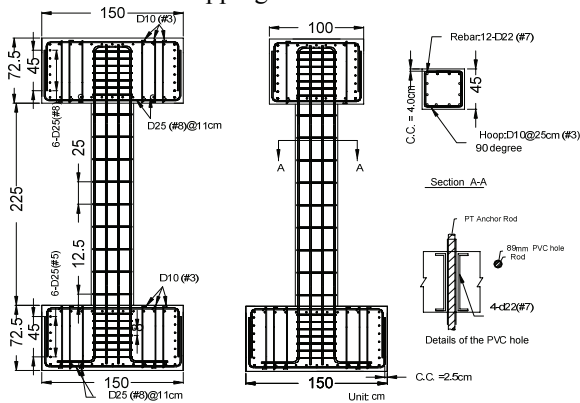


Fig. 3 Specimen design details

Specimen Design and Test Setup

A total of five specimens were designed in this research following the old building codes in Taiwan. There are twelve reinforcing bars with diameter of 22mm. The column height is 2250mm and the section is 450mm x 450mm. The diameter of stirrups is 10 mm with 250mm spacing. Figure 3 shows the design details of the un-retrofitted specimens. The tensile test results of reinforcements are shown in Table 1 and the compression test results of concrete cylinders are

shown in Table 2.

Table 1 Tensile test results of reinforcements

Bar Size	Nominal Strength (MPa)	Yield Strength (MPa)	Ultimate Strength (MPa)
#3	280	354	580
#5	280	368	521
#7	420	491	658
#8	420	423	664

Table 2 Compression test results of cylinders

Events	Nominal Strength (MPa)	Compression Strength (MPa)
Foundation	21	25.0
Column	21	22.3

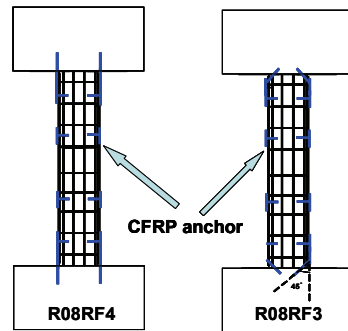


Fig. 4 Specimen R08RF3 and Specimen R08RF4

Table 3 Instruction of tested specimens

Specimen	Retrofit Target	Retrofit Scheme
R08BM	benchmark	—
Group1	R08RF1 shear strength/ductility	CFRP
	R08RF2 shear strength/ductility	CFRP & CFRP anchors
Group2	R08RF3 shear strength / flexural strength /ductility	CFRP & CFRP anchors
	R08RF4 shear strength / flexural strength /ductility	CFRP & CFRP anchors

Specimen R08BM is a benchmark sample to be compared with other four retrofitted specimens. These four retrofitted specimens could be divided into two major groups: 1) two specimens for increasing the shear capacity, and 2) the other two for enhancing the flexural strength and ductility. Specimen R08RF1 and Specimen R08RF2 are in Group 1. They were both wrapped with three layers of CFRP sheets in transverse direction. In addition, the CFRP anchors were used in Specimen R08RF2.

Specimen R08RF3 and Specimen R08RF4 are in Group 2. Both of them were wrapped with two layers of CFRP sheets in transverse direction and two additional layers of CFRP sheets in longitudinal direction to retrofit the flexural strength. CFRP anchors were used in both specimens, however, with different link mechanisms between the foundation and the CFRP sheets as shown in Fig. 4 were applied.

Each specimen was named as described in Table 3.

It is relevant to have the test specimens be subjected to constant axial force and reverse-curvature moment to reflect the real boundary conditions of RC columns. An L-shaped test frame was adapted to satisfy the boundary conditions of the columns. Test setup is shown in Fig.5. Two horizontal hydraulic actuators provided lateral force and the other two vertical hydraulic actuators provided axial load. The horizontal actuators were displacement-controlled by the external transducer (MTS Temposonic III). One of the two vertical actuators was force-controlled and the other one was slaved to the force-controlled actuator with same displacement. The control algorithm enabled the specimen subjected to constant total axial force of 850kN without rotation on the top of the crosshead. The displacement time history is shown in Fig.6. The test ended once the strength of the specimen is lower than 80% of its ultimate strength.



Fig. 5 Test Setup

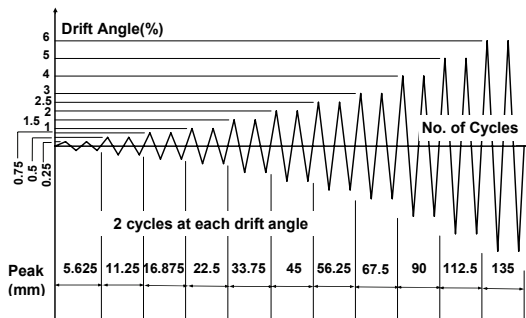


Fig. 6 Displacement-controlled loading protocol

Test Results

Specimen R08BM was designed to have flexural-shear failure mode. When the drift ratio reached 0.75% radian, shear cracks occurred at the top and bottom of the column. Meanwhile, the associated shear force was still increasing. When the drift ratio reached 1.5% radian, the strength of the specimen decayed and shear failure occurred. Figure 7 shows the hysteresis loop of Specimen R08BM. The ultimate moment caused by the maximum shear force was close to the plastic moment capacity. It is

demonstrated that the specimen behaved as it was expected. Figure 8 shows the failure mode of Specimen R08BM.

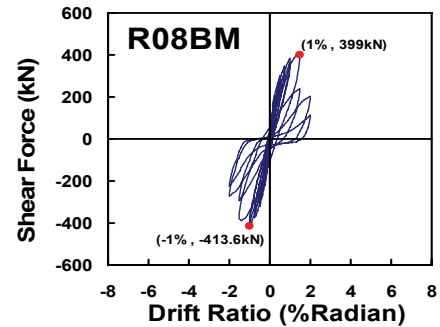


Fig. 7 The hysteresis loop of Specimen R08BM



Fig. 8 The failure modes of Specimen R08BM

Group 1: Both two specimens reached 7% radian drift ratio without loss of strength. The behavior of the two specimens were almost the same. Larger displacement was not available due to the stroke limit of the lateral actuators. Hence, repeated cyclic loading with drift ratio of 7.0% radian was applied to the two specimens until the CFRP wrapping broke. Specimen R08RF1 failed due to the fracture of the CFRP at the bottom of the column during the 3rd cycle. However, Specimen R08RF2 failed in the 5th cycle due to the low cycle fatigue of the reinforcements. The CFRP sheets were still bonded to the column face. Obviously, the usage of CFRP anchors delayed the fracture time of CFRP sheets and changed the failure mode from brittle failure of the CFRP sheets to the flexural failure of the reinforcements. Figure 9 shows the hysteresis loops of the specimens in Group1. To compare with Specimen R08BM, both the ductility and the strength were enhanced significantly. Figure 10 shows the failure modes of the specimens in Group 1.

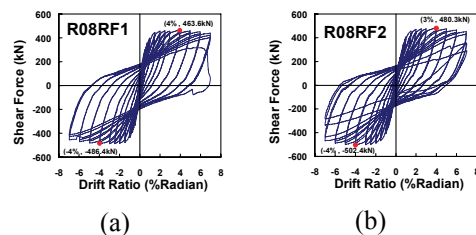


Fig. 9 The hysteresis loops of the specimens in Group 1 (a) R08RF1 (b) R08RF2

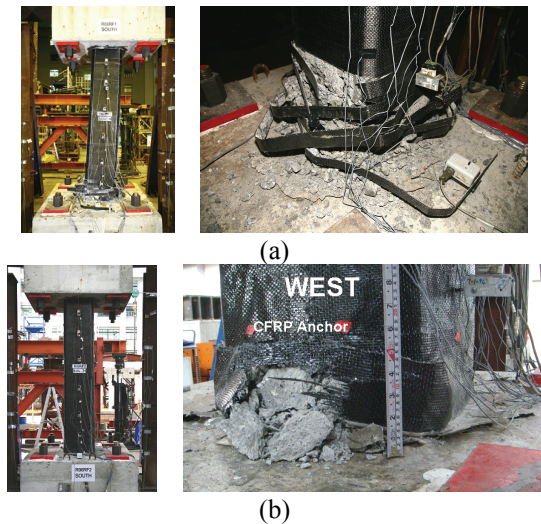


Fig. 10 The failure modes of the specimens in Group 1 (a) R08RF1 (b) R08RF2

Group 2: Both of the two specimens reached 7% radian drift ratio without loss of strength. Again, repeated cyclic loading with drift ratio of 7.0% radian was applied to the two specimens until the fracture occurred. The CFRP anchors linked the longitudinal CFRP sheets and the foundation by plugging the CFRP anchors with an angle of 45° into the foundation at Specimen R08RF3. However, the CFRP anchors were plugged into the foundation vertically at Specimen R08RF4. It was expected that larger flexural strength by wrapping the CFRP sheets in longitudinal direction and the linking systems could be developed. Unfortunately, the links of both specimens broke under large deformation. Figure 11 shows the hysteresis loops of the specimens in Group 2. The initial stiffness of the two specimens increase slightly, but neither of the moment capacities increased evidently. Figure 12 shows the failure modes of the specimens in Group 2.

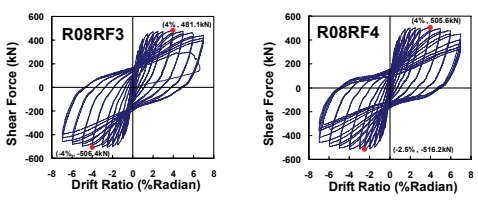


Fig. 11 The hysteresis loops of the specimens in Group 2 (a) R08RF3 (b) R08RF4

Conclusions

1. The breaks of the CFRP caused the failure of the Specimen R08RF1 and Specimen R08RF2. However, the ductility of Specimen R08RF2 was better than that of Specimen R08RF1 due to the use of CFRP anchors.
2. The link mechanisms of Specimen R08RF3 and Specimen R08RF4 were not so good. The moment capacity was not enhanced evidently.

3. Further researches on different structural components such as RC walls and RC beams are necessary to evaluate the performance of those retrofitted by CFRP wrapping and CFRP anchors.

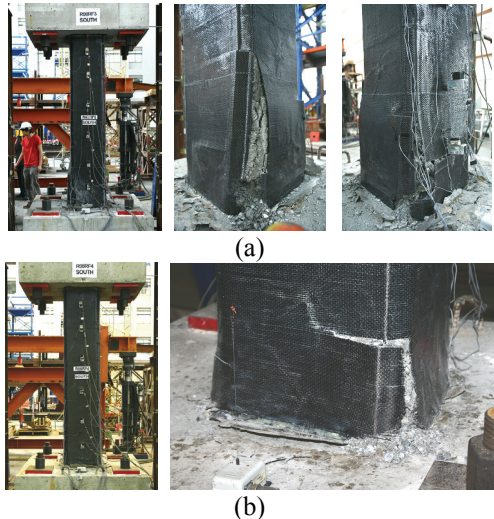


Fig. 12 The failure mode of the specimens in Group 2 (a) R08RF3 (b) R08RF4

References

Tsai, K. C., and Lin, M.L., "Steel Jacket Retrofitting of Rectangular RC Bridge Columns to Prevent Lap Splice and Shear Failures," National Center for Research on Earthquake Engineering, Report No. NCREE-02-015 (2002).

Tsai, K. C., and Lin, M.L., "Seismic Jacketing of RC Columns for Enhanced Axial Load Carrying Performances," National Center for Research on Earthquake Engineering, Report No. NCREE-02-016 (2002).

Lin, M.L., Chen, P.C., Tsai, K. C., and Wu, Y.H., "Retrofit Tests on RC Columns Subjected to High Axial Force and Reverse-Curvature Moment," National Center for Research on Earthquake Engineering, Report No. NCREE-08-025 (2008).

Ghobarah, A., and Elmandooh Galal, K., "Seismic Rehabilitation of Short Rectangular RC Columns", Journal of Earthquake Engineering, Vol. 8, No.1, 45-68, 2004.

Shaking Table Tests on Model Piles in Liquefiable Sand

Tzou-Shin Ueng¹, Chia-Han Chen² and Yong-Cheng Tseng³

翁作新¹、陳家漢²、曾永成³

Abstract

For the study of the soil-pile interaction in a liquefiable soil under earthquake shakings, shaking table tests on model piles in the large biaxial laminar shear box filled with saturated sand were conducted at the National Center for Research on Earthquake Engineering (NCREE), Taiwan. The model piles made of two different materials were used in the shaking table tests. Each model pile was placed in the shear box containing saturated clean fine sand. The pile tip was fixed at the bottom of the shear box to simulate the condition of a pile foundation embedded in rock or within a firm soil stratum. Strain gauges and accelerometers were installed on the pile surface to observe the behavior of the pile during shaking. The near- and far-field soil responses, including pore pressure changes, accelerations, and settlements were also measured. One- and multi-directional shaking table tests were performed on the model pile in the shear box with and without soil. The shakings included sinusoidal and recorded earthquake accelerations. The results of this study can be used for design of pile foundations under seismic loadings.

Keywords: pile, shaking table test, liquefaction, earthquakes, soil-pile interaction

Introduction

In the previous large earthquakes, such as 1964 Japan Niigata Earthquake, 1989 US Loma Prieta Earthquake, 1995 Japan Kobe Earthquake and 1999 Taiwan Chi-Chi Earthquake, there are many cases of pile foundation failures due to soil liquefaction, which caused loss of soil supports for the piles or induced lateral spreading. Therefore, many studies on soil-pile interactions for pile foundations in a liquefiable stratum were conducted recently in order to understand the mechanism of the dynamic loading on the piles (soil-pile interaction) and their responses under earthquake loading. The results of these studies provide the bases for aseismic design criteria for structures with pile foundations.

Lateral loading tests in the field or in the laboratory and shaking table tests on model piles within soil specimens, under either 1 g or centrifugal conditions, have been used to investigate the pile behaviors and soil-pile interaction in liquefiable soils (e.g., Ashford et al., 2006; Dobry and Abdoun, 2001; Tokimatsu et al., 2005). These tests are mostly under one-dimensional shaking and can not consider the

effect of multidirectional shaking on the pile foundations. Besides, the inertial effect by the super structure and the pile and the kinematic loading by the surrounding ground cannot be separately identified and understood. This research used the large biaxial laminar shear box developed at NCREE as the soil container and the instrumented model pile was installed inside the shear box filled with saturated sand. Static and cyclic lateral loading tests on the model pile were conducted utilizing the reaction wall at NCREE to acquire the basic pile properties and soil-pile interaction under simple conditions. The biaxial shear box with the model pile in a saturated sand specimen was then placed on the shaking table at NCREE; one- and multi-directional sinusoidal and recorded earthquake accelerations were applied from the shaking table. The soil and pile responses and their interaction under these types of shakings were studied.

Model Piles and Sand Specimen

Two different types of model piles were used in the shaking table tests. One was made of a stainless steel pipe, 1.50 m in length, with an outer diameter of 101.6

¹ Professor, Department of Civil Engineering, National Taiwan University, ueng@ntu.edu.tw.

² Assistant Research Fellow, National Center for Research on Earthquake Engineering, chiaham@ncree.org.tw.

³ Former graduate Students, Department of Civil Engineering, National Taiwan University

mm, a wall thickness of 3 mm and a flexural rigidity, EI , of $186.05 \text{ kN}\cdot\text{m}^2$; the other was made of an aluminum alloy pipe, 1.60 m in length, with the same diameter and wall thickness and $EI = 77.62 \text{ kN}\cdot\text{m}^2$. Strain gauges and accelerometers were placed at different locations to measure bending moments and accelerations along the pile. The pile was fixed at the bottom of the shear box to simulate the condition of a pile foundation embedded in rock or within a firm soil stratum. A rigid steel adapter for application of lateral force was fixed to the top of the steel pile, while up to 6 disks of masses were fixed to the top of the aluminum pile to simulate various conditions of the superstructure. Each disk of mass weighs about 37.10 kg. The model pile with instrumentation inside the shear box was set up before preparation of the sand specimen, as shown in Figure 1.

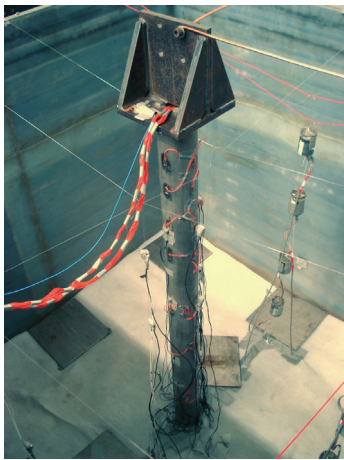


Fig. 1 Model pile with instrumentation

We used clean fine silica sand from Vietnam for the sand specimen inside the laminar shear box. This sand has been used in the shaking table tests for liquefaction studies at NCREC (Ueng et al. 2006). The maximum and minimum void ratios are 0.887~0.912 and 0.569~0.610, respectively. The sand specimen was prepared using the wet sedimentation method after the placement of the model pile and instruments in the shear box. The sand was rained down into the shear box filled with water to a pre-calculated depth. The size of sand specimen is $1.880 \text{ m} \times 1.880 \text{ m}$ in plane and about 1.40 m in height before shaking tests. The saturation of the specimen was checked by the P-wave velocity measurements across the specimen horizontally. Details of the sand specimen preparation and the mechanism of the biaxial laminar shear box were described in Ueng et al. (2006).

Shaking Table Tests

Shaking table tests were first conducted on each model pile without sand specimen to evaluate the dynamic behavior of the pile itself. Sinusoidal and white noise accelerations with amplitudes from 0.03 to 0.075 g were applied in X- and Y-directions. The model pile within the saturated sand specimen was then tested

under one- and multi-directional sinusoidal (1~24 Hz) and recorded earthquake accelerations with amplitudes ranging from 0.03 to 0.15 g. White noise accelerations were also applied in both X- and Y-directions to investigate the behavior of the model pile and the sand specimen after every several shakings. Figure 2 shows a shaking table test of the model pile in the sand specimen.



Fig. 2 The model pile with mass on its top in saturated sand specimen on the shaking table

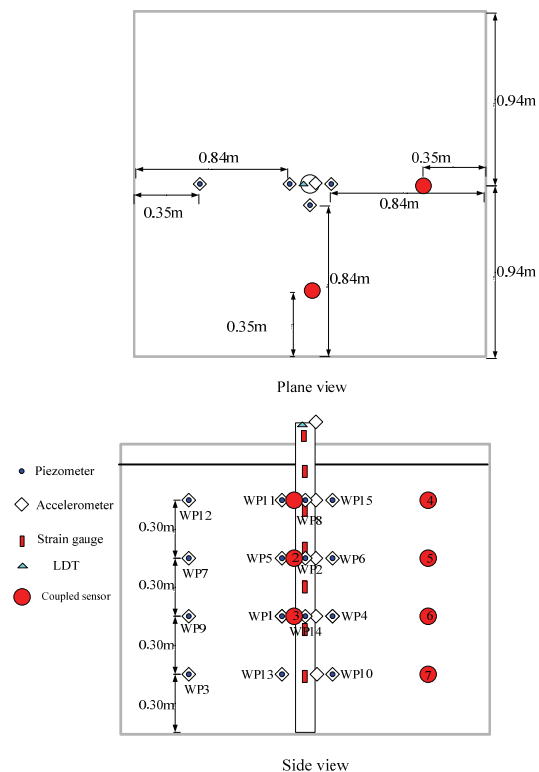


Fig. 3 Instrumentation on the pile and within the sand specimen

Figure 3 is the layout of instrumentation on the model pile and in the sand specimen. During every test, pile top displacements, strains and accelerations at different depths on the pile, and pore water pressures and accelerations in the sand specimen (near field and far field) were measured. Besides, the frame movements

at different depths of the laminar shear box were also recorded to evaluate the responses and liquefaction of the sand specimen using displacement transducers and accelerometers. Pore water pressures inside the sand specimen were measured continuously until sometime after the end of shaking to observe the dissipation of the water pressures. The height of the sand surface after each test was obtained for the settlement and density of the sand specimen. Soil samples were taken using short thin-walled cylinders at different depths after completion of the shaking tests to obtain the densities of the sand specimen.

Preliminary Results

Characteristics of model pile

The flexural rigidity of the steel model pile was verified with the results of the lateral load tests on model pile without soil specimen. An additional equivalent rotational spring was considered to take into account the possible rotation at the pile tip at the bottom of the shear box. Shaking table tests on both model piles without sand specimen were conducted to evaluate the dynamic behaviors of the model piles themselves. The dynamic characteristics can be evaluated based on the forced vibration of white noise shaking. The amplification curve was derived from the Fourier spectral ratio of the measured accelerations of the pile top to those of the input motions. The predominant frequency was also verified with observations of free vibrations after the end of the input motions. Table 1 lists the predominant frequencies of the steel and aluminum model piles according to the test data. It was found that a single hinged-end beam with a rotational spring can well simulate the dynamic behavior of the model pile in our tests.

Table 1. Predominant frequencies of the model piles

Mass on pile top	Steel pile	Aluminum pile
	Freq., Hz	Freq., Hz
No mass	—	23.4
Rigid adapter	13.62	—
1 disk of mass	—	5.55
3 disks of masses	—	3.11
6 disks of masses*	—	2.07

* The frequency was evaluated by numerical method.

Dynamic characteristics of soil and soil-pile system under small amplitude of shaking

Figure 4 shows the amplification factors for the steel pile top and the free-field ground surface under the white noise accelerations and sinusoidal vibrations of various frequencies with amplitude of 0.03 g. It is found that the predominant frequencies of both free-field soil and the pile in soil are nearly the same with a value of about 11.5 Hz. Table 2 lists the predominant frequencies of soil and the pile in soil specimens of different densities for the case of the steel model pile. It can be seen that the predominant frequencies of soil and the pile in soil are almost the

same and these frequencies increase with relative density of the soil specimen. This infers that the kinematic effect from the soil motion dominates the pile response because of the small inertia force from the superstructure and the pile.

Table 3 lists the predominant frequencies of soil and soil-pile system for the aluminum pile in soil of various relative densities. It can be found that, for the model pile without mass and with one disk of mass, the predominant frequencies of both soil and the soil-pile system are almost the same and these frequencies increase with the relative density of the soil specimen. For the pile with 6 disks of masses, the predominant frequency of soil-pile system is significantly lower than that of the soil specimen. Comparing the predominant frequencies of the aluminum pile without and with soil specimen (Table 1 and Table 3), one can find that, except for the case without mass on the pile top, the predominant frequencies of the model pile in the soil specimen were higher than that without soil due to the constraint of the soil on the pile. The lower predominant frequency of the model pile without mass in the soil specimen might be attributed to the kinematic effect from the soil motion, which has a lower frequency, dominates the pile response because of the small inertia force from the superstructure. Therefore, these observations suggest that the mass and inertia force induced by the superstructure can have an important effect on the soil-pile interaction.

Table 2. The predominant frequencies of soil and soil-pile system for the steel pile in different soil densities

Density of soil Dr, %	Predominant frequency, Hz	
	Soil	Pile in soil
37.13	11.5	11.5
50.78	12.5	12.38
70.58	12.9	12.9

Table 3. Predominant frequencies of soil and soil-pile system for the aluminum pile in the soil specimen of different relative densities

Mass on pile top	Soil-Pile	Soil	Dr
	Freq., Hz	Freq., Hz	%
No mass	10.49	10.49	7.5
No mass	11.7	11.68	30.6
1 disk of mass	11.7	11.8	31.7
1 disk of mass	11.7	11.8	40.5
6 disks of masses	4.88	13.1	56.6
6 disks of masses	5.1	13.2	65.4

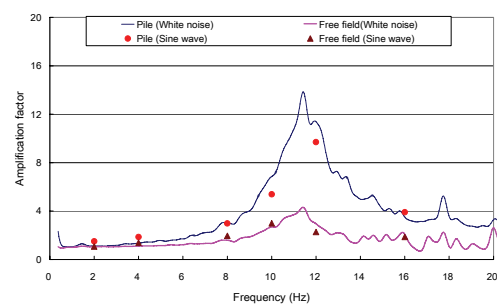


Fig. 4 Amplification factors versus frequency for free-field soil and steel pile in soil (Dr = 37.13 %)

Response of model piles in liquefiable soil

Figure 5 shows the measured time histories of accelerations and displacements of the aluminum pile with 6 masses on its top and accelerations of the free-field soil, and excess pore water pressure ratios (r_u) at various depths in the specimen during one-dimensional sinusoidal shaking with frequency of 4 Hz and amplitude of 0.15 g, respectively. The depth of liquefaction was determined based on the measurements of mini-piezometers in the sand specimen and accelerometers on the inner frames (Ueng et al. 2009). In this shaking, the sand specimen was fully liquefied. It was found that the maximum accelerations along the pile occurred before liquefaction of the sand specimen. After liquefaction, the accelerations of the pile reduced and remain steady while the accelerations of the soil diminished. This phenomenon can be interpreted as that the stiffness of the soil almost vanished when the specimen was fully liquefied. The reason might be attributed to the lower predominant frequency of the aluminum pile with masses because of the lack of soil constraint. These results suggest that the acceleration and displacement of the pile with a mass may decrease due to soil liquefaction, but the stability of the pile-structure system should depend on the depth of liquefaction, the conditions of superstructure and the load capacity of the pile foundation.

Conclusions

Lateral load tests and shaking table tests were conducted on a model pile in the biaxial laminar shear box with and without saturated sand specimen. The displacements, strains and accelerations at different depths of the model pile were measured. The dynamic behavior of the model pile and the pile-soil system were evaluated based on the test results. Further tests and analyses of the test data will be performed to understand the soil-pile interaction, such as the relationship of ground reaction on the pile, and pore water pressure generation versus pile displacements (p-y curve) and their coupling. Based on these results, aseismic design criteria for pile foundations in liquefiable soils can be established for engineering practices.

References

Ashford, S.A., Juirnarongrit T., Sugano T., and Hamada M. (2006). "Soil-pile response to blast-induced lateral spreading. I: field test," *J. Geotechnical and Geoenvironmental Engineering*, 132(2), 152-162.

Dobry, R.D. and Abdoun T. (2001). "Recent Studies on Seismic Centrifuge Modeling of Liquefaction and its Effect on Deep Foundations," *State-of-the-Art Report (SOAP3), Proc. 4th International Conference on Recent Advances in Geotechnical Earthquake Engineering and Soil*

Dynamics, San Diego, CA, March 26-31, Vol. 2.

Tokimatsu, K., Suzuki, H., and Sato, M. (2005) "Effect of Inertial and Kinematic Interaction on Seismic Behavior of Pile with Embedded Foundations," *Soil Dynamics and Earthquake Engineering*, 25, 2005, pp. 753-762.

Ueng, T.S., Wang, M.H., Chen, M.H., Chen, C.H. and Peng, L.H. (2006). "A large biaxial shear box for shaking table tests on saturated sand," *Geotechnical Testing Journal, ASTM, Vol.29 (1):* 1-8.

Ueng, T.S., Wu, C.W., Cheng, H.W. and Chen, C.H. (2009). "Settlements of saturated clean sand deposits in shaking table tests," Submitted for publication.

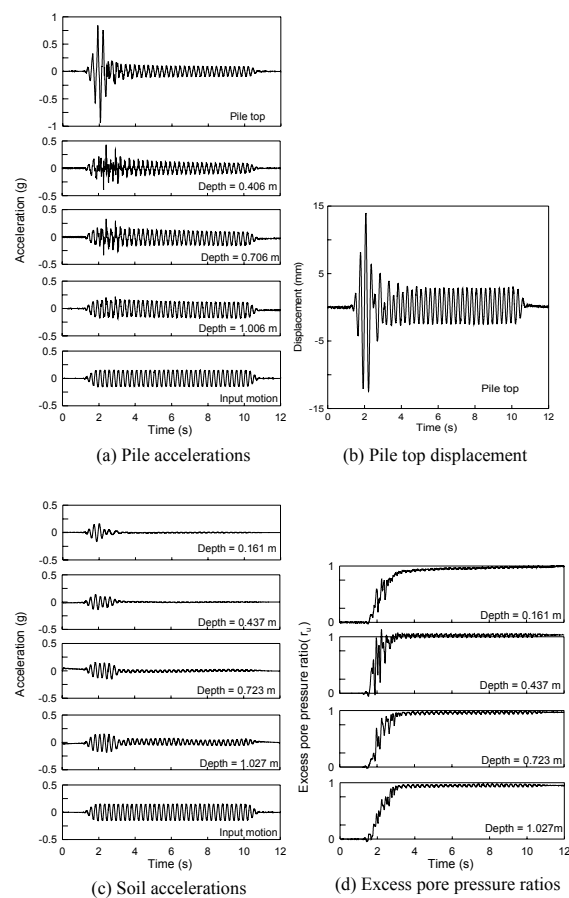


Fig. 5 Time histories of accelerations of the aluminum pile and the far-field soil, pile top displacement and excess pore pressure ratios in the sand specimen ($Dr = 64.7\%$)

Parametric Study on Ductility Capacity of Fixed-Head Piles

Juinn-Shyang Chiou¹

邱俊翔¹

Abstract

This study used SAP2000 to perform a parametric study on the ductility capacity of fixed-head piles. The Winkler-beam model was adopted in which the nonlinearity of the soils and the pile can be considered. The nonlinear secant subgrade reaction coefficient proposed by the Architecture Institute of Japan was followed to consider the soil nonlinearity, and the distributed plastic hinge model was applied to simulate the pile nonlinearity. In this study, the pile was considered as a limited ductility structure which conditionally allows the pile to enter a plastic state during larger loadings, such as a severe earthquake. The effects of variables, such as the axial force, pile diameter, longitudinal steel amount, and soil stiffness, were investigated in the parametric study. Besides, the over-strength ratio which represents the whole effect of structural property (character) of the pile section was introduced. Results showed that the over-strength ratio significantly influences the ductility of the pile; as the ratio increases, the displacement ductility capacity increases. When the ratio is zero, no displacement ductility can be developed. On the other hand, as the over-strength ratio is fixed, the displacement ductility capacity decreases with the soil stiffness.

Keywords: Ductility, piles, parametric study.

Introduction

In the conventional seismic design, piles are designed as elastic structures because it is preferable to force the plasticity into the superstructure without occurring in the piles. However, in many design conditions such that a severe earthquake may occur, it becomes impractical to keep the piles always being in the elastic stage. Especially for a fixed-head pile whose pile head is restrained by a slab or a pile cap, the pile head usually sustains a larger curvature demand which easily damages the piles. It is cost-effective to design the piles to have plasticity and provide a function for energy dissipation. Therefore, the ductility capacity of piles is of concern in seismic design. Generally, since the difficulty of damage inspection and the high-cost foundation repair, the pile damage is limited to ensure that the full ductility capacity of the pile will not develop under the design load. Such structures are termed as Limited Ductility Structures by ATC-32 (1996). Budek et al. (2000) parameterized the height of pile head above the

ground level and the soil stiffness to conduct parametric analyses for examining the ductility capacity of piles. Their study did not investigate the effect of structural property of the piles. Song et al. (2005) used a concentrated plastic-hinge model to relate the displacement ductility of a fixed-head pile with the curvature ductility of the pile section. However, the concentrated hinge model is unable to reflect plasticity propagation in piles because the range of plasticity of this model has been specified beforehand and is thus unchanged in the whole analysis process (Chiou, et al, 2009).

The objective of this study is to conduct extensive parametric studies for fixed head piles by considering the effects of the axial force level, pile diameter, longitudinal reinforcement amount and soil strength for clearly identifying the influencing factors on the displacement ductility of piles. In addition, instead of using the concentrated plastic hinge model, a distributed plastic hinge model for the nonlinear behavior of piles was used.

¹ Associate Research Fellow, National Center for Research on Earthquake Engineering, jschiou@ncree.org.tw.

Pushover Model

This study adopted the Winkler-beam model to build a pushover model for parametric analyses in which the pile was modeled by a beam and the soil reactions were modeled by the spring elements.

To model the pile material nonlinearity, the plastic hinge approach was employed where the distributed plastic hinge model was used to capture completely the development of the plastic zone. The distributed hinge model locates many potential plastic hinges over an expected plastic zone. The procedure in determining the property of the distributed plastic hinges can refer to Chiou, et al. (2009) which is based on the moment-curvature relation of the pile section. In this distributed model, it is unnecessary to set the plastic-hinge length for plastic hinges and the plasticity propagation of the pile can be easily modeled.

The soil p - y spring model was based on the subgrade reaction coefficient suggested by the Architecture Institute of Japan, as the equation shown below:

$$k_{h1} = 80 \cdot E_0 \cdot D^{-0.75} \quad (1)$$

where k_{h1} (kN/m³) is the subgrade reaction coefficient when the lateral displacement reaches 0.01m; E_0 is the soil modulus, which can be estimated from an empirical equation as $E_0=0.7N$ (kN/m²), in which N is the blow number of Standard Penetration Test (SPT); D is the pile diameter in centimeter.

Further, to consider the effects of soil nonlinearity, the following relation was adopted;

$$k_h = k_{h1} \cdot (y_0 / y_1)^{-0.5} \quad (2)$$

where k_h is the subgrade reaction coefficient when the lateral displacement y_0 (m) is larger than y_1 . And It was assumed that the soil reaction reaches its ultimate pressure when the lateral displacement reaches one-tenth of the pile diameter ($D/10$).

Parametric Studies

Figure 1 displays a pile-soil model for parametric studies where a fixed-head pile with a length of 25 m is embedded in uniform soils. The concrete strength is 28 MPa. The yield strength of rebar is 414 MPa. The concrete cover is 0.075 m. The ratio of transverse steel is set to 1%. Four parameters are considered in the parametric analyses: (1) axial force level, (2) longitudinal reinforcement ratio, (3) pile diameter, and (4) SPT-N of the soil stratum. The values of these four parameters adopted in the analyses are specified and listed in Table 1. A total of 64 combinations for those parametric values were performed.

Moment-Curvature Relation

Except for the SPT-N value, all the other parameters considered above may affect the section property of the pile. This section will demonstrate their effects on the moment-curvature relation of the pile.

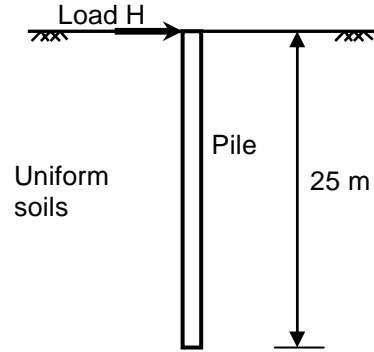


Fig. 1 Pile-soil model for parametric studies

When the pile is designed as a limited ductility structure, the limit state of damage control for steel strain limit at tension and concrete strain limit at compression are set to 0.018 and 0.06 according to Kowalsky (2000). The moment-curvature relation was computed based on nonlinear stress-strain relations of concrete and steel concrete. For concrete, Mander et al. (1988) model was applied to consider confined effects from stirrups; for steel, the nonlinear hardening stress-strain model was considered. The nonlinear moment-curvature relation was further simplified as a bilinear curve which is defined in terms of the effective yield point and the ultimate point for easy modeling. The equal-energy rule was employed in the bilinearization process. Two parameters including the curvature ductility μ_ϕ and the over-strength ratio α_M , were defined to describe the nonlinear character of the section. They are

$$\mu_\phi = \phi_u / \phi_y \quad (3)$$

$$\alpha_M = M_u / M_y \quad (4)$$

where ϕ_u is the ultimate curvature; ϕ_y is the effective yield curvature; M_u is the ultimate moment, and M_y is the effective yield moment.

Table 1 Parametric cases

Parameter	Values
Axial force level ($P/f_c'A_g$)	-0.1, 0.0, 0.1, 0.2
Pile Diameter (m)	1.0, 1.5
Longitudinal steel ratio (%)	1, 2
SPT-N value	5, 10, 20, 30
Note: P is the axial force, f_c' is the compressive strength of concrete, and A_g is the gross area of the pile section.	

Figure 2 shows the moment-curvature relations for the various axial load levels. It can be seen that the stiffness and strength of the pile section increases with the axial force level. The curvature ductility capacity of each curve is close, about 17-20. As the axial load approaches zero, the curvature ductility capacity is largest, and when the axial load increases or decreases from zero, the curvature ductility capacity decreases. On the other hand, the over-strength ratio increases as the axial load decreases.

Figure 3 displays the moment-curvature relations for the pile diameters of 1m and 1.5m. It can be seen that the stiffness and strength of the pile section increases with the pile diameter as well as the over-strength ratio which significantly increases. The curvature ductility for the diameter of 1.0m is about 20.1, which is a little higher than that for the diameter of 1.5m whose capacity is about 18.4.

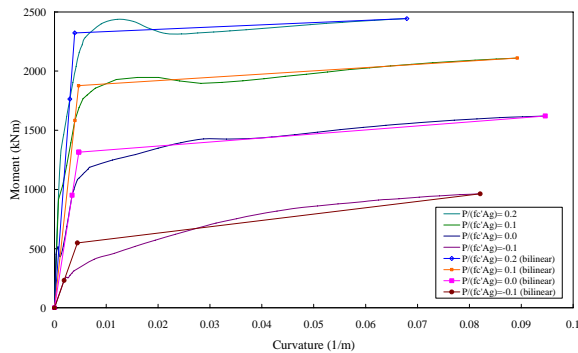


Fig. 2 Moment-curvature relationships for various axial force levels

Figure 4 shows the moment-curvature relations for the longitudinal steel ratios of 1% and 2%. It can be seen that the stiffness and strength of the pile section increases with increasing steel ratio. The over-strength ratio also significantly increases with the steel ratio. The curvature ductility for the ratio of 2% is about 18.18, which is a little lower than that for the ratio of 1% whose curvature ductility capacity is about 20.1.

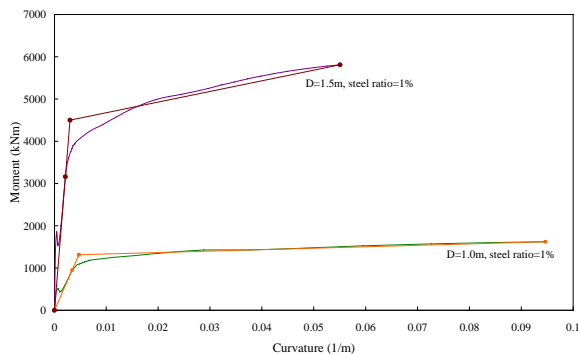


Fig. 3 Moment-curvature relationships for $D=1.0m$ and $1.5m$ at zero axial force

Under the specified limit state of concrete and steel materials, the strength and over-strength ratio significantly varies with the axial force level, pile diameter, and longitudinal steel ratio; however, the

curvature ductility capacity varies within a narrow range.

Nonlinear soil p - y Springs

Based on the soil p - y spring models described above, this study applied several SPT-N values to change the stiffness and strength of the p - y springs of the soil. For example, Fig. 5 shows the p - y curves for $D=1m$ at SPT-N=5, 10, 20, and 30. The higher SPT-N value implies a stiffer ground.

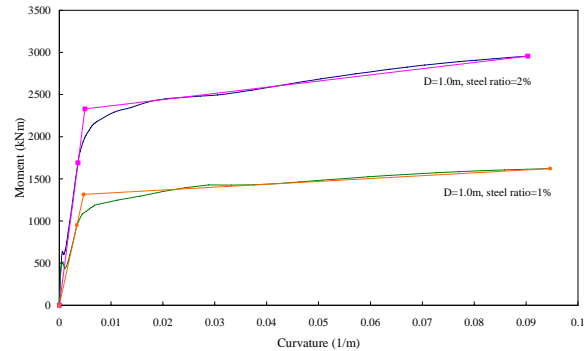


Fig. 4 Moment-curvature relationships for steel ratios of 1% and 2% at zero axial force

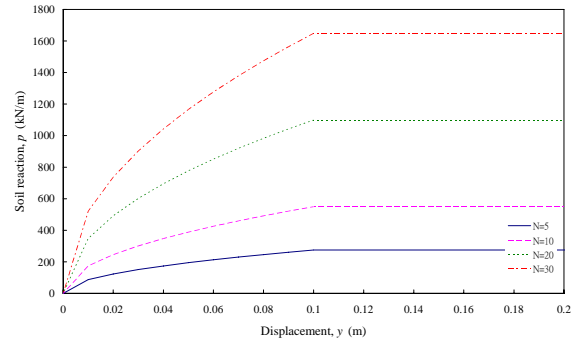


Fig. 5 P - y curves for $D=1.0m$

Pushover Curves

On the basis of the set moment-curvature relations and the p - y soil springs in the pile-soil system, a series of pushover analyses were conducted to obtain the pile-head pushover curves by using SAP2000.

Here, define the pile-head displacement ductility capacity as follows:

$$\psi = U_u / U_y \quad (5)$$

where U_u is the ultimate displacement, and U_y is the yield displacement.

Figure 6 shows the pushover curves for the different axial force levels. In this figure, it can be seen that the strength of the pushover curve depends on the strength of the moment-curvature curve, and it can be observed that the higher axial force level gives the lower displacement ductility capacity.

Figure 7 depicts the pushover curves for the pile diameters of 1m and 1.5m. It can be seen that the

larger pile-diameter yields the stiffer pushover curve and the higher displacement ductility.

Figure 8 shows the pushover curves for the longitudinal steel ratios of 1% and 2%. This figure shows that the higher steel ratio gives the stiffer p - y curve and the higher displacement ductility capacity.

Figure 9 shows the pushover curves for the different SPT-N values. Here, the higher SPT-N value yields the stiffer pushover curve, but the lower displacement ductility capacity.

Figure 10 compares the displacement ductility of the pushover curves with the over-strength ratio of the pile section. Note that the displacement ductility increases with the over-strength ratio increases. In addition, the scatters in the ductility values for each over-strength ratio are due to the changes of soil properties (the ductility capacity is lower when the soil is stiffer). For the section with the low over-strength ratio (close to one), the scatter is small.

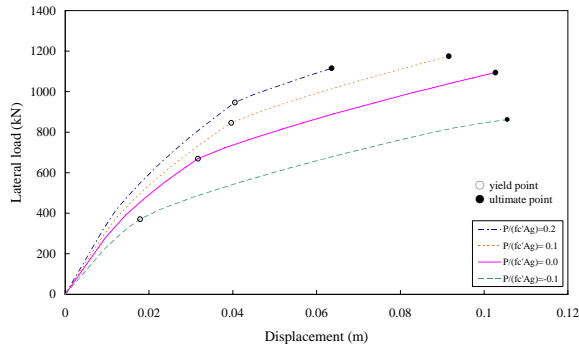


Fig. 6 Pushover curves for different axial force levels

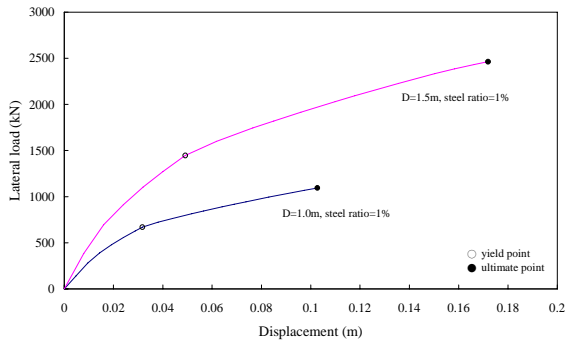


Fig. 7 Pushover curves for $D=1.0\text{m}$ and 1.5m

Conclusions

From this parametric study, it can be found that the over-strength ratio is a significant factor to the pile-head displacement ductility capacity. The displacement ductility capacity decreases with SPT-N of the soil stratum; however, the influence of soil stiffness is small, especially at a very low over-strength ratio.

References

Applied Technology Council ATC-32. (1996). Improved seismic design criteria for California

bridges: Provisional recommendations. Redwood City, California.

Budek A.M., Priestley, M.J.N., and Benzoni, G. (2000). "Inelastic seismic response of bridge drilled-shaft RC pile/columns." *Journal of Structural Engineering*, 126(4), 510-517.

Chiou, J.S., Yang, H.H., and Chen, C.H. (2009). "Use of plastic hinge model in nonlinear pushover analysis of a pile," *Journal of Geotechnical and Geoenvironmental Engineering*.

Mander, J.B., Priestley, M.J.N., and Park, R. (1988). "Theoretical stress-strain model for confined concrete." *Journal of the Structural Division (ASCE)*, 114(8), 1804-1826.

Kowalsky, M.J. (2000). "Deformation limit states for circular reinforced concrete bridge columns." *Journal of Structural Engineering*, 126(8), 869-878.

Song S.T., Chai, Y. H., and Hale, T. H. (2005). "Analytical model for ductility assessment of fixed-head concrete piles." *Journal of Structural Engineering*, 131(7), 1051-1059.

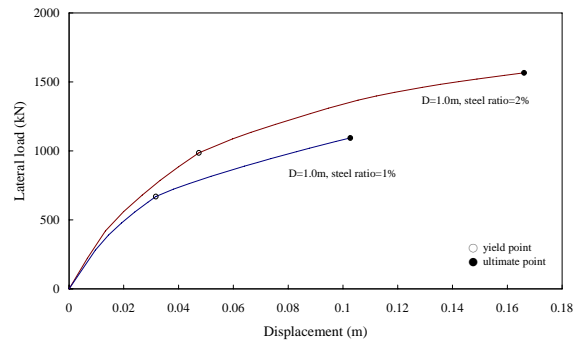


Fig. 8 Pushover curves for longitudinal steel ratios of 1% and 2%

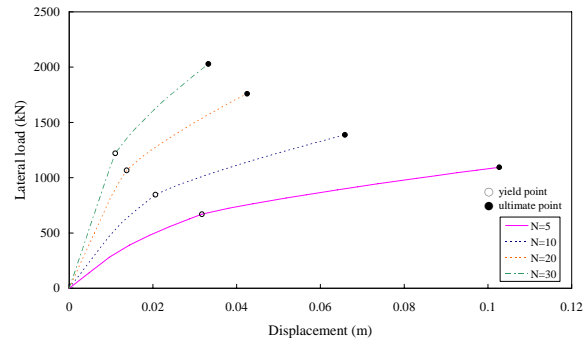


Fig. 9 Pushover curves for different soil properties

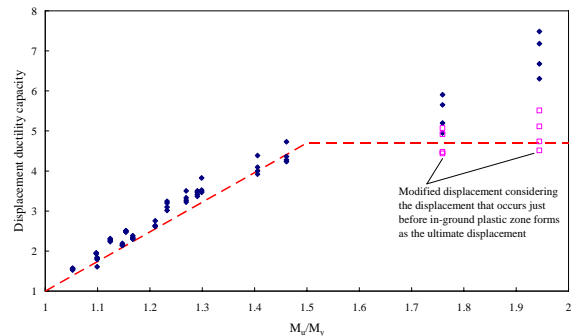


Fig. 10 Displacement ductility vs. over-strength ratio

An Investigation on the Effective Damping Ratio Considering Soil-Structure Interaction (I)

Shang-Yi Hsu¹ Cheng-Hsing Chen² Jiunn-Shyang Chiou³

Abstract

To incorporate the effects of Soil-Structure Interaction (SSI) into the structural design, the most important issue is to quantify the effects of SSI for a soil-structure system. For design purpose, it is well recognized that the natural frequency and associated damping ratio are the key parameters for structural analysis. The natural frequency and associated damping ratio of the Equivalent Fixed-Base (EFB) model constructed can be calculated through explicit equations, and can represent the dynamic characteristics of the original soil-structure system. In this study, preliminary comparisons between the recommended provisions for Seismic Regulations considering SSI effect of FEMA450 and the EFB model of a SDOF structure are advanced and discussed.

Keywords: Soil-structure interaction, foundation impedance, equivalent fixed-base model, seismic regulation

Introduction

To incorporate the effects of soil-structure interaction (SSI) into the structural design, the most important issue is to quantify the effects of SSI for a soil-structure system. For design purpose, it is known that the predominant frequency and associated damping ratio are the key parameters for structural analysis. The former is used to locate where the maximum response will be and the latter controls the magnitude of maximum response. Based from such understanding, this study aimed at quantifying the effects of SSI on a soil-structure system. Since the phenomenon of SSI is very complex for a general structure with large number of degrees-of-freedom, this study will use a simple structure founded on elastic half-space as the fundamental model to deduce how the predominant frequency and associated damping ratio are affected by the effects of SSI. Once these two parameters are quantified for a soil-structure system then an Equivalent Fixed-Base (EFB) model, which had taken the effects of SSI into account, can be constructed. This equivalent model is actually a rigid-base model that can be conveniently applied in a conventional structural analysis for engineering design.

Furthermore, a complete and positive procedure of

seismic design for buildings considering soil-structure interaction, the Recommended Provisions for Seismic Regulations for New Buildings and Other Structures (FEMA 450), has been proposed by the Building Seismic Safety Council of the National Institute of Building Sciences in 2004. In this study, an in situ seismic test at Hualien and various numerical cases for general building seismic design were used to verify and review the suitability of the EFB model proposed herein and FEMA 450.

SSI Equivalent Fixed-Base Model

The typical model usually used in describing the effects of soil-structure interaction is a lumped SDOF elastic structure supported on elastic half-space. The structure is characterized by the mass m and mass moment of inertia J of the roof, the mass m_0 and mass moment of inertia J_0 of the basemat, the lateral stiffness k , and the damping coefficient c . The height of the structure is denoted by h . For simple case, it is assumed that the basemat is rigid and perfectly bonded to the underlying soils. When the system is subjected to earthquake excitations, denoted by ground acceleration \ddot{x}_g , the response of the system can be depicted as shown in Fig. 1.

¹ Associate Research Fellow, National Center for Research on Earthquake Engineering, syhsu@ncree.org

² Professor, Department of Civil Engineering, National Taiwan University, chchen2@ntu.edu.tw

³ Research Fellow, National Center for Research on Earthquake Engineering, jschiou@ncree.org

In order to simplify the equations of motion obtained, it is convenient to define the parameter $\omega_s = \sqrt{k/m}$ be the natural frequency of the lumped SDOF structure if it is assumed to be fixed on a rigid base, and introduce the dimensionless parameters defined as follows: the structure damping ratio $\xi = c/(2m\omega_s)$, $\beta = \omega/\omega_s$, $a = m_0/m$, $b = (J + J_0)/mh^2$, $a_1 = 1 + a$, $b_1 = 1 + b$, $S = K_{VV}(i\omega)/k$, $C = K_{VM}(i\omega)/kh$, $R = K_{MM}(i\omega)/kh^2$. Herein, $K_{VV}(i\omega)$, $K_{VM}(i\omega)$ and $K_{MM}(i\omega)$ are the impedance coefficients corresponding to the translational, coupling and rocking motions, respectively, of the rigid massless basemat supported on elastic half-space. Therefore, the dynamic equilibriums of the whole soil structure system in the frequency domain can be written in matrix form as follows:

$$\begin{bmatrix} 1 - \beta^2 + i2\xi\beta & -\beta^2 & -\beta^2 \\ -\beta^2 & -a_1\beta^2 + S & -\beta^2 + C \\ -\beta^2 & -\beta^2 + C & -b_1\beta^2 + R \end{bmatrix} \begin{Bmatrix} X(i\omega) \\ X_f(i\omega) \\ h\Theta(i\omega) \end{Bmatrix} = - \begin{Bmatrix} \beta^2 \\ a_1\beta^2 \\ \beta^2 \end{Bmatrix} \frac{\ddot{X}_g(i\omega)}{\omega^2} \quad (1)$$

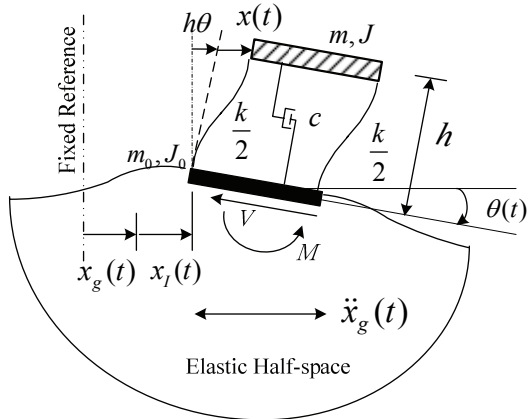


Fig. 1 Simplified model for SSI analysis

Since the coupling terms of soil impedance in Eq.(1) are very small compared to the diagonal terms, they can be neglected for simplification. For derivation, the total displacement amplitude of roof mass in the frequency domain which is the summation of the structure deformation X , the lateral translation of foundation X_f and the interaction displacements Θh resulted from rocking motion of foundation, is substituted and introduced the complex-valued structure stiffness $k^* = k(1 + i2\xi\beta)$ to further simplify the Eq.(1). into the following form

$$m\ddot{X}_f + k^* \left(\frac{1 + \frac{a\beta^2}{-a\beta^2 + S}}{1 + \frac{a_1}{-a\beta^2 + S} + \frac{1}{-b\beta^2 + R}} \right) X_f = -m\ddot{X}_g \quad (2)$$

Now, equation (2) has been transformed into the equation of motion of a SDOF fixed-base model but in terms of the relative displacement. That is to say, the original soil-structure system can be replaced by an equivalent fixed-base model, in which the equation of motion can be written as

$$m\ddot{X}_f + \tilde{k}^* X_f = -m\ddot{X}_g \quad (3)$$

The equivalent fixed-base model has a structure mass same as the original roof mass, but with a modified complex-valued stiffness \tilde{k}^* , expressed as

$$\tilde{k}^* = k^* \cdot [F_{SSI}]_{3dof} \quad (4a)$$

$$F_{SSI} = \frac{1 + \frac{a\beta^2}{-a\beta^2 + S}}{1 + \frac{a_1}{-a\beta^2 + S} + \frac{1}{-b\beta^2 + R}} \quad (4b)$$

In the above equation, the stiffness modification factor of the equivalent fixed-base model is denoted as F_{SSI} , called the factor of SSI, because Eq. (3) is exactly the same as the original structure except that the stiffness is modified. This modification process considers the effects of SSI.

Quantification of SSI effects

Based from the EFB model, the dynamic characteristics of the system, such as the natural frequency and damping ratio, can be easily determined as follows.

The predominant frequency of the EFB model, called $\tilde{\omega}_1$, thereafter, will represent the predominant frequency of the original soil-structure system. From equations (3) and (4) the modification factor μ for predominant frequency of the soil-structure system compared to the same structure founded on a fixed-base can be determined by

$$\mu^2 = (\tilde{\omega}_1 / \omega_s)^2 = [F_{SSI}]_{RE} \quad (5)$$

where $[F_{SSI}]_{RE}$ represents the real part of F_{SSI} and the structure damping is neglected for dimensionless frequency $a_0 = \omega r_0 / C_s$ less than 1, the values of k_{VV} and k_{MM} can be regarded as frequency independent and replaced by averaged values \bar{k}_{VV} and \bar{k}_{MM} .

Under such circumstance, equation (5) can be simulated by a hyperbolic function of $E_0(Gr_0/k)$ and represented by

$$\mu^2 = \frac{E_0(Gr_0/k)}{E_0(Gr_0/k) + 1} \quad (6)$$

where and $E_0 = f(a, b, r_0, h, \bar{k}_{VV}, \bar{k}_{MM})$, the initial slope of the hyperbola, is a function of the configuration of the structure and the foundation. For a given soil-structure system, the value of E_0 can be calculated in advance according to its definitions. It can be seen that the value of μ is decreased when $E_0 (Gr_0/k)$ is decreased. The more flexible the soil is, the lower the natural frequency of the soil-structure system will be.

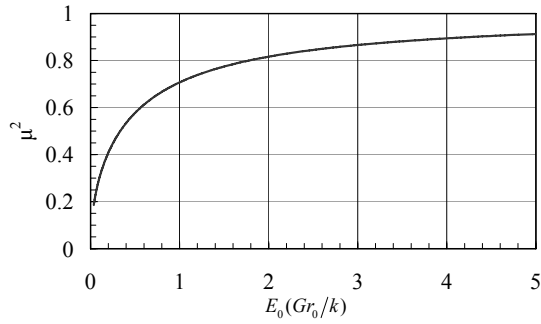


Fig. 2 The modification factor of predominant frequency of the soil-structure system (By normalized hyperbolic function method)

Another important issue is to calculate the damping ratio of the equivalent fixed-base model. In this current study, it is suggested to choose the damping ratio corresponding to the natural frequency $\bar{\omega}_1$ and regarded as a frequency-independent damping ratio of the system. It will be called the equivalent damping ratio $\tilde{\xi}_1$ of the fixed-base model.

$$\tilde{\xi}_1 = \xi\mu + \frac{1}{2\mu^2} \cdot [F_{SSI}]_{IM} \quad (7)$$

From this equation, it can be noted that the equivalent damping ratio $\tilde{\xi}_1$ is the combination of the structural damping and the imaginary part of the SSI factor F_{SSI} . The contribution from the part of the structural damping will decrease with the decreasing of μ , while the contribution from the SSI effects will increase with the decreasing of μ .

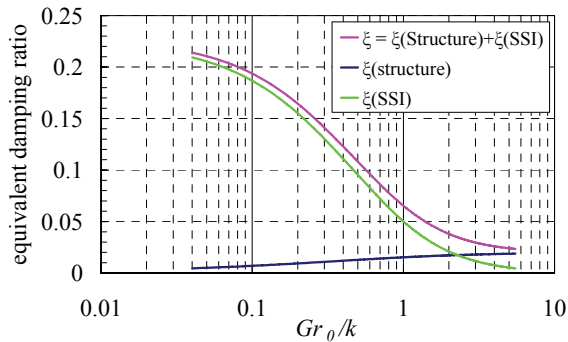


Fig. 3 The equivalent damping ratio of EFB model

SSI Analysis Procedures of FEMA 450

The effective period of the flexibly supported structure, \tilde{T} , shall be determined as follows

$$\tilde{T} = T \sqrt{1 + \frac{k}{K_y} \left(1 + \frac{K_y \bar{h}^2}{K_\theta} \right)} \quad (8)$$

where T is the fundamental period of the structure ; \bar{h} is the effective height of the structure which shall be taken as 0.7 times the total height, h ; K_y and K_θ are the lateral and rocking stiffness of the foundation, respectively ; k , the stiffness of the fixed-base structure, is defined by the following:

$$k = 4\pi^2 W / gT^2 \quad (9)$$

Alternatively, for structures supported on mat foundations that rest at or near the ground surface where the poisson's ratio of ground is equal to 0.4, the effective period of the structure may be determined from:

$$\tilde{T} = T \sqrt{1 + \frac{25\alpha r_a \bar{h}}{V_s^2 T^2} \left(1 + \frac{1.12 r_a \bar{h}^2}{\alpha_\theta r_m^3} \right)} \quad (10)$$

where $\alpha = W / \gamma A_0 \bar{h}$ is the relative weight density of the structure and the soil (γ is the average unit weight of the soils and A_0 is the area of the foundation), V_s is the average shear wave velocity for the soils, r_a and r_m are the characteristic foundation lengths for equivalent area and equivalent static moment of the foundation respectively, and α_θ is the dynamic foundation stiffness modifier for rocking.

If the structure damping ratio is equal to 0.05, then the effective damping factor for the structure foundation system, $\tilde{\beta}$, shall be computed as follows

$$\tilde{\beta} = \beta_0 + \frac{0.05}{\left(\frac{\tilde{T}}{T} \right)^3} \quad (11)$$

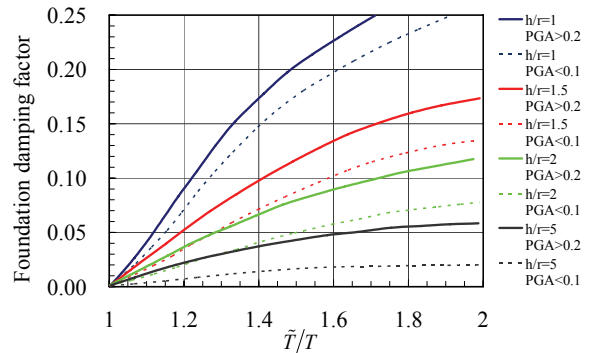


Fig. 4 Foundation Damping Factor (FEMA 450)

where β_0 is the foundation damping factor as specified in Fig. 4. The value of $\tilde{\beta}$ computed from Eq. (11) shall in no case be taken less than 0.05 or greater than 0.20.

In-suit Test and Numerical Cases Analysis

A Large Scale Seismic Test (LSST) had been carried out at Hualien, Taiwan, to investigate the effects of SSI during dynamic loadings. It is an in-situ test program sponsored by EPRI and NRC of USA, CEA and EdF of France, TEPCO and CRIEPI of Japan, KINS and KEPCO of Korea and TPC of Taiwan. The first phase forced vibration test (FVT-1) was conducted under the condition when the containment model had been completed but without any embedment (i.e., before backfilled). The Unified Ground Model for FVT-1 based on all geotechnical investigations conducted at site is shown in Fig. 5.

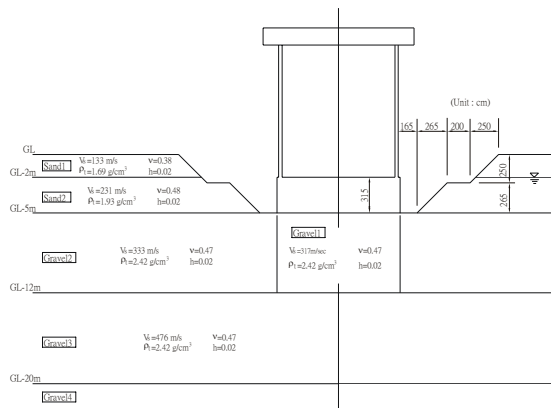


Fig. 5 Unified ground model for FVT-1 analysis

The correlation of the FVT-1 test results to the effective period and the effective damping factor calculated by EFB model and FEMA 450 procedure is shown in Table 1. From the results obtained, it can be found that the EFB rocking model has a natural frequency of 4.3 Hz and an equivalent damping ratio of 3.9%. Both of them are very close to the results of FVT-1.

Tab. 1. The analysis results of FVT-1 test

	EFB	FEMA	FVT-1
W (t)		520	
r (m)		5.41	
H (m)		15.38	
Vs (m/s)		317	
T (s)	0.113		—
\tilde{T} (s)	0.233	0.191	0.217
ζ_{SSI}	0.039	0.068	0.037

Furthermore, to investigate the variation of SSI effects with different structural period and different sites, a series of numerical case studies on general RC

buildings had been conducted in this study. Three SDOF structures, S1, S2, and S3, with the same roof mass of 1000 tons and rigid massless surface foundation with a diameter of 10 m, have total height of 5 m, 10 m, and 15 m, respectively (i.e. the structure periods are 0.234 sec, 0.394 sec, and 0.534 sec, respectively). Those buildings are located at different sites with soil shear wave velocity of 400 m/s (hard), 250 m/s (medium), and 150 m/s (soft) individually. The effective period and the effective damping factor of these cases computed by EFB model and FEMA 450 procedure are shown in Table 2. Both analysis revealed that the effect of SSI is most notable when a short period structure is located at soft (long period) ground.

Tab. 2. The analysis results of numerical cases

Vs (m/s)		S1		S2		S3	
		T(s)	ζ_{SSI}	T(s)	ζ_{SSI}	T(s)	ζ_{SSI}
400	EFB	0.96	5.6%	0.98	5.1%	0.98	5.0%
	FEMA	0.97	5.4%	0.99	5.2%	0.99	5.2%
250	EFB	0.90	7.4%	0.95	5.5%	0.96	5.1%
	FEMA	0.94	6.1%	0.97	5.5%	0.98	5.4%
100	EFB	0.78	14.1%	0.87	7.4%	0.89	5.8%
	FEMA	0.73	15.7%	0.83	10.0%	0.86	10.3%

Conclusions

The Equivalent Fixed-Base (EFB) model proposed in this study has been used to characterize the effects of soil-structure interaction completely. This equivalent model is actually a rigid-base model that can be conveniently applied in a conventional structural analysis for engineering applications and seismic design.

References

- Building Seismic Safety Council of National Institute of Building Sciences, "Recommended Provisions for Seismic Regulations for New Buildings and Other Structures (FEMA 450)", 2003 Edition, Washington, D.C., 2004.
- Chen, C.H., Hsu, S.Y., "Equivalent Fixed-Base Model for Soil-Structure Interaction Analysis," Journal of Mechanics, Vol. 22, No. 3, 2007, pp. 167-180.
- CRIEPI, "The Unified Model of the Ground for FVT-1 Analysis", Report, Central Research institute of Electric Power industry, Tokyo, Japan, 1993.

Preliminary Study of Seismic Response and Disaster Prevention Information System

Hui-Ping Wang¹, Wei-Jen Chen², Wei-Chang Chen³, Chin-Hsun Yeh⁴

Abstract

Along with the development and updating of Taiwan Earthquake Loss Estimation System (TELES), the databases and seismic disaster assessment models have been fully developed in National Center for Research on Earthquake Engineering (NCREE). However, those valuable data and research results could not be shared with public due to expensive GIS software and for protection of intellectual property right. From the information sharing point of view, NCREE planed to build an information system through the web geographic information system (Web-GIS) technology. Starting in 2008, "Seismic Response and Disaster Prevention Information System" was set up; it integrated the result of early assessment of seismic disaster and provided information to rescue organizations

Keywords: Taiwan Earthquake Loss Estimation System (TELES), Web-Geographic Information System (Web-GIS), Seismic Disaster Simulation, Early Assessment of Seismic Disaster.

Introduction

The main objective of this research is to establish a seismic response and disaster reduction information system on internet so that the damage estimates of general building stocks, various kinds of facilities and lifeline systems can be used more effectively; and also it offers valuable information to all rescue organizations or emergency decision-making units within the shortest period of time after an earthquake happens. The software and technologies we used to build "Seismic Response and Disaster Prevention Network System" are MapInfo's MapXtreme and Microsoft VS.NET, AJAX, HTML, and XML. The tasks of setup "Seismic Response and Disaster Prevention Information System" include (1) exhibit and inquiry system of transportation network and major facilities, (2) seismic disaster information management system, (3) seismic early assessment and seismic disaster simulation system, and (4) website of TELES.

Exhibit and Inquiry System of Transportation Network and Major Facilities

In recent years, NCREE collected various types of seismic disaster prevention databases, including earthquake catalogs, strong earthquake records, distribution of active faults, engineering borehole data, general and school buildings, roads and bridges, electricity system, potable water and gas pipelines, etc. However, because of the price of GIS tool, data ownership, and privacy constraint, those valuable databases and research results cannot be effortlessly shared with public. In view of this, this study not only expects to build an information display and query system through the Web-GIS technology, but also integrates different information websites into one platform for serving more users, academic researchers, and disaster prevention units.

"Exhibition and inquiry system of transportation network and major facilities" contains two parts of functionalities; one is roads or landmarks searching, and the other one is layer controlling. Also, users can experience some basic functions, for example, zoom in, zoom out, pan, and ten default scale levels.

¹ Beginning Technician, National Center for Research on Earthquake Engineering

² Beginning Technician, National Center for Research on Earthquake Engineering

³ Assistant Research Fellow, National Center for Research on Earthquake Engineering

⁴ Research Follow, National Center for Research on Earthquake Engineering

In order to facilitate users to query data, the search function provides several querying criteria including the dropdown lists of counties, towns, and types, and inputting keywords. For convenience, the system will list out the corresponding town to dropdown list of town while county has been selected. Moreover, users can set inquiry types such as roads, government agencies, cultural and educational institutions, transport stations, public facilities, restaurants and hotels, bridges, and disaster reports. The results not only sort by name, county, and town, but also display and locate in the center of the map.



Fig. 1 Example of exhibition and inquiry of facilities

“Exhibition and Inquiry of Transportation network and major Facilities System” also has layer control utility. It divides base map layers into three categories, such as landmarks, roads, and others (rivers, lakes, and satellite). In the landmarks category, it includes government agencies, cultural and educational institutions, transport stations, public facilities, landscapes, restaurants and hotels, and bridges. Additionally, the transportation system has been separated into seven different types of roads for instance highways, expressways, provincial roads, county roads, village and town roads, city roads, and lanes. The users can not only easily choose to exhibit specific layers by their demand; but also clearly identify landmarks and roads by different symbols and colors.



Fig. 2 Use of layer control to select visible layers

Seismic Disaster Information Management System

In order to provide seismic disaster evaluation and analysis to rescue organization, and coordinate with each year earthquake prevention training hosting by Nation Disaster Prevent and Protection Commission, the Seismic Disaster Simulation Division in National Center for Research on Earthquake Engineering established a seismic disaster information upload and management system. When strong earthquake occurs, NCREE will offer a group of well trained staffers to disaster area; there are disaster evaluation, collection, and investigation teams and administrative support group. For the disaster investigation team, these are responsible to investigate actual disaster in disaster area, and give disaster information back to NCREE. Then, disaster collection team will assemble all the information and upload to “Seismic Disaster Information Upload and Management System”; the system can also arrange disaster information and pictures issued by electronic media.

As a result, the purpose of “Seismic Disaster Information Upload and Management System” is to record the earthquake disaster in detail. It offers seven types of loss survey form such as building, road and bridge, non-structural building, harbor and airport, the geology, living system, and historic monument; also, the multimedia and pictures files are available to store in the database. The “Disaster Information Upload and Management System” integrates MapXtreme Web Map, AJAX, and Microsoft Silverlight technologies to provide asynchronous data update, precise disaster loss point positioning, reviewing and verifying disaster report, and seismic information exhibits. Once the new seismic disaster information adds to database, the contents of the information or report will be evaluated and reviewed in carefully; then released to public as an official seismic disaster report. In addition to exhibit and query the seismic disaster information, it also builds a Web Service interface for external releasing; it shares data and integrates with other Web-GIS systems.

This system has been used and modified during the “Wen-Chuan earthquake, China 2008”. Furthermore, to prevent abuse by general users, its login system is combined with “NCREE Friends”; the logged in user can access or upload disaster based on his or her permissions.

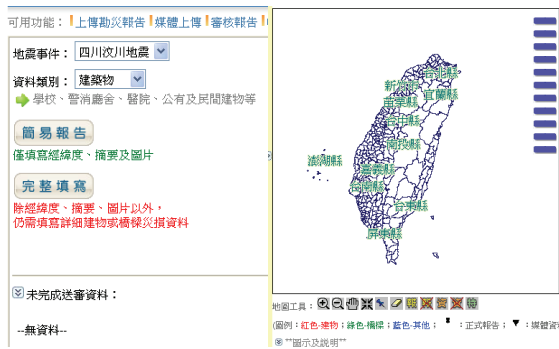


Fig. 3 Interface of seismic disaster information and management system

Display of Seismic Early Assessment and Disaster Simulation

"Taiwan Earthquake of Loss Estimates System" is an earthquake disaster simulation system. For effective and accurate simulation of the disaster of earthquake, it must have a complete database and analysis models. Although NCREE offers TELES application for free, it currently does not provide database to general users. In order to offer variety of seismic evaluation results to public and disaster prevention units, we established a "Seismic Early Assessment and the Seismic Disaster Simulation System" by using Web-GIS technology.

Results of Seismic Early Assessment

Taiwan Earthquake of Loss Estimation System starts to simulate seismic disaster after receiving the earthquake message from Central Weather Bureau by email; based on the seismic parameters from the email, TELES evaluates the building damages, casualties and economic loss. The result of assessment can be viewed or accessed on the website immediately. Through the website, the disaster rescuers can clearly view the thematic map of earthquake events, the location of earthquake epicenter, faults direction, and disaster loss distribution. Furthermore, the researchers can download related data for follow-up study.

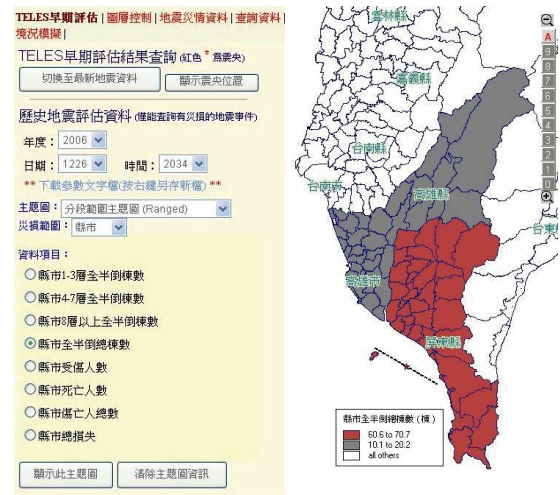


Fig. 4 Query results and thematic map of seismic early assessment

This system can also exhibit the seismic disaster reports, which come from "The Disaster Information Upload and Management System". The user can view the detail of the seismic disaster report, for example location of disaster losses, information of latitude and longitude, and hyperlink of complete report. All the result of seismic early assessment and disaster report can show on the same map; it really assists disaster assessment and provides more precise information to commander of rescue.



Fig. 5 Exhibition of seismic disaster report

Results of Seismic Disaster Simulation

Using TELES earthquake simulation technology can build a seismic loss simulation database, which contains potential seismic hazards analysis, general building damage assessment, casualties and economic losses. In this study, we establish online seismic disaster simulation distribution and inquiry system to combine the pre-built seismic loss database, and to provide a variety of seismic disaster simulation results on the Web-GIS.

Users can set earthquake scale (5.1~7.3 scale), focal depth (10~90 km.), epicenter location (latitude 21.1~25.9, longitudes 119.1~122.9), and faults (0~135 degree) to simulate earthquake disaster. The result is not only shown on the map, but is also exhibited by different types of thematic maps such as range, dot density, individual values, pie chart, or bar chart, spatial units (counties or towns), and the simulation subjects (building damage, casualties, fire, shelter, debris). Also, this function is very useful for general seismic disaster education and training.



Fig. 6 Assessment results and thematic map of seismic disaster simulation

Website of TELES

NCREE has devoted developing of “Taiwan Earthquake of Loss Estimation System—TELES” in recent years. Based on the knowledge and information sharing, Seismic Disaster Simulation Division in National Center for Research on Earthquake Engineering established a “Taiwan Earthquake of Loss Estimation System Website” to provide general TELES information to public. All the seismic disaster analysis results, research reports, training material and user manual, software, and database are available to download from the website.



Fig. 7 homepage of TELES Website

During this year, Seismic Disaster Simulation Division in NCREE processes web page layout and services update of Taiwan Earthquake of Loss Estimation System Website, the new services include: (1) integration of Login System, (2) Download site of Software and Database, and (3) Setup of a Technical Forum; all the details address as follows:

Integration of Login System

Taiwan Earthquake of Loss Estimation System Website provides a lot of valuable research results, such as computing software, reference databases and research reports. In order to carry out the statistics and analysis of users, Taiwan Earthquake of Loss Estimation System Website needs a member database and login system. However, the users usually visit both NCREE and Taiwan Earthquake of Loss Estimation System websites. Therefore, we combined Taiwan Earthquake of Loss Estimation System and NCREE member database into a unique member database. It allows users to access and download data through the “NCREE Friends’ Login System”.

Download Site of Software and Database

In the past, the application of software and example data of TELES (Taipei area only) needed to be requested through the official document or the application form. After receiving it, NCREE would send out data sources CD-ROM by mail or files by FTP (File Transfer Protocol). In order to make work flow more efficient, the program files and sample databases have been uploaded to website, as long as the user is able to log on to “NCREE Friends”. The latest version of execution file, user manual, training materials, technical reports, and sample databases can be easily downloaded.

Setup of a Technical Forum

TELES website set up a technical forum area to interact with users. Through the Forum, users can post questions or suggestions on the website; all the requests will have professional researchers to reply answers and recommendations.

Conclusion

In this study we have shown that through the Web-GIS technology, the TELES has become well-known in public. It provides general educations to users and the information of early assessment of seismic disaster to rescue decision-makers. In order to prevent serious disaster and accelerate seismic rescue, the TELES Web-GIS system will improve the performance of display data and add the satellite photographs layer to base map in the further studies.

A Preliminary Study on the Performance Assessment of Water Network Systems Following Earthquakes

Gee-Yu Liu¹ and Hsiang-Yuan Hung²

劉季宇¹、洪祥瑗²

Abstract

In this research work, a methodology for assessing the seismic performance of water systems has been preliminarily proposed based on earthquake scenario simulation and pipe flow hydraulic analysis. The water system of Taipei metropolitan area was selected as a test bed and its serviceability following earthquakes was investigated.

Keywords: water systems, serviceability, seismic scenario simulation

Background

Water systems are one of the most essential infrastructures in modern societies. The disruption of water supply following earthquakes may cause serious inconvenience to the daily life of people in the disastrous areas. Medical caring, sanitation, fire-fighting and so forth may be seriously affected, too. Moreover, the time needed for the recovery of water supply is usually much longer than that for, says, electricity or telecommunication due to the difficulties raised by the damage in buried water pipelines. As a result, it is highly desirable to facilitate water utility managers with a seismic scenario simulation tool for estimating the likely service disruption following earthquakes. Measures could be taken then to improve the seismic preparedness and emergency response more appropriately. One that best exemplifies this is the software called GIRAFFE (Graphical Iterative Response Analysis for Flow Following Earthquakes) [Shi, 2006; Wang, 2006]. It was developed by O'Rourke and co-workers in the Cornell University. Since 2006, LADWP (the Los Angeles Department of Water and Power) has formally adopted GIRAFFE as a decision-supporting tool for its water system [MCEER]. On the other hand, the similar technology for the assessment of seismic serviceability of water systems is yet to be developed in Taiwan.

Pipe Damage and Negative Pressure

In this study, the pipe damage model summarized

by Shi and Wang [Shi, 2006; Wang, 2006] has been adopted. This model includes pipe break and various types of pipe leaks, and the probability that each will occur in various pipe materials, and also the hydraulic models and parameters for each type of pipe damage. Following their findings from water pipelines and their damages in past earthquakes in the U.S., water pipe materials could be classified into 5 types: cast iron, ductile iron, jointed concrete, riveted steel and welded steel. For the first four pipe materials, the total number of repairs consists of roughly 80% of pipe leaks and 20% of pipe breaks, respectively. While for welded steel pipes, only 20% of the total repairs are pipe leaks, and the rest damages are merely deformation and won't affect the pipe's ability to carry water. Furthermore, there are five different types of pipe leaks, namely the annular disengagement, round crack, longitudinal crack, local loss of pipe wall, and local tear of pipe wall at welded slip joint, as illustrated in Figure 1.

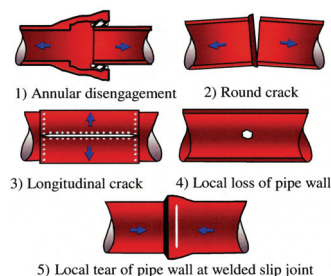


Fig. 1 Schematic views of five types of pipe leaks [Shi et al., 2006]

¹ Associate Research Fellow, National Center for Research on Earthquake Engineering, karl@ncree.org.tw

² Assistant Research Fellow, National Center for Research on Earthquake Engineering, hyhung@ncree.org.tw

Shi and co-workers further proposed the hydraulic models for pipe breaks and leaks, respectively [Shi et al., 2006]. The hydraulic model for a pipe break is depicted in Figure 2. At each of the broken ends, a reservoir and a check valve are added to mimic the condition of water flowing to the atmosphere. Hydraulically, a pipe leak is equivalent to a sprinkler with a specific discharge coefficient and an orifice size. The sprinkler can be modeled as fictitious pipe linking the original pipe and an added reservoir, as depicted in Figure 3. A check valve is designated to the fictitious pipe to ensure that water flows from the leaking pipe to the reservoir.

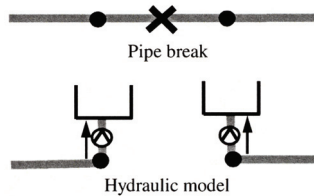


Fig. 2 Hydraulic model for a pipe break [Shi et al., 2006]

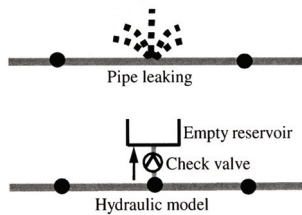


Fig. 3 Hydraulic model for a pipe leak [Shi et al., 2006]

While performing hydraulic analysis of a water network with damaged pipelines, it is likely to predict negative pressure at some of the nodes. Negative pressure is generated here due to the employment of the assumption that the pipe flows are always full and pressurized. However, water pipelines are not air-tight, especially when they are damaged, and the assumption no longer holds somewhere and sometime. Usually, hydraulic analysis of a damaged water network tends toward overestimating its ability to convey water if the elimination of negative pressure is not dealt with during analysis. In this study, the approach proposed by Ballantyne et al. [1990], which assumes that no water will flow through negative pressure nodes, was employed.

Seismic Assessment Procedure for Water Networks

The procedure for the assessment of seismic serviceability of a water network system is illustrated in the flow chart in Figure 4, which reads:

- (1) Read the input file for the hydraulic analysis of the interested water system. This file is usually prepared by the water utilities and is compatible

with the employed analysis software in terms of data formatting. All attributes of the components in the water system (e.g. reservoirs, tanks, pumps, nodes and pipes) are defined in the file.

- (2) Simulate the pipeline damage of the water system based on an earthquake scenario. A pre-processor has been developed in this study to decide the locations and attributes of pipe breaks and leaks in the pipeline network in a probabilistic way, and then to modify the input file according to the simulated pipeline damage. It takes into account the seismic hazard and the pipe repair rate (see below), and the pipe damage model provided by Shi and Wang [Shi, 2006; Wang, 2006] was employed.
- (3) Check the connectivity of all nodes to the system with simulated pipeline damage. Remove the disconnected nodes by further modifying the input file.
- (4) Perform hydraulic analysis using EPANET.
- (5) Check the pressure at all nodes from the result of Step (4) and, following the approach proposed by Ballantyne et al. [1990], summarize the water supply by eliminating the demands at nodes of negative pressure.

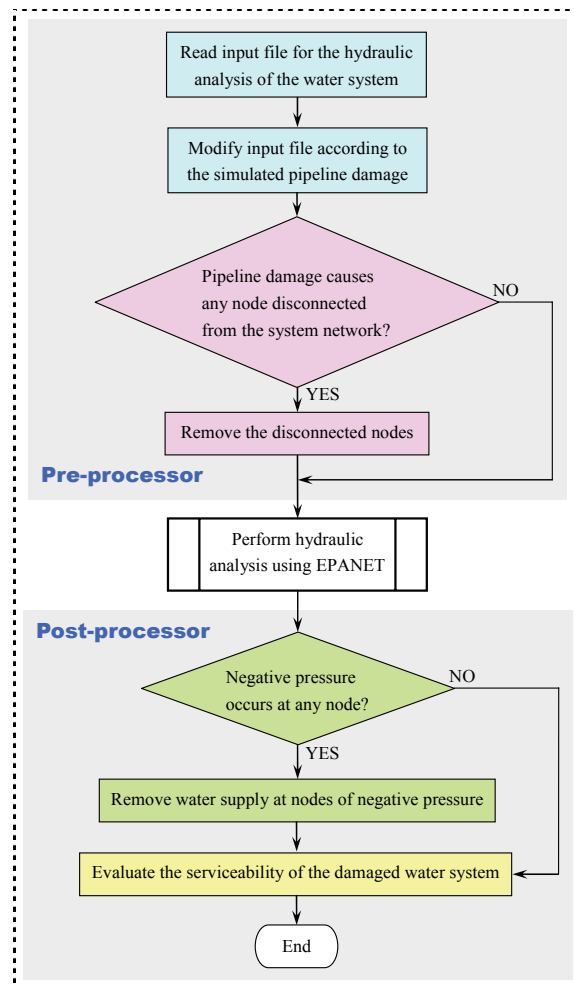


Fig. 4 Flow chart for the assessment of seismic serviceability of water systems

In Step (4), the software EPANET is a computer program developed and maintained by the U.S. Environmental Protection Agency for the simulation of hydraulic and water quality behavior within a pressurized pipe network [Rossman, 2000]. It is free software and has been widely adopted by commercial packages, e.g. WaterCAD and MIKE NET, as the hydraulic engine. GIRAFFE employs the computer codes of EPANET for hydraulic analysis, too.

Case Study

The water system of the Taipei metropolitan area has been selected as a test bed for case study. It is operated by the Taipei Water Department (TWD). It provides service to the Taipei City as well as four other cities of the Taipei County. TWD has a service region of 434 square kilometer, and serves water to 1.51 million customers or 3.85 million people. The daily water supply is around 2.5 million tons. The entire water system is hydraulically separated into 10 service areas, as illustrated in Figure 5. Table 1 summarizes the statistics of each service area including the numbers of nodes, pipes, pumps, tanks, reservoirs and total pipe length.

Regarding the repair rate (RR , the number of repairs or damage points per km) for the pipe damage caused by earthquake ground shaking (in terms of PGA in gal), the following equation was tentatively employed in this study:

$$RR = \begin{cases} 1.2 \times 10^{-3} \cdot PGA^{0.9735} & \phi \leq 300\text{mm} \\ 0.8 \times 10^{-3} \cdot PGA^{0.9735} & 300\text{mm} < \phi \leq 500\text{mm} \\ 0.4 \times 10^{-3} \cdot PGA^{0.9735} & 500\text{mm} < \phi \end{cases}$$

Two earthquake scenarios have been considered. They are the M5.9 earthquake associated with the Sanchiao fault and the M7.5 earthquake associated with the Hsincheng fault. The two fault lines are depicted in Figure 6. For each earthquake scenario, the assessment procedure has been conducted 100 times for the pipe network of each service area. The simulated distributions of serviceability index for the TWD water system are depicted in Figures 7 and 8 for the M5.9 and M7.5 earthquake scenarios, respectively. Here, the serviceability index (SI), the ratio of flow at demand nodes before and after the earthquake, is used to quantify the water network seismic performance in each service area. In the M5.9 case, the SI values vary between 0.45 and 0.89. While in the M7.5 case, the SI values vary between 0.44 and 0.92.

Conclusions

A methodology has been preliminarily proposed for the seismic assessment of water network systems. It consists of earthquake scenario simulation and pipe flow hydraulic analysis. The water system of Taipei metropolitan area has been selected for case study and

its capability to convey water following earthquakes has been estimated. Implementation of the proposed methodology will benefit urban earthquake disaster preparedness and mitigation.

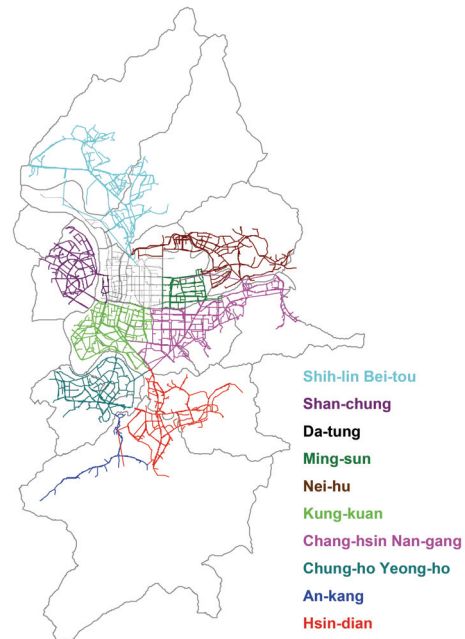


Fig. 5 Pipe networks of the 10 TWD service areas

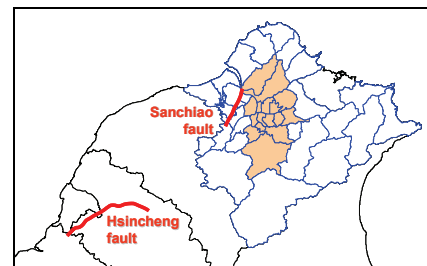


Fig. 6 The Sanchiao and Hsincheng fault lines and their relation with the TWD service region

Table 1. Pipe network statistics of the TWD system

	Nodes	Pipes	Pumps	Tanks	Reservoirs	Pipe Length (km)
01	3,254	3,376	40	10	0	171,359
02	2,289	2,366	18	3	0	102,684
03	4,288	4,421	27	2	0	143,565
04	1,769	1,822	18	2	0	68,446
05	2,591	2,673	10	2	0	116,349
06	3,691	3,796	17	2	0	142,553
07	4,985	5,127	32	3	1	193,524
08	2,338	2,394	5	1	0	98,039
09	587	601	12	2	0	28,829
10	2,716	2,799	20	3	0	130,933
Sum	28,508	29,375	199	30	1	1,196,281

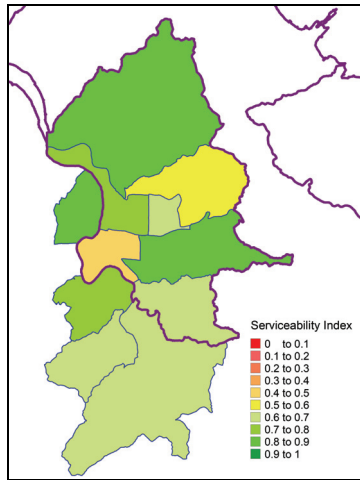


Fig. 7 The simulated distribution of SI value for the TWD water system following the considered M5.9 earthquake

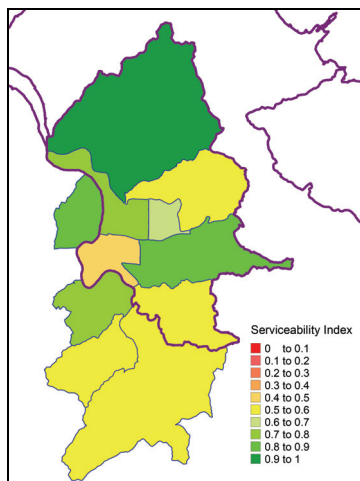


Fig. 8 The simulated distribution of SI value for the TWD water system following the considered M7.5 earthquake

Shi, P. (2006). Seismic Response Modeling of Water Supply Systems, Ph.D. Dissertation, Cornell U., Ithaca, NY.

Shi, P., O'Rourke, T. D. and Wang, Y. (2006). "Simulation of Earthquake Water Supply Performance", Proc. 8th U.S. Nat. Confer. Earthquake Eng., Paper No. 1295, San Francisco, CA.

Wang, Y. (2006). Seismic Performance Evaluation of Water Supply Systems, Ph.D. Dissertation, Cornell U., Ithaca, NY.

Acknowledgement

This research work was funded by the National Science Council, Taiwan under Grant No. NSC-96-2625-Z-492-007, and was carried out using the network data of the Taipei Water Department for hydraulic analysis. Both are gratefully acknowledged.

References

Ballantyne et al. (1990). Earthquake Loss Estimation Modeling of the Seattle Water System, Technical Report, Kennedy/Jenks/Chilton, Federal Way, WA.

MCEER, http://mceer.buffalo.edu/publications/bulletin/06/20-02/03_ladwp.asp.

Rossman, L. A. (2000). EPANET 2 User's Manual, EPA, Cincinnati, OH.

Development of A Prototype of Strong Ground Motion Estimation System

Tao-Ming Chang¹

張道明¹

Abstract

Although disastrous earthquakes may not happen everyday, governments in various countries need one decision support system for managing emergency response during such events. To support such a system, the Center for Research on Earthquake Engineering (NCEE) is now developing a Strong Ground Motion Estimation System. This system is designed to work with the Taiwan Earthquake Loss Estimation System (TELES) which developed by NCEE, and wish to become the prototype system for Taiwan. The Strong Ground Motion Estimation System (SGMES) needs to obtain some relevant waveform data immediately after an earthquake event in computing the focal mechanism and in solving the earthquake rupture patterns within 30~60 minutes after an earthquake. In remote regions and countries, this system still can fetch seismograms from global seismic network via internet after 30~60 minutes and to solve the focal mechanism and earthquake rupture patterns for additional 60 minutes. After this earthquake source resolving process, various computation techniques can be applied to make synthetic seismograms for the earthquake affected regions. Local site responses can be corrected if the site information is available. The PGA and SA contour maps can be produced to check soil liquefactions and landslides. The response spectrums can be also produced also to check immediately the status of bridges and relevant structures.

Keywords: strong ground motion estimation

Introduction

In NCEE, a “Strong Ground Motion Estimation System” or SGMES has been proposed for the purpose of supporting hazard mitigation, refining building codes, and obtaining better seismic-resistant designs.

Various methods are included in the SGMES. First is to set up a seismic network in monitoring micro earthquakes and in understanding current source rupture patterns of active faults. Second is to develop computation codes in dealing with the near fault ground motion. Third is to study the site effects using four major methods. Fourth is to monitor the concentration of soil Radon which is one of the earthquake precursors. Fifth is to solve the earthquake rupture patterns. Last is to combine all the aforementioned methods to complete the SGMES. The system framework is shown in Fig.1. This proposed system can be further worked with TELES

(Taiwan Earthquake Loss Estimation System) which is a major project by NCEE. In the future, the proposed system could be a very important tool for central and local governments of Taiwan.

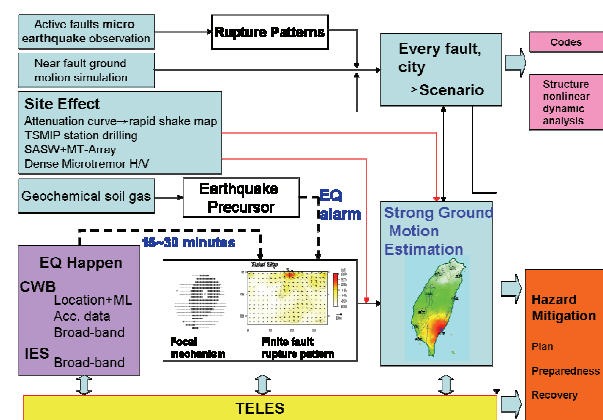


Fig.1 Framework of Strong Motion Estimation System

¹ Associate Research Fellow, National Center for Research on Earthquake Engineering, tmchang@ncee.org.tw.

Micro Earthquake Monitoring Networks

Roughly about 90% of Taiwan's population lives in the western part of Taiwan. In this region, at least 30 active faults were identified. Most of them are located in the western foothill region. To fully understand the possible rupture pattern of a future disaster earthquake which related to active faults, the current source rupture patterns has to be studied. The best tool to achieve such task is to set up dense micro-earthquake monitoring networks. So far, two micro-earthquake monitoring networks were setup in Hsinchu-Miaoli area and in Tainan-Chiayi area. Another seismic network will be deployed before the end of 2008 to cover the Taichung-Nantou area. It is believed that if these micro-earthquakes have been studied carefully, some important insights about the seismic zone can be obtained. A large amount of micro-earthquakes were observed. The number is 2~3 times than Central Weather Bureau's S13 network. For the northern network, most of them are in the Sanyi-Puli seismic zone, the Shih-Tan fault, and in the foothill regions. For the southern network, the earthquakes are strongly related to the Chuko fault.

Site Effect

In NCREE, there are several researches related to the so-called site effect. They are: (1) Using the TSMIP (Taiwan Strong Motion Instrumentation Program) data to get local amplification factors for each TSMIP acceleration station this is useful to quickly estimate the shake-map after a strong earthquake happen, (2) Study the geological condition of TSMIP stations by drilling the geological descriptions and STP-N values are obtained and the seismic V_p and V_s velocity profiles are obtained by PS suspension logging method, (3) Obtain deeper V_s velocity profile by using micro-tremor array method, and (4) Perform micro-tremor measurements for a large area to study the site effects.

Geotechnical Database

To maximize the use of TSMIP data, the clear site condition are indispensable. NCREE collaborates with CWB (Central Weather Bureau) to drill each TSMIP station after the 1999 921 earthquake. There are three major items in the Geotechnical Database of Taiwan. The first item is the general information of the station site, including latitude and longitude of the station, ground water level, geographical/ topographical conditions, and list of surrounding structures. The second item is the physical properties of soils. The SPT-N value, water content, unit weight, soil classification, and grain size distribution were obtained by on-site boring, sampling, and laboratory testing. After drilling the borehole, the suspension P-S

logging technique was used to measure the wave velocity of the stratum in every 0.5 m depth. The wave velocity of the stratum is an important index for site classification, thus it was selected as the third item in the database. If the geological condition of the station site is classified as the rock outcrop, only the general environmental investigation was performed to collect the basic information of the station. This project has been conducted for eight years. Up to now, the site investigations at 295 station sites were completed, including 60 stations in 2000, 65 stations in 2001, 50 stations in 2002, 54 stations in 2003, 37 stations in 2004, and 29 stations in 2005. Those stations are located on the alluvial deposit, gravel or even rock sites. All the results are summarized on a web page.

Most studies on site effect for earthquake ground motion were based on the soil properties in the upper 30 m. In the 1997 UBC and 1997 NEHRP provisions in the USA, the average of the shear wave velocity for the top 30 m soil layer is used as an index for the site classification. In the site classification of Taiwan free-field strong-motion stations, the site conditions are classified as class B (rock), class C (soft rock or very dense soil), class D (stiff soil), and class E (soft soil) according to the geological age, rock type, and the average of SPT-N values for the upper 30 m of the stratum. With detailed subsurface soil profile and quantitative soil properties (SPT-N values and wave velocities) on a station site, the site effect of ground motions can be analyzed for a certain class of site conditions. Engineers may evaluate appropriate peak ground acceleration for the earthquake-resistant design of structures.

Dense Microtremor Measurements

In the last five years, NCREE has measured more than 4000 microtremor data in Taiwan. The measured regions include most populated cities and plains where people live. The average spacing for these data is roughly 2 kilometers for most plains; 1 kilometers for Ilan plain, and 700 meters for Taipei and Kaohsiung cities. For some special regions such as Science Parks, the microtremor measurements will be very dense.

The Science Parks of Taiwan have become the centers for catering various different types of industries and contributed 16% GDP of Taiwan. But their locations are very susceptible to earthquakes events due to Taiwan's tectonic activities. To reduce possibly the losses during the shaking of strong earthquakes, it is therefore necessary to have a sound and reliable hazard mitigation plan. So far, such a plan is not completely conceived because of lack in some critical and relevant factors. In this project, two factors are aimed to be produced for that purpose. First, is to estimate the status of active faults near these Science parks and second, is to measure the site effect on these Science parks.

Up to now, dense microtremor measurements are being performed for most Science Parks. The

measurement is very dense spatially at the average distance between every two measurements is about 150–200 meters inside the Science Parks, and about 300–400 meters in the surrounding areas. The microtremor data has been processed using the spectrum H/V ratio method. For example, the dominant frequency map of the Taichung Science Parks can be identified. The Taichung Science Park is located at the east flank of Dadu mountain. From the dominant frequency map, it is concluded that the thickness of top loose sediment layer is thickening along the west to east direction. This phenomenon is consistent with the nearby topography.

Microtremor, also called as earth noise, is the summation of many seismic signals caused by various sources including nature and man-made vibrations. The vibration sources include, for example, biological activities, traffic, wind, ocean tides etc. Short period microtremor consists of Rayleigh waves induced by local traffic vibrations from different directions. The major advantage of microtremor survey is the less cost, fast, convenient, and its easiness to be analyzed. The microtremor data is easier to obtain than the traditional strong ground motion data which require installing acceleration seismometers and be observed for many years. Microtremor survey is very efficient also, especially in the urban areas where seismic reflection survey and drilling wells are not easy to be done.

Using microtremor data to study the underground geological structures, Professor Kanai (1962) of Tokyo University did a lot of pioneer works. One of his conclusions is that the amplitudes of certain period waves existing in the alluvium or weathered sediment sites are larger than those at rock sites. This is because the multiple reflections and resonance of seismic signals in the sediment layers. After that, Kanai and Tanaka (1962) discuss the relation between predominant period and geological layer structures using the distribution curves of seismic wave periods. Katz (1976) did similar research using power spectrums of microtremor. Microtremor can be applied to various purposes, such as investigation on structure vibrations, characteristics of geological structures, site selection for important facilities, sediment thickness, velocity structures of sediments, amplification effect of soft soils etc.

The most commonly used method in studying the effect of site response or the amplification effect of soft soil layer is the two station spectrum ratio method (Borcherdt, 1970; Chávez-Gracia et al., 1990; Field et al., 1992) which is a simple and effective way to eliminate the source and propagating path effects on the regions where numerous earthquakes happened (Lermo and Chávez-García, 1993; Field and Jacob, 1995; Bonilla et al., 1997; Riepl et al., 1998). The critical point in using two-station spectrum ratio method is that a good reference site can be identified with respect to the soil site to be studied. Usually the

reference site is the site on the outcrop of bedrock generally not too far away from the soil site, therefore the spectrum ratio can really eliminate the source and path effects for the strong motion data from the same earthquake. However it is really difficult to find a good reference site thus this limit the use of the said method. To overcome this difficulty in searching a good reference site, Nakamura(1989) proposed an empirical single station horizontal/vertical spectrum ratio (H/V Ratio) method which utilizes the microtremor data measured in situ to study the site effect. In the beginning, the H/V ratio method is applied in studying site response regarding the use of microtremor data. Lermo and Chávez-Gracia(1993) applied the same technique to strong motion data of Mexico and suggested similar site response results were obtained from S wave of strong motion data and microtremor data in the four Mexican cities studied.

Field *et al.*(1990) pointed out that microtremor data can be used in site response and micro-zonation studies. Lermo and Chávez-Gracia(1994) analyzed the weak motion, strong motion and microtremor data of Mexico city, and found that the microtremor data can be used in estimating the predominant frequency and amplification factor of sediment layers. Most microtremor researches confirm that the dominant frequency of soft sediments can be perfectly identified using Nakamura H/V ratio method. Nakano *et al.* (2000) showed a detailed dominant frequency distribution map established using 341 microtremor measurements, strong ground motion data and local geology, and thus has proposed for future seismic micro-zonation and seismic design standards.

Velocity Profile Measurement using Micro Tremor Array Method

As mentioned above, the drilling of TSMIP station stops typically at 30 meters below existing ground level. However, the western coastal plain are much thick than 100 meters. Therefore deeper Vs profiles are required in some sites. In NCREE, Micro-Tremor Array Method was used estimate the Vs velocity profile in such condition. The field setup of the micro-tremor array method utilizes ten seismometers which were arranged in an array with three concentric circles of maximum radius of 32 or 64 m. In each circle, three recorders were arranged in an angle of 120-degree. Each concentric circle has a radius in an order of 2. The total time for measurement at one station must be at least one hour. After the frequency-wave number analysis of data, a dispersion curve for the site will be obtained. By using an inversion process using genetic algorithm search method, the velocity structure can be obtained as depicted in Fig. 2. The result of CHY015 shows minor difference in the used methods. So far, NCREE have performed micro-tremor array method in more than 130 TSMIP stations.

Determine Source Rupture Pattern

Before the strong ground motion of an earthquake can be estimated, a detailed source rupture pattern is needed. There are many methods which can be used to obtain such information and in this particular the generalized ray method has been chosen to generate the tele-seismic P-wave waveforms. The wave-number integration method to generate the local seismograms (usually integrated from the acceleration data) was also used. The multistation waveforms will be fitted by a Genetic Algorithm search method. The best searched result is described as many subevents which have its own locations, magnitude, time delays and source time functions. This information is useful in estimating strong ground motions.

Ground Motion Estimation

In recent years, computer technology has developed tremendously, allowing some complicated and difficult tasks which can not be done ten years ago to be now affordable for individual researcher by using PC-clusters. In this study, wave-number integration method was utilized to compute the synthetic seismograms. The source, propagation path effect and velocity model are discussed in the succeeding paragraphs.

Since 1950s, Thomson (1950) has used the matrix method to deal with the wave propagation in 1-D layered media, and Haskell (1953) promoted it into computing seismic wave propagation which is considered as the modern seismology step into its fast growing stage. Nowadays, seismologists are very familiar with the synthetic seismograms computation method for 1-D layer model. Wave-number integration is one of these methods. The advantage of this method is that various type of waves, such as body waves and surface waves can be calculated simultaneously, and it can deal with the elastic and inelastic attenuation properties of the media. Comparing with other 3-D wave propagation techniques, wave-number integration method needs very small memory spaces and generates high frequency seismic signals. However it fails in dealing with the scattered waves. But when the near-field seismic vibrations from a moderate to big earthquake are required, the source (rupture fault plane) becomes a plane source instead of a point source. Under such situation, the synthetic seismograms computed using wave-number integration are acceptable to be used because the seismograms are now sensitive to source rupture patterns instead of scattered waves. The regions of disaster are close to the epicenter thus the wave-number integration method with the plane source is a proper way to study the strong ground motion patterns. To generate high frequency seismic signals from a plane source, the fault plane needs to be divided into many subfaults and thus, the finite

subfault area will have shorter source time functions which mean the higher frequency seismic signals.

In some cases, the strong ground motion numerical simulations will be done in the following manner. First, the rupture plane will be constructed using the source parameters published by Harvard University and USGS. Second, the rupture fault plane will be divided into many subfaults. The size of each subfault is 1km by 1km. Third, the source rupture parameters will be set and is explained as follows: The earthquake depth will be different for different scenarios. When the earthquake began to rupture, the front of rupture will propagate outward using roughly 0.85Vs and the maximum fault displacement will be decreased exponentially outward from the earthquake focus. The rupture velocity, source time function, slip length, slip direction, the initial rupture time for each subfault will be changed slightly and randomly.

Conclusions

In this study, the ongoing development of Strong Ground Motion Estimation System in NCEE is elucidated. The said system is designed to resolve the earthquake focal mechanism using local acceleration data right after an earthquake event. The detailed source rupture pattern is needed to be derived within 60 minutes. Then, a lot of synthetic seismograms should be computed for affected regions to evaluate the situations of some important buildings, bridges and relevant structures.

References

- Field, E. H., Hough S. E. and Jacob K. H. 1990. Using microtremors to assess potential earthquake site response : a case study in Flushing Meadows, New York City. *Bull. Seism. Soc. Am.* 80:1456-1480.
- Haskell, N. A., 1953. The Dispersion of Surface Waves in Multilayered Media, *Bull. Seism. Soc. Am.* 43:17-34.
- Kanai, K. and Tanaka 1962. On the predominant period of earthquake motions. *Bull. Earthq. Res. Inst.* 40:855-860.
- Lermo, J. and Chávez-García F. J. 1993. Site effect evaluation using spectral ratios with only one station. *Bull. Seism. Soc. Am.* 83:1574-1594.
- Nakamura, Y., 1989. A method for dynamic characteristics estimation of subsurface using microtremor on the ground surface, *QR of RTRI*, 30(1): 25-33.
- Thomson W. T. 1950. Transmission of elastic waves through a stratified solid. *J. of Applied Physics* 21:89-93 .

The Engineering Geological Database for Strong Motion Stations in Taiwan

Kuo-Liang Wen¹² and Hung-Hao Hsieh³

溫國樑¹²、謝宏灝³

Abstract

More than 680 seismic stations all over Taiwan have been established by the Central Weather Bureau (CWB) to record ground motion data. In order to obtain the geological conditions and soil profiles at these strong motion stations, a site investigation project was developed by the National Center for Research on Earthquake Engineering (NCREE) and CWB in 2000. The site investigation mainly consists of three parts: the basic description of a site, the on-site boring, and the Suspension P-S Logger technique which is used to determine the P and S wave velocities of the stratum at various depths. The Suspension P-S Logger technique, using a single down-hole probe with one source and two receivers, allows continuous measurements of wave velocities with high resolution. There are 31 seismic stations which were investigated in 2008. With reference to Kyoshin Net in Japan and ROSRINE in USA, a preliminary engineering geological database for 377 seismic stations investigated during 2000 to 2007 has been constructed on NCREE's website for researchers' convenient access to their needed data.

Keywords: Geological Database, Wave Velocity, Seismic Station, P-S Logger, Suspension P-S Velocity Logging System

Introduction

Taiwan is located on the Circum-Pacific seismic belt --- the most active seismic region in the world. Preventing severe losses of lives and properties caused by large earthquake is a major concern for the people in this region. The Taiwan Strong Motion Instrumentation Program (TSMIP) was initiated by CWB in 1991 to monitor ground motions at over 680 free-field stations around Taiwan. Once a major earthquake happens, all the records of ground motions from TSMIP provide useful information for the operation of hazard mitigation. The ground responses monitored by seismographs reveal the characteristics of ground motions in different geological conditions, and these can be used to improve the design spectrum and the current building codes.

More than 1,000 seismic stations have been installed in Japan to monitor ground responses during an earthquake. Researchers can download the data on ground responses via a web site called "Kyoshin Net".

The basic information of a station site, physical properties of soils, and wave velocity of the stratum measured by the down-hole velocity logging technique are also available on the site. After 1994 Northridge earthquake, a project called "Resolution of Site Response Issues from the Northridge Earthquake", ROSRINE, was conducted to study the site responses in the USA. Related information can be accessed in the said web site to download the geological information and the wave velocity profile of a specified station.

The distribution of seismic stations in Taiwan is the densest in the world, although the amount of seismic stations installed by CWB is less than that in Japan and USA. However, the application of earthquake data is being restricted by having an incomplete geological database. Therefore, in 2000, NCREE and CWB collaborated to perform the site investigation to obtain basic soil properties and wave velocity of the stratum. There are 31 seismic stations

¹ Professor, Dep. of Earth Science & Inst. of Geophysics, National Central University.

² Division Head, National Center for Research on Earthquake Engineering.

³ Assistant Research Fellow, National Center for Research on Earthquake Engineering.

which were investigated in 2008 and are shown in Figure 1. The code of the stations is listed in Table 1. All of the stations drilled 35 meters except TAP092. TAP092 is just doing surface investigation. There are 408 seismic stations which were investigated during the period 2000 to 2008 and are shown in Figure 2. With reference to Kyoshin Net in Japan and to ROSRINE in USA, a preliminary engineering geological database for the 377 seismic stations investigated during the year 2000 to 2007 has been constructed on NCREE's website for convenient information access. This is named, "Geological Surveyed Database of CWB Strong Motion Station" and its website address is at <http://geo.ncree.org.tw> (as shown in Figure 3).

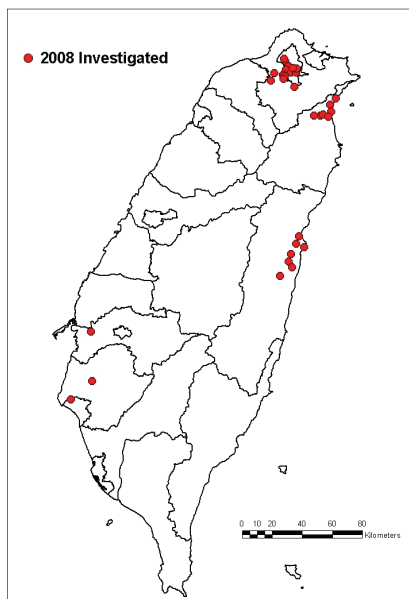


Figure 1. The 31 seismic stations investigated in 2008.

Table 1. The seismic stations investigated in 2008.

Sta. Code	Sta. Code	Sta. Code
CHY108	ILA002	TAP026
CHY116	ILA012	TAP027
CHY123	ILA015	TAP037
HWA012	ILA034	TAP043
HWA017	ILA036	TAP086
HWA018	ILA040	TAP088
HWA027	TAP005	TAP091
HWA048	TAP008	TAP092
HWA051	TAP012	TAP096
HWA052	TAP021	
ILA001	TAP025	

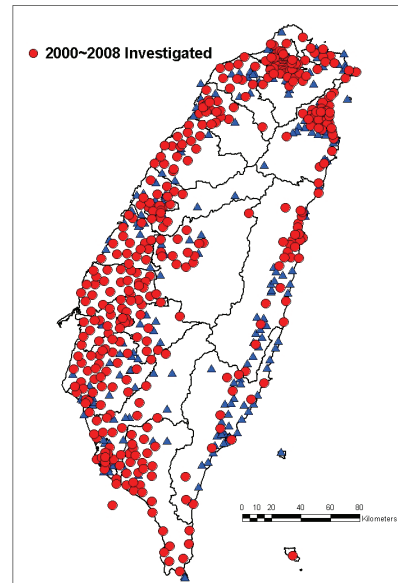


Figure 2. The 408 seismic stations investigated during 2000~2008.



Figure 3. "Geological Surveyed Database of CWB Strong Motion Station" Website

The local site conditions play an important role in determining ground responses during an earthquake. Different site conditions could induce amplification or de-amplification at different period ranges in the response spectra. It is called the "site effect". Besides, in a seismic hazard analysis, the motion at a site's bed rock is predicted by the attenuation low from the earthquake source. According to the 2000 Uniform Building Code (UBC), 1997 National Earthquake Hazards Reduction Program (NEHRP) provisions in the USA, and the revised Earthquake-resistant Code in Taiwan, the ground motion at free field is evaluated by the response at bed rock times the coefficient of site effect. The coefficient of site effect is related to the magnitude of earthquake and the local site conditions. Thus, a complete geological database is essential to the evaluation of site effect for earthquake engineering.

Suspension P-S Logging Technique

The Suspension P-S Logging Technique developed by the OYO Corporation in Japan is used in this project to measure the primary wave velocity (V_p) and the shear wave velocity (V_s) of the stratum. The

source and the receiver of this measuring system were integrated into a single probe within a short distance. Therefore, the wave velocities of the stratum can be measured continuously and precisely.

A borehole was first drilled at the chosen site and then filled with water. If the surrounding soil on a borehole is not stable and is easily eroded, the borehole may be lined with a plastic tube. The probe was then put into the borehole at a specified depth. A primary wave or a shear wave may be generated by the source in the probe. The primary wave was propagated through the surrounding soil in the direction perpendicular to the borehole axis (horizontal direction). Also, the shear wave was propagated through the soil along the vertical direction. Each receiver consists of a hydrophone and a geophone for receiving the primary wave and the shear wave, respectively. A normal pulse and a reverse pulse were triggered by the source in order to check the received signals. The time histories of those received signals should then be in the same shape but with 180 degrees of the phase difference, since the two shear waves were propagated through the same soil media.

Typical measured signals of the primary waves and the shear waves from the logging computer are shown in Figure 4, where H1 and /H1 represent the signals received by the upper receiver in normal and reverse directions, H2 and /H2 represent the signals received by the lower receiver in normal and reverse directions, V1 and /V2 represent the signals received by the upper and lower receivers, respectively. From the time histories of H1 and H2, the first arrival time for the upper receiver and the lower receiver was picked as t_{s1} and t_{s2} . Since the distance between the two receivers is 1 m, the shear wave velocity can be determined as:

$$v_s \text{ (m/sec)} = \frac{1}{t_{s1} - t_{s2}} \quad (1)$$

Similarly, the primary wave velocity is:

$$v_p \text{ (m/sec)} = \frac{1}{t_{p1} - t_{p2}} \quad (2)$$

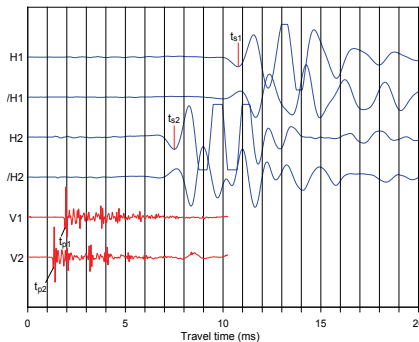


Figure 4. Typical measurements from the Suspension P-S Logging System.

Engineering Geological Database

There are three major items in the Engineering Geological Database in Taiwan. The first item is the general information of the station site that includes latitude and longitude of the station site, ground water level, geographical/topographical conditions, and surrounding structures. The second item refers to the physical properties of soils. The SPT-N value, water content, unit weight, soil classification, and grain size distribution are obtained by on-site boring, sampling, and laboratory testing. After the borehole was drilled, the Suspension P-S Logging Technique was utilized to measure the wave velocity of the stratum at depth for every 0.5 m. The wave velocity of the stratum is an important index for site classification, so it is selected as the third item in the database. If the geological condition of the station site is classified as a rock outcrop, only the general environmental investigation was performed to collect the basic information of the station.

This project has been conducted for nine years. At present, site investigations at 408 station sites were completed, distributed as follows: 44 stations in 2000, 65 stations in 2001, 49 stations in 2002, 54 stations in 2003, 40 stations in 2004, 26 stations in 2005, 50 stations in 2006, 49 stations in 2007 and 31 stations in 2008. These stations are located on the alluvial deposit, gravel, or even rock sites. The results are summarized on NCREE's website. For example, as shown in Figure 5, the general information for station TTN023 (the photo of the seismograph, the plan section and the cross section of the surrounding environment), the soil profile, the SPT-N value, the shear wave velocity, and the primary wave velocity of the stratum are all available on NCREE's website.

Most studies of site effect for earthquake ground motion are based on soil properties of the upper 30-m layer. In the 1997 UBC and 1997 NEHRP provisions in the USA, the average of the shear wave velocity for the top 30-m layer of soils is used as an index for the site classification. In the site classification of Taiwan free-field strong-motion stations, the site conditions were classified as class B (rock), class C (soft rock or very dense soil), class D (stiff soil), and class E (soft soil) according to the geological age, rock type, and the average SPT-N values for the upper 30-m layer of the stratum. With detailed subsurface soil profile and quantitative soil properties (SPT-N values and wave velocities) on a station site, the site effect of ground motions can be analyzed easily for a certain class of site conditions. Engineers may evaluate appropriate peak ground acceleration for the earthquake-resistant design of structures. According to the Classified Code of average shear wave velocity on the top 30-m soil layer (Table 2), the 46 seismic stations, which were investigated in 2007 except KAU040, KAU047 and TAP028, can then be classified. The classification is shown in Table 3.

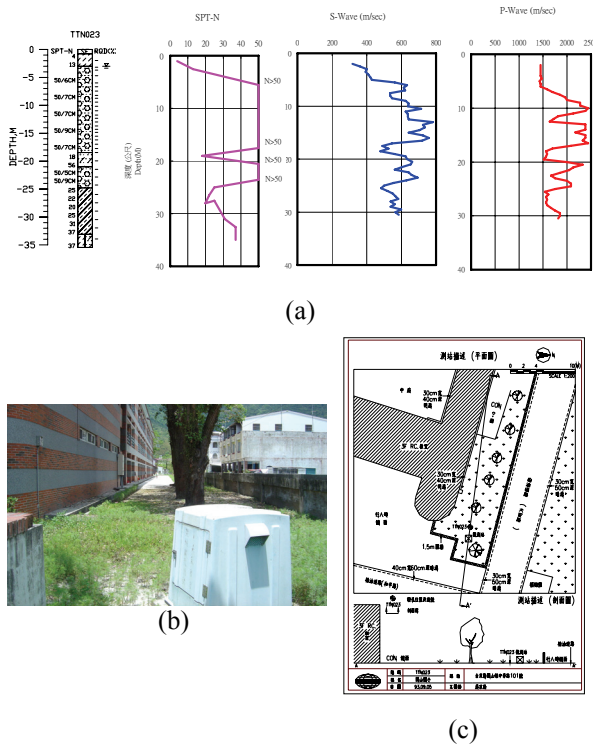


Figure 5. The information for station TTN023 in the database shown on NCREE's website.
 (a) The soil profile, SPT-N value, and wave velocity profile.
 (b) The photo of the seismic station in the field.
 (c) The description of the plan section and the cross section in the field.

Table 2. The shear wave velocity for the top 30m classified code (1997 UBC and NEHRP provision).

Classification	The average of the shear wave velocity for the top 30m (V_{30})
A	$V_{30} \geq 1500\text{m/sec}$
B	$760\text{m/sec} \leq V_{30} < 1500\text{ m/sec}$
C	$360\text{m/sec} \leq V_{30} < 760\text{m/sec}$
D	$180\text{m/sec} \leq V_{30} < 360\text{m/sec}$
E	$V_{30} < 180\text{m/sec}$

Table 3. The classification of 30 seismic stations which were investigated in 2008.

Station Code	Classification	Station Code	Classification
CHY108	D	ILA036	D
CHY116	D	ILA040	D
CHY123	D	TAP005	D
HWA012	C	TAP008	D
HWA017	C	TAP012	D

HWA018	C	TAP021	E
HWA027	C	TAP025	D
HWA048	D	TAP026	D
HWA051	C	TAP027	D
HWA052	C	TAP037	D
ILA001	B	TAP043	C
ILA002	D	TAP086	B
ILA012	D	TAP088	C
ILA015	B	TAP091	D
ILA034	D	TAP096	E

Conclusions

The site investigation at 408 TSMIP stations was completed by NCREE in cooperation with Taiwan's CWB. By sampling of soils in the borehole and using the Suspension P-S Logger Technique, specific geological and geotechnical data were obtained including soil profile, physical properties of soils, and wave velocities of the stratum. All the results of investigation were organized systematically in the database available in a preliminary web site. This project will be performed continuously in the following years. Combining with the GIS technique, the engineering geological database for strong motion stations in Taiwan will be more convenient for web usage. If an engineering project site is close to the strong-motion station, engineers may retrieve the geological and geotechnical properties of soils from the database to evaluate the site's ground response. Thus, this database is helpful for site effect analysis and earthquake-resistant design.

References

- Kuo, C. H., Wen, K. L., Hsieh, H. H., "Evaluating V_{s30} assessors via borehole data in Taipei" Proceedings of the 2008 Taiwan-Japan Symposium on the Advancement of Urban Earthquake Hazard Mitigation Technology, pp.89-92, Taiwan, 2008.
- Kuo, C.H., Wen, K.L., Chang, T.M., Hsieh, H.H. and Cheng, D.S., "Comparison of different methods for investigation of shallow shear wave velocity structures." 4th International Conference on Earthquake Engineering (ICEE), Taipei, Taiwan, October 12-13, 2006.
- <http://geo.ncree.org.tw>

Preliminary Study on Online Updating Hybrid Simulation

Yuan-Sen Yang (楊元森)¹, Keh-Chyuan Tsai (蔡克銓)²,

Amr S. Elnashai³, Oh-Sung Kwon⁴, Sheng-Lin Lin (林聖霖)⁵

Abstract

This work proposes a framework of a new method to run a hybrid simulation, which is named online updating hybrid simulation. An online updating hybrid simulation is a hybrid simulation in which numerical model parameters of its numerical substructure(s) are adjustable and instantly updated based on the instantaneously-measured responses of experimental substructures. This work is a collaborative work between the National Center for Research on Earthquake Engineering (NCREE) and the Mid-America Earthquake (MAE) Center, which is located at University of Illinois at Urbana Champaign, USA. The MAE Center group plans to develop the near term neural network-based approach to updating the response of the repetitive analytical components in hybrid simulation (*e.g.*, beam-column connections) based on the instantaneously-measured response of the experimental component. NCREE is planning on developing algorithms for the updating of material models used in finite element analysis using measured data, during the same test.

This report is a four-page shortened version of a progress report of the first year work on online updating hybrid simulation. Figures in this report are resized. Full-size figures can be found at NCREE report 09-001 [1]. Most of the research work written in this report was completed during the first author's one-month short visit at the MAE Center under supervision and discussion of the third author of this report. Further details of the upcoming work will be described in the near future.

Keywords: Hybrid simulation, online updating, numerical model, optimization, neural network

Introduction

Hybrid simulation is an experiment manner combining numerical simulation technology and experimental technology, and is getting popular in earthquake engineering researches. To simulate the dynamic response of a structure, a part of the structure (or a substructure) can be simulated by one or more physical specimens in laboratories, while the remaining part of the structure can be simulated by numerical simulation. Commonly, the numerical parts of the structure are the parts where researchers have reasonable numerical models to simulate, while the experimental parts of the structure are more unknown. As shown in Fig. 1, a hypothesis bridge structure with two short piers and two long piers is tested using hybrid simulation. Assuming the short piers would encounter more violent deformation and would go into

severer damages than the long ones while subjecting to earthquakes, the behaviors of the short piers are not well known and are more difficult to simulate numerically. The two short piers are simulated by two physical substructure specimens, while the longer piers and other components of the bridge are numerically simulated in the hypothesis hybrid simulation.

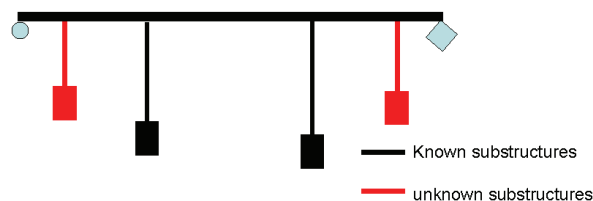


Fig. 1: A hybrid simulation with two physical substructure specimens

¹ Associate Research Fellow, National Center for Research on Earthquake Engineering (NCREE), ysyang@ncree.org.tw

² Director, NCREE; Professor, National Taiwan University, kctsay@ncree.org.tw

³ Director, MAE Center, USA; Professor, University of Illinois at Urbana-Champaign, USA

⁴ Assistant Professor, Missouri University of Science and Technology, USA

⁵ PhD Student, University of Illinois at Urbana Champaign, USA

However, in some cases, there are many unknown parts in a structure, and it is not practical to construct specimens for all of these parts because of high experimental cost of multiple substructure hybrid simulation. An idea of online updating of numerical models during a hybrid simulation is proposed by Elnashai [2] to improve the consistency among substructures in a hybrid simulation, as shown in Fig. 2. Conceptually, researchers learn more about the structural behaviors of the experimental substructures during the progress of the test, and have more information to tune the presumed parameters of the numerical models.

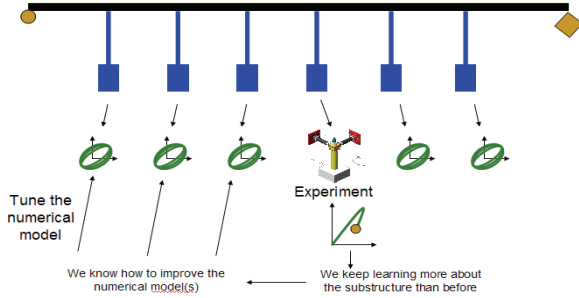


Fig. 2: An online updating hybrid simulation with one physical substructure and many roughly identical online updating numerical substructures

Online Updating Hybrid Simulation Framework

The basic concept and its development of hybrid simulation is described in many papers (*e.g.*, [3, 4]). To distinguish with an online updating hybrid simulation, a hybrid simulation without online hybrid simulation is called conventional hybrid simulation in this paper. The flowchart of a conventional hybrid simulation is as shown in Fig. 3. The procedure of an online updating hybrid simulation is basically based on a conventional one, except that there is an additional parameter analysis module, and the original numerical substructure module is modified so that it allows updates of some of its numerical parameters (as shown in Fig. 4). The parameter analysis module calculates a set of parameters for the numerical model based on the experimental data. The par_{i+1}^N is a set of calculated parameters for the numerical model at time step $i+1$. The modified numerical substructure module updates the numerical model according to par_{i+1}^N and calculates its resisting force \tilde{r}_{i+1}^N regarding to the displacement \tilde{u}_{i+1}^N .

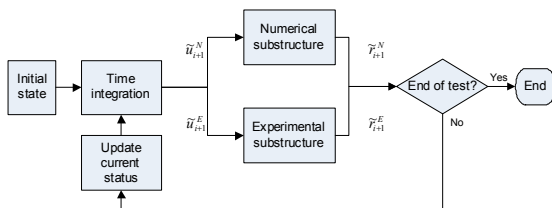


Fig. 3: Flowchart of a conventional hybrid simulation [1]

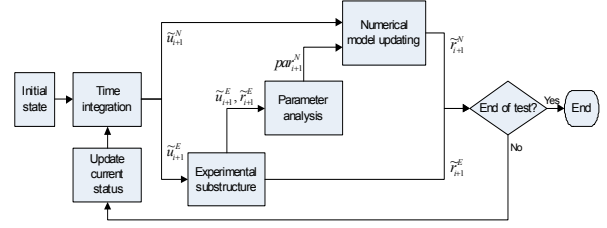


Fig. 4: Online updating hybrid simulation flowchart [1]

Online updating hybrid simulation is based on the following assumptions:

- (1) Assumption of similarity of numerical models: It is assumed that we have a numerical model for the experimental substructure, and the numerical model is similar to that of the numerical substructure. For detail description and formulations, please refer to the full report [1].
- (2) Assumption of small change of resisting force history: It is assumed that the change or updating of the numerical model does not lead to a significant change on their past history. For detail description, formulations and figures, please refer to the full report [1].

The parameter analysis module calculates a set of parameters for the numerical model based on the experimental data. Figure 5 shows a flowchart of the parameter analysis procedure. For detail description and formulations, please refer to the full report [1].

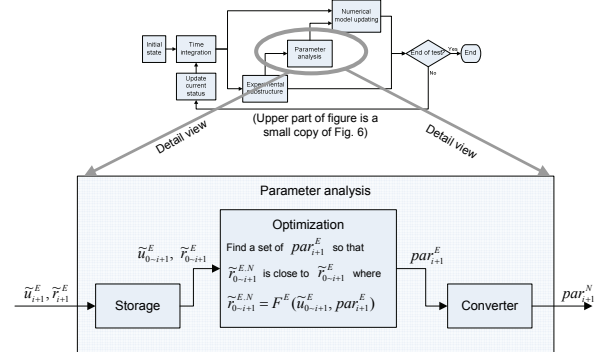


Fig. 5: Flowchart of the parameter analysis*

*The upper part of the figure is a small copy of Fig. 4. The small unrecognizable words in the upper part can be seen in Fig. 4). Full-size figure can be found in report [1].

The numerical model updating module carries out a loop to check and tune the parameters par_{i+1}^N if it is necessary, as shown in Fig. 6. The j is the loop number in the numerical model updating module. The check may include:

- (1) Upper and lower bounds of par_{i+1}^N : Researchers may pre-set upper and lower bounds of the parameters to ensure that the calculated parameters is within a reasonable range.
- (2) Consistency of resisting force history: As mentioned, it is assumed that the change of the numerical parameters par_{i+1}^N leads to a small

change of resisting force history, as shown in Fig. 7a. If the change of par_{i+1}^N leads to an unreasonable change of resisting force history (as shown in Fig. 7b), the par_{i+1}^N may need to be tuned. The error of the resisting force history should be recorded, so that the accuracy or reliability of the online updating hybrid simulation can be evaluated.

To prevent the loop in the numerical model updating becoming an unlimited loop, a maximal number of loop checking may be needed. However, it increases the risk that the resisting force history may be inconsistent.

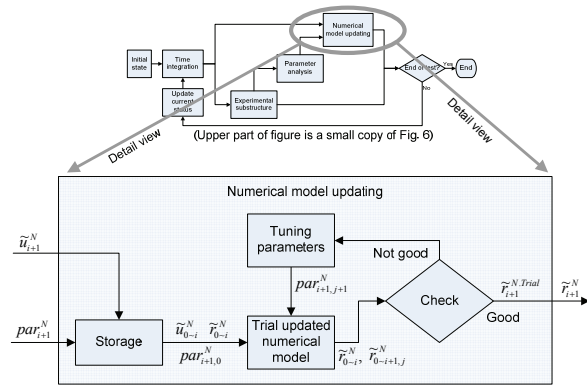


Fig. 6: Flowchart of the numerical model updating *
 *The upper part of the figure is a small copy of Fig. 4. The small unrecognizable words in the upper part can be seen in Fig. 4). Full-size figure can be found in report [1].

3. Design of a Preliminary Test

In this work, a simple test example is roughly sketched to preliminarily verify the online updating hybrid simulation. The preliminary test is a software simulation. The structure is divided into three parts:

- (1) Adjustable numerical substructure: This part of substructure is the numerical substructure in which some of the parameters can be updated.
- (2) Experimental substructure: This part of substructure is to simulate the behavior of an experimental specimen. The numerical model should be more sophisticated than the adjustable numerical substructure to represent that the actually specimen's behavior is complicated than its numerical model.
- (3) Remaining part: The remaining part of the structure is numerically simulated, where numerical model does not change during the hybrid simulation.

Figure 7 shows the structure of the test example. It is a two dimensional bridge structure with two piers. To simplify the test, the mass and vertical loads are lumped to the tops of the piers.

The optimization module finds a reasonably optimized set of parameters so that the experimental substructure's numerical model approaches the experimental result as shown in Fig. 8. For detail descriptions and formulations, refer to report [1].

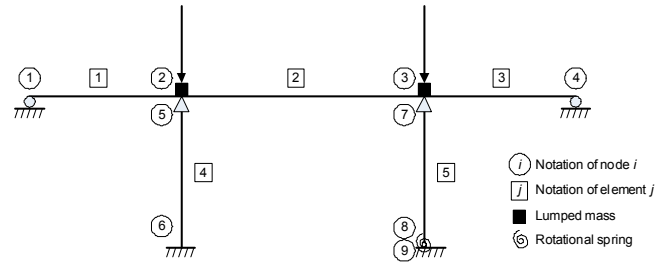


Fig. 7: Elevation of a bridge structure for a test

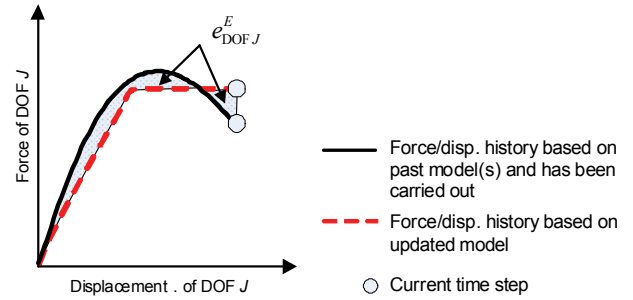


Fig. 8: Strain energy error between experimental and updated numerical results

The second stage is to check the consistency of resisting force history. It is required that the updated numerical model using the optimized parameters does not change the resisting force history significantly. The consistency of the resisting force history is based on the strain energy error, which is shown as the gray area in Fig. 9. Refer to report for details [1].

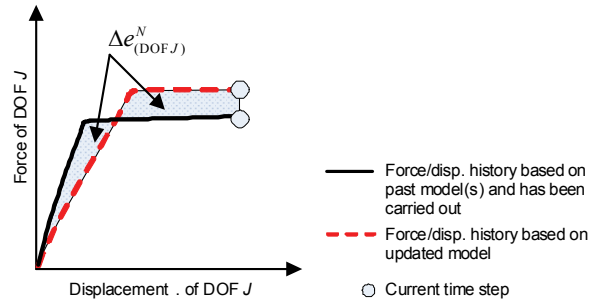


Fig. 9: Strain energy error between and after numerical model is updated

In addition to the aforementioned hypothetical bridge structure, an example of a bridge or building structure with a number of identical isolators is being prototyped. An isolated structure is typically supported by a number of isolators. The basic mechanical behaviors of an isolator can be tested at laboratories. Full-scale test of an isolator typically requires a large experimental facility because the gravity load of isolator bears is very large. A multi-axial testing system at NCEE, named MATS, was completed in 2008, which can apply up to 40 MN (mega-Newton) (about 4000 metric tons) of vertical loads and 4 MN of horizontal loads with 1.2 meters of horizontal displacement in dynamics. The capacity allows MATS to run a performance test a full-scale isolator. However, it is not likely to run a hybrid

simulation with more than one full-scale isolator due to the high cost of the experimental facility like MATS. The online updating hybrid simulation is a possible solution. Figs. 10 and 11 present hypothetical online updating hybrid simulation on a bridge structure using isolators and an isolated building. The design and implementation of the software simulation of the two tests will be carried out in the near future.

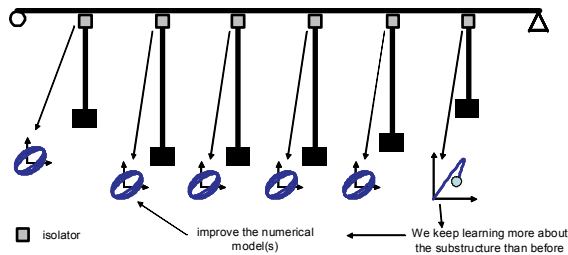


Fig. 10: A hypothetical online updating hybrid simulation of an isolated bridge

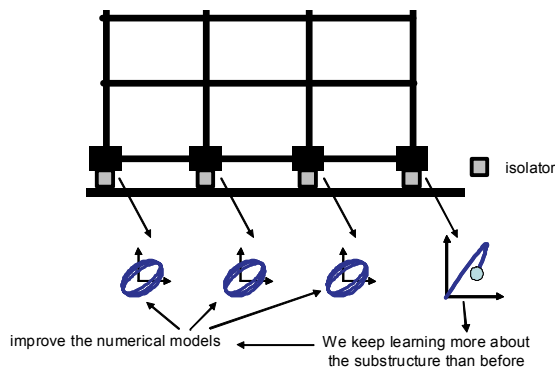


Fig. 11: A hypothetical online updating hybrid simulation of a building with base isolation

The software development for the preliminary test will be started in the following work. The following software simulations are aimed to be carried out using ISEE and UI-SimCor hybrid simulation environment are aimed to be employed [5,6,7] :

- (1) A numerical simulation of the two-pier bridge and/or an isolated building structure subjecting to a ground motion. Both piers are simulated by simple numerical models. However, this test may be skipped because it is not heavily related to the focus of this work.
- (2) A software-based hybrid simulation of the two-pier bridge and/or an isolated building structure using a conventional hybrid simulation approach, where one of the pier is simulated by a sophisticated numerical model, while the other is simulated by a simple numerical model.
- (3) A hybrid simulation of the two-pier bridge and/or an isolated building structure using the proposed online updating hybrid simulation, where one of the pier is simulated by a sophisticated numerical model, while the other one is initially simulated by a simple numerical model and updated online during the test.

- (4) A sophisticated numerical model representing the real (or ideal) responses of the structure. Both piers are simulated by the sophisticated numerical model.

The following data will be monitored or be gathered for statistics:

- (1) The dynamic responses of the piers and the bridge system and/or an isolated building structure,
- (2) The elapsed time of running these simulations,
- (3) The history of adjustable parameters of the online updating hybrid simulation,
- (4) The resisting force consistency error monitored during the online updating hybrid simulation, and the influence of the consistency error tolerance to the online updating hybrid simulation result.

Summary

An online updating hybrid simulation framework is proposed in this report. The online updating hybrid simulation is based on a conventional hybrid simulation, a parameter analysis module, and a numerical model updating module. A software-based preliminary test of an online updating hybrid simulation is preliminarily designed. Structural design of this test will be completed soon. The test will be carried out in a software-based manner to demonstrate the feasibility and reliability of the proposed online updating hybrid simulation. Refer to report [1] for further details of this four-page article.

References

1. Yang, Y.S., Tsai, K.C., Elnashai, A.S., Kwon, O.S., Lin, S.L. (2009). "Preliminary Study on Online Updating Hybrid Simulation," NCREC Report 09-001. National Center for Research on Earthquake Engineering, Taipei, Taiwan.
2. Elnashai, A. S. 2008. Personal communication.
3. Takashi, K., Nakashima, M. 1987. "Japanese activities on on-line testing," *Journal of Engineering Mechanics*, ASCE, 113(7), 1014-1032.
4. Mahin, S.A., Shing, P.B., Thewalt, C.R., Hanson, R.D. 1989. "Pseudodynamic test method - Current status and future direction," *Journal of Structural Engineering*, ASCE, 115(8), 2113-2128.
5. Yang, Y.S., Hsieh, S.H., Tsai, K.C., Wang, S.J., Wang, K.J., Cheng, W.C., Hsu, C.W. 2007. "ISEE: Internet-based simulation for earthquake engineering Part I: database approach," *Earthquake Engineering and Structural Dynamics*, 36(12), 2291-2306.
6. Wang, K.J., Tsai, K.C., Wang, S.J., Cheng, W.C., Yang, Y.S. 2007. "ISEE: Internet-based simulation for earthquake engineering Part II: the application protocol approach," *Earthquake Engineering and Structural Dynamics*, 36(12), 2307-2323.
7. Kwon, O.S., Nakata, N., Elnashai, A.S., Spencer, B. 2005. "A framework for Multi-site distributed simulation and application to complex structural systems," *Journal of Earthquake Engineering*, 9(5), 741-753.

Image-based Surface Strain Field Measurement in an RC-Wall Cyclic Test

Yuan-Sen Yang¹, Chang-Wei Huang², Bei-Ting Chen³, Chiun-lin Wu⁴

楊元森¹、黃仲偉²、陳北亭³、吳俊霖⁴

Abstract

Image analysis technology is employed in this work for concrete surface strain field measurement of a post-tensioned RC-wall cyclic test. The surface strain fields of each cyclic control step are estimated by analyzing a pair of images taken by two digital cameras. Camera calibration is carried out using a user friendly MATLAB toolbox called Bouguet's toolbox. Image distortion effect is considered using cameras' intrinsic parameters. Stereo 3D image analysis is performed to render the 3D geometry of the measurement concrete surface. Digital Image Correlation (DIC) using template matching technique is adopted to trace the displacement change of grids on the measurement surface using a widely known high performance open source library for computer vision called OpenCV. The strain fields are estimated by the traced displacement fields. The measurement error is preliminarily estimated.

This report is a four-page short version of a progress report of the first year work on image-based strain measurement [13]. A similar publication of this work has been published at The Eleventh East Asia-Pacific Conference on Structural Engineering & Construction (EASEC-11), which was held on November 19-21, 2008, Taipei, Taiwan [12]. Further details of the upcoming work will be written in the near future.

Keywords: Image-based measurement, image processing, camera calibration, stereo triangulation, template matching, strain measurement,

Introduction

Strain measurement plays an important role in structural experiments. A strain field presents the deformation distribution of a part of the tested structure, providing plenty of information to researchers and engineers. Locations with high tension, compression or shear strains may indicate high risk of different types of failure. Conventionally, strain gauges are commonly used for strain measurement. A strain gauge is a device with insulating flexible backup which supports a metallic foil pattern and is attached on an object to be measured. A strain gauge actually measures the tension or compression deformation along a single direction. With multiple strain gauges, a strain field distributed within a region can be estimated. Although using strain gauges is an

inexpensive and accurate way for strain measurement, there are still limitations. When the region of interest is a large region, it is impractical to paste hundreds or thousands of strain gauges distributed within this region of interest. Too many strain gauges may lead to the complexity of the experiment. Strain gauges and their ubiquitously distributed wires may obstruct researchers and engineers to observe the surface of the structure. In addition, for regions that are difficult for people to reach, it is not easy to send someone to deploy hundreds or thousands of strain gauges, their wires and data acquisition.

Image analysis offers an alternative way for strain measurement [11]. By taking photos of structural specimens, the shapes and the surfaces of the specimens can be recorded in an image form. Their

¹ Associate Research Fellow, National Center for Research on Earthquake Engineering, ysyang@ncree.org.tw

² Assistant Professor, Department of Civil Engineering, Chung-Yuan University

³ Graduate Student, Department of Civil Engineering, Chung-Yuan University

⁴ Associate Research Fellow, National Center for Research on Earthquake Engineering

changes during the experiment can be recorded and analyzed as well. As the improvement of digital technology, digital cameras which are easily available on the consumer electronic market are now capable to carry out basic and practical image-based measurement in structural experiments. Considering the rapid soaring digital technology, it is believed that image-based measurement will be an important technique for measurement in structural experiments and health monitoring. Several researches have adopted image analysis technique for experiment measurement [1,2,3,4]. Due to limited space, their valuable achievements are not introduced in this paper.

This work estimated reinforce-concrete (RC) surface plane strain fields in a large-scale post-tensioned RC wall experiment using a set of photos taken by digital consumer cameras. The post-tensioned RC wall was subjected to a set of cyclic loadings at the top of the wall during the experiment [5]. Two rectangular regions at the bottom of the wall, which were supposed to suffer major internal forces in this experiment, were photographed by four consumer digital single lens reflex (SLR) cameras. Further discussions about the post-tensioned RC wall structure can be found in [6]. The surface plane strain fields of these two regions of concrete were estimated through image analysis of the photos taken during the experiment. This paper presents the procedures, image analysis techniques, and software developed in this work. Image analysis techniques employed in this work include camera calibration, stereo triangulation, image correction for unexpected camera movement, image template matching for displacement analysis, and image measurement error analysis. Based on ImPro [4], a 2D displacement analysis tool developed by the authors, a software framework, called ImPro Strain, was developed in this work employing some existing state-of-the-art image analysis toolboxes to complete the strain measurement work. The software developed in this work is believed to be useful for other similar structural experiment, and has been publicly open for free download on the Internet.

Setup for Measurement

Two experiments are briefly introduced in this paper. The first one is a zero-strain test, which is simply to estimate the error of strain measurement using the adopted approach in this work. The second experiment is a large-scale post-tensioned reinforced concrete (RC) wall tested in the NCREE's laboratory [5] in March 2008.

As shown in Fig. 1, a zero-strain test is to measure the strain field of a non-deformed board. Since there is no external force applied on the board, the strains of the board are seen as zero. The measured strain using image-based measurement can be seen as the error of

the measurement. Two boards were used: the calibration board has a regular checkerboard pattern on its surface; while the zero-strain board has a randomly distributed spots of painting so that images at different locations are distinct from others,



Figure 1: zero-strain test which is good for template matching. The random pattern was generated by using a special spray. Two cameras are used to take a set of photos of the calibration board and the zero-strain board.

The large-scale post-tensioned RC wall experiment was carried at NCREE's laboratory in March, 2008 [5]. The experiment was conducted collaboratively by NCREE, Iowa State University, and University of Auckland (in New Zealand). As shown in Fig. 2, the post-tensioned RC wall was subjected to a series of cyclic lateral forces by a set of hydraulic actuators at the south side of the specimen during the test. The east sides of two bottom corners were measured in this work (Fig. 3).



Fig. 2: The post-tensioned RC wall [5]

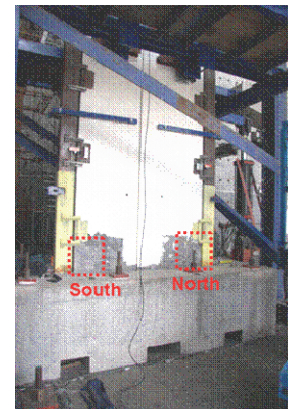


Fig. 3: Measured regions of two corners

Each corner was taken by a pair of digital cameras. Calibration is carried out to obtain the intrinsic parameters of each camera and extrinsic parameters of each pair of cameras. A set of photos taken before the RC wall was deformed was taken as the initial status. Other taken photos were used to measure the strain of the two corners of the wall. Further details of the setup of the measurement can be found at [13].

Analysis Procedure

In this work, an image analysis approach is used to carry out image-based strain field measurement. This approach triangulates (calculates) 3D positions of sampling points [9] within the measurement region plane using image analysis and triangulation, and then calculates the plane strain fields.

In this approach, as is shown in the flowchart in Fig. 4, the Image Analysis process gets an image pair, and selects a number of pairs of sampling points on the images. Each sampling point on an image has a unique corresponding sampling point on the other image, and the two points on the images represent the same point in the real world. It should be noted that an assumption is implied in this approach:

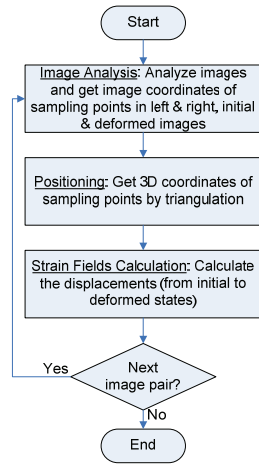


Fig. 4: Analysis flowchart

The view angles and the sizes of the measurement region in the left image and the right image are reasonably close, so that a sub-image of the left image can be a template to match on the right image.

Further discussion about this approach can be found in [13] and is not presented here.

Setup for Measurement

Here we show very limited analysis result of the zero-strain test and the post-tensioned RC wall experiment due to limited space. See reference [13] for more complete results.

Table 1 presents a series of zero-strain tests. It can be imagined that the more coarsened the grid is, the better accuracy of strain is obtained. Although the strain accuracy is still insufficient for accurate strain measurement for structural experiments because material with a 7×10^{-4} of strain would be close to yielding status, it achieves an equivalent displacement measurement accuracy between neighboring grids of about 0.03 to 0.06 pixels, which the authors believe is close to the inherent limit of image analysis limitation. It is also observed, but not shown here, that the error increases as the displacement between the initial and deformed status is larger. Similar situation was also observed by [10]. The authors believe that the error mainly comes from the camera calibration error, which is the higher order of the camera distortion that a limited order of camera calibration model can not well calibrate.

Table 1: Zero-strain test results

Strain type	Grid size	Minimal strain	Maximal strain	Average strain	Equivalent displacement measurement accuracy
ϵ_{XX}	20 x 20	0.065e-3	0.670e-3	0.368e-3	0.055 pixels
ϵ_{YY}	20 x 20	0.062e-3	0.643e-3	0.316e-3	0.043 pixels
ϵ_{XY}	20 x 20	-0.299e-3	0.422e-3	-0.043e-3	0.031 pixels
ϵ_{XX}	40 x 40	-0.576e-3	1.282e-3	0.361e-3	0.052 pixels
ϵ_{YY}	40 x 40	0.714e-3	1.649e-3	0.311e-3	0.055 pixels
ϵ_{XY}	40 x 40	-1.342e-3	1.633e-3	-0.042e-3	0.061 pixels

* The e-3 denotes a thousandth (i.e., $\times 1/1000$)

Due to limited accuracy of the image-based strain measurement, the authors believe that the concrete surface strains within $\pm 10^{-4}$ can not be measured, and strains within $\pm 10^{-3}$ can be measured but may not be certainly accurate. In addition, photographing environment conditions of the post-tensioned RC wall experiment were not good. The duration of the experiments was two days. Cameras were occasionally slightly moved, probably due to carelessness touching or instability of tripods. The environment light in the morning was different from that in the afternoon and evening. Therefore, only photos of specimens with large strains and visible cracks are presented in this paper. More details of the measurement results can be found in the NCREE research report to be published in the near future. Fig. 5 shows the main part of the roof drift ratio history of the experiment.

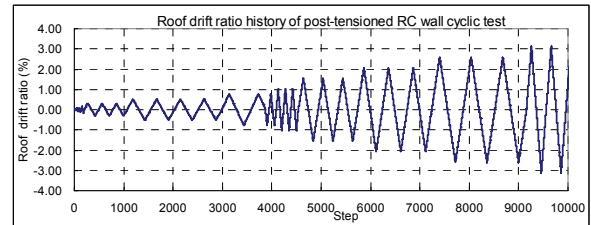


Fig. 5: Measured regions of two corners

Table 2: Selected analysis results of the experiment

	Step 4683 DR = 1.6%	Step 5238 DR = -1.6%	Step 7718 DR = -2.6%
ϵ_{XX}			
ϵ_{YY}			
ϵ_{XY}			

Strain field color bars range from -0.1 to 0.1. Strains exceeding color range may indicate concrete cover peeled.

The analysis engine adopted in this work is based on a MATLAB-based Bouguet's toolbox [7] and a C++ based OpenCV library [8], which are well known in the computer vision discipline. Taking advantage of the good reliability and high performance of these tools, the strain measurement tool developed in this work performs well in the presented tests. The strain and displacement field measurement shown in Table 2 only requires less than 1 hour on a laptop with an Intel Core 2 Duo 2GHz CPU.

Summary

This work employed state-of-the-art image analysis techniques, toolbox and library and developed a tool to measure plane surface strain and displacement fields in structural experiments. A MATLAB-based camera calibration toolbox, called Bouguet's toolbox, and a well known library in the computer vision discipline, called OpenCV, were employed to support the tool developed in this work.

A zero-strain test was carried out to estimate the strain measurement accuracy of the proposed image measurement approaches. The tested strain measurement accuracy is about 7×10^{-4} for measurement grid 20 by 20, and about 1.7×10^{-3} for measurement grid 40 by 40 within a 30cm by 30cm region. The equivalent relative displacement accuracy between grids may achieve 0.031 to 0.109 pixels in the presented zero-strain tests. The authors believe that it is close to the inherent limit of image analysis limitation. However, the strain accuracy is still insufficient for accurate strain measurement for structural experiments. Higher accuracy image-based strain measurement may rely on higher resolution of digital cameras or using more cameras sharing the same size of measurement region.

This work then estimated concrete surface plane strain fields in a large-scale post-tensioned RC wall experiment using a set of photos taken by digital consumer cameras. The post-tensioned RC wall was subjected to a set of cyclic loadings at the top of the wall during the experiment. Two rectangular regions at the bottom of the wall, which were supposed to suffer major internal forces in this experiment, were photographed by four consumer digital single lens reflex (SLR) cameras. The surface plane strain fields of these two regions of concrete were estimated through image analysis of the photos taken during the experiment. This paper presents the procedures, image analysis techniques, and software developed in this work. Image analysis techniques employed in this work include camera calibration, stereo triangulation, image correction for unexpected camera movement, image template matching for displacement analysis, and image measurement error analysis.

The result shows that the image-based measurement is capable to capture not only visible cracks of concrete surface, but also growing cracks before they are visible by human naked eyes. The capability may be even improved if higher resolution digital cameras are adopted.

The authors believe that the digital cameras available nowadays provide sufficient quality and resolution to partially replace some labor intensive work in structural experiments, such as RC crack depiction. Although it is not yet sufficient to supersede conventional strain gauges in terms of accuracy, image-based measurement is a safe alternative way for crack observations, especially

considering the potential danger induced by local or global failure of damage structures when researchers or participating students depict cracks. Concrete debris may fall down and damage precious lives of researchers and/or their students due to unpredicted local failure during experiments. Unpredicted global failures or collapses, even though not highly possible, should be considered seriously due to the possibility of misuse of actuators control, controllers' failure, or controlling software bugs. Image-based measurement is a compromise solution between research purposes and life safety.

References

1. Capéran, P. "Displacement and Strain Field Photogrammetric Measurements of a Reinforced Concrete Slab Submitted to an Earthquakes Loading," *Proceedings of the OPTIMESS2007 Workshop*, Leuven, Belgium, May 28-30, 2007.
2. Capart, H., Young, D.L., & Zech, Y. (2002). "Voronoi Imaging Methods for the Measurement of Granular Flows," *Experiments in Fluids*, 32(1), pp. 121-135.
3. Shih, M. H., Tung, S. H., Kuo, J. C., & Sung, W. P. "Application of Digital Image Correlation Method for Crack Observation", *The Eighth International Conference on Computational Structures Technology*, Las Palmas de Gran Canaria, Spain, September 12-15, 2006.
4. Yang, Y. S., Wu, C. L., Loh, C. H., Yang, C. M., Tu, W. H., Shih, M. H., Tung, S. H. & Capéran, P. "Preliminary Study on Image-based Measurement," Technical Report NCREE-08-013, National Center for Research on Earthquake Engineering, Taipei, Taiwan, 2008.
5. Chen, P. C. "International Collaborative Test on Post-tensioned RC Shear Wall," *NCREE Newsletter*, Vol. 3, No. 1, 2008, pp.6.
6. Rahman, M.A. & Sritharan, S. (2006). "An evaluation of force-based design vs. direct displacement-based design of jointed precast post-tensioned wall systems," *Earthquake Engineering & Engineering Vibration*, 5(2), pp. 285-296.
7. Bouguet, J. Y. (2007). "Camera Calibration Toolbox for MATLAB," Web page: http://www.vision.caltech.edu/bouguetj/calib_doc/index.html (Accessed: Jul. 1, 2008)
8. Intel Corp. "Open Source Computer Vision Library," Web page: <http://www.intel.com/research/mrl/research/opencv> (Accessed: Jan. 31, 2008)
9. Wikipedia Foundation Inc. "Triangulation," Web page: <http://en.wikipedia.org/wiki/Triangulation> (Accessed: Jul. 1, 2008).
10. Lu, Y. Y. "On Anisotropy of Indentation Induced Piling-up by using Optical Microstrain measurement," Master thesis, National Cheng Kung University, Tainan, Taiwan, 2006.
11. David, E. R. *Machine Vision Theory Algorithms Practicalities*, 3rd Edition, Elsevier, UK, 2005.
12. Yang, Y. S., Huang, C. W., Chen, B. T. and Wu, C. L. "Image-based Surface Strain Field Measurement of a Post-Tensioned RC-Wall Cyclic Test," *Proceedings of the Eleventh East Asia-Pacific Conference on Structural Engineering & Construction (EASEC-11)*, Taipei, Taiwan, November 19-21, 2008.
13. Yang, Y. S., Huang, C. W., Chen, B. T. And Wu, C. L. "Image-based Surface Strain Field Measurement of an RC-wall Cyclic Test," NCREE Report 09-002, National Center for Research on Earthquake Engineering, Taipei, Taiwan, 2008.

Construction and Application of NCREE Information and Knowledge Services

Kuang-Wu Chou¹, Wen-Hsiang Tu², Chun-Yi Lin², Shang-Hsien Hsieh³,
and Hsien-Tang Lin⁴

周光武¹、涂文祥²、林峻毅²、謝尚賢³、林顯堂⁴

Abstract

In order to manage and disseminate the accumulated knowledge and experiment experience from NCREE, this work developed helpers for knowledge management, constructed information service systems that are needed, and extended the functionalities of the existing information systems to meet the new requirements. For NCREE's knowledge management, the ontology for earthquake engineering was developed. Considering ontology could enable communication between computers, far more effective sharing of knowledge becomes possible. On the other hand, to preserve and manage NCREE's experiment data and knowledge, this work developed the experiment flow management system that cooperates with two already-online systems (NCREE experiment online-application system and NCREE Data Center) to provide more complete experiment services than before. Besides, the service extent of the conference website manage system was expanded from the NCREE employees to faculties outside NCREE. Also the NCREE video database was constructed to provide users with the online query for the international training programs that NCREE held in 2005 and 2006.

Keywords: ontology, experiment flow management, experiment online-application, experiment data management, conference website management, video database

Introduction

The National Center for Research on Earthquake Engineering (NCREE) has delivered valuable research and accumulated extensive knowledge in areas such as large-scale experiments; innovative experimental technologies; seismic design, evaluation, and retrofit of structures; and seismic hazard simulation. If the knowledge gets managed, disseminated, and demonstrated effectively, it may form the basis of further research and be used to solve more problems in the field of earthquake engineering. Therefore, one focus of this work is on managing the NCREE knowledge base and extending its applications. The earthquake engineering ontology as one type of effective media to manage and disseminate knowledge was developed. In addition, this work developed the

experiment flow management system. This system cooperates with the already-online NCREE online experiment application system and NCREE Data Center to manage all the knowledge and information that an experiment can provide or use, and to maximize the potential reuse and application of the knowledge and information from experiments.

Another focus of this work is on developing the NCREE information services and on raising the quality of the existing services provided for users from either inside or outside NCREE. In 2008, the NCREE video database was constructed for the NCREE staff to access and apply. In addition, the Conference Website Management System was expanded so that any user from outside NCREE could create and

¹ Associate Technologist, National Center for Research on Earthquake Engineering, kwchou@ncree.org.tw

² Assistant Technologist, National Center for Research on Earthquake Engineering, whtu@ncree.org.tw

³ Professor, Department of Civil Engineering, National Taiwan University; Division Head, National Center for Research on Earthquake Engineering, shhsieh@ntu.edu.tw

⁴ PH.D. candidate, Department of Civil Engineering, National Taiwan University, d93521003@ncree.org.tw

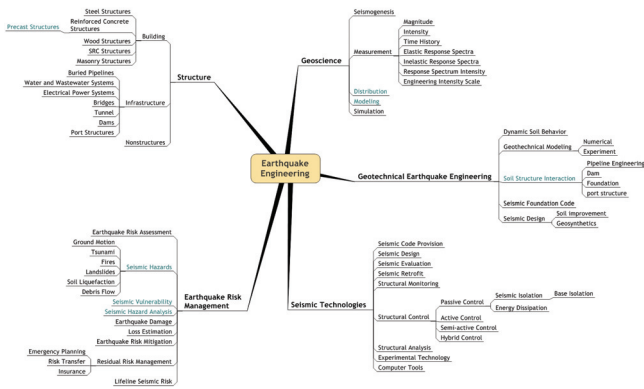


Fig. 4 Upper-level concept map of earthquake engineering domain

```

<rdf:RDF xml:base="Example.owl">
  <owl:Ontology rdf:about="">
    <owl:Class rdf:ID="Structural dynamics">
      <rdfs:subClassOf rdf:resource="http://www.w3.org/2002/07/owl#Thing"/>
    </owl:Class>
    <owl:Class rdf:ID="Evaluation of damping">
      <rdfs:subClassOf rdf:resource="#Structural dynamics"/>
    </owl:Class>
    <owl:Class rdf:ID="Response spectra">
      <rdfs:subClassOf rdf:resource="#Structural dynamics"/>
    </owl:Class>
    <owl:Class rdf:ID="Acceleration response spectra">
      <rdfs:subClassOf rdf:resource="#Response spectra"/>
    </owl:Class>
  </rdf:RDF>

```

Fig. 5 OWL example for class hierarchy representation

Experimental data Management

Released in last year, NCREE Data Center serves as a uniform and central environment for users to store and manage their experimental data. In addition, NCREE Data Model has been proposed to support the management of NCREE's experimental data; NCREE Data Model has been implemented in NCREE Data Center. However, it still takes considerable time and manpower for users to organize their data and the relationships among data after any experiment is finished. To further facilitate data management and reduce extra workload, a subcommittee composed of senior technologists and researchers is responsible for establishing the data management policies.

The integration of all the experiment-related systems mentioned in the following could reduce the effort of management on the experimental data. Now the NCREE experiment online-application system is refined and integrated with NCREE Data Center. In addition, the experiment flow management system (See Fig. 6), which is responsible for confirming the related experimental data storage in every experiment phase, is also developed to work with the two systems mentioned above. From experiment application to experiment finish, there are five phases to deal with the experimental data: application, review, plan, execution, and finish. The application and review phases are taken care of by the experiment online-application system. The applicants could trace

their applications and the experiment application form will be reserved through the web-based interface provided by the experiment online-application system. The plan, execution, and finish phases are taken care of by the experiment flow management system. The applicants have to plan and arrange their experiments, including uploading specimen specification, channel and sensor setup plan, etc. in the plan phase. The technologists will setup experimental environment and execute experiment in the process phase according to the information provided by the applicants in the plan phase. In the experiment finish phase, the system also provides a web-based interface for users to retrieve the data which records the behavior of the specimen. Moreover, the operations in the experiment flow management system will establish automatically the corresponding entities of the NCREE Data Model in the NCREE Data Center. It reduces the workloads that users have to re-arrange their experimental data on the NCREE Data Center.

The NCREE Data Model is also extended to be compatible with the experiment application and flow. Based on the NCREE Data Model, the integration of experimental application, experimental flow and experiment data management system completely records and reserves the experiment-related data and experiment procedure. Such integration makes Non-project members understand the background of the projects they are interested in.



Fig. 6 Experiment flow management system

NCREE Web Information Services

The International Training Programs (ITP) for earthquake engineering held in NCREE have been recorded into videos for several years. Those videos not only contain knowledge but also education content for technologies of earthquake engineering. Therefore, those videos are so valuable that they should get stored and organized into the earthquake engineering knowledge base. To meet this demand, this work classified these videos, and made them easily searchable and accessible. In 2008, the videos of 2005 and 2006 were first compiled into a video database

correspondingly. As shown in Fig. 7 the user can access this video database by contacting with the website of ITP2005. Currently, this video database is only available for the NCREE employees, helping them collect and access the knowledge they need.

Since 2006, the Conference Website Management System (CWMS) has helped NCREE construct many conference websites. By using this system, any NCREE employee can quickly create a conference's website and let it serve people interested in this conference. Meanwhile, the NCREE employee may carry out back-end management on registration, file sharing, and related data transmission. In short, such an electronic operating procedure is developed to help people reduce tedious work. On the other hand, this system fulfils environmental protection because people from either inside or outside NCREE need no paper printing while using this system.

CWMS was designed only for NCREE employees to construct conference websites. It was certainly unable to match what the other faculties need for conference website construction. To help them construct and customize their conference website, this work modified and expanded the framework of CWMS so that they can apply CWMS as smoothly as the NCREE employees can. Now CWMS has already served the user outside NCREE as shown in Fig. 8.



Fig. 7 ITP 2005 Video database



Fig. 8 The CWMS expanded for the user outside NCREE

Conclusions

The ontology this work developed embodies and stores part of the earthquake engineering knowledge. Capable of establishing agreements about knowledge, this ontology may enable the communication between NCREE's knowledge bases or systems so that the knowledge management in NCREE could be fulfilled more effectively with the support of knowledge sharing between machines. In addition, the procedures this work proposed to construct this ontology could help researches of other domain save human effort on ontology development. Besides, the construction of the experimental flow management system can effectively help an experiment preserve information and data throughout its three stages: plan, execution, and finish. Cooperating with the NCREE experiment online application system and the NCREE Data Center, the experiment flow management system is expected to facilitate the accumulation of the experiment-related knowledge and experience. Moreover, through the construction of NCREE video database, the knowledge of NCREE technologies can be maintained and then accumulated year by year. The knowledge could therefore get disseminated through people's access to the NCREE video database. Finally, the fact that CWMS helped people outside NCREE construct and customize their conference website will promote NCREE's people-visible performance if they indeed appreciate this service.

References

- Chen, W. F., and Scawthron, C.(2003), "Earthquake Engineering Handbook", CRC Press, Boca Raton, Florida.
- Gruber, T. R. (1993), "Toward Principles for the Design of Ontologies Used for Knowledge Sharing", Technical Report, KSL 93-04, Knowledge Systems Laboratory, Stanford University, Palo Alto, CA, USA.
- Herman, I., and Marshall, M. (2000), "GraphXML-An XML-based graph description format", Proceedings of Symposium on Graph Drawing (GD 2000), volume 1984 of LNCS, pp.52-62, Springer.
- Lin, H. T., Hsieh, S. H., Chou, K. W., and Lin, K. Y. (2009), "Construction of Engineering Domain Ontology through Extraction of Knowledge from Domain Handbooks", ASCE International Workshop on Computing in Civil Engineering, June 24-27, Austin, Texas, USA.(Submitted)
- Wikipedia(2009), "Ontology (information science)", [http://en.wikipedia.org/wiki/Ontology_\(information_science\)](http://en.wikipedia.org/wiki/Ontology_(information_science))

Earthquake Source Parameters and Micro-tremor Site Characteristics Study-Geochemical Monitoring (IV)

Vivek Walia¹, S. J. Lin², T. F. Yang³ and K. L. Wen⁴

瓦里亞¹、林世榮²、楊燦堯³、溫國樑⁴

Abstract

Soil-gas emissions along active zones are demonstrated as a geochemical tool to identify and monitor tectonic activity in the region. The present work is focused on Hsincheng fault in Hsinchu area and the Hsinhua fault in Tainan for earthquake monitoring using soil gas method to determine the influence of such formations on enhanced concentrations of different gases in soil to monitor the tectonic activity in the region. Along with some preliminary field surveys in Ilan area in 2008 to find appropriate site for establishing geochemical monitoring station. To carry out the present investigation variation in temporal soil-gases compositions was measured at continuous earthquake monitoring station established along Hsincheng and Hsinhua faults in Hsinchu and Tainan areas, respectively. Observations have shown potential precursory signals for some major earthquakes in the region.

Results have shown that Hsinhua and Hsincheng faults have different tectonic settings. Hsinhua soil-gas variations show precursory signals for earthquakes occurring in south or south eastern part of Taiwan, whereas, for Hsincheng fault most of soil-gas variation precursory signals were recorded for the earthquakes that occurred along Okinawa Trough and Ryukyu Trough. Hsinchu monitoring station has shown better confidence level (i.e. 2.8) than monitoring station along the Hsincheng fault, hence seems to be a better station. During the preliminary survey in Ilan area, five profiles has been completed so far in which in about 46 samples were collected and analysed. Distributions of radon values have shown anomalous values along the Nanao fault and other tectonic features..

Keywords: Soil-gas, Fault, Earthquake, Helium, Radon, CO₂.

Introduction

The island of Taiwan is a product of the arc-continent collision between Philippine Sea plate and Eurasian plate which make it a region of high seismicity. Looking at the tectonic map of Taiwan, one can find about 42 identified active faults. The present work is focused on Hsincheng fault in Hsinchu area and the Hsinhua fault in Tainan for earthquake monitoring using soil gas method. It is well established that distribution of soil gas compositional variations can be employed as the precursors for earthquakes (Walia et al., 2005b; Yang et al., 2006) and for mapping of fault zones (Walia et. al, 2005a; Fu et al., 2005). Studies on

diffuse degassing from sub-surface carried out have clearly shown that gases can escape towards the surface by diffusion and by advection and dispersion as they are transported by rising hot fluids and migrate along preferential pathways such as fractures and faults (Yang et al., 2003). To explain radon migration over large distances, several models have been elaborated and it has been established that radon is transported by underground water or carrier gases (Etiope and Martinelli, 2002).

Presently we have focused on temporal geochemical variations of soil-gas composition at established geochemical observatories along the Hsincheng and the Hsinhua faults in Hsinchu and

¹ Associate Research Fellow, National Center for Research on Earthquake Engineering, walia@ncree.org.tw

² Assistant Research Fellow, National Center for Research on Earthquake Engineering, sjlin@ncree.org.tw

³ Professor, Department of Geosciences National Taiwan University, tyang@ntu.edu.tw

⁴ Deputy Director, National Center for Research on Earthquake Engineering, wenkl@ncree.org.tw

Tainan areas of Taiwan, respectively and to determine the influence of enhanced concentrations of soil gases to monitor the tectonic activity in the region. Along with some preliminary field surveys in Ilan area to find appropriate site for establishing geochemical monitoring station.

Methodology

To carry out the present investigation, temporal soil-gases compositions variation were measured regularly at continuous earthquake monitoring stations established along Hsincheng and Hsinhua faults in Hsinchu and Tainan areas, respectively using RTM2100 (SARAD) for radon and thoron measurement (for details see previous reports).

Results and Discussions

Investigations during the observation period have shown potential precursory signals for some major earthquakes in the region. Both the above said faults are located on/near National Science Industrial Park (NSIP), the industrial hub of Taiwan, and can be cause of concern making it necessary to check the activity to these faults. During the observation we have found that in some cases number of earthquakes happened in short span of time i.e within 1-5 days, these earthquakes can be considered as aftershocks/foreshocks of big earthquakes or different earthquakes. In the present study we have considered these as one seismic event.

Hsincheng Fault

During the observation period (i.e Jan., 2006 until Dec., 2008) potential precursory signals have been recorded for some earthquakes that occurred in the region (Fig. 1). About 40 seismic events were observed during the observation period at this monitoring station and 17 of these have shown precursory signals. Those which have shown no precursory signals are deep focus earthquakes or monitoring station may be effected by the heavy rainfall during that period. During the period of observation, about 29 anomalies were observed and out of these 17 anomalies can be correlated with the seismic events (Table 1). Most of non-correlated events are either having no soil-gas data or deep focused events. During heavy rains, water percolated down and affected the gas emanation thus prevented gas to migrate towards the surface. For the above mentioned period of observation, about 59% of anomalies can be correlated with seismic events in the region and the rest of anomalies may have occurred due to on going crustal deformation in the region which is not mature enough to produce an earthquake. The confidence level of monitoring station along the Hsincheng fault is found be 1.2 and indicative the monitoring station is good for earthquake monitoring.

Hsinhua Fault

A continuous monitoring station was established at selected point at end of October, 2006 using radon detectors RTM 2100 along with carbon-di-oxide detector (Fig. 2). In the observation period potential precursory signals were recorded for some earthquakes that occurred in the region

Totally, about 34 seismic events were recorded and 35 anomalies were also recorded at the monitoring station. From this, 26 can be correlated with the seismic events. All of non-correlated events occurred during heavy rainy season and thus no anomalies can be detected for these events. This monitoring station has shown better confidence level (i.e. 2.8) than monitoring station along the Hsincheng fault, hence seems to be a better station (Table1). It has been found during year 2008 we have recorded more number of seismic events as well as number of precursory anomalies at Hsinhua as compare to Hsincheng fault which may indicate the this region may be getting more seismically active.

Ilan Area

In addition to continues monitoring at established monitoring stations, we are trying to find appropriate site to build new monitoring stations on other active faults, so that we can have dense network of monitoring stations. For that in 4th phase of the project we did some preliminary field surveys in Ilan area using the soil-gas sampling procedure (reported in previous reports) has been undertaken.

In total 5 profiles has been completed so far in which in about 46 samples were collected and analysed ^{222}Rn , ^4He , CO_2 , CH_4 , Ar , O_2 etc. Out of these five profiles three preformed in Ilan area where as two were taken near the Nanao fault present in Ilan Plain (Fig. 3). Nanao fault is supposed to be non active geologically. Preliminary results shows show large spatial variation in gas concentrations along the tectonic features present in that area. Distribution of radon values have shown anomalous values along the Nanao fault and other tectonic features (Fig. 3).

Conclusions

From the above results, it can be concluded that both Hsinhua and Hsincheng faults have different tectonic setting. Hence, it can be said that soil-gas variations at Hsincheng fault were disturbed by the stress variation due to tectonic activities along Okinawa Trough and Rkukyu Trough (Fig. 4) which are located in north and central eastern part of Taiwan, respectively. Whereas in the case of Hsinhua fault, soil-gas variations were observed to be due to tectonic activities along the Luzon Arc and

other tectonic activities in southern part of Taiwan. So, soil-gas variations at Hsinhua monitoring station show precursory signals for earthquakes occurring south or south eastern part of Taiwan (Fig. 5), whereas, for Hsincheng faults, most of soil-gas variation precursory signals were recorded for the earthquakes that occurred along Okinawa Trough and Rkukyu Trough. The result from the present study shows that the soil-gas method may be useful for fault and earthquake monitoring studies along the Hsincheng fault, Hsinchu area of NW Taiwan. Long time continuous and comprehensive monitoring may be needed to find correlation of earthquakes with degassing along the established monitoring station to understand the characteristics of earthquakes.

From the temporal variation of soil-gas during the observation at both the monitoring stations it has been found that both the faults have different characteristics which are indicated by the different anomaly pattern. It has been observed along Hsinhua fault monitoring station that the soil gas shows diurnal and nocturnal variations in silent period. But this variation was found to be disturbed before some seismic event and considered to be a precursory anomaly. Whereas in the case of Hsincheng Fault soil gas variation don't show diurnal and nocturnal variations and values above the threshold values can be denied as precursory anomaly. To filter out the effect of diurnal and nocturnal variations we prepared online database where we can find the values average values of soil gas ranging from 1 hour to 24 hours. For data analysis and identifying anomalies we use 24 hour average values of soil-gas for both the stations.

From the above preliminary data it can be concluded that the soil gas anomalies patterns observations can supply useful information in the recognition of possible tectonic activities. The results show that, analyses of two more than two gas species gives more reliable information which is clearly seen from temporal distribution of the anomalies of the gas species used to understand tectonic setting of area. From the spatial distribution of radon the trace of Nanao fault and neotectonic features can be identified.

References

- Etioppe, G., Martinelli, G. (2002). "Migration of carrier and trace gases in the geosphere: an overview". *Phys. Earth Planet. Int.*, 129, 185-204.
- Fu, C.C., Yang, T.F., Walia, V., Chen, C-H. (2005). "Reconnaissance of soil gas composition over the buried fault and fracture zone in southern Taiwan". *Geochemical Journal*, 39,427-439.
- Walia, V., Su, T. C., Fu, C. C., Yang, T. F. (2005a). "Spatial variations of radon and helium

concentration in soil gas across Shan-Chiao fault, Northern Taiwan". *Radiat. Meas.*, 40, 513-516.

- Walia, V., Virk, H.S., Yang, T. F., Mahajan, S., Walia, M. and Bajwa, B.S. (2005b). "Earthquake prediction studies using radon as a precursor in N-W Himalayas, India: a case study". *TAO*, 16(4), 775-804.
- Yang, T.F., Chou, C.Y., Chen, C-H, Chyi, L.L., Jiang, J.H. (2003). "Exhalation of radon and its carrier gases in SW Taiwan". *Radiat. Meas.* 36, 425-429.
- Yang, T.F., Fu, C.C., Walia, V., Chen, C-H., Chyi, L.L., Liu, T.K., Song, S.R., Lee, M., Lin, C.W., Lin, C.C., (2006). Seismo-geochemical variations in SW Taiwan: multi-parameter automatic gas monitoring results, *Pure Appl. Geophys.*, 163, 693-709.

Table.1. Statistical analysis of recorded data at both the monitoring stations.

Station Name	Total anomalies (a)	Total seismic events (b)	Anomalies related with events (c)	Anomalies not related with seismic events (d)	Signal (%) (e/a)	Noise (%) (d/a)	Confidence level (Signal/Noise)
Hsincheng Fault	29	40	17	12	59%	41%	1.2
Hsinhua Fault	35	34	26	9	74%	26%	2.8

竹科觀測站 Hsinchu Station

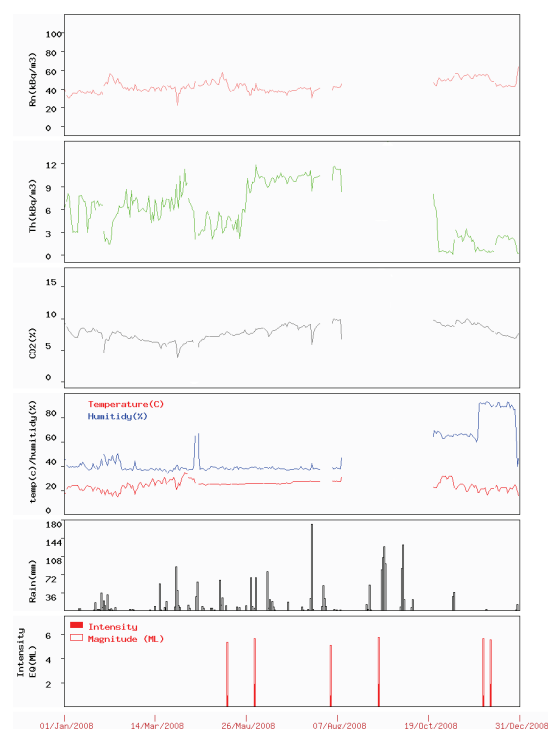


Fig.1. Variations of radon, thoron, carbon dioxide and rainfall at Hsinchu monitoring station and its correlation with earthquakes.

新化觀測站 Hsinhua Station

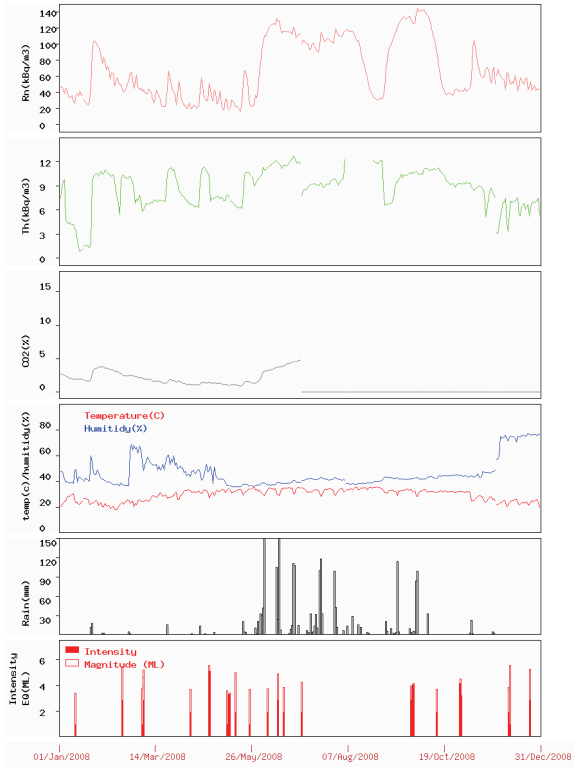


Fig.2. Variations of radon, thoron, carbon dioxide and rainfall at Hsinchu monitoring station and its correlation with earthquakes.

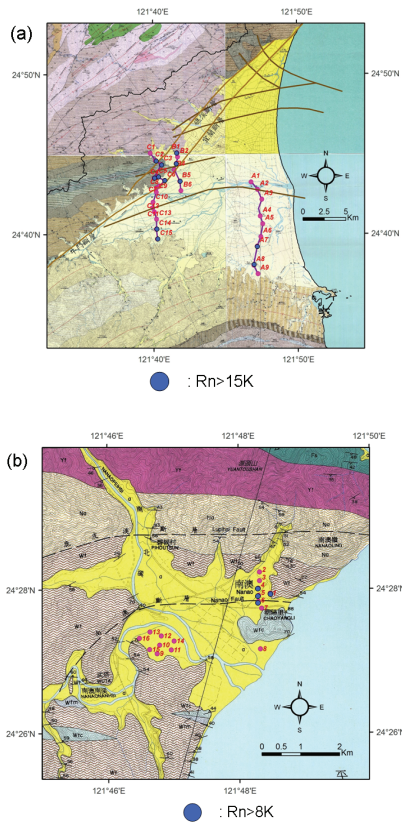


Fig.3. Distribution of radon anomalies (blue dot) along profiles in (a) Ilan Plain (b) Nanao Fault, of Ilan area.

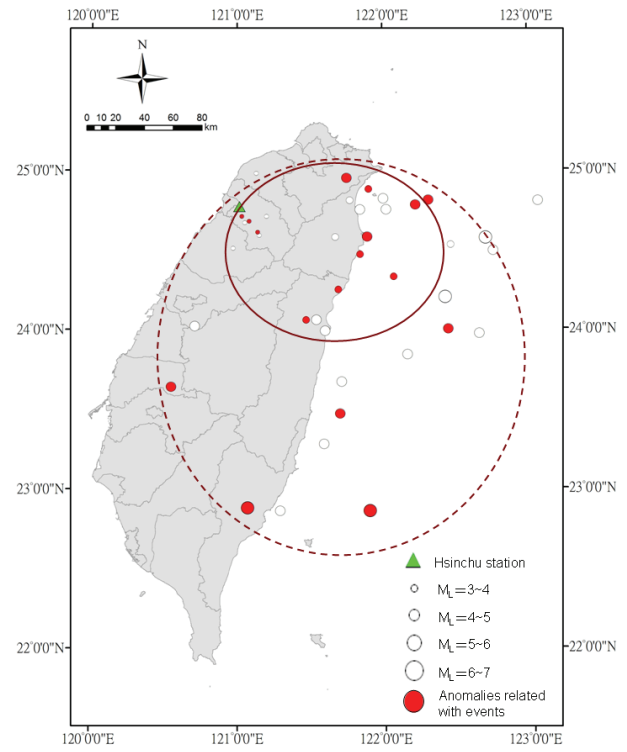


Fig.4. Distribution of events recorded at monitoring station along Hsincheng fault in Hsinchu area.

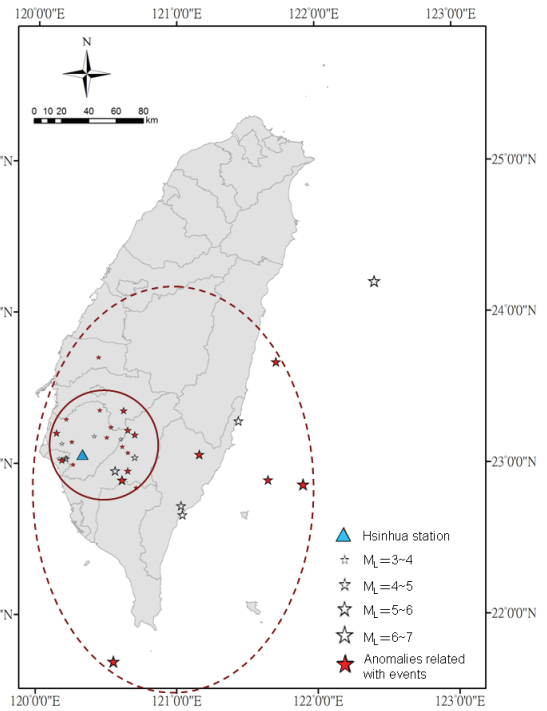


Fig.5. Distribution of events recorded at monitoring station along Hsinhua fault in Tainan area.

Development of an Object-Oriented Program for Structural Collapse Analysis of Framed Structures

Ren-Zuo Wang¹, Keh-Chyuan Tsai² and Ming-Chieh Chuang³

王仁佐¹、蔡克銓²、莊明介³

Abstract

The object of this project is to develop numerical analysis code using vector form intrinsic finite element (VFIFE, or V-5) method. In this work, this code design and implementation of an object-oriented technology. The code name is called SUV-5 which has a user friendly interface to simulate nonlinear static analysis, nonlinear dynamics analysis and collapse analysis of structures. An easy-to-use and user-friendly interface was developed at the National Center for Research on Earthquake Engineering(NCREE). In this project, this interface is called GISA3D which has modified in the SUV-5. In addition, the project also has successfully developed a fiber section element. The element cross-section can be a fiber section using different stress-strain models. These materials include the reinforced steel, steel, well-confined concrete and not well-confined concrete. Finally, the accuracy of SUV-5 was demonstrated by comparing experimental and numerical results.

Keywords: vector form intrinsic finite element, SUV-5, GISA3D, fiber section element

Introduction

This research aimed to develop an interface of Windows programs with the core of Vector Form Intrinsic Finite Element (V-5) and to build numerical software that can analyze collapse of structures. The Windows programs can be used to build various kinds of numerical analysis models of space structure and also to check the result of analysis. The combined V-5 method and Windows programs is then called SUV-5 numerical software. The foundation of Windows program was based from the graphical user interface of nonlinear static/dynamic 3D structural analysis program. The Windows interface of GISA3D was developed to support the PISA3D program. The SUV-5 and the PISA3D software have different calculating core. The SUV-5 software can not only be used to analyze the nonlinear large deformation behavior of continuum, but also can be used to simulate the collapse, impact and fracture behavior of structure. Hence, the key point of this research to the extension of the GISA3D framework to integrate the V-5 method.

In science research, the development of a

nonlinear static and dynamic structural analysis programs focus mainly in the efficiency of analysis, then the National Center for Research on Earthquake Engineering developed the graphical user interface of inelastic structural analysis for 3D systems or GISA3D. Through object-oriented design and the application of various design patterns, the system framework of SUV-5 Program can be established with more elasticity and expansibility.

This project has formulated also the frame element of a fiber section. The element's cross-section can be a fiber section using different stress-strain models for various fibers within the cross-section such as steel, concrete, concrete with FRP model. Through the comparison between numerical simulation of SUV-5 software and laboratory experiments, the accuracy of the SUV-5 software was demonstrated. A numerical example on the collapse analysis of structure is presented to illustrate the capability and user-friendly interface of the SUV-5 software.

¹ Associate Research Fellow, National Center for Research on Earthquake Engineering, rzwang@ncree.gov.tw.

² Director of NCREE, Professor of Civil Engineering, Dept of Civil Engineering, National Taiwan University

³ Assistant Research Fellow, National Center for Research on Earthquake Engineering,

The system framework of SUV-5 program

In order to build a numerical analysis program on the collapse of a structure, the system framework of SUV-5 program was developed by object-oriented design and has been applied with design pattern as shown in Fig.1.

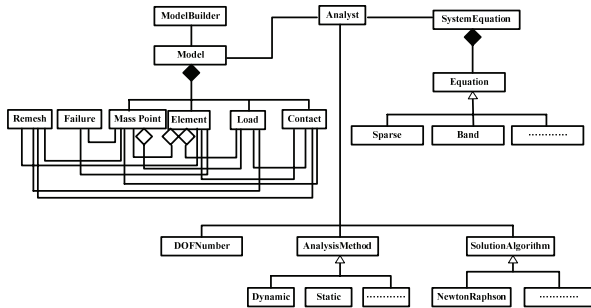


Fig 1. The system framework of SUV-5 program

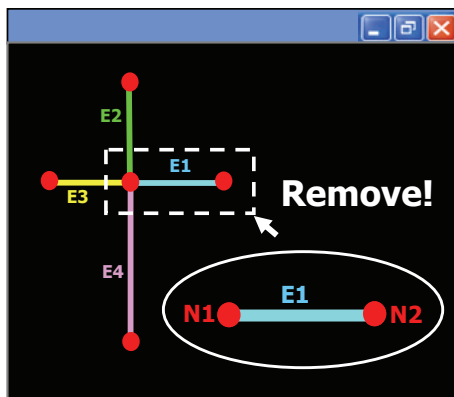


Fig 2. Beam-column joint

The user-friendly interface of GISA3D has been adopted to improve the framework of the proposed analysis program. In the future, in order to provide a more user-friendly interface under various requirements, the model method using object-oriented design for GISA3D needs to work on modifying the mesh method. Thus, this can maximize efficient use of the software and keep the GISA3D well maintained. Due to traditional finite element and V-5 methods for the structure models needs to define the geometry by many different categories of elements. The analysis engine (PISA3D or V-5) and various material models have been considered also to work under object-oriented design. The user-friendly interface of GISA3D must control these kinds of interaction conditions during program admini

The PISA3D can analyze nonlinear dynamic response of frame structure, but the number of degree of freedom can not be added in the PISA3D. Using the V-5 method computer simulation of structural collapse. The end nodes for each frame elements will be cracked in structural collapse analysis of framed structures under impact loads and seismic excitations. The degree of freedom will be added for cracked joint of the elements during dynamic analysis. Thus, the difference between

PISA3D and V-5 method are the post-processing models output. For example, the beam-column connection system is as shown in Fig.2. this system are combined with four frame elements. If the element node N1 is failure, we need to add new degree of freedom at N1 node. It is very important problem for simulation of structural collapse. In order to solve this problem, we need to modify the program of GISA3D and add new design Pattern. Thus, the observer pattern is adopted. This Pattern can clearly describe relationship of the nodes and elements, when there are separated. The observer pattern is used in SUV-5 as shown in Fig.3.

The purpose of research is to integrate graphics interface GISA3D and the V-5 method in postprocessing file. The GISA3D successful used the design pattern to build complete system framework. The PISA3D already provided data integration and visualization system for structural dynamics analysis. In addition, the input file has a good solution which is Strategy Pattern for V-5 and PISA3D as shown in Fig. 4. The new framework of GISA3D can be used to analyze collapse behavior of structural systems.

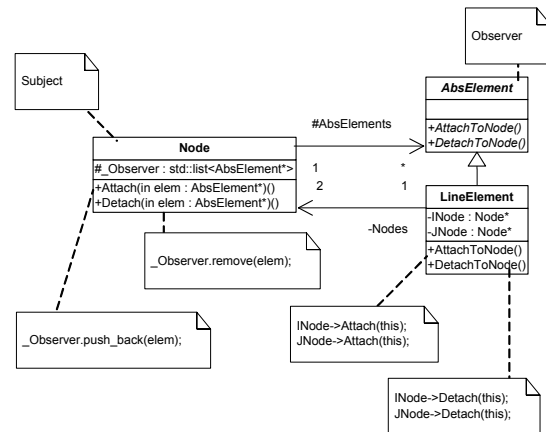


Fig 3. Observer Pattern for each nodes and elements

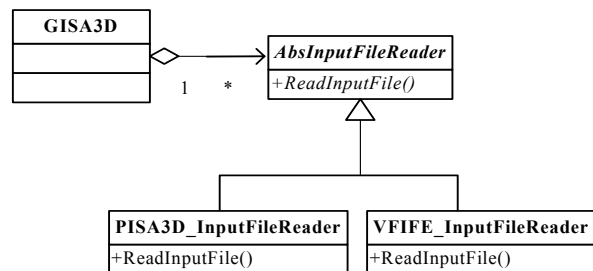


Fig 4. Strategy pattern for V-5 and PISA3D

Fundamentals of the V-5 method

In this study, the V-5 method is extended in order to analyze nonlinear structural systems containing multiple deformable bodies with the following characteristics: (1) interact with each other, (2) or are discontinuous, (3) undergo large deformations and arbitrary rigid body motions. Since

the conventional finite element method (FEM) is an energy-based method, it does not require the balance of forces within each element. Since these unbalanced residual forces will do some work under virtual rigid body motion it will cause inaccuracy and nonconvergence of the computed results. In order to solve these problems, the V-5 method has been proposed by Ting et al. (2004). The V-5 method includes 4 main procedures: (1) construct the equation of motion using Newton's Law at the mass points, (2) update the material frame, (3) compute the fictitious reversed rotations (4) determine the deformation coordinates. These aforementioned computation procedures have some points in common with the concept of the modern FEM. However, the key concept of the V-5 is that V-5 maintains the intrinsic nature of the original FEM. The V-5 makes use of the strong form of equilibrium at each element. All the forces are balanced within each element. These forces are obtained from the principle of virtual work. The associated nodal displacements satisfy the compatibility condition.

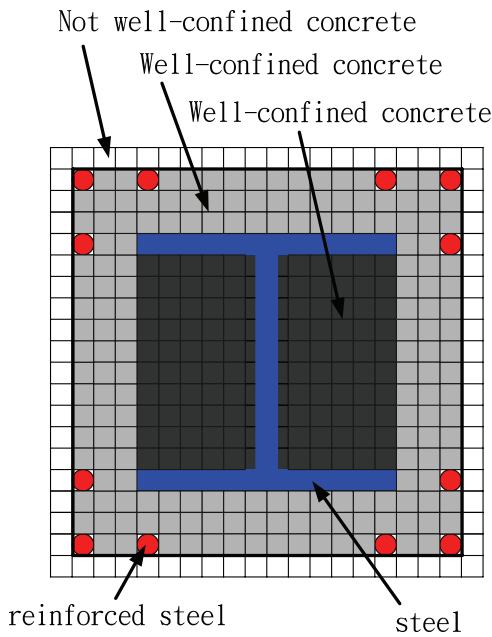


Fig. 5 Fiber section for Modeling of Frame element

Fiber Section for Modeling of Frame Element

The internal force of the elastic frame has been developed by Ting et al. (2004). Recently, the fiber elements is developed in the V-5 method for large deformation analysis of nonlinear structures. The fiber section method can analyze various material on crass section of the frame elements as shown in Fig.5. These materials include the reinforced steel, steel, well-confined concrete and not well-confined concrete. The fiber section method can consider the effects of frame element for axial force-bending moment interaction in the dynamic response of large deformation. In this study, we focus on numerical

analysis of reinforced concrete structures. The element cross-section can be modeled as a fiber section using different stress-strain models for different fibers. In this project, the Mander concrete model was adopted on different fibers as show in Fig.6.

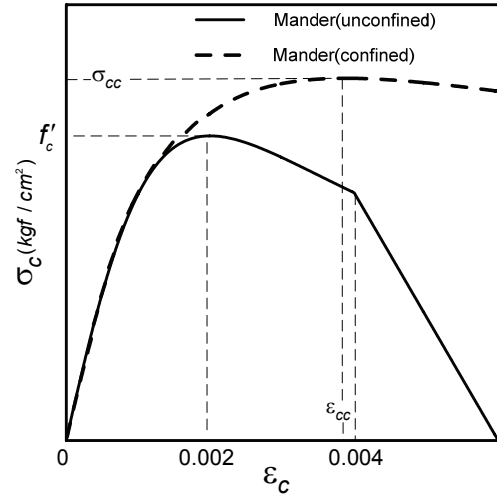


Fig. 6 Mander concrete model

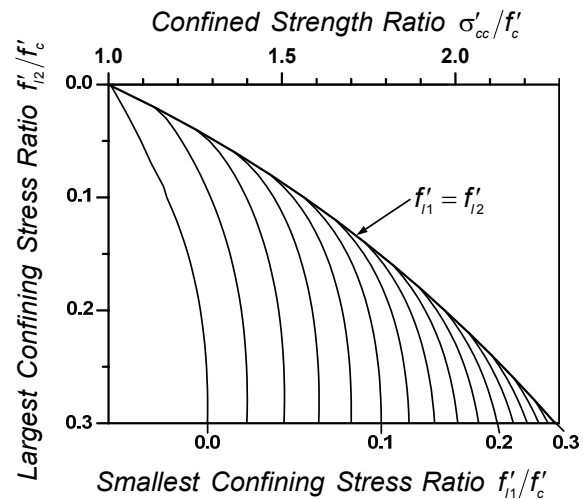


Fig. 7 Smallest confining stress ration verse largest confining stress ratio from Wang and Restrepo, (2001) formulation

Wang and Restrepo, (2001) have suggested a formulation of Mander concrete model on rectangular section as shown in Fig.7. This formulation was adopted in SUV-5 program. This formulation can be expressed as:

$$\sigma_{cc} = \alpha_1 \alpha_2 f'_c \quad (1)$$

where

$$\alpha_1 = \left[1.4 \frac{f'_{11}}{f'_{12}} - 0.6 \left(\frac{f'_{11}}{f'_{12}} \right)^2 - 0.8 \right] \sqrt{\frac{f'_{12}}{f'_c}} + 1 \quad (2)$$

$$\alpha_2 = 1.25 \left(1.8 \sqrt{1 + \frac{7.94 f'_{12}}{f'_c}} - 1.6 \frac{f'_{12}}{f'_c} - 1 \right) \quad (3)$$

$$f'_{l2} = \max[f'_{lx}, f'_{ly}] \quad (4)$$

$$f'_{l1} = \min[f'_{lx}, f'_{ly}] \quad (5)$$

The $f'_{lx} = k_e f_{lx}$ and the $f'_{ly} = k_e f_{ly}$ are the effective lateral confining stress for rectangular confined concrete in the spiral of x and y direction. the k_e is effective confined coefficient. The modified Mander confined model is used to analyze numerical simulation analysis of column with FRP. For steel material model, the stress-strain relation of steel (Mirza and MacGregor, (1979)) is adopted.

Numerical simulation of SUV-5

In this project, there were three numerical examples. Two examples for comparing experiments of reinforced concrete, FRP column and numerical results of SUV-5 are studied. There are experimental size of RC1 and RC2 as fig.8 by Hong, (1998). The accuracy of SUV-5 was demonstrated by comparing experimental and numerical results. As shown in fig.9 and fig.10.

The three examples is studied for the structural collapse analysis of frame structures. This structure collapse analysis using SUV-5 program is as shown in fig.11. The purpose of this example, in order to show the user friendly interface of SUV-5 is developed in this project.

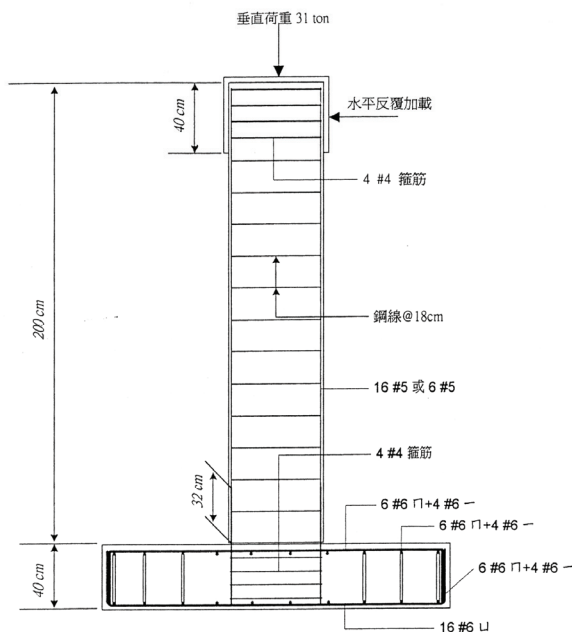


Fig 8. Experimental size of RC1 and RC2 by Hong, (1998)

Conclusions

In this project, the numerical analysis of structure collapse using the system of object-oriented is developed. The framework of SUV-5 program is successfully adopted the new framework of GISA3D windows interface and the V-5 method. This project

also developed a fiber section element in V-5 method. The element cross-section can be used different stress-strain models (FRP-confined concrete, well-confined concrete, not well-confined concrete, steel) for different fibers. In the future, National Center for Research on Earthquake Engineering (NCREE) will keep to modify the user friendly interface and to develop another function of SUV-5.

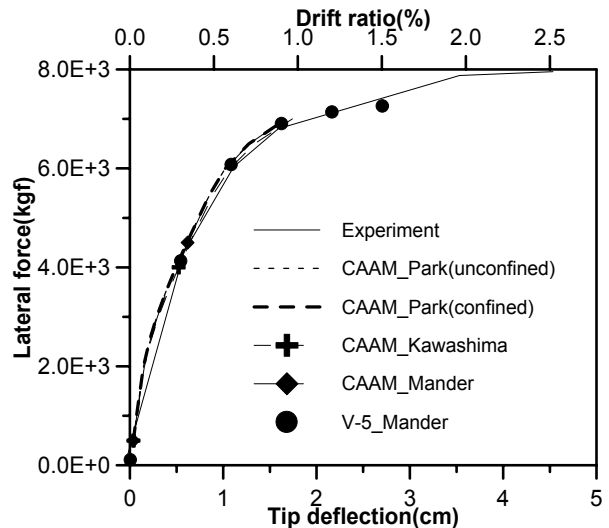


Fig. 9. Comparison experimental and numerical results (RC1)

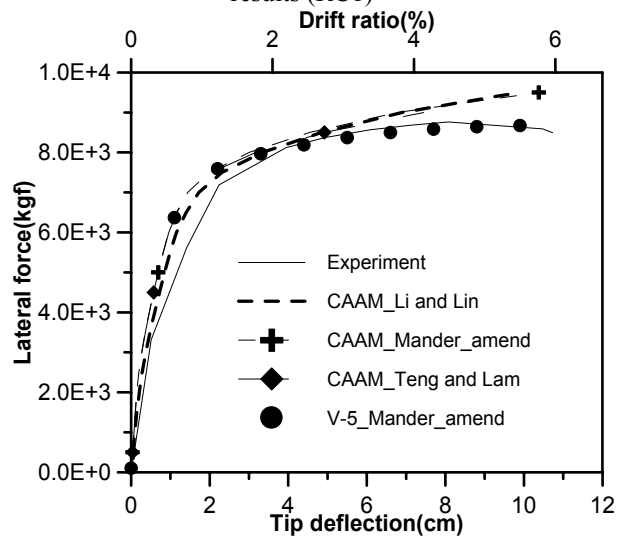


Fig. 10. Comparison experimental and numerical results (RC2)

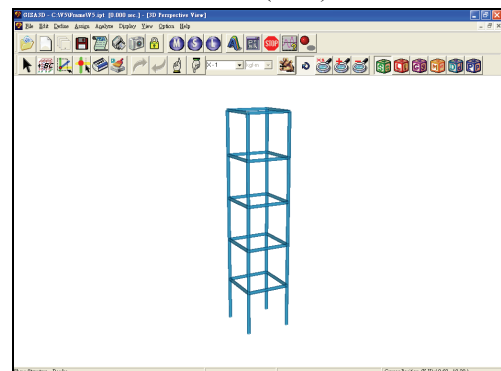


Fig. 11. The user friendly interface of SUV-5